

Renormalisation Group Study  
of Broken Symmetry States  
in Strongly Correlated Electron Systems

Johannes Bauer

A thesis presented for the degree of  
Doctor of Philosophy of the University of London  
and the  
Diploma of Imperial College  
August 2007

Supervisor: Dr AC Hewson  
Imperial College London



# Declaration

Hereby I declare that the work presented in this thesis is my own and all other sources used have been referenced.

London, ..... ..



# Abstract

In recent years the extraordinary behaviour in condensed matter materials such as high temperature superconductors and heavy fermions has attracted much attention. Attempts to understand it are mostly based on local and lattice models of strongly correlated electrons. These systems show a rich behaviour with states of broken symmetry. In the strong coupling regime the relevant models are, however, not easy to understand with standard perturbative approaches. Renormalisation group methods in contrast constitute a reliable approach to describe these strong correlation effects. The objective of this thesis is to contribute to (a) the development of renormalisation group methods for states with broken symmetry and (b) the description of the low energy properties for certain specific symmetry breakings.

The calculations presented are based on the Anderson impurity model (AIM) and the Hubbard model. We develop and apply the numerical renormalisation group (NRG) and the renormalised perturbation theory (RPT). The extension of these methods from the local model to the lattice model is within the dynamical mean field theory (DMFT) framework. First we focus on the application of NRG and RPT to local models. We study magnetic symmetry breaking in the AIM in equilibrium and non-equilibrium. This includes calculating dynamic response functions and all relevant quasiparticle parameters. We also investigate the AIM with superconducting symmetry breaking in the medium. The analysis is then extended to infinite dimensional lattice models by using the DMFT approach. Thus, results are presented for field induced magnetic ordering and antiferromagnetic symmetry breaking in the Hubbard model. We also give a preliminary study of the crossover from weak to strong coupling in the attractive Hubbard model with superconducting symmetry breaking.



# Contents

<b>Introduction</b>	<b>1</b>
<b>I Models and Methods</b>	<b>7</b>
<b>1 Models of strongly correlated electrons</b>	<b>9</b>
1.1 The Anderson Impurity Model (AIM)	9
1.1.1 General features and model parameters	9
1.1.2 The Spin-Isospin Transformation	14
1.2 The Hubbard Model	15
1.2.1 General features and model parameters	15
1.2.2 The Spin-Isospin transformation and symmetry breaking	16
<b>2 Methods for strong correlation physics</b>	<b>19</b>
2.1 The Numerical Renormalisation Group (NRG)	19
2.1.1 NRG setup for the Anderson impurity model	20
2.1.2 Static and dynamic quantities from NRG calculations	23
2.2 The Renormalised Perturbation Theory (RPT)	27
2.2.1 The RPT setup	28
2.2.2 Functional integral description in the 1PI formalism	30
2.2.3 Alternative formulations and extensions	34
2.3 The Dynamical Mean Field Theory (DMFT)	36
<b>II Locally Correlated Systems</b>	<b>39</b>
<b>3 Field dependent quasiparticle dynamics in the Anderson impurity model</b>	<b>41</b>
3.1 Strongly correlated electrons in a field	41
3.2 Field dependent renormalised parameters	42
3.3 Low temperature response	47
3.4 Beyond the Low Energy Regime	51
3.4.1 NRG method	51

---

3.4.2	RPT method . . . . .	53
<b>4</b>	<b>The Anderson impurity model in magnetic field in non-equilibrium</b>	<b>63</b>
4.1	Transport through a quantum dot . . . . .	63
4.2	Formal setup for the non-equilibrium theory . . . . .	67
4.2.1	The two channel Anderson model and Keldysh formalism . . . . .	67
4.2.2	Low voltage asymptotics for the self-energy . . . . .	71
4.3	Differential conductance for low voltage . . . . .	72
4.3.1	Effect of the voltage on the differential conductance for small field . . . . .	73
4.3.2	Critical field for peak splitting . . . . .	74
4.4	Higher voltages and non-equilibrium RPT calculations . . . . .	76
4.4.1	Non-equilibrium repeated quasiparticle scattering . . . . .	76
4.4.2	Single particle dynamics in zero magnetic field . . . . .	78
4.4.3	Dynamics and differential conductance in finite magnetic field . . . . .	80
<b>5</b>	<b>Locally correlated electrons in a superconducting bath</b>	<b>83</b>
5.1	Kondo physics and BCS superconductors . . . . .	83
5.2	The Anderson model with superconducting medium . . . . .	85
5.2.1	NRG approach . . . . .	85
5.2.2	Relevant Green's functions . . . . .	86
5.2.3	Andreev bound states . . . . .	88
5.3	Bound state behaviour for the symmetric model . . . . .	90
5.4	Spectral functions . . . . .	94
5.5	Away from particle hole symmetry . . . . .	98
<b>III</b>	<b>Correlated Lattice Systems</b>	<b>101</b>
<b>6</b>	<b>The Hubbard model in magnetic field</b>	<b>103</b>
6.1	Magnetic states in the Hubbard model . . . . .	103
6.2	Setup for the DMFT with a magnetic field symmetry breaking . . . . .	104
6.3	Results at Half-filling . . . . .	108
6.3.1	Weakly correlated regime . . . . .	108
6.3.2	Intermediate coupling regime . . . . .	110
6.3.3	Strong coupling regime . . . . .	113
6.4	Results away from half filling . . . . .	114
6.4.1	Quarter Filled Case . . . . .	114
6.4.2	Near half filling . . . . .	115

---

<b>7</b>	<b>Renormalised quasiparticles in metallic Antiferromagnets</b>	<b>119</b>
7.1	Antiferromagnetic order in the Hubbard model . . . . .	119
7.2	General setup and DMFT approach . . . . .	121
7.3	Quasiparticle analysis . . . . .	124
7.3.1	Quasiparticle weight . . . . .	125
7.3.2	Renormalised chemical potential . . . . .	126
7.3.3	The quasiparticle interaction . . . . .	127
7.4	Spectra . . . . .	128
7.4.1	Local Spectra . . . . .	128
7.4.2	$k$ -resolved Spectra . . . . .	129
<b>8</b>	<b>The attractive Hubbard model</b>	<b>137</b>
8.1	The BCS-BEC crossover . . . . .	137
8.2	The DMFT setup . . . . .	139
8.3	Renormalised quasiparticle description . . . . .	141
8.4	Results . . . . .	143
	<b>Conclusions</b>	<b>147</b>
	<b>Appendix</b>	<b>153</b>
<b>A</b>	<b>Spectral functions in the full density matrix (FDM) approach</b>	<b>153</b>
A.1	General expressions . . . . .	153
A.2	Details for Quantum numbers $Q, S_z$ . . . . .	155
A.2.1	Reduced density matrix . . . . .	155
A.2.2	Expressions for the dynamic correlations functions . . . . .	157
<b>B</b>	<b>Renormalised parameters from NRG calculations</b>	<b>159</b>
<b>C</b>	<b>Renormalised Perturbation Theory</b>	<b>163</b>
C.1	Proof for the feasibility of the RPT approach . . . . .	163
C.2	Alternative Setup for the RPT . . . . .	166
C.3	Functional integral description in the 2PI formalism . . . . .	167
C.4	Non-equilibrium renormalised perturbation theory . . . . .	170
	<b>Bibliography</b>	<b>175</b>
	<b>Acknowledgement</b>	<b>185</b>



*There is a theory which states that if ever anyone discovers exactly what the Universe is for and why it is here, it will instantly disappear and be replaced by something even more bizarre and inexplicable. There is another theory which states that this has already happened.*

Douglas Adams

# Introduction

In many fields of research, ranging from sociology over finance to biology and physics, a fundamental concept is that of *correlations* between certain entities. When analysing certain events, or the behaviour of a system in terms of its constituents, one often asks to what degree the subunits of the system are correlated and what the implication of the correlations are. In many cases in nature, the fundamental behaviour of an isolated constituent is rather unspectacular, whereas the collective behaviour of the whole system can show remarkable features. For illustration consider a living organism based on individual cells or a magnetically ordered state formed from itinerant electrons. That such an organised state persists in spite of omnipresent natural fluctuations can often be understood in terms of correlated behaviour.

This thesis deals with many-body systems in the field of condensed matter physics. There, models of strongly correlated electrons have attracted an enormous amount of attention in the last four decades. A number of materials, such as heavy fermions, high temperature superconductors and mesoscopic systems like quantum dots, show behaviour which can only be explained when strong local interactions are taken into account. These strong electronic interactions can be of various kinds, such as direct Coulomb interactions or mediated by exchange bosons, for instance lattice phonons. At low temperature, when there are few thermal fluctuations, the quantum mechanical behaviour of these many-body systems is most visible. Then they can assume a large variety of different states, such as a normally conducting or insulating state, they can spontaneously order magnetically and also become superconducting. It is this variety of phases with broken symmetry, which makes these systems so interesting to study. The appearances of these different phases can often be understood in terms of the high degree of correlation of the particles. A small change in a parameter can alter the state of the system completely. Along certain axes in the relevant parameter space, zero temperature quantum phase transitions can be observed. The rich phase diagram of many of these systems is due to the delicate interplay of kinetic and potential energy as well as that of charge and spin fluctuations. Often it is a challenge to identify the dominant mechanism that drives the system into a certain state.

Before introducing the specific models to describe these systems of strongly correlated electrons, we outline a few general considerations. It is remarkable that - as realised in the 1920s and 1930s - in spite of the generally large Coulomb repulsion between two

electrons in a solid state system at short distances, many metals are exceptionally well described by a gas of non-interacting fermions. Experimental studies showed that the electric and magnetic response of these materials is essentially that of a Fermi gas, however, with effective parameters, slightly renormalised from their bare value. This phenomenon could be understood through ideas dating back to Landau (1957), who saw that a natural extension of the Fermi gas is a Fermi liquid, which at low temperature shows excitations of similar nature to the Fermi gas, albeit with renormalised parameters. The Fermi liquid thus is an effective description of an interacting system. One of the main ideas is that the low energy excitations are in a one to one correspondence with the original electronic excitations. This description applies well for itinerant, metallic systems, such as copper, but is even valid for insulators, where the band structure is such that the Fermi energy falls into the gap. One reason that this works so well is not that the Coulomb energy for two electrons is as small as compared to the kinetic energy, but that the positive background charge leads to a screening of the interaction. Such a picture emerges most naturally for largely overlapping atomic orbitals, which lead to wide conduction bands. The situation changes, however, if the itinerant electrons belong rather to more localised orbitals, such as in transition metals. Here the interaction plays a significant role if two or more electrons occupy the same orbital. This leads to strong correlation effects, and as a result it can happen that a material with a half filled band is actually an insulator because of the interaction - this possibility was first pointed out by Mott (1949, 1968). It is remarkable that the quasiparticle excitations of many of these strongly correlated systems are still well characterised by Landau's Fermi liquid theory.

In the 1960s various simple models for such situations were introduced. One model, which is of paramount importance for condensed matter studies, is the Anderson impurity model (Anderson 1961). It describes an atomic orbital (impurity) in which local Coulomb interactions play an important role. It is surrounded by a non-interacting band of electrons, which hybridises with this impurity. In the simplest case the impurity does not have degenerate states (s-orbital) and can therefore maximally be occupied by two electrons with opposite spin. The Anderson impurity model has served as a sensible model for physics of dilute impurities in metals and forms the basis for understanding the celebrated Kondo effect. It has been the subject of many theoretical studies and is accepted as the standard model of locally strongly correlated electron systems. It has attracted renewed attention in recent years, since it can be considered as an appropriate model for the description of nanoscale quantum dot systems in certain instances.

A model which takes into account local Coulomb interactions on every site of a lattice is the Hubbard model. This model was motivated by describing the basic magnetic and electric properties of condensed matter materials in the 1960s. For real materials it is maybe too simplified, but up to the present date it is one of the most important models for studying strong correlation effects in matter. Revived interest in the model was generated by the discovery of high temperature superconductors in the 1980s and more recently by

---

cold atomic gas systems in optical lattice, which apart from an additional confinement potential have all the characteristics of the Hubbard model. For this thesis the Hubbard model is considered as the standard lattice model of strong electron correlations, which due to its rich phase diagram is worthwhile to study in detail. Moreover, it is, as the Anderson impurity model, a good testing ground for methods of different kinds.

The simplicity of these models is both an advantage and a drawback. The first since it allows for a fairly simple analysis in terms of few parameters, and yet a rich behaviour in terms of broken symmetry phases can be explored. The obvious drawback is that in order to model “real systems” and compare to experimental measurements other effects such as orbital degeneracies, disorder, nearest neighbour interaction, lattice phonons, etc. have to be taken into account. Some of these extensions can be incorporated without major difficulties, whereas for others the methods we describe here become inapplicable in practice. We want to stress that the purpose of this work is not to explain the properties of a particular material. It is rather to discuss generic strong correlation effects and the development of reliable methods. The emphasis for this is to include symmetry breaking effects, since they lead to very interesting behaviour characteristic for these materials with strongly correlated electrons.

In physics, a concept of paramount importance to understand the state of matter is that of symmetry breaking. The concept is ubiquitous from cosmology and the generation of matter over high energy physics and the fundamental interactions to the well known cases in condensed matter physics such as magnetic ordering, superconductivity or simply the actual condensation from gas to fluid and solid state ordered form. Generally, most systems are invariant under a larger group of symmetry transformations at high temperature. This is quite intuitive as strong thermal fluctuations tend to wash out any symmetry breaking structure. At low temperature, however, it is possible to stabilise a certain state, such as a ferromagnetic ordering which in turn breaks the rotational invariance. It is important to note that the interactions of the particles are very important for an ordering transition. In other words a non-interacting system of fermions does not order even at zero temperature and simply remains a Fermi gas with the corresponding occupation rules. This is different for bosons, which undergo Bose-Einstein condensation at low temperature. For a non-interacting system of bosons, however, no truly superfluid state is adopted. In this thesis we deal with systems of strongly interacting fermions mostly at low temperature. It is therefore to be expected that a number of symmetry breakings can occur. Symmetry breaking does not necessarily occur spontaneously for a certain temperature. We can also bring a system into an ordered state by applying an external field which breaks the symmetry. The simplest case in the context of strongly correlated electrons systems is to subject the system to a magnetic field and study its paramagnetic response.

The strongly interacting nature of the electrons in these models poses severe difficulties for an accurate analysis of their behaviour. Since the potential energy is by no means small compared to the kinetic energy, it is more than questionable to analyse these models in

terms of standard, weak coupling, perturbative methods. Therefore, theoretical research has focused on the development of non-perturbative methods such as numerical techniques like exact diagonalisation or Quantum Monte Carlo. Due to the exponential increase of the underlying Hilbert space the application of these is, however, often limited to fairly small system sizes. Another class of non-perturbative methods are renormalisation group (RG) approaches, which were first developed in the 1960s and 70s, and have contributed to the understanding of many strong coupling problems. Essentially one generates a transformation by which the system is considered on different energy scales, and studies the behaviour for successive applications of the transformation. This transformation is usually invoked by integrating out high energy degrees of freedom. One major aim is the identification and characterisation of different low energy fixed points. This thesis focuses on the application and development of the RG methods numerical renormalisation group (NRG) and renormalised perturbation theory (RPT). Both are directly applicable to the Anderson impurity model (AIM). In the beginning of the 1990s it was shown that in the limit of large dimensions the Hubbard model can be described by an effective AIM, which has to be determined self-consistently within the dynamical mean field theory (DMFT) framework. With the help of the DMFT we can therefore use RPT and NRG to study the Hubbard model and certain symmetry breakings.

Having introduced the relevant topics we can formulate the main goal of this thesis. The objective of the work is twofold:

1. **Advancement of Methods**, i.e. to contribute to the development of the RG methods NRG and RPT and their extension to cases with symmetry breaking.
2. **Physical insight**, i.e. we want to understand the low energy behaviour of these systems of strongly correlated electrons in states with broken symmetry.

The main unifying question of this thesis can then be stated:

- What are the properties of the quasiparticle excitations of strongly correlated fermions in local and lattice models subject to certain symmetry breakings and how can we analyse them?

Figure 1 gives an overview of the structure and contents of the thesis in terms of models, methods and applications. The thesis is divided into three parts. The first introduces the models and methods, the second discusses results for the local models, and in the third part results for the lattice models are presented. On the top of figure 1 we can see the two types of models under consideration. In practice, we will study the AIM as an impurity model and the Hubbard model as a lattice model. We will give a brief introduction to them in chapter 1, establishing the necessary notation. The analysis is in terms of a combination of the RPT and NRG methods which are linked to the corresponding application (box in figure 1) by a line. These methods as well as the DMFT are briefly introduced in chapter

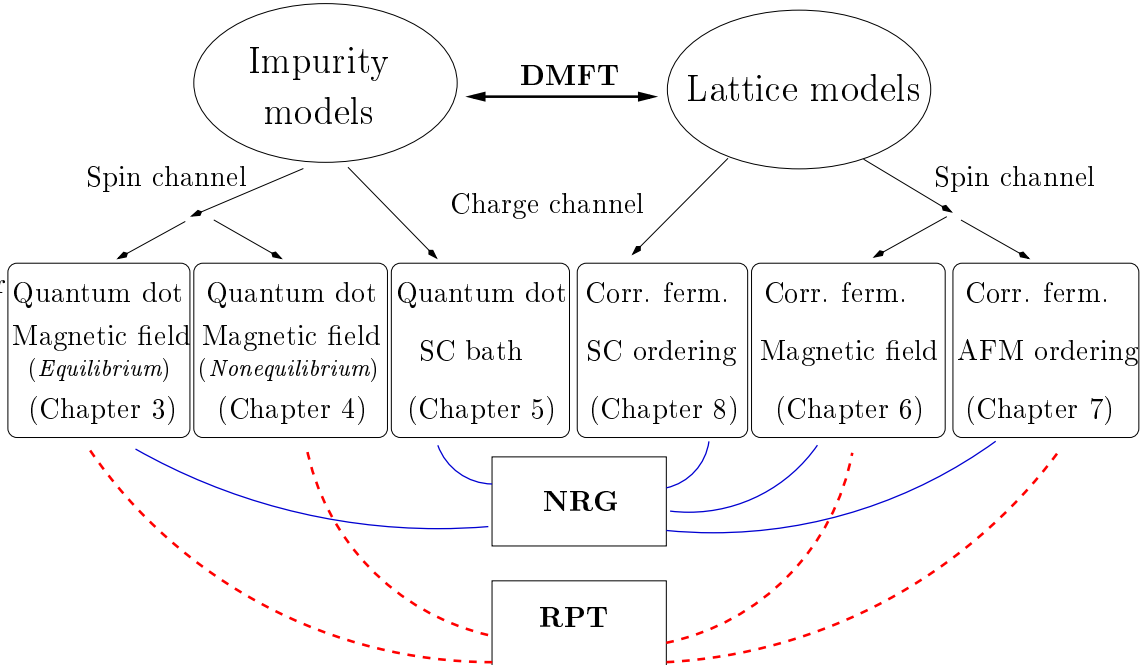


Figure 1: Scheme of relevant models, methods and their range of application.

2. Chapter 1 and 2 form the first part of the thesis. In the second part we study two types of symmetry breaking in the AIM, in the spin and in the charge channel. The AIM does not possess a spontaneously ordered state so the ordering is an induced one. In the spin channel we study the influence of a magnetic field, which is the subject of chapter 3. It will turn out that in order to describe measurements of the current in quantum dot system in a magnetic field, the theory has to be extended to non-equilibrium and a two channel model, which is the focus of chapter 4. The following chapter 5 considers a symmetry breaking in the charge channel. The bath of the model is given by a BCS superconductor there, and we study the effect of this on the impurity. The third part of the thesis deals with correlated fermions in the lattice model. First we study symmetry breaking in the spin channel. Chapter 6 deals with field induced magnetic ordering in the Hubbard model. Spontaneous antiferromagnetic ordering in the doped lattice system is analysed in chapter 7. In chapter 8 we consider symmetry breaking in the charge channel and focus specifically on spontaneous superconducting order in the attractive model.

Let us anticipate some of the main results of this work. For the locally correlated systems with magnetic symmetry breaking we will see that a description in terms of field dependent renormalised parameters allows one to characterise the free quasiparticles and many static response quantities, the low temperature response, the low energy dynamics and the behaviour in small but finite voltage. With the renormalised perturbation expansions we can extend the analysis to higher energies and voltages, and it proves very useful to base the considerations on the field dependent renormalised parameters. We also discuss

NRG results for static and dynamic quantities in the equilibrium case, and the comparison with corresponding results from RPT calculations gives good agreement. We show that the situation for an impurity in a BCS superconductor can be described accurately with the NRG method. In the locally repulsive case the lowest excitations correspond to bound states in the superconducting gap and we give an accurate description of their position and weight. We also analyse the ground state transition which occurs with changing the system parameters, and present results for spectral functions.

In the third part of the thesis we focus on the symmetry breaking in lattice models within the DMFT description. When studying the paramagnetic response of the Hubbard model to a homogeneous magnetic field in terms of static and dynamic response functions, we find regimes with qualitatively different behaviour. At half filling we observe metamagnetic behaviour accompanied by a field induced metal insulator transition. In the doped case no metamagnetic behaviour occurs, but the spin dependent effective masses of the quasiparticles differ markedly. As for the local models the description in terms of quasiparticles with field dependent renormalised parameters proves to be useful here. We also give a detailed analysis of the nature of the renormalised quasiparticle in a metallic antiferromagnet and develop an accurate description of the renormalised quasiparticle bands. Renormalised parameters can be deduced as before, but the symmetry breaking nature leads to expressions for the spectral quasiparticle weight and the effective mass enhancement different from the ones in the normal state. For the attractive system we study the broken symmetry state with superconducting order. We show that the crossover of static quantities and spectral functions from the BCS superconducting regime at weak coupling to the BEC regime of tightly bound fermions at strong coupling occurs smoothly.

The author is aware that the thesis is of considerable length. As a variety of different issues are addressed, it seemed difficult in the preparation to restrain the length of the document without losing clarity in the exposition. However, as much of the discussion of the results in each chapter is self-contained, apart from linking remarks and common methods, the reader is encouraged to focus selectively on topics of personal preference.

## Part I

# Models and Methods



*The art of the model-building is the exclusion of real but irrelevant parts of the problem, and entails hazards for the builder and the reader.*

Philip W. Anderson

## Chapter 1

# Models of strongly correlated electrons

In this chapter we introduce the details of the models relevant for this thesis. First we discuss the Anderson impurity model, its basic behaviour and parameter ranges. The symmetries of the model are identified and it is shown how the attractive and repulsive model are related by a mapping. Similarly, the Hubbard model, its parameters and behaviour in limiting cases are introduced. We discuss symmetries, symmetry breaking terms and the mapping from the attractive to the repulsive model.

### 1.1 The Anderson Impurity Model (AIM)

#### 1.1.1 General features and model parameters

Historically the Anderson impurity model (AIM) was proposed in order to describe metals with magnetic impurities in a simplified microscopic model. The Hamiltonian of the AIM is given by (Anderson 1961)

$$H_{\text{And}} = \sum_{\mathbf{k},\sigma} \varepsilon_{\mathbf{k}} c_{\mathbf{k},\sigma}^{\dagger} c_{\mathbf{k},\sigma} + \sum_{\sigma} \varepsilon_d c_{d,\sigma}^{\dagger} c_{d,\sigma} + \sum_{\mathbf{k},\sigma} V_{\mathbf{k}} (c_{\mathbf{k},\sigma}^{\dagger} c_{d,\sigma} + \text{h.c.}) + U c_{d,\uparrow}^{\dagger} c_{d,\uparrow} c_{d,\downarrow}^{\dagger} c_{d,\downarrow}. \quad (1.1)$$

The model describes an impurity ( $d$ -site) with energy  $\varepsilon_d$  in a metallic bath with dispersion  $\varepsilon_{\mathbf{k}}$ . There is a hopping term from the bath to the impurity site whose amplitude is characterised by the parameter  $V_{\mathbf{k}}$ . This term leads to a hybridisation between the bath and the impurity level. The last term is the on-site interaction with strength  $U$ . The spin label  $\sigma$  here and in the rest of this thesis assumes values  $\sigma = \pm 1$  and therefore the impurity corresponds to an s-orbital. In many situations where an impurity in metal is modelled a higher orbital degeneracy (d- or f-orbital) would be more realistic. In this work we will, however, focus on the singly degenerate case. In the following we briefly establish some simple features and terminology commonly used. Unless otherwise stated we will assume

throughout the course of this work that the Fermi energy  $\varepsilon_F$  is at zero energy,  $\varepsilon_F = 0$ . For  $\varepsilon_d = -U/2$  and for a half filled conduction band the Hamiltonian (1.1) is invariant under the particle hole transformation

$$c_{d,\sigma} \leftrightarrow -c_{d,\sigma}^\dagger \quad c_{\mathbf{k},\sigma} \leftrightarrow c_{-\mathbf{k},\sigma}^\dagger. \quad (1.2)$$

Hence, this case is termed particle hole symmetric case or simply symmetric AIM. We will also refer to it as half filled case in analogy to the corresponding lattice situation. Without hybridisation,  $V_{\mathbf{k}} \rightarrow 0$ , the model can be trivially solved (atomic limit) and the ground-state energy  $E_0$  only depends on the impurity electronic occupation  $n_d$ . For  $n_d = 0$  we have  $E_0 = 0$ , for single occupation,  $n_d = 1$ ,  $E_0 = \varepsilon_d$ , and the doubly occupied impurity has energy  $E_0 = 2\varepsilon_d + U$ . We can see that for the symmetric AIM zero and double occupation are degenerate and if  $\varepsilon_d < 0$  the lowest energy is given by the singly occupied state. For  $U > 0$  therefore the ground state is singly occupied. This argument can be extended in a simplified picture to the case with finite hybridisation,  $V_{\mathbf{k}} \neq 0$ . The delta-function atomic limit peak is then broadened by the hybridisation with the conduction band.

In the non-interacting case,  $U = 0$ , the model can be solved with the Green's functions technique as already done in the original work by Anderson (1961). From the equations of motion we find the Fourier transform of the retarded impurity Green's function at  $T = 0$ ,

$$G_d(\omega) = \langle\langle c_{d,\sigma}; c_{d,\sigma}^\dagger \rangle\rangle_\omega = -i \int_{-\infty}^{\infty} dt e^{-i\omega t} \theta(t) \langle\{c_{d,\sigma}(t), c_{d,\sigma}^\dagger(0)\}\rangle. \quad (1.3)$$

The explicit expression for  $U = 0$  is

$$G_d^0(\omega) = \frac{1}{\omega^+ - \varepsilon_d - K(\omega)}, \quad (1.4)$$

where  $\omega^+ = \omega + i\eta$ ,  $\eta \rightarrow 0$ .  $K(\omega)$  is generally referred to as the hybridisation function. With the Dirac identity

$$\frac{1}{x \pm i\eta} = \mathcal{P} \frac{1}{x} \mp i\pi\delta(x) \quad (1.5)$$

the hybridisation term in the denominator becomes

$$K(\omega) = \sum_{\mathbf{k}} \frac{|V_{\mathbf{k}}|^2}{\omega + i\eta - \varepsilon_{\mathbf{k}}} = \mathcal{P} \sum_{\mathbf{k}} \frac{|V_{\mathbf{k}}|^2}{\omega - \varepsilon_{\mathbf{k}}} - i\pi \sum_{\mathbf{k}} |V_{\mathbf{k}}|^2 \delta(\omega - \varepsilon_{\mathbf{k}}) \equiv \Lambda(\omega) - i\Delta(\omega). \quad (1.6)$$

In the AIM it is common to assume a flat conduction band density of states ( $\rho_c \equiv 1/2D$ ) and a broad band ( $\varepsilon_{\mathbf{k}} \in (-D, D)$ , where  $D$  is the largest parameter in the problem). Then for the usual range of  $\omega$  the real part of the expression  $\Lambda(\omega) \simeq \Delta(0) \ln(\frac{\omega-D}{\omega+D})$  is small and can be neglected or absorbed in a renormalisation of  $\varepsilon_d$  [for a discussion see (Hewson 1993a, chapter 1)]. Approximating the hybridisation by the value at the Fermi level,  $V_{\mathbf{k}} \simeq V_{\mathbf{k}_F} \equiv V$ ,  $\Delta(\omega) = \pi\rho_c(0)V^2 = \pi V^2/2D \equiv \Delta$  independent of  $\omega$ , which will be used throughout this thesis, when the local model is considered. In the DMFT framework we

have to consider an effective impurity model and the hybridisation function  $K(\omega)$  retains its frequency dependence. Here for the impurity model, however, we find the simplified expression for (1.4)

$$G_d^0(\omega) = \frac{1}{\omega^+ - \varepsilon_d + i\Delta}, \quad (1.7)$$

which is what is commonly used as the free retarded Green's function for the AIM. The corresponding spectral function  $\rho_d^0(\omega) = -\text{Im}G_d^0(\omega)/\pi$  is a Lorentz curve centred at  $\varepsilon_d$  with half width at half maximum (HWHM)  $\Delta$ ,

$$\rho_d^0(\omega) = \frac{\Delta/\pi}{(\omega - \varepsilon_d)^2 + \Delta^2}. \quad (1.8)$$

It is therefore clear to see that the hybridisation broadens the local level  $\varepsilon_d$  in the spectral density. From the atomic limit analysis we have another level at energy  $\varepsilon_d + U$ , which is also found to be broadened by the hybridisation. Based on these considerations we can distinguish the following

### Parameter regimes:

1. The local moment regime, where  $\varepsilon_d \ll \varepsilon_F$  and  $|\varepsilon_F - (\varepsilon_d + U)| \gg \Delta$ , constitutes a singly occupied impurity with a spin (local moment) coupling to the conduction bath. In this regime charge fluctuations on the impurity site are largely suppressed, and a transformation by Schrieffer and Wolff (1966) to the Kondo model is applicable. The interaction term then has the form

$$H_{\text{int}} = \sum_{\mathbf{k}, \mathbf{k}'} J_{\mathbf{k}, \mathbf{k}'} [S^+ c_{\mathbf{k}, \uparrow}^\dagger c_{\mathbf{k}', \downarrow} + S^- c_{\mathbf{k}, \downarrow}^\dagger c_{\mathbf{k}', \uparrow} + S^z (c_{\mathbf{k}, \uparrow}^\dagger c_{\mathbf{k}', \uparrow} - c_{\mathbf{k}, \downarrow}^\dagger c_{\mathbf{k}', \downarrow})]. \quad (1.9)$$

$\mathbf{S}$  is the impurity spin,  $S^\alpha = c_{d, \sigma}^\dagger \sigma_{\sigma\sigma'}^{(\alpha)} c_{d, \sigma'}$  ( $\alpha$ : Cartesian component),  $S^\pm = S^1 \pm iS^2$ . This is the regime, where Kondo physics is dominant at low temperature and the spectral density shows a narrow peak at the Fermi level.

2. The intermediate valence regime where,  $|\varepsilon_d - \varepsilon_F| \simeq \Delta \simeq |\varepsilon_F - (\varepsilon_d + U)|$  and thus the two levels lie within the width of  $\Delta$ . Real charge fluctuations of electrons hopping on and off the impurity are important in this regime.
3. The non-magnetic regime,  $\varepsilon_d - \varepsilon_F \gg \Delta$ , where it costs energy to occupy the impurity. This is the case, for instance, in the symmetric model with attractive interaction,  $U < 0$ . The system is in this regime also for  $|\varepsilon_d - \varepsilon_F| \gg \Delta$ ,  $|\varepsilon_F - (\varepsilon_d + U)| \gg \Delta$ , such that the impurity is either always doubly occupied or empty.

If we restrict ourselves to the symmetric model,  $\varepsilon_d = -U/2$ , a mean field analysis shows that only the ratio  $U/\pi\Delta$  is relevant for the characterisation of the behaviour (Anderson 1961). One finds an instability towards a magnetic solution for  $U/\pi\Delta > 1$ . Although this

is an artefact and restored by fluctuations it is common to distinguish the regimes by this ratio, i.e. a weak coupling regime for  $U/\pi\Delta < 1$ , an intermediate coupling regime,  $U/\pi\Delta \simeq 1$ , and strong coupling regime,  $U/\pi\Delta > 1$ . For large enough  $U$ , in practice  $U/\pi\Delta > 2$ , the last case corresponds to the first regime mentioned above. An important quantity for this regime is the Kondo temperature  $T_K$ , which can be defined for the symmetric model as (Horvatic and Zlatic 1985)

$$T_K = \sqrt{(U\Delta/2)}e^{-\pi U/8\Delta + \pi\Delta/2U}. \quad (1.10)$$

It is the energy scale where the perturbation theory of Kondo (1964) diverges, and it is the only relevant low energy scale. The ratio of the spin susceptibility of the impurity  $\chi_s$  and the linear  $T$  coefficient of the specific heat  $\gamma_d$ , which is referred to as Sommerfeld or Wilson ratio,

$$R = 4\pi\chi_s/3(g\mu_B)^2\gamma_d, \quad (1.11)$$

describes the transition from weak coupling to Kondo behaviour;  $\mu_B = \frac{e\hbar}{2m_e}$  is the Bohr magneton. One has  $R = 1$  for noninteracting electrons (weak coupling limit) and  $R = 2$  in the strong coupling case.

The low energy behaviour of the AIM can be expressed in terms of the renormalised quasiparticles of a local Fermi liquid, which is described by a renormalised version of the same model (Hewson 1993a,b),

$$\begin{aligned} \tilde{H}_{\text{And}} = & \sum_{\mathbf{k},\sigma} \varepsilon_{\mathbf{k}} c_{\mathbf{k},\sigma}^\dagger c_{\mathbf{k},\sigma} + \sum_{\sigma} \tilde{\varepsilon}_d c_{d,\sigma}^\dagger c_{d,\sigma} + \sum_{\mathbf{k},\sigma} \tilde{V}_{\mathbf{k}} (c_{\mathbf{k},\sigma}^\dagger c_{d,\sigma} + \text{h.c.}) \\ & + \tilde{U} : c_{d,\uparrow}^\dagger c_{d,\uparrow} c_{d,\downarrow}^\dagger c_{d,\downarrow} :, \end{aligned} \quad (1.12)$$

where the colon brackets indicate that the expression within them must be normal-ordered. This Hamiltonian corresponds to the low energy fixed point of the Wilson numerical renormalisation group transformation of the discretised Anderson and Kondo models, with the leading irrelevant terms (Wilson 1975, Krishna-murthy et al. 1980a, Hewson 1993a). The advantage of describing the fixed point in this way, as a renormalised Anderson model rather than as a strong coupling fixed point of the Kondo model, even in the strong correlation or Kondo limit, is that it clearly brings out the 1-1 correspondence of the low-lying single particle excitations with those of the non-interacting model (Hewson et al. 2004, Hewson 1993a, 2005). Furthermore, it is applicable in all parameter regimes, from weak to strong coupling and for all occupation values for the local site. The effective level,  $\tilde{\varepsilon}_d$ , the effective resonance width  $\tilde{\Delta} = \pi\tilde{V}^2/2D$ , and effective local interaction,  $\tilde{U}$ , define the quasiparticles of this renormalised model. A more rigorous definition of these renormalised parameters in terms of the self-energy and vertex function is given in chapter 2. The free quasiparticle density of states is given by replacing the bare parameters in (1.8) by the renormalised parameters ,

$$\tilde{\rho}_d^0(\omega) = \frac{\tilde{\Delta}/\pi}{(\omega - \tilde{\varepsilon}_d)^2 + \tilde{\Delta}^2}. \quad (1.13)$$

For particle hole symmetry  $\tilde{\varepsilon}_d = 0$ , and the corresponding Lorentz peak  $\tilde{\rho}_d^0(\omega)$  describes the Kondo quasiparticle resonance at the Fermi level.

The spin susceptibility  $\chi_s = \chi_{\text{imp}}/(g\mu_B)^2$  can be related to the renormalised parameters (Hewson 1993a)

$$\chi_s = \frac{\tilde{\rho}_d^0(0)}{2}[1 + \tilde{U}\tilde{\rho}_d^0(0)], \quad (1.14)$$

and since the specific heat coefficient in Fermi liquid theory is given by

$$\gamma_d = \frac{2\pi^2}{3}\tilde{\rho}_d^0(0), \quad (1.15)$$

we can express the Wilson ratio (1.11) as

$$R = 1 + \tilde{U}\tilde{\rho}_d^0(0). \quad (1.16)$$

Since the only one energy scale in the Kondo regime is  $T_K$ , it possible to relate the renormalised parameters to the Kondo temperature, and one finds  $\pi\tilde{\Delta} = \tilde{U} = 4T_K$ .

### Symmetries and symmetry breaking

The total spin operator of the system  $\mathbf{S} = \sum_{\mathbf{k}} \mathbf{S}_{\mathbf{k}} + \mathbf{S}_d$  commutes with the Hamiltonian (1.1) and due to this  $SU(2)$  symmetry the total spin is a conserved quantum number of the AIM. This is not the case anymore if we couple the electrons to a magnetic field  $\mathbf{H}_{\text{ext}}$  at the  $d$ -site. Conveniently, we choose the field along the  $z$ -axis,  $\mathbf{H}_{\text{ext}} = H_z \mathbf{e}_z$  such that the coupling term is of the form  $H'_{\text{mag}} = -\mu_d H_z = h(n_{d,\uparrow} - n_{d,\downarrow})$ , where  $h := \frac{g\mu_B H_z}{2}$  with the electronic  $g$ -factor. Such a term implies that a positive magnetic field decreases the energy of a down spin electron and thus favours an antiparallel alignment of the electrons along the field axis, as it is usually the case in nature. Theoretically, it is, however slightly more convenient to have a magnetisation and field with the same sign and therefore it is common to choose

$$H_{\text{mag}} = -h(n_{d,\uparrow} - n_{d,\downarrow}) = -h \sum_{\sigma} \sigma n_{d,\sigma}, \quad (1.17)$$

a convention we will comply with throughout this thesis. In the wide band conduction limit we can neglect any magnetic field acting on the band electrons. Any polarisation only affects the impurity via the hybridisation  $\Delta$  and any change to the conduction band density due to an applied field is only at the band edges ( $\pm D$ ) and therefore negligible in the wide band limit (Hewson et al. 2005). The AIM in magnetic field is subject of chapter 3 and 4.

The Hamiltonian of the AIM (1.1) is also invariant under a  $U(1)$  gauge transformation and therefore conserves the total particle number  $N = \sum_{\mathbf{k},\sigma} n_{\mathbf{k},\sigma} + n_d$  or charge. This symmetry is broken if the electron bath is in a superconducting state rather than a metallic state. This situation will be subject of the study in chapter 5.

### 1.1.2 The Spin-Isospin Transformation

We can map the symmetric AIM ( $U > 0$ ) with magnetic field to an attractive AIM without magnetic field by employing a “spin-charge”-transformation, or spin-isospin transformation  $T$ .<sup>1</sup> Denote the unoccupied impurity site  $|\square\rangle \equiv |\downarrow\rangle$  by isospin  $T_{d,z} = -\frac{1}{2}$ , and in analogy the doubly occupied site ( $T_{d,z} = \frac{1}{2}$ ) by  $|\uparrow\downarrow\rangle \equiv |\uparrow\rangle$ .  $T$  maps a spin state to an isospin state, i.e.

$$|\uparrow\rangle \xrightarrow{T} |\uparrow\rangle \text{ and } |\downarrow\rangle \xrightarrow{T} |\downarrow\rangle. \quad (1.18)$$

In order to write this formally for the Anderson model it is convenient to use Hubbard operators,  $X_{ab} := |a\rangle\langle b|$ . The impurity site operator thus can be written as

$$c_{d,\uparrow}^\dagger = X_{\uparrow,\downarrow} + X_{\uparrow,\uparrow} \text{ and } c_{d,\downarrow}^\dagger = X_{\downarrow,\downarrow} - X_{\uparrow,\uparrow}. \quad (1.19)$$

The spin-charge transformation has the effect

$$Tc_{d,\uparrow}^\dagger T^{-1} = X_{\uparrow,\downarrow} + X_{\uparrow,\uparrow} = c_{d,\uparrow}^\dagger, \text{ but } Tc_{d,\downarrow}^\dagger T^{-1} = X_{\downarrow,\downarrow} - X_{\uparrow,\uparrow} = c_{d,\downarrow}$$

and vice versa.

The symmetric AIM local magnetic field  $H$  in positive  $z$ -direction is given by (1.1) with  $\varepsilon_d = -U/2$  plus (1.17). We find that  $n_{d,\uparrow} = X_{\uparrow,\uparrow} + X_{\uparrow,\uparrow}$  is invariant under  $T$ ,  $Tn_{d,\uparrow}T^{-1} = n_{d,\uparrow}$ . However,  $n_{d,\downarrow} = X_{\downarrow,\downarrow} + X_{\uparrow,\uparrow}$  transforms to  $\mathbb{1} - n_{d,\downarrow}$ , where  $\mathbb{1} = X_{\uparrow,\uparrow} + X_{\downarrow,\downarrow} + X_{\uparrow,\uparrow} + X_{\downarrow,\downarrow}$  was used. Thus, we see that the spin operator  $S_{d,z}$ ,

$$S_{d,z} = \frac{1}{2}(n_{d,\uparrow} - n_{d,\downarrow}) \xrightarrow{T} \frac{1}{2}(n_{d,\uparrow} + n_{d,\downarrow} - 1) =: \hat{T}_{d,z}, \quad (1.20)$$

transforms to the isospin operator  $\hat{T}_{d,z}$  with the property  $\hat{T}_{d,z}|\uparrow\rangle = \frac{1}{2}|\uparrow\rangle$ ,  $\hat{T}_{d,z}|\downarrow\rangle = -\frac{1}{2}|\downarrow\rangle$ .

The interaction term transforms as  $n_{d,\uparrow}n_{d,\downarrow} = X_{\uparrow,\uparrow} \xrightarrow{T} X_{\uparrow,\uparrow}$ . Omitting the conduction band and the hybridisation term one finds

$$T(H_{\text{And}} + H_{\text{mag}})T^{-1} = -2hX_{\uparrow,\uparrow} - (\varepsilon_d + h)(X_{\uparrow,\uparrow} + X_{\downarrow,\downarrow}) + \varepsilon_d + h \quad (1.21)$$

by particle-hole symmetry and using the expression for the unit operator  $\mathbb{1}$ . This can be compared with parameters  $\varepsilon'_d, U'$  for an Anderson model without magnetic field, neglecting an additional constant,

$$H'_{\text{And}} = (2\varepsilon'_d + U')X_{\uparrow,\uparrow} + \varepsilon'_d(X_{\uparrow,\uparrow} + X_{\downarrow,\downarrow}). \quad (1.22)$$

The comparison of (1.21) with (1.22) shows that it is possible to transform the symmetric Anderson model with local repulsion ( $U > 0$ ) and with a local magnetic field to an asymmetric Anderson model with negative  $U' = -U$  and the identification for the asymmetric parameters with the magnetic field is

$$h = -\left(\varepsilon'_d + \frac{U'}{2}\right). \quad (1.23)$$

<sup>1</sup>This is equivalent to a particle hole transformation for the down spin particles.

Clearly, the symmetric case ( $\varepsilon'_d = -\frac{U'}{2}$ ) corresponds to zero magnetic field. For  $\varepsilon'_d < |\frac{U}{2}|$   $h$  is negative. The appropriate transformation for the band electrons is

$$Tc_{\mathbf{k},\uparrow}^\dagger T^{-1} = c_{\mathbf{k},\uparrow}^\dagger, \text{ and } Tc_{\mathbf{k},\downarrow}^\dagger T^{-1} = c_{-\mathbf{k},\downarrow},$$

if  $\varepsilon_{-\mathbf{k}} = -\varepsilon_{\mathbf{k}}$  and  $V_{-\mathbf{k}} = V_{\mathbf{k}}^*$ .

The dynamic response functions in the charge and spin channel map onto each other under the spin-isospin transformation  $T$ . The diagonal and transverse spin ( $\chi_s$  and  $\chi_t$ ) and charge susceptibilities ( $\chi_c$  and  $\chi_c^t$ ) are given by the following equations

$$\chi_s(\omega) = \langle\langle n_{d,\uparrow} - n_{d,\downarrow}; n_{d,\uparrow} - n_{d,\downarrow} \rangle\rangle_\omega, \quad (1.24)$$

$$\chi_c(\omega) = \langle\langle n_{d,\uparrow} + n_{d,\downarrow} - 1; n_{d,\uparrow} + n_{d,\downarrow} - 1 \rangle\rangle_\omega, \quad (1.25)$$

$$\chi_t(\omega) = \langle\langle c_{d,\uparrow}^\dagger c_{d,\downarrow}; c_{d,\downarrow}^\dagger c_{d,\uparrow} \rangle\rangle_\omega, \quad (1.26)$$

$$\chi_c^t(\omega) = \langle\langle c_{d,\uparrow}^\dagger c_{d,\downarrow}^\dagger; c_{d,\downarrow} c_{d,\uparrow} \rangle\rangle_\omega. \quad (1.27)$$

One finds easily that

$$\chi_s(\omega) \xleftrightarrow{T} \chi_c(\omega) \quad \text{and} \quad \chi_t(\omega) \xleftrightarrow{T} \chi_c^t(\omega). \quad (1.28)$$

## 1.2 The Hubbard Model

### 1.2.1 General features and model parameters

Probably the simplest lattice model to study strong correlation physics including microscopic charge and spin degrees of freedom, is the model suggested and discussed by Hubbard (1963, 1964a,b), Kanamori (1963), and Gutzwiller (1963). The Hamiltonian - referred to as the Hubbard model - in the grand-canonical formalism reads

$$H = - \sum_{i,j,\sigma} (t_{ij} c_{i,\sigma}^\dagger c_{j,\sigma} + \text{h.c.}) - \mu \sum_{i\sigma} n_{i\sigma} + U \sum_i n_{i,\uparrow} n_{i,\downarrow}, \quad (1.29)$$

where the first term describes hopping of electrons from a lattice site  $i$  to  $j$  with amplitude  $t_{ij} = 1/N_s \sum_{\mathbf{k}} e^{i\mathbf{k}(\mathbf{R}_i - \mathbf{R}_j)} \varepsilon_{\mathbf{k}}$ ;  $N_s$  is the number of lattice sites. Hopping is often restricted to neighbouring sites and the amplitude is taken to be the same for all sites  $t$ .  $\mu$  is the chemical potential, whose value is determined by the filling factor  $x$ . The third term in  $H$  constitutes the on-site electron-electron interaction of strength  $U$ . The model we consider here is for a band of s-orbitals such that each site is maximally occupied by two electrons. Extension to higher degeneracies are not considered in this thesis, but are certainly of interest for the description of real materials. If a certain hopping amplitude  $t$  is given the band dispersion energy can be calculated, and for instance, for nearest neighbour hopping on a cubic lattice with lattice constant  $a$  we have in  $d$  dimensions

$$\varepsilon_{\mathbf{k}} = -t \sum_{\langle i,j \rangle} e^{-i\mathbf{k}(\mathbf{R}_i - \mathbf{R}_j)} = -2t \sum_{\alpha=1}^d \cos(k_\alpha a). \quad (1.30)$$

For large  $U$  and half filling ( $x = 1$ ) every lattice space is likely to be occupied by only one electron. Starting from such a configuration one can calculate corrections in a perturbation theory in the hopping term and one obtains the so called  $t$ - $J$ -model, where a Heisenberg spin coupling term,

$$H_J = \frac{J}{2} \sum_{\langle i,j \rangle} \mathbf{S}_i \cdot \mathbf{S}_j, \quad (1.31)$$

with  $J = 4t^2/U$ , is generated. This is analogous to the mapping of the AIM to the Kondo model for strong coupling. For the  $t$ - $J$ -model away from half filling the hopping term with amplitude  $t$  [cf. eq. (1.29)] has to be considered, but double occupancy is always forbidden. Since  $J$  is positive an anti-ferromagnetic ordering is expected in the parameter regime where the doping is not too large.

In the atomic limit,  $\varepsilon_{\mathbf{k}} = t_0$  (zero bandwidth) or  $t_{ij} = \delta_{ij}t_0$ , the equations of motion for the retarded Green's function can be solved exactly, which yields for  $\mu = 0$

$$G_{ij,\sigma}^{\text{al}}(\omega) = \delta_{ij} \left( \frac{1 - \langle n_{-\sigma} \rangle}{\omega^+ - t_0} + \frac{\langle n_{-\sigma} \rangle}{\omega^+ - (t_0 + U)} \right). \quad (1.32)$$

This gives two delta-peaks at  $t_0$  and  $t_0 + U$  similar as in the atomic limit for the AIM. These excitations are broadened for finite band width and then are referred to as lower and upper Hubbard peaks.

The Hubbard Hamiltonian (1.29) has a number of symmetries. It is invariant under a global gauge transformation,

$$c_{j,\sigma}^\dagger \rightarrow e^{i\alpha} c_{j,\sigma}^\dagger, \quad (1.33)$$

and correspondingly the electron number is conserved. (1.29) is also invariant under rotations in spin space  $U(\boldsymbol{\lambda}) = e^{i\boldsymbol{\lambda} \cdot \mathbf{S}}$  ( $SU(2)$  symmetry), where  $\mathbf{S} = \sum_i \mathbf{S}_i$ , and therefore the total spin is a conserved quantity. Similar as the AIM the Hubbard model for half filling, a bipartite lattice and  $\mu = U/2$  is invariant under a particle-hole transformation

$$c_{i,\sigma} \leftrightarrow -c_{i,\sigma}^\dagger. \quad (1.34)$$

Other symmetries for specific lattice structures exist, but we will not consider any of these in detail.

### 1.2.2 The Spin-Isospin transformation and symmetry breaking

Similar as in the AIM described in section 1.1.2 there is a canonical transformation which maps the attractive model with arbitrary chemical potential to a half-filled repulsive model with a magnetic field. The details of this transformation are given in the appendix of the review article by Micnas et al. (1990). Starting point is the attractive Hubbard Hamiltonian in the form

$$H_- = - \sum_{i,j,\sigma} (t_{ij} c_{i,\sigma}^\dagger c_{j,\sigma} + \text{h.c.}) - \mu \sum_{i,s} n_{i,\sigma} - U \sum_i n_{i,\uparrow} n_{i,\downarrow} = H(t_{ij}^{(1)}, \mu^{(1)}, U^{(1)}), \quad (1.35)$$

where  $U^{(1)} = -U < 0$ . Note that the chemical potential  $\mu^{(1)} = \mu$  here can take arbitrary values, such that a certain filling is achieved. This model is not magnetically ordered since electrons tend to form local pairs due to the attraction term (Lieb 1989). As a consequence one has

$$\sum_i \langle S_i^\alpha \rangle = 0, \quad \sum_i e^{i\mathbf{q}_0 \mathbf{R}_i} \langle S_i^\alpha \rangle = 0, \quad (1.36)$$

$\alpha = +, -, z$ , i.e. no ferromagnetic order and no commensurate anti-ferromagnetic order.  $\mathbf{q}_0$  such that  $e^{i\mathbf{q}_0 \mathbf{R}_i}$  changes sign from one sublattice to another. The perfect nesting condition  $\varepsilon_{\mathbf{k}} = 1/N_s \sum_{ij} t_{ij} e^{i\mathbf{k}(\mathbf{R}_i - \mathbf{R}_j)} = -\varepsilon_{\mathbf{k} + \mathbf{q}_0}$  is satisfied. The canonical transformation

$$c_{i,\downarrow}^\dagger = e^{i\mathbf{q}_0 \mathbf{R}_i} b_{i,\downarrow}, \quad c_{i,\uparrow}^\dagger = b_{i,\uparrow}^\dagger, \quad (1.37)$$

$$c_{i,\downarrow} = e^{-i\mathbf{q}_0 \mathbf{R}_i} b_{i,\downarrow}^\dagger, \quad c_{i,\uparrow} = b_{i,\uparrow}, \quad (1.38)$$

such that  $n_{i\uparrow} = n'_{i\uparrow}$  but  $n_{i\downarrow} = 1 - n'_{i\downarrow}$ , maps  $H(t_{ij}^{(1)}, \mu^{(1)}, U^{(1)})$  to  $H(t_{ij}^{(2)}, \mu^{(2)}, U^{(2)}) + H_{\text{mag}}(h) + C$  in terms of the  $b$  operators,

$$H_{\text{mag}}(h) = -h \sum_i (n'_{i,\uparrow} - n'_{i,\downarrow}). \quad (1.39)$$

The parameters are related by  $t_{ij}^{(1)} = t_{ij}^{(2)} = t_{ij}$ ,  $U^{(2)} = -U^{(1)} = U > 0$ ,  $\mu^{(2)} = U/2$  and  $h = -(U/2 + \mu)$ .  $C = \mu N_s$  and can be omitted as a constant. Spin quantities transform into charge quantities and vice versa, as has been seen above in the AIM. Condition (1.36) becomes  $1/N_s \sum_i \langle n_i \rangle = 1$ , which corresponds to half filling.

We want to look at the relevant symmetry breaking terms in the charge and spin channel. The symmetry breaking of interest for the repulsive model is an external field coupling to the spin degrees of freedom and we introduce the general term

$$H_{\text{sb}}^+ = \sum_i \mathbf{H}_i \cdot \mathbf{S}_i = \sum_i H_i^1 S_i^1 + H_i^2 S_i^2 + H_i^3 S_i^3. \quad (1.40)$$

We can introduce the two operators  $S_i^+ = c_{i,\uparrow}^\dagger c_{i,\downarrow}$  and  $S_i^- = c_{i,\downarrow}^\dagger c_{i,\uparrow}$  such that

$$S_i^1 = \frac{1}{2}(S_i^+ + S_i^-), \quad S_i^2 = -\frac{i}{2}(S_i^+ - S_i^-), \quad S_i^3 = \frac{1}{2}(n_{i,\uparrow} - n_{i,\downarrow}). \quad (1.41)$$

A special case for magnetic symmetry breaking is homogeneous magnetic symmetry breaking  $H_i^1 = H_i^2 = 0$  and  $H_i^3 = -2h$ , which corresponds to choosing a field along the  $z$ -axis. The symmetry breaking term then just has the simple form (1.39). Another symmetry breaking is the antiferromagnetic symmetry breaking with the  $z$ -axis as preferred orientation. This requires a bipartite lattice structure with an  $A$  and  $B$  sublattice. The symmetry breaking field has the form  $H_i^1 = H_i^2 = 0$  and  $H_i^3 = -2h$  for  $i \in A$  and  $H_i^3 = 2h$  for  $i \in B$ .

For the attractive Hubbard model  $H_-$  the natural symmetry breaking term is a coupling to the charge degrees of freedom. In analogy to the spin operators we can introduce an

isospin operator reflecting the different charge degrees for freedom,  $T_i^\alpha = \frac{1}{2}\mathbf{C}_i^\dagger \sigma^{(\alpha)} \mathbf{C}_i$ , where  $\mathbf{C}_i^\dagger = (c_{i,\uparrow}^\dagger, c_{i,\downarrow}^\dagger)$ . We introduce similar as above  $T_i^+ = c_{i,\uparrow}^\dagger c_{i,\downarrow}^\dagger$ ,  $T_i^- = c_{i,\downarrow} c_{i,\uparrow}$  such that

$$T_i^1 = \frac{1}{2}(T_i^+ + T_i^-), \quad T_i^2 = -\frac{i}{2}(T_i^+ - T_i^-), \quad T_i^3 = \frac{1}{2}(n_{i,\uparrow} + n_{i,\downarrow}). \quad (1.42)$$

The symmetry breaking term for the attractive model has then the standard form

$$H_{\text{sb}}^- = \sum_i \mathbf{M}_i \cdot \mathbf{T}_i = \sum_i M_i^1 T_i^1 + M_i^2 T_i^2 + M_i^3 T_i^3. \quad (1.43)$$

There are two types of symmetry breaking of particular interest in the attractive Hubbard model. The first one is a charge density wave (CDW) state. For this we need to consider a bipartite lattice and the order parameter corresponds to  $\langle T_i^3 - T_{i+1}^3 \rangle \neq 0$ , where  $i \in A$  and  $i+1 \in B$ . Such a symmetry could be invoked by a symmetry breaking field of the form  $M_i^1 = M_i^2 = 0$  and  $M_i^3 = \varepsilon_d$  for  $i \in A$  and  $M_i^3 = -\varepsilon_d$  for  $i \in B$ . Another symmetry breaking of interest is superconducting order which can be induced by choosing  $M_i^1 = \text{Re}\Delta_{\text{sc}}^0$  and  $M_i^2 = \text{Im}\Delta_{\text{sc}}^0$  and  $M_i^3 = 0$ . This is an offdiagonal symmetry breaking and has the explicit form

$$H_{\text{sc}}^- = \sum_i (\text{Re}\Delta_{\text{sc}}^0 - i\text{Im}\Delta_{\text{sc}}^0) T_i^+ + (\text{Re}\Delta_{\text{sc}}^0 + i\text{Im}\Delta_{\text{sc}}^0) T_i^- = \sum_i [\Delta_{\text{sc}}^0]^* c_{i,\uparrow}^\dagger c_{i,\downarrow}^\dagger + \Delta_{\text{sc}}^0 c_{i,\downarrow} c_{i,\uparrow}$$

We saw above that the attractive and the repulsive model with field are related by a canonical transformation as given in (1.38). Let us investigate how the symmetry breaking term transforms under this transformation. We find  $T_i^+ \rightarrow S_i^+ e^{i\mathbf{q}_0 \mathbf{R}_i}$  and  $T_i^- \rightarrow S_i^- e^{-i\mathbf{q}_0 \mathbf{R}_i}$  and thus apart from additional constants

$$T_i^1 \rightarrow \frac{1}{2} S_i^+ e^{i\mathbf{q}_0 \mathbf{R}_i} + S_i^- e^{-i\mathbf{q}_0 \mathbf{R}_i}, \quad T_i^2 \rightarrow -\frac{i}{2} S_i^+ e^{i\mathbf{q}_0 \mathbf{R}_i} - S_i^- e^{-i\mathbf{q}_0 \mathbf{R}_i}, \quad T_i^3 \rightarrow S_i^3, \quad (1.44)$$

which explicitly shows that apart from phase factors spin is transformed into isospin and vice versa. We can write

$$H_{\text{sb}}^- \rightarrow \sum_i (M_i^1 - iM_i^2) e^{i\mathbf{q}_0 \mathbf{R}_i} S_i^+ + (M_i^1 + iM_i^2) e^{-i\mathbf{q}_0 \mathbf{R}_i} S_i^- + M_i^3 S_i^3$$

Since the symmetry breaking term in the spin channel (1.40) can be written as

$$H_{\text{sb}}^+ = \sum_i H_i^+ S_i^+ + H_i^- S_i^- + H_i^z S_i^3, \quad (1.45)$$

where  $H_i^+ = H_i^1 - iH_i^2$  and  $H_i^- = H_i^1 + iH_i^2$ , we can relate symmetry breaking fields by  $M_i^z = H_i^z$  and  $H_i^+ = (M_i^1 - iM_i^2) e^{i\mathbf{q}_0 \mathbf{R}_i}$  and  $H_i^- = (M_i^1 + iM_i^2) e^{-i\mathbf{q}_0 \mathbf{R}_i}$ . It is therefore easy to see that the diagonal antiferromagnetic ordering in the repulsive model corresponds to charge density wave ordering in the attractive model, and the superconducting symmetry breaking (offdiagonal in the charge channel) in the attractive case corresponds to transverse ordering in the spin channel for the repulsive case. More details concerning different types of ordering can be found in the review article by Micnas et al. (1990).

*Most of the unsolved problems of physics and theoretical chemistry are of the kind the renormalization group is intended to solve (other problems usually do not remain unsolved for long).*

Kenneth G. Wilson

## Chapter 2

# Methods for strong correlation physics

In this chapter the methods relevant for this thesis are described. First we focus on the renormalisation group methods directly applicable to the AIM. The most important aspects of the numerical renormalisation group, including all the recent extensions to calculate spectral functions, are outlined. Then we dedicate a large part of the chapter to the detailed description of the renormalised perturbation theory approach and illustrate the approach with a few examples of low order expansions. In the last section of the chapter we give the main equations for the dynamical mean field theory, which links the solution of an effective impurity model to that of a lattice model.

### 2.1 The Numerical Renormalisation Group (NRG)

The renormalisation group (RG) for statistical physics is an approach designed to understand the behaviour of systems with many coupled degrees of freedom. Let the system be characterised by a Hamiltonian  $H$ . Mathematically, the RG can then be defined as a homomorphism  $\mathcal{R}$  on the space of Hamiltonians  $\mathcal{V}_H$ ,  $\mathcal{R} : \mathcal{V}_H \rightarrow \mathcal{V}_H$ . It can be more convenient to understand a Hamiltonian  $H \in \mathcal{V}_H$  in terms of its physical couplings  $\mathbf{g}$ , such that  $H = H(\mathbf{g})$  is a family of Hamiltonians for different  $\mathbf{g}$ . Then the RG mapping acts on the space of couplings  $\mathcal{V}_g$ ,  $r : \mathcal{V}_g \rightarrow \mathcal{V}_g$ . Usually, this mapping is invoked by decreasing the energy scale, for instance the high energy cut-off, or coarse graining of space. In practice, this can be done, for instance, by changing the fundamental length scale of the problem by a parameter,  $b$  say, and integrating out the degrees of freedom within the old and new fundamental scale. Usually, the RG involves a rescaling step in order to make the Hamiltonian before and after the transformation comparable. We can characterise the transformation by the parameter  $b$ ,  $r = r_b$  and a mathematical group law is realised for successive application of the mapping via  $r_{b_2}(r_{b_1}(\mathbf{g})) = r_{b_2+b_1}(\mathbf{g})$ . Since in general an inverse

of the transformation does not exist (the degrees of freedom which are integrated out are not accessible anymore), the renormalisation group is mathematically a semi-group only. A fixed point for the transformation in the coupling space  $\mathbf{g}^*$  is defined by  $r(\mathbf{g}^*) = \mathbf{g}^*$ , and thus implies invariance of the Hamiltonian under the RG transformation. Physically, the fixed point Hamiltonian can represent the essence of the low energy physics of the problem (Coleman 2002).

In many cases one aims to identify all the fixed points of a model, and to find out for which initial couplings a certain fixed point in the coupling space is favoured and whether it is stable. An interpretation of the RG is to see it as a scaling approach, where a fixed point is reached, when the cut-off energy drops below the lowest energy scale in the problem, such that no further changes occur and the Hamiltonian remains invariant. Before a fixed point is reached a crossover from one effective model description to a different one can occur. This happens, when the energy cut-off becomes smaller than a characteristic energy scale for the model. Therefore, a particular class of high energy excitations can only occur through virtual processes and therefore the Hamiltonian description alters. An example is the passage from the AIM to the Kondo model, where in the latter case real charge fluctuations are eliminated.

In this thesis we deal with a renormalisation group approach in the numerical form, NRG, which was explored and applied to the Kondo model by Wilson (1975) and later also to the AIM (Krishna-murthy et al. 1980a,b). It contributed substantially to a complete picture of the Kondo Problem [see Hewson (1993a)]. One progresses iteratively to lower energy scales whilst observing the behaviour of the energy spectrum of the Hamiltonian. One can regard the RG here as method to split the full problem with (too) many degrees of freedom into smaller problems on a certain energy scale, which can be solved. By comparing the solution of these “sub-problems” the behaviour of the original “full system” can be analysed. The details of the application to the AIM are given in the following section.

### 2.1.1 NRG setup for the Anderson impurity model

The numerical renormalisation group (NRG) for the Kondo and Anderson impurity model has been the subject of a large number of publications and has for instance recently been reviewed by Bulla et al. (2007). We will therefore keep our explanations here to a minimum and refer the reader for more details to references (Hewson 1993a, Bulla et al. 2007, Bauer 2007) and the original papers (Krishna-murthy et al. 1980a,b).

The starting point is the Hamiltonian of the AIM (1.1) with a constant density of states in the conduction band. For the NRG approach it is mapped to a discrete form, the so called linear chain Hamiltonian,

$$H_{\text{And}}^N = 1/D(\varepsilon_d + \frac{1}{2}U) \sum_{\sigma} c_{d,\sigma}^{\dagger} c_{d,\sigma} + \frac{U}{2D} \left( \sum_{\sigma} c_{d,\sigma}^{\dagger} c_{d,\sigma} - 1 \right)^2$$

$$+ \sqrt{\frac{\Delta}{\pi D}} \sum_{\sigma} (f_{0,\sigma}^{\dagger} c_{d,\sigma} + \text{h.c.}) + \sum_{\sigma, n=0}^{N-1} \gamma_{n+1} (f_{n,\sigma}^{\dagger} f_{n+1,\sigma} + \text{h.c.}), \quad (2.1)$$

which is also depicted in figure 2.1.

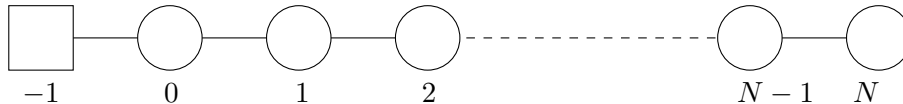


Figure 2.1: Linear chain model which corresponds to Hamiltonian (2.1).

This Hamiltonian has been scaled by half the bandwidth  $D$ . As we can see the impurity part (first line) of the Hamiltonian (2.1) is the same as in the original continuum model (1.1). The conduction band and hybridisation term (second line) have taken a different form and are written in terms of an  $f_{n,\sigma}$ -operator basis. It is important that in this basis only the states corresponding to  $f_{0,\sigma}$  couple directly to the impurity term. We will briefly sketch the steps of the transformation to get from (1.1) to (2.1).

The major goal of the transformation is to clearly separate how states of different energy scales in the electron band couple to the impurity degrees of freedom. A first step is to exploit the spherical symmetry of the problem and to expand the band electron operators into spherical harmonics, where only the s-wave states are important since they couple to the impurity. The next step is a logarithmic discretisation of the band into intervals  $I_n = (\Lambda^{-(n+1)}, \Lambda^{-n})$  with length  $l_n = \Lambda^{-n} - \Lambda^{-(n+1)}$  characterised by the parameter  $\Lambda > 1$ . Note that  $\Lambda \rightarrow 1$  corresponds to the continuum model and  $l_{n+1}/l_n = \Lambda^{-1}$  gives the ratio by which the interval length decreases. The idea of the logarithmic discretisation is that the energies are clearly separated in different orders of magnitude (energy scale separation). In each interval the operators are expanded in a Fourier series. An approximation in the approach is to neglect higher  $p$ -states in the Fourier expansion and focus on the lowest component. This turns out to be a good approximation for  $\Lambda \simeq 2$  as analysed by Krishna-murthy et al. (1980a). Crucial for the setup of an iterative procedure is a basis change. The starting point is a spatially localised state at the impurity, which is a superposition of states from all intervals  $I_n$ . It is created by  $f_{0,\sigma}^{\dagger}$  on the “0th site” of a linear chain and is the only state that couples directly to the impurity. The rest of the basis states are generated in a hopping (tridiagonal) Hamiltonian form with offdiagonal elements  $\gamma_n$  as seen in equation (2.1).

From the Hamiltonian (2.1) we can easily find the recurrence relation

$$H_{\text{And}}^{N+1} = H_{\text{And}}^N + \gamma_{N+1} (f_{N\sigma}^{\dagger} f_{N+1,\sigma} + \text{h.c.}) \quad (2.2)$$

and thus (2.1) can be used to generate an iterative diagonalisation scheme, when it is considered for steps  $N = 0, \dots, N_{\text{max}}$ . The numerical RG transformation is defined by

$$\mathcal{R}(H_N) = H_{N+1} := \sqrt{\Lambda} H_N + \xi_{N+1} (f_{N\sigma}^{\dagger} f_{N+1,\sigma} + \text{h.c.}). \quad (2.3)$$

The definition of the linear chain parameters  $\gamma_N$  and  $\xi_N$  is (Hewson 1993a),

$$\gamma_n = \frac{\frac{1}{2}(1 + \Lambda^{-1})\Lambda^{(-n-1)/2}(1 - \Lambda^{-n})}{(1 - \Lambda^{-2n-1})^{1/2}(1 - \Lambda^{-2n+1})^{1/2}}, \quad \xi_n = \frac{D(1 + \Lambda^{-1})(1 - \Lambda^{-n})}{2(1 - \Lambda^{-2n-1})^{1/2}(1 - \Lambda^{-2n+1})^{1/2}}. \quad (2.4)$$

The  $\gamma_n$  the property of falling off with  $n$ , which implies that one couples to lower energetic contributions at later NRG steps. This is very important for the NRG approach, since the high energy physics should not be altered anymore, when we descend to lower energies along the chain. Note that a scaling factor  $\sqrt{\Lambda}$  is included in the transformation. It is chosen such that the hopping at step  $N$  is of order one and allows one to compare excitations from different NRG steps. This is illustrated in figure 2.2.

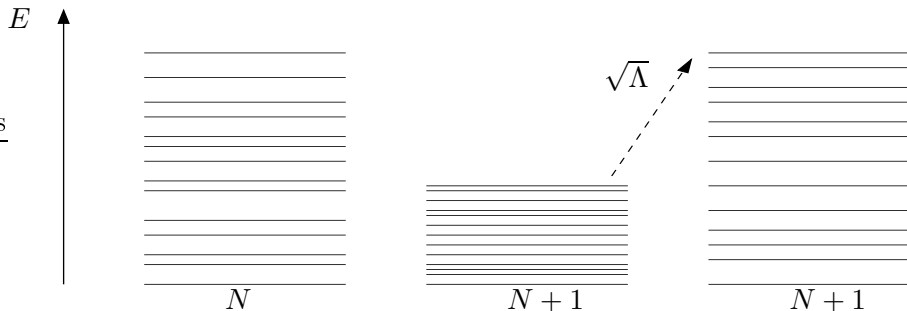


Figure 2.2: Discrete energies from the diagonalisation: Descending to lower energies and rescaling in order compare with earlier steps.

In the iterative diagonalisation procedure we start by considering the decoupled impurity problem, which can easily be solved. After this one considers the two site Hamiltonian  $H_{\text{And}}^0$  involving the impurity and the “0-site”, and solves this numerically. Then for each successive step  $N$ , the basis is always enlarged by an additional site on the linear chain and the Hamiltonian diagonalised. Since the Hilbert space increases exponentially the corresponding matrices become too large to be handled numerically for a certain iteration. At this point a truncation sets in, where states corresponding to energies higher than a certain cutoff are neglected. This is motivated by the RG idea that higher energies are integrated out and do not contribute any more to the low energy physics. The eigenstates can be characterised in terms of conserved quantum numbers. As mentioned in chapter 1 for the Hamiltonian (1.1), the total charge and total spin are symmetries and give good quantum numbers  $Q_N$  and  $S_N$ . For the linear chain model the charge and spin operators have the form (measured relative to number of sites),

$$\hat{Q}_N = \sum_{\sigma, n=0}^N f_{n,\sigma}^\dagger f_{n,\sigma} + c_{d,\sigma}^\dagger c_{d,\sigma} - N - 2 \quad (2.5)$$

and

$$\mathbf{S}_N = \sum_{\sigma, n=0}^N \mathbf{S}_{n,f} + \mathbf{S}_d \quad (2.6)$$

(Quantum number  $\langle \mathbf{S}_N^2 \rangle = S_N(S_N + 1)$ ). Details about the extension of the basis at each NRG step can be found in (Krishna-murthy et al. 1980a, appendix).

In this series of transformations (2.3) the lowest excitations from the ground-state can be followed when the energy scale after each step is rescaled as described above. By fitting effective models to the converged low energy spectra different fixed points characterising the behaviour of the model can be identified. It is possible that for intermediate energy scales a crossover from one fixed point to another can be observed, depending on the parameters initially chosen for the RG flow. It is not straightforward to give an RG transformation for the coupling constants in the AIM. As described by Hewson et al. (2004) one can, however, identify renormalised parameters as introduced in section 1.1 for all NRG steps, which characterise the behaviour of the model. How this is achieved is illustrated in appendix B. In section 2.2 on the renormalised perturbation theory we will describe the approach based on these renormalised parameters.

The major subject of this thesis is the study of situations with broken symmetry. Various modifications occur to this standard setup when the NRG is applied to situations with symmetry breaking and in the DMFT framework. We will point out later what the main differences are.

### 2.1.2 Static and dynamic quantities from NRG calculations

There are a number of extensions to the original scheme described above, which allow one to calculate static and dynamic quantities, such as the occupation number, the one-particle Green's function and spin and charge susceptibilities (Sakai et al. 1989, Costi et al. 1994). In this section we will briefly explain the methods relevant for this thesis.

Static expectation values like the single occupancy  $\langle n_{d,\sigma} \rangle$  and the double occupancy  $\langle n_{d,\uparrow} n_{d,\downarrow} \rangle$  can be calculated from matrix elements and the ground state energies only. For a scalar operator  $\mathcal{O}$  the expectation value is given by

$$\langle \mathcal{O} \rangle = \frac{1}{Z} \text{tr}[e^{-\beta H} \mathcal{O}] = \frac{1}{Z} \sum_m e^{-\beta E_m} \langle m | \mathcal{O} | m \rangle, \quad (2.7)$$

in terms of an eigenbasis  $\{|m\rangle\}$  of  $H$ . The energy eigenvalues  $E_m$  are calculated at each NRG step by diagonalising the Hamiltonian. We also need to evaluate the matrix elements, which can be done easily for the isolated impurity and then at each iteration by transforming them with the corresponding orthogonal matrices for the basis change. For details we refer to Bauer (2007).

One can also calculate the retarded impurity Green's function

$$G_{d,\sigma}(t) := -i\theta(t) \langle \{c_{d,\sigma}(t), c_{d,\sigma}^\dagger(0)\} \rangle = -i\theta(t) \text{tr}(\rho \{c_{d,\sigma}(t), c_{d,\sigma}^\dagger(0)\}). \quad (2.8)$$

Inserting an eigenbasis of the Hamiltonian and writing out the Heisenberg operators  $c_{d,\sigma}(t) = e^{iHt} c_{d,\sigma} e^{-iHt}$ , we find with the standard expression  $\rho = e^{-\beta H} / Z$  and after Fourier

transformation,  $G_{d,\sigma}(\omega) = \int dt e^{i\omega t} G_{d,\sigma}(t)$  that the spectral density  $\rho_{d,\sigma}(\omega) = -\text{Im}G_{d,\sigma}(\omega)$  can be displayed in the Lehman representation as a sum of delta functions

$$\rho_d(\omega) = \frac{1}{Z} \sum_{m,n} |\langle m|c_d^\dagger|n\rangle|^2 \delta[\omega - (E_m - E_n)](e^{-\beta E_m} + e^{-\beta E_n}). \quad (2.9)$$

The real part of  $G_{d,\sigma}(\omega)$  can be obtained via principal value integration. The matrix elements  $\langle m|c_{d,\sigma}^\dagger|n\rangle$  are defined for the isolated impurity system and are then calculated at each NRG step with the help of the corresponding basis transformation (Krishna-murthy et al. 1980a). The NRG calculations in this thesis are carried out at zero temperature. In practice, it is usually sufficient to use a value for the temperature  $1/\beta$  which is smaller than all the other energies appearing in the calculation. In order to obtain a continuous spectrum we have to broaden the excitation peaks in (2.9) numerically,

$$\rho(\omega) = \sum_i w_i f_b(\omega, i), \quad (2.10)$$

where  $w_i$  is the weight,

$$w_{i(m,n)} = \frac{1}{Z} |\langle m|\mathcal{O}_\alpha|n\rangle|^2 (e^{-\beta E_m} + e^{-\beta E_n}), \quad (2.11)$$

for a certain excitation energy  $E_{i(m,n)} = E_m - E_n$ . As described by Bulla et al. (1998) a suitable broadening function  $f_b$  is an exponential on a logarithmic scale,

$$f_b(\omega, i) = \frac{e^{-\frac{b^2}{4}} e^{-(\log|\omega| - \log E_i)^2 / b^2}}{b|E_i|\sqrt{\pi}}. \quad (2.12)$$

Results obtained for this thesis make use of this broadening function unless otherwise stated. (2.12) has the advantage of broadening the spectral data according to the information available, i.e. the few peaks for higher energies are broadened out more than the ones on lower energies, where a lot of information is available. In the interpretation of the spectra one only has to bear in mind that the broadening function displays some asymmetry. In practice in this simple scheme, we have to use matrix elements and excitations from different NRG iterations and merge this information to obtain a spectral density on all energy scales. The idea behind this is that the most accurate information for a typical energy  $\omega$  is given by the iteration  $N$  where  $\omega \simeq \Lambda^{-(N-1)/2}$ .

### Reduced density matrix scheme

The method to obtain spectra described in the last section works well in many cases (Hewson 1993a, Bulla et al. 2007). It is, however, important to note that the first few NRG iterations, which describe the high energy features are not accurate enough to capture a small symmetry breaking, for instance induced by a magnetic field. Therefore, the dynamical quantities at high energies are not necessarily calculated with the correct ground

state, and, for instance, the magnetisation obtained from a sum over the spectral weight does not give correct values when compared with exact results (Hofstetter 2000). Only for later steps, for lower energy scales, the symmetry breaking is calculated correctly and, therefore, the right ground-state obtained. As pointed out by Hofstetter (2000) in an improved calculation of spectra one really has to start with the ground-state obtained in the last iteration. It is possible to do this by storing the information from all the NRG steps and calculating the spectra “backwards” from the ground state at the last NRG iteration. The correct implementation rests on the concept of the reduced density matrix  $\rho^{\text{red}}$ , where we think at step  $m$  of the sites  $n > m$  as environment. This is illustrated in figure 2.3. Such a procedure makes use of the full information obtained in the iterative diagonalisation.

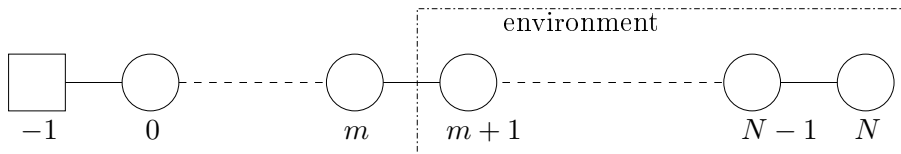


Figure 2.3: Linear chain model, where iterations  $n > m$  are treated as environment for step  $m$ .

This concept of the reduced density matrix can be used to calculate a more accurate impurity Green’s function (2.8). Since the density matrix is only diagonal at the last step of the NRG we obtain a different expression for the Lehmann sum (2.9),

$$\rho_{d,\sigma}(\omega) = \sum_{m,n} \alpha_{mn} \delta[\omega - (E_m - E_n)], \quad (2.13)$$

with

$$\alpha_{mn} := \langle m | c_{d,\sigma}^\dagger | n \rangle^* \left( \sum_l \langle m | c_{d,\sigma}^\dagger | l \rangle \langle l | \rho | n \rangle + \langle m | c_{d,\sigma}^\dagger | n \rangle \sum_l \langle m | \rho | l \rangle \langle l | c_{d,\sigma}^\dagger | n \rangle \right). \quad (2.14)$$

Details of the implementation are described in reference Bauer (2007). This approach has still an unsatisfactory aspect as we have to mix information from different iterations to patch together the spectral function on all energy scales. A more rigorous scheme also involving the concept of a reduced density matrix is explained in the following section.

### Full density matrix (FDM) approach

A different approach to spectral functions within the NRG framework is based on the complete basis set of the full linear chain of length  $N$  which has been identified by Anders and Schiller (2005). The idea is to consider the linear chain model (figure 2.3) at step  $m < N$  as the full chain with all the hopping elements for connecting sites  $i > m$  set to zero rather than thinking of the chain being extended by one site at each NRG step. A typical Fock basis state for this set of “environment” sites is denoted by

$$|e_m\rangle := |J_{m+1}\rangle \otimes \dots \otimes |J_N\rangle, \quad (2.15)$$

where usually  $J_m = 1 \dots 4$ , numbering the basis state at site  $m$ , from empty to double occupation. With this a basis state at iteration  $m$ , denoted by  $|r\rangle_m$  can be extended to a basis state for the full chain of length  $N$  as a product state

$$|r, \mathbf{e}_m\rangle_N := |r\rangle_m \otimes |\mathbf{e}_m\rangle \equiv |r, \mathbf{e}; m\rangle, \quad (2.16)$$

where the last expression corresponds to the notation used by Anders and Schiller (2005). Due to the truncation of the Hilbert space and discarding of states during the NRG procedure it is not straight forward to see how one can construct a complete basis set. We will use the notation, which labels kept states  $|r\rangle_K$  with  $|k\rangle$  and discarded states  $|r\rangle_D$  with  $|l\rangle$ .

We denote the iteration at which the truncation first sets in by  $m_0$ . Then the set of all states

$$\{|k, \mathbf{e}; m_0\rangle\}, \{|l, \mathbf{e}; m_0\rangle\}, \quad (2.17)$$

i.e. the set of all kept states equipped with the rest of the chain environment together with the set of all discarded states plus environment, form a basis for the full Wilson chain. Going one step further to  $m_0 + 1$  a moment's thought shows that

$$\{|k, \mathbf{e}; m_0 + 1\rangle\}, \{|l, \mathbf{e}; m_0 + 1\rangle\} \quad (2.18)$$

is only a subset of a complete basis for the chain, since we have discarded the states  $\{|l, \mathbf{e}; m_0\rangle\}$  at the step before. If, however, we collect the states

$$\{|k, \mathbf{e}; m_0 + 1\rangle\}, \{|l, \mathbf{e}; m_0 + 1\rangle\}, \{|l, \mathbf{e}; m_0\rangle\}, \quad (2.19)$$

we obtain again a complete basis for the full chain. This can be extended to the last iteration  $N$  and if we think of all states for this last step as discarded (just for notational convenience), then we can define the Anders-Schiller (AS) basis as the set of all discarded states equipped with environment,

$$\{|l, \mathbf{e}; m\rangle\}_{m=m_0, \dots, N}. \quad (2.20)$$

This is a complete basis for the full NRG chain.

By definition of the AS basis we know that for the Hamiltonian at stage  $m$ ,  $H_{\text{And}}^m$ ,  $|k, \mathbf{e}; m\rangle$  and  $|l, \mathbf{e}; m\rangle$  are exact eigenstates,  $H_{\text{And}}^m |\alpha, \mathbf{e}; m\rangle = E_m^\alpha |\alpha, \mathbf{e}; m\rangle$  for  $\alpha = l, k$ . In order to calculate spectral functions one makes the fundamental approximation to assume that they are also eigenstates of the Hamiltonian for the full chain  $H = H_{\text{And}}^{N_{\text{max}}}$ . This amounts to saying that the effect of further environment sites, which due to the NRG setup couple with decreasing energies, is only a small perturbation, and therefore

$$H |\alpha, \mathbf{e}; m\rangle \approx E_m^\alpha |\alpha, \mathbf{e}; m\rangle. \quad (2.21)$$

In this sense the AS basis is an approximate eigenbasis for the linear chain model. This fact can be used to evaluate spectral functions (Peters et al. 2006, Weichselbaum and von Delft

2006). As we trace out the environment states this approach involves the reduced density matrix  $\rho^{\text{red}}$  introduced before. Since we are using a complete basis set one can easily see, that for chains of any length, sum rules are satisfied exactly. The details for the manipulations for a general spectral function of the form,

$$G_{AB}(t) = -i\theta(t)\text{tr}(\rho[A(t), B]_\varepsilon) \quad (2.22)$$

( $\varepsilon = -1$  bosonic,  $\varepsilon = 1$  fermionic), are given in appendix A.

### Self-energy with higher $F$ -Green's function

Once the impurity Green's function has been calculated according to the procedure described above it is possible to extract the impurity self-energy from the Dyson equation

$$\Sigma_{d,\sigma}(\omega) = G_{d,\sigma}^0(\omega)^{-1} - G_{d,\sigma}(\omega)^{-1}. \quad (2.23)$$

It turns out, however, that a better method to calculate the self-energy is to employ a higher Green's function (Bulla et al. 1998), since the difference in (2.23) can lead to large numerical errors for small  $\omega$ . The relevant expressions can be found in an equations of motion approach, where one finds the relation

$$(\omega - \varepsilon_d - K(\omega))G_{d,\sigma}(\omega) - UF_\sigma(\omega) = 1, \quad (2.24)$$

with the higher  $F$ -Green's function,

$$F_\sigma(\omega) = \langle\langle c_{d,\sigma} c_{d,-\sigma}^\dagger; c_{d,\sigma}^\dagger \rangle\rangle_\omega \quad (2.25)$$

and  $K(\omega)$  was given in (1.6). Identifying the self-energy as

$$\Sigma_\sigma(\omega) = U \frac{F_\sigma(z)}{G_\sigma(\omega)}, \quad (2.26)$$

yields in equation (2.24) the standard expression for the Green's function

$$G_\sigma(\omega) = \frac{1}{\omega - \varepsilon_d - K(\omega) - \Sigma_\sigma(\omega)}. \quad (2.27)$$

Hence,  $\Sigma_\sigma(\omega)$  can be calculated from equation (2.26) once  $G_\sigma(\omega)$  and  $F_\sigma(z)$  have been determined.

## 2.2 The Renormalised Perturbation Theory (RPT)

In section 1.1 we have heuristically introduced renormalised parameters for the AIM and shown that static response quantities can conveniently be expressed in terms of them. Quite generally in strongly correlated systems, physical couplings can change their effective value substantially, when one descends from the band energy to typical low energy scales. A

prominent example of such a behaviour is Anderson's poor man's scaling (Anderson 1970), where the antiferromagnetic spin-spin coupling  $J$  is seen to increase when the energy is lowered. In fact, since the ideas of Landau's Fermi liquid theory it is well known that the low energy physics of interacting particles can be described in terms of effective parameters which differ from their original value (Abrikosov et al. 1963). As a prominent example consider heavy fermion systems, where the effective mass of charge carriers can vary up to a factor of 500 from their bare mass. In models of strongly interacting electrons the original parameters are usually of the order of the band width. In locally correlated systems, however, the behaviour is generally dominated by a low energy scale, for instance the Kondo temperature  $T_K$ . If we are interested in the properties of the order  $T_K$  it is very convenient to choose the corresponding effective low energy parameters as a starting point for the description of the behaviour.

For a perturbative approach it is important to choose an expansion point with an appropriate energy scale such that other effects enter as corrections. Therefore, it is a good strategy in systems where the renormalisation effects are large to work with renormalised couplings on the low energy scale rather than the bare parameters. Such an approach, a renormalised perturbation theory, can be constructed, and for the AIM it has the property that the lowest order results are asymptotically exact (Hewson 1993b, 2001). One has to be careful, however, since by using effective parameters renormalisation effects are implicitly taken into account and must not be included again. Similar as in the high energy field theoretic approaches (Ryder 1996) counter-terms, which are introduced there to cancel divergences, have to be introduced in order to satisfy renormalisation conditions (Hewson 1993b, 2001). In the following sections we explain the details for the formalism of the RPT based on these Fermi liquid parameters for the AIM in a magnetic field.

### 2.2.1 The RPT setup

For the setup of the RPT it is convenient to work in the functional integral formalism. The Anderson impurity model from equation (1.1) is expressed as

$$\mathcal{Z}_{\text{AIM}} = \int \mathcal{D}(d_\sigma, \bar{d}_\sigma) \mathcal{D}(c_{\mathbf{k},\sigma}, \bar{c}_{\mathbf{k},\sigma}) e^{-\int_0^\beta d\tau \mathcal{L}_{\text{AIM}}(\tau)}, \quad (2.28)$$

with

$$\begin{aligned} \mathcal{L}_{\text{AIM}} = & \sum_{\mathbf{k},\sigma} \bar{c}_{\mathbf{k},\sigma}(\tau) \left( \frac{\partial}{\partial \tau} + \varepsilon_{\mathbf{k}} \right) c_{\mathbf{k},\sigma}(\tau) + \sum_{\sigma} \bar{d}_\sigma(\tau) \left( \frac{\partial}{\partial \tau} + \varepsilon_{d,\sigma} \right) d_\sigma(\tau) + \\ & \sum_{\mathbf{k},\sigma} V_{\mathbf{k}} (\bar{c}_{\mathbf{k},\sigma}(\tau) d_\sigma(\tau) + \text{h.c.}) + U n_{d,\uparrow}(\tau) n_{d,\downarrow}(\tau) \equiv \mathcal{L}_{\text{AIM}}(\varepsilon_{d,\sigma}, \Delta, U), \end{aligned} \quad (2.29)$$

where we have allowed for a magnetic field  $h$ ,  $\varepsilon_{d,\sigma} = \varepsilon_d - \sigma h$  and  $\Delta = \pi V^2/2D$  in the wide conduction band limit as explained in the first chapter.  $c_{\mathbf{k},\sigma}(\tau)$  and  $d_\sigma(\tau)$  are Grassman

fields here. Rescaling the band electron fields  $c_{\mathbf{k},\sigma} \rightarrow c_{\mathbf{k},\sigma}/V_{\mathbf{k}}$  and integrating them out the total action becomes

$$S = - \sum_{\sigma} \int_0^{\beta} d\tau \int_0^{\beta} d\tau' \bar{d}_{\sigma}(\tau) G_0(\tau - \tau')^{-1} d_{\sigma}(\tau') + U \int_0^{\beta} d\tau n_{d,\uparrow}(\tau) n_{d,\downarrow}(\tau) \equiv S_0 + S_U, \quad (2.30)$$

where

$$G_0(\tau) = \frac{1}{\beta} \sum_n e^{-i\tau\omega_n} \frac{1}{i\omega_n - \varepsilon_{d,\sigma} + i\Delta \text{sgn}(\omega_n)}. \quad (2.31)$$

The full  $d$ -site retarded Green's function (analytically continued to the real axis  $\omega \in \mathbb{R}$ ), which takes through the self-energy  $\Sigma_{\sigma}(\omega, h)$  all interaction effects into account, reads

$$G_{d,\sigma}(\omega) = \frac{1}{\omega - \varepsilon_{d,\sigma} + i\Delta - \Sigma_{\sigma}(\omega, h)}. \quad (2.32)$$

The action (2.30) is a common starting point for perturbation theory in the bare interaction  $U$ , by which an approximation for  $\Sigma_{\sigma}(\omega, h)$  can be calculated.

As explored by Hewson (1993b, 2001) the Fermi liquid properties of the AIM, can be expressed in terms of renormalised parameters, which are obtained by expanding the self-energy at  $\omega = 0$ . This approach rests on basic properties of the self-energy,  $-\text{Im}\Sigma_{\sigma}(\omega) \sim \omega^2$  (Luttinger 1961), which essentially define the Fermi liquid regime. With the usual definition of the wavefunction renormalisation

$$z_{\sigma}(h)^{-1} := 1 - \frac{\partial}{\partial \omega} \text{Re}\Sigma_{\sigma}(\omega = 0, h), \quad (2.33)$$

the renormalised parameters are defined by

$$\tilde{\Delta}_{\sigma}(h) := z_{\sigma}(h)\Delta, \quad \tilde{\varepsilon}_{d,\sigma}(h) = z_{\sigma}(h)[\varepsilon_{d,\sigma} + \text{Re}\Sigma_{\sigma}(0, h)]. \quad (2.34)$$

The remainder of the expansion of the self-energy  $\Sigma_{\sigma}^{\text{rem}}(\omega, h)$  defines the renormalised self-energy  $\tilde{\Sigma}_{\sigma}(\omega, h)$ ,

$$\tilde{\Sigma}_{\sigma}(\omega, h) = z_{\sigma}(h)\Sigma_{\sigma}^{\text{rem}}(\omega, h). \quad (2.35)$$

With these parameters we can write the impurity Green's function (2.32) equivalently as

$$G_{d,\sigma}(\omega) = \frac{z_{\sigma}(h)}{\omega - \tilde{\varepsilon}_{d,\sigma}(h) + i\tilde{\Delta}_{\sigma}(h) - \tilde{\Sigma}_{\sigma}(\omega, h)}. \quad (2.36)$$

A renormalised interaction  $\tilde{U}(h)$  is defined by the full, antisymmetrised, renormalised four point vertex function at zero frequency,

$$\tilde{U}(h) = \tilde{\Gamma}_{\uparrow,\downarrow}(0, 0; h) = z_{\uparrow}(h)z_{\downarrow}(h)\Gamma_{\uparrow,\downarrow}(0, 0; h). \quad (2.37)$$

This quantity is usually interpreted as the interaction between quasiparticles in Fermi liquid theory (Abrikosov et al. 1963).

In analogy to the renormalised perturbation theory in quantum field theory (Ryder 1996, chapter 9), where the theory is written as  $\mathcal{L}_B = \mathcal{L} + \mathcal{L}_{ct}$  ( $\mathcal{L}_B$  bare Lagrangian,  $\mathcal{L}_{ct}$  counter-terms) we can define a renormalised perturbation theory by identifying

$$\mathcal{L}_{\text{AIM}}(\varepsilon_{d,\sigma}, \Delta, U) = \mathcal{L}_{\text{AIM}}^r(\tilde{\varepsilon}_{d,\sigma}, \tilde{\Delta}, \tilde{U}) + \mathcal{L}_{ct}^r(\lambda_1, \lambda_2, \lambda_3), \quad (2.38)$$

where the counter-term Lagrangian reads

$$\mathcal{L}_{ct}^r(\lambda_1, \lambda_2, \lambda_3) = \sum_{\sigma} \bar{d}_{\sigma}^r(\tau) (\lambda_2 \frac{\partial}{\partial \tau} - \lambda_1) d_{\sigma}^r(\tau) + \lambda_3 n_{d,\uparrow}^r(\tau) n_{d,\downarrow}^r(\tau). \quad (2.39)$$

Note that in the renormalised theory we are working with renormalised fields  $d_{\sigma}^r(\tau) = d_{\sigma}(\tau)/\sqrt{z_{\sigma}}$  in  $\mathcal{L}_{\text{AIM}}^r(\tilde{\varepsilon}_d, \tilde{\Delta}, \tilde{U})$  and  $\mathcal{L}_{ct}^r(\lambda_1, \lambda_2, \lambda_3)$ . The parameters  $\lambda_i$  have to be determined by the renormalisation conditions for the renormalised self-energy

$$\tilde{\Sigma}_{\sigma}(0, h) = 0, \quad \frac{\partial \tilde{\Sigma}_{\sigma}(0, h)}{\partial \omega} = 0, \quad (2.40)$$

and for the full renormalised vertex at zero frequency

$$\tilde{\Gamma}_{\uparrow,\downarrow}(0, h) = \tilde{U}(h). \quad (2.41)$$

These have to be satisfied to all orders in perturbation theory such that renormalisation effects are not over-counted. The parameter  $\lambda_1$  also carries a spin label for the symmetric model with magnetic field and  $\lambda_2$  becomes spin-dependent in the asymmetric model with magnetic field. We have omitted such a notation for simplicity. In order to set up such an RPT it is useful to introduce source terms and define generating functionals as done in the following section.

## 2.2.2 Functional integral description in the 1PI formalism

The generating functional for the renormalised theory is given by

$$\mathcal{Z}^r[J] = \int \mathcal{D}(d_{\sigma}^r, \bar{d}_{\sigma}^r) e^{-S^r[d_{\sigma}^r, \bar{d}_{\sigma}^r] - S^c[d_{\sigma}^r, \bar{d}_{\sigma}^r] - S_J[d_{\sigma}^r, \bar{d}_{\sigma}^r]}. \quad (2.42)$$

The renormalised parameter action  $S^r$  can be obtained from  $\mathcal{L}_{\text{AIM}}(\tilde{\varepsilon}_{d,\sigma}, \tilde{\Delta}, \tilde{U})$  by integrating out the band electrons as in the last section,

$$S^r = - \sum_{\sigma} \int_0^{\beta} d\tau \int_0^{\beta} d\tau' \bar{d}_{\sigma}^r(\tau) \tilde{G}_{\sigma}^0(\tau - \tau')^{-1} d_{\sigma}^r(\tau') + \tilde{U} \int_0^{\beta} d\tau n_{d,\uparrow}^r(\tau) n_{d,\downarrow}^r(\tau) \quad (2.43)$$

where

$$\tilde{G}_{\sigma}^0(\tau) = \frac{1}{\beta} \sum_n e^{-i\tau\omega_n} \frac{1}{i\omega_n - \tilde{\varepsilon}_{d,\sigma} + i\tilde{\Delta}_{\sigma} \text{sgn}(\omega_n)} \quad (2.44)$$

The action for the counter-terms can be written as

$$S^c = - \sum_{\sigma} \int_0^{\beta} d\tau \int_0^{\beta} d\tau' \bar{d}_{\sigma}^r(\tau) G_{\sigma}^{c,0}(\tau - \tau')^{-1} d_{\sigma}^r(\tau') + \lambda_3 \int_0^{\beta} d\tau n_{d,\uparrow}^r(\tau) n_{d,\downarrow}^r(\tau), \quad (2.45)$$

where

$$G_{\sigma}^{c,0}(\tau) = \frac{1}{\beta} \sum_n e^{-i\tau\omega_n} \frac{1}{\lambda_2 i\omega_n + \lambda_1}. \quad (2.46)$$

The one-particle irreducible (1PI) source term is defined as

$$S_J = \sum_{\sigma} \int_0^{\beta} d\tau [\bar{J}_{\sigma} d_{\sigma}^r(\tau) + \bar{d}_{\sigma}^r(\tau) J_{\sigma}(\tau)]. \quad (2.47)$$

As usual we can introduce a generating functional for connected Green's functions,

$$W^r[J] = \log \mathcal{Z}^r[J], \quad (2.48)$$

and the renormalised one-particle Green's function can be calculated as

$$G_{d,\sigma}(i\omega_n) = - \left. \frac{\delta^2 W^r[J]}{\delta \bar{J}_{\sigma}(i\omega_n) \delta J_{\sigma}(i\omega_n)} \right|_{J=0}. \quad (2.49)$$

### Standard Setup of the renormalised perturbation theory

The standard way to generate a renormalised perturbation expansion from (2.42) is to write

$$\mathcal{Z}^r[J] = \int \mathcal{D}(d_{\sigma}^r, \bar{d}_{\sigma}^r) e^{-S_0^r[d_{\sigma}^r, \bar{d}_{\sigma}^r] - S_{\bar{U}}^r[d_{\sigma}^r, \bar{d}_{\sigma}^r] - S_0^c[d_{\sigma}^r, \bar{d}_{\sigma}^r] - S_{\lambda_3}^c[d_{\sigma}^r, \bar{d}_{\sigma}^r] - S_J[d_{\sigma}^r, \bar{d}_{\sigma}^r]} \quad (2.50)$$

$$= e^{-S_{\bar{U}}^r[\delta_{J_{\sigma}}, \delta_{\bar{J}_{\sigma}}] - S_0^c[\delta_{J_{\sigma}}, \delta_{\bar{J}_{\sigma}}] - S_{\lambda_3}^c[\delta_{J_{\sigma}}, \delta_{\bar{J}_{\sigma}}]} \int \mathcal{D}(d_{\sigma}^r, \bar{d}_{\sigma}^r) e^{-S_0^r[d_{\sigma}^r, \bar{d}_{\sigma}^r] - S_J[d_{\sigma}^r, \bar{d}_{\sigma}^r]} \quad (2.51)$$

$$= e^{-S_{\bar{U}}^r[\delta_{J_{\sigma}}, \delta_{\bar{J}_{\sigma}}] - S_0^c[\delta_{J_{\sigma}}, \delta_{\bar{J}_{\sigma}}] - S_{\lambda_3}^c[\delta_{J_{\sigma}}, \delta_{\bar{J}_{\sigma}}]} \mathcal{Z}_0^r[J]. \quad (2.52)$$

where by Gaussian integration

$$\mathcal{Z}_0^r[J] = e^{-\sum_{\sigma} \int_0^{\beta} d\tau \int_0^{\beta} d\tau' \bar{J}_{\sigma}(\tau) \tilde{G}_{\sigma}^0(\tau - \tau') J_{\sigma}(\tau')}. \quad (2.53)$$

In this setup all the counter-terms  $e^{-S_0^c}$  and  $e^{-S_{\lambda_3}^c}$  are treated directly as interaction terms and this is how the counter-terms are usually introduced in quantum field theory (Ryder 1996, chapter 9). They give rise to three additional Feynman rules for the diagrams:

1. A contraction multiplied by  $\lambda_1$ , which we will denote by  $(\circ)$  in the diagrams.
2. A contraction with the additional factor  $\lambda_2 i\omega_n$  or  $\lambda_2 \omega$  for  $T = 0$  after Fourier transformation, which we will denote by  $(\square)$  in the diagrams.

3. An interaction term with constant  $\lambda_3$ , which has exactly the same structure as the standard AIM interaction term and can be denoted by an interaction vertex with side-script  $\lambda_3$ .

The easiest way to analyse (2.52) is by expanding the exponential in  $\mathcal{Z}_0^r[J]$  in terms of free propagators, as given in (2.44), first and then act with the functional derivatives from the interaction terms in  $S_{\tilde{U}}[\delta_{J_\sigma}, \delta_{\tilde{J}_\sigma}]$ ,  $S_0^c[\delta_{J_\sigma}, \delta_{\tilde{J}_\sigma}]$  and  $S_{\lambda_3}^c[\delta_{J_\sigma}, \delta_{\tilde{J}_\sigma}]$  as a contraction to vertices. In order to calculate the one-particle Green's function one needs to leave two external source terms open for the last functional derivatives, as seen from (2.49), and for the two-particle Green's function (and full vertex) one needs four. Graphically, this is usually written out with lines (—) for the propagators  $G_0^r$  and crosses (x) for the source terms  $J$ . The functional derivative  $\delta_{J_k(\tau)}$  then just takes the cross away and relates it to time  $\tau$ . It is convenient to calculate diagrams after Fourier transformation. Rather than the Green's functions we focus on the self-energy and vertex function.

An inductive proof that such a renormalised perturbation theory can be carried out order by order is given in appendix C. We need to prove that the renormalisation conditions (2.40) and (2.41) can always be satisfied. For this it is helpful to classify the contributions to the proper self-energy into three different types:

- (a) terms  $\Sigma_{\tilde{U}}(i\omega_n)$  coming purely from AIM interaction term  $e^{-S_{\tilde{U}}^r}$ . They correspond to the diagrams in the standard perturbation theory of the AIM.
- (b) terms coming purely from  $e^{-S_0^c}$ , which correspond to trivial counter-terms which can be collected to a self-energy contribution  $\Sigma^{ct}(i\omega_n) = -[\lambda_1 + \lambda_2 i\omega_n]$ .
- (c) mixed terms  $\Sigma_{\lambda_1, \lambda_2, \lambda_3}^{\text{mix}}(i\omega_n)$  generated by the combination  $e^{-S_{\tilde{U}}^r}$ ,  $e^{-S_0^c}$ , and  $e^{-S_{\lambda_3}^c}$ .

The perturbative renormalised self-energy to order  $n$  is given by

$$\tilde{\Sigma}^{(n)}(i\omega_n) = \sum_{k=1}^n \left[ \sum_m \Sigma_{\tilde{U}}^{(k,m)}(i\omega_n) + \sum_m \Sigma_{\lambda_1, \lambda_2, \lambda_3}^{\text{mix},(k,m)}(i\omega_n) \right] + \Sigma^{ct}(i\omega_n), \quad (2.54)$$

where  $\Sigma^{(k,m)}$  denotes the  $m$ th diagrammatic contribution to the self-energy of order  $k$ . We have omitted the spin index for notational simplicity. In order to classify different orders of the perturbation theory it is useful to think of the counter-term parameters as expanded in  $\tilde{U}$  (Hewson 2001),

$$\lambda_i = \sum_k \lambda_i^{(k)} \tilde{U}^k. \quad (2.55)$$

Then for each order of the perturbation theory we have to determine the coefficients  $\lambda_i^{(n)}$  in this expansion, such that (2.40) and (2.41) are satisfied, whilst all mixed terms for the renormalised self-energy are included.

In order to illustrate how the RPT works we will briefly discuss the expansion to second order for the symmetric AIM with zero magnetic field at  $T = 0$ . The first and

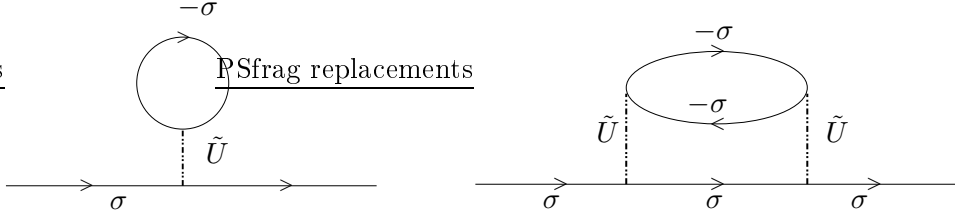


Figure 2.4: First and second order diagrams for the renormalised self-energy.

second order standard diagrams are displayed in figure 2.4. To first order we have to consider the diagram in figure 2.4 (left) which gives

$$\Sigma_{\tilde{U},\sigma}^{(1)} = \tilde{U} \int_{-\infty}^0 d\omega [-\text{Im}\tilde{G}_{-\sigma}^0(\omega)]/\pi \equiv \tilde{U}\tilde{n}_{-\sigma}. \quad (2.56)$$

The full vertex to first order is trivial and the second renormalisation condition (2.41) yields  $\lambda_3^{(1)} = 0$ .  $\Sigma_{\sigma}^{ct}(\omega)$ , shown in figure 2.5 (left), is determined from (2.56) and the first renormalisation condition (2.40) gives  $\lambda_1^{(1)} = \tilde{n}_{-\sigma}$  and  $\lambda_2^{(1)} = 0$ .

Up to second order the only dynamic diagram contributing is the one in figure 2.4 (right), which we denote by  $\Sigma_{\tilde{U},\sigma}^{(2,1)}(\omega)$ . A static term arises from the double tadpole diagram similar to the one in 2.4 (left), which gives  $\Sigma_{\tilde{U},\sigma}^{(2,2)} = \tilde{U}^2\tilde{n}_{-\sigma}^2$ . We also get a contribution to  $\Sigma^{\text{mix}}$  (c), which comes from mixing the first order counter-term contribution and the first order diagram,

$$\Sigma_{\sigma}^{\text{mix},(2,1)} = -i\frac{\tilde{U}^2\lambda_1^{(1)}}{2\pi} \int_{-\infty}^{\infty} d\omega \tilde{G}_{-\sigma}^0(\omega)^2 = -\tilde{U}^2\lambda_1^{(1)}\tilde{\rho}_{d,-\sigma}^0(0, h) \quad (2.57)$$

It is shown in figure 2.5 (middle). Another diagram, which could appear in principle is the tadpole diagram with  $\lambda_3$  interaction  $\Sigma_{\sigma}^{\text{mix},(2,2)} = \lambda_3^{(2)}\tilde{U}^2\tilde{n}_{-\sigma}$ .

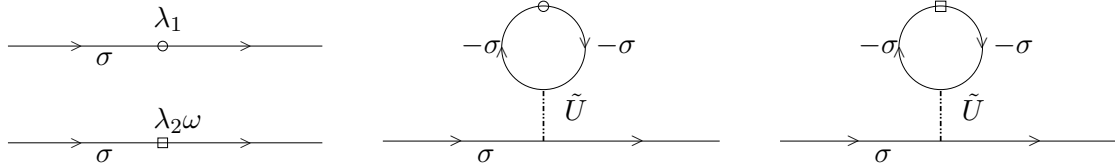


Figure 2.5: Examples of counter-term diagrams.

In order to determine the coefficient in the expansion for  $\lambda_3$  we have to determine the antisymmetric up-down full vertex at zero frequency. To second order there are two contributions which are shown in figure 2.6. For zero field and particle hole symmetry they give the same contribution with opposite sign and therefore we find  $\lambda_3^{(2)} = 0$ . From this we find that the parameters to second order have to be given by  $\lambda_1^{(2)} = \tilde{U}^2\tilde{n}_{-\sigma}^2 + \Sigma_{\sigma}^{\text{mix},(2,1)}$ ,

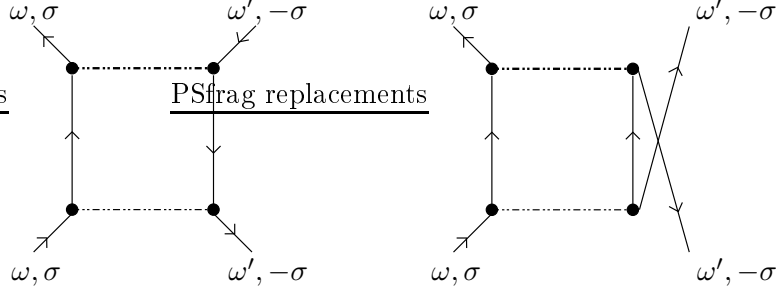


Figure 2.6: Second order diagrams for the vertex function.

where we used  $\Sigma_{\tilde{U},\sigma}^{(2,2)}(0) = 0$ , and  $\lambda_2^{(2)} = \Sigma_{\tilde{U},\sigma}^{(2,2)}(0)' / \tilde{U}^2$ . This determines the renormalised self-energy to second order with all contributions according to (2.54). To clarify how the second additional Feynman rule would be incorporated we give the simplest diagram for this term in figure 2.5 (right), which is actually of third order.

$$\Sigma_{\sigma}^{\text{mix},(3,1)} = -i \frac{\tilde{U}^3 \lambda_2^{(2)}}{2\pi} \int_{-\infty}^{\infty} d\omega \omega \tilde{G}_{-\sigma}^0(\omega)^2. \quad (2.58)$$

Whilst for this case it is straight forward to carry out the RPT one can imagine that for higher order calculations with larger number of standard and mixed diagrams it becomes more and more cumbersome to compute all contributions to the RPT. Third order calculations have been discussed by Hewson (2001). It might be easier to alter the setup of the RPT slightly in order not to deal with all the counter-terms separately and we will discuss a possibility in the following section.

### 2.2.3 Alternative formulations and extensions

The perturbation theory can be given in a different formulation by including the “free counter-terms” derived from  $S_0^c$  into the propagator, which then takes the form

$$G_{\sigma,\lambda_1,\lambda_2}^r(\omega) = \frac{1}{\omega - \tilde{\epsilon}_{d,\sigma} + i\tilde{\Delta}_{\sigma} + \lambda_1 + \lambda_2\omega}. \quad (2.59)$$

Since the counter-term interaction term  $S_{\lambda_3}^c$  has the same form as the standard interaction term, also these terms can be collected and the perturbation theory carried out in  $\tilde{U}_1 \equiv \tilde{U} + \lambda_3$ . The renormalisation conditions become self-consistency equations in that case. Although such a setup at first sight appears promising due the much simpler structure of the perturbation expansion it turns out that it is difficult to carry out the expansion in this form. We had seen in the last section that the counter-term parameters include contributions to different order in  $\tilde{U}$  [cf eq. (2.55)]. The setup defined by (C.15) and the free propagator (2.59) implies that counter-term contributions to all orders are included even in the low order diagrams discussed in the last section. In fact, if the exact expressions of the counter-terms, which can be derived from the identity (2.38), were used in this

approach the theory would formally lead back to the bare perturbation theory and nothing new would have been achieved. More details for this kind of approach are described in the appendix C.

The idea of expanding in an effective renormalised interaction  $\tilde{U}_1$  turns out to be fruitful, when we consider an RPT expansion, which sums up a certain class of diagrams to all orders rather than all diagrams up to certain order in  $\tilde{U}$ . This is best illustrated for the dynamic transverse spin susceptibility  $\chi_t(\omega)$  as defined in equation (1.26), which we can calculate by an RPA-like sum of repeated quasiparticle scattering diagrams (Hewson 2006). This is depicted in figure 2.7.

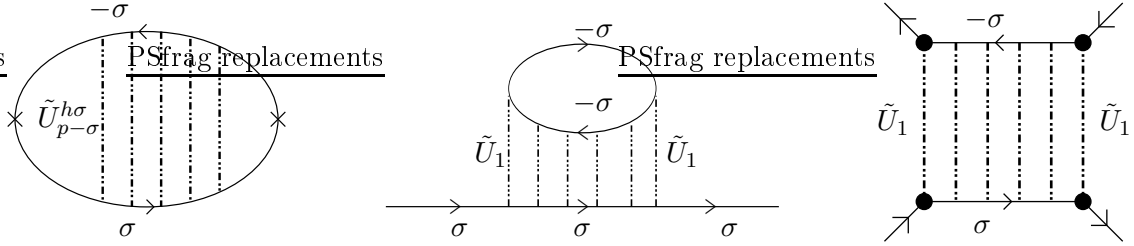


Figure 2.7: Typical diagrams for repeated quasiparticle scattering for the susceptibility (left), the renormalised self-energy (middle) and the full vertex (right).

The lines correspond to the free quasiparticle propagators in equation (2.44) and the interaction term vertex is given by  $\tilde{U}_1 = \tilde{U}_{p-\sigma}^{h\sigma}$ . Here the series in terms of repeated quasiparticle scattering yields the expression

$$\chi_t(\omega) = \frac{1}{2} \frac{\Pi_{p-\sigma}^{h\sigma}(\omega)}{1 - \tilde{U}_{p-\sigma}^{h\sigma} \Pi_{p-\sigma}^{h\sigma}(\omega)}, \quad (2.60)$$

with the appropriate effective interaction  $\tilde{U}_{p-\sigma}^{h\sigma}$ . We have introduced the pair propagator  $\Pi_{p-\sigma}^{h\sigma}(\omega)$ , which is given by

$$\Pi_{p-\sigma}^{h\sigma}(\omega) = - \int \frac{d\omega_1}{2\pi i} \tilde{G}_\sigma^0(\omega + \omega_1) \tilde{G}_{-\sigma}^0(\omega_1). \quad (2.61)$$

It can be solved analytically and the expression is given in section 3.4.2 in the next chapter. Note that  $\Pi_{p-\sigma}^{h\sigma}(0) = \tilde{\rho}_d^0(0)$ . We still have to satisfy the renormalisation conditions (2.40) and (2.41), but as we have not calculated the self-energy or vertex this seems difficult. How can we therefore determine the quantity  $\tilde{U}_{p-\sigma}^{h\sigma}$ ? As illustrated by Hewson (2006) we can use the exact static result for the susceptibility from the first chapter (1.14) to determine this quantity by equating the result for  $\omega \rightarrow 0$  in (2.60) to (1.14). Hence, we find

$$\tilde{U}_{p-\sigma}^{h\sigma} = \frac{\tilde{U}}{1 + \tilde{U} \tilde{\rho}_d^0(0)}. \quad (2.62)$$

It turns out that the dynamic susceptibility can be described quite accurately in such a formulation on all energy scales (Hewson 2006).

For the renormalised self-energy one can make a similar approximation and sum up the repeated scattering terms as shown in figure 2.7,

$$\Sigma_{\sigma}^{r,\text{ph}}(\omega) = \tilde{U}_1^2 \int \frac{d\omega_2}{2\pi i} 2\chi_{s\perp}^{\sigma}(\omega_2) \tilde{G}_{-\sigma}^0(\omega - \omega_2). \quad (2.63)$$

The processes of spin fluctuations taken into account in such a summation are likely to be the most dominant ones in the Kondo regime. The effective interaction  $\tilde{U}_1$  has to be found from the renormalisation condition (2.41) for the full vertex, which for this simple RPA like approximation is just a sum of the terms as shown in figure 2.7. From this we find

$$\tilde{U}_1 = \frac{\tilde{U}}{1 + \tilde{U}\tilde{\rho}_d^0(0)}. \quad (2.64)$$

which agrees with the earlier result for the susceptibility. In order to calculate the renormalised self-energy  $\tilde{\Sigma}_{\sigma}(\omega)$  we still have to include the counter-terms and in the most straightforward approach is to only take the trivial counter-terms  $\Sigma^{ct}(\omega)$  into account and determine  $\lambda_1$  and  $\lambda_2$  by the condition (2.40). Results for this kind of calculations will be presented in chapter 3.

An extension of this simple repeated scattering analysis can be given by considering a self-consistent theory with fully dressed propagators. This is most conveniently described in the two-particle irreducible (2PI) framework and an approach based on a Luttinger Ward functional. We have described the details for such an approach in appendix C.3.

## 2.3 The Dynamical Mean Field Theory (DMFT)

So far in this chapter we have concentrated on the description of methods suitable for the solution of impurity models like the AIM. Another subject of this thesis is, however, to study strong correlation effects in lattice models like the Hubbard model. As realized by Metzner and Vollhardt (1989), and elaborated on by Müller-Hartmann (1989), it is enlightening for the understanding of correlation effects in lattice models to study the limit of infinite dimensions,  $d \rightarrow \infty$ . With the appropriate scaling of the hopping amplitude, it was found that the self-energy becomes a local quantity, i.e. does not depend on  $\mathbf{k}$  anymore, but retains the full frequency dependence. The limit thus generates a large simplification without making the problem trivial. Based on these considerations an approach linking the solution for a lattice model to that of a local model was developed, the dynamical mean field theory (DMFT). The essential idea of the DMFT is to map the lattice model to a single site quantum impurity model embedded in an effective medium (Georges et al. 1996), which is determined self-consistently [also Local Impurity Self-consistent Approximation (LISA)]. In contrast to standard mean-field or Hartree Fock theory, DMFT fully takes into account local quantum fluctuations and hence the many-body character of the problem is retained. One can show that DMFT is exact in the limit  $d \rightarrow \infty$ . For details of the derivation of the main equations we refer to the review article by Georges et al. (1996).

To be more specific, we consider the Hubbard model (1.29) which is written conveniently in the imaginary time path integral formulation as

$$\mathcal{Z} = \prod_i \int \mathcal{D}(c_{i,\sigma}, \bar{c}_{i,\sigma}) e^{-S[c_{i,\sigma}(\tau), \bar{c}_{i,\sigma}(\tau)]} \quad (2.65)$$

with the action

$$S[c_{i,\sigma}(t), \bar{c}_{i,\sigma}(t)] = \int_0^\beta d\tau \sum_{i,j,\sigma} \bar{c}_{i,\sigma}(\tau) (\delta_{ij} \frac{\partial}{\partial \tau} - t_{ij} - \delta_{ij} \mu) c_{i,\sigma}(\tau) + U \sum_i n_{i\uparrow}(\tau) n_{i\downarrow}(\tau). \quad (2.66)$$

The DMFT approach is based on deriving an effective action for a special lattice site, usually termed the “0”-site. This is achieved by formally integrating out the degrees of freedom of the other lattice sites. The effective action on the “0”-site reads

$$S_{\text{eff}} = - \int_0^\beta d\tau \int_0^\beta d\tau' \sum_\sigma c_{0,\sigma}^\dagger(\tau) \mathcal{G}_0^{-1}(\tau - \tau') c_{0,\sigma}(\tau') + U \int_0^\beta d\tau \sum_i n_{0,\uparrow}(\tau) n_{0,\downarrow}(\tau), \quad (2.67)$$

where we have not explicitly allowed for any kind of symmetry breaking. We have introduced the effective Weiss field (or dynamical mean field)  $\mathcal{G}_0^{-1}(\tau)$  for the “0”-site. In analogy to classical mean field theory it has to be determined self-consistently, but in contrast to the latter  $\mathcal{G}_0^{-1}(\tau)$  is function of  $\tau$ , which mimics the lattice dynamics. For a given  $\mathcal{G}_0^{-1}(\tau)$ ,  $S_{\text{eff}}$  in (2.67) determines the dynamics at the 0-site, which is still an interacting problem. In the DMFT approach the lattice self-energy is entirely local and the lattice Green’s function can be written in the form

$$G_{\mathbf{k}}^{\text{lat}}(i\omega_n) = \frac{1}{i\omega_n + \mu - \varepsilon_{\mathbf{k}} - \Sigma^{\text{lat}}(i\omega_n)}. \quad (2.68)$$

From this we can define the local lattice Green’s function  $G^{\text{loc}}(i\omega_n)$  by

$$G^{\text{loc}}(i\omega_n) := \frac{1}{N} \sum_{\mathbf{k}} G_{\mathbf{k}}^{\text{lat}}(i\omega_n) = \int d\varepsilon \frac{\rho_0(\varepsilon)}{i\omega_n + \mu - \varepsilon - \Sigma^{\text{lat}}(i\omega_n)} = \text{HT}[\rho_0](\zeta), \quad (2.69)$$

where  $\zeta := i\omega_n + \mu - \Sigma^{\text{lat}}(i\omega_n)$ .  $\text{HT}[\rho_0](\omega)$  is the Hilbert transform of the free electron density of states  $\rho_0(\varepsilon) = \sum_{\mathbf{k}} \delta(\varepsilon - \varepsilon_{\mathbf{k}})$ ,

$$\text{HT}[\rho_0](\zeta) = \int d\xi \frac{\rho_0(\xi)}{\zeta - \xi}. \quad (2.70)$$

In the derivation of the DMFT equations [see Georges et al. (1996)] one finds quite generally the Dyson-like relation between the effective Weiss field, the local lattice Green’s function and the self-energy,

$$\mathcal{G}_0^{-1}(i\omega_n) = \Sigma^{\text{lat}}(i\omega_n) + \frac{1}{\text{HT}[\rho_0](\zeta)} = \Sigma^{\text{lat}}(i\omega_n) + G^{\text{loc}}(i\omega_n)^{-1}. \quad (2.71)$$

In the DMFT framework the lattice self-energy  $\Sigma^{\text{lat}}(i\omega_n)$  is the same as the self-energy of the effective impurity problem  $\Sigma^{\text{imp}}(i\omega_n)$ ; also the Green's function of the effective impurity model and  $G^{\text{loc}}(i\omega_n)$  coincide. As an effective impurity problem (2.67) we can consider the AIM in the path integral formalism (2.29) with the effective action

$$S = - \sum_{\sigma} \int_0^{\beta} d\tau \int_0^{\beta} d\tau' \bar{d}_{\sigma}(\tau) G_0(\tau - \tau')^{-1} d_{\sigma}(\tau') + U \int_0^{\beta} d\tau n_{d,\uparrow}(\tau) n_{d,\downarrow}(\tau) \quad (2.72)$$

where generally

$$G_0(\tau) = \frac{1}{\beta} \sum_n e^{-i\tau\omega_n} \frac{1}{i\omega_n - \varepsilon_d - K(i\omega_n)}. \quad (2.73)$$

with  $K(i\omega_n)$  given in the earlier equation (1.6).

By comparison of (2.72) with (2.67) one can formally identify  $\mathcal{G}_0^{-1}(\tau - \tau') = G_0(\tau - \tau')^{-1}$ . Therefore, the properties of the medium have to be encoded in the generally complex and  $i\omega_n$ -dependent hybridisation function  $K(i\omega_n)$  (often denoted as complex  $\Delta(i\omega_n)$ ). For this reason it cannot be identified with just an imaginary constant  $i\Delta$ , as for the impurity model with a flat conduction band density of states. In this framework we find therefore an explicit expression for the Weiss effective field

$$\mathcal{G}_0^{-1}(i\omega_n) = i\omega_n + \mu - K(i\omega_n), \quad (2.74)$$

where one identifies  $\varepsilon_d = -\mu$ . This relates the DMFT approach (2.67) to an effective AIM as the corresponding impurity model to be studied.

In practice, we use a certain input for the medium,  $K^{(0)}(i\omega_n)$ , to calculate the self-energy of the corresponding effective impurity problem  $\Sigma^{\text{imp}}(i\omega_n)$  with the NRG approach. This self-energy is identified with the local lattice self-energy  $\Sigma^{\text{lat}}(i\omega_n)$  and used to calculate the local lattice Green's function with (2.69). From equation (2.71) we can then calculate the new effective Weiss field  $\mathcal{G}_0^{-1}(i\omega_n)$  and  $K^{(1)}(i\omega_n)$  from (2.74). This closes the self-consistency cycle, which has to be iterated until convergence,  $K^{(m)}(i\omega_n) = K^{(m+1)}(i\omega_n)$ , is reached. This approach is completely general and does not rely on a specific density of states  $\rho_0(\varepsilon)$ . For the Bethe lattice with a semicircular density of states,

$$\rho_0(\varepsilon) = \frac{1}{2\pi t^2} \sqrt{4t^2 - \varepsilon^2}, \quad |\varepsilon| < 2t, \quad (2.75)$$

analytic expressions for the Hilbert transforms can be given and the equations simplify (Georges et al. 1996). In this thesis we employ the NRG as solver for the effective impurity problem, and therefore have to map a given hybridisation function  $K(i\omega_n)$  onto the corresponding linear chain problem [cf. equation (2.1)]. A procedure to do this has been devised by Bulla et al. (1997), and is also described by Bauer (2007) for different cases. For situations with broken symmetry some of the expressions have to be modified, but the general setup is as described here.

## Part II

# Locally Correlated Systems



*Try to learn something about everything and everything about something.*

Thomas H. Huxley

## Chapter 3

# Field dependent quasiparticle dynamics in the Anderson impurity model

In the following three chapters, which form the the second part of the thesis, we present results for locally strongly correlated electrons in the Anderson impurity model (AIM). As a common theme of this thesis we are interested in the situation with broken symmetry. The AIM does not order spontaneously in any parameter range, it is, however, interesting to study its response to an external symmetry breaking. In this chapter we study the effect of a magnetic field. The analysis is a combination of analytical and numerical methods based on the NRG and RPT framework. First we describe the behaviour of the field dependent renormalised parameters and show how the low energy response can be characterised in terms of them. In later sections we present dynamic response function for higher energies deduced from NRG and RPT calculations.

### 3.1 Strongly correlated electrons in a field

Electrons in strongly correlated systems are particularly sensitive to the application of magnetic fields. One reason is that strong correlations are usually a consequence of the interaction of electrons with enhanced spin fluctuations, and these fluctuations couple strongly to a magnetic field. Another reason is that there is a low temperature scale  $T^*$  ( $T^* \ll T_F$ ) induced which plays the role of an effective Fermi temperature  $T_F$ . The effects of a magnetic field  $H$  in general depend on the ratio of the two energy scales  $\mu_B H$  and  $k_B T_F$ . In a weakly correlated metal  $\mu_B H/k_B T_F \ll 1$ , but in a strongly correlated system the relevant ratio is  $\mu_B H/k_B T^*$ , which can be of order unity. This sensitivity means that a magnetic field is an important tool in the experimental investigation of strongly correlated metallic systems, such as magnetic impurities, quantum dots, heavy

fermions and transition metal oxides. In the next section we show how it is possible to describe the quasiparticles in a magnetic field in the Fermi liquid regime by field dependent parameters. We focus on the particle-hole symmetric Anderson model in the next sections as in reference Hewson, Bauer and Koller (2006). The non-symmetric case is studied in a similar approach in Bauer and Hewson (2007a). The AIM (1.1) with the local magnetic field term (1.17) forms basis for the calculations. For the symmetric AIM, the calculations can be carried out either directly with the field dependent model or we can use the mapping to the negative  $U$  model, which is not symmetric for finite field, as explained in section 1.1.2. For the NRG calculation the latter has the advantage of preserving all spin and charge quantum numbers as a symmetry and thus reducing the numerical effort.

First we discuss the field dependent behaviour of the renormalised parameters introduced earlier. Once the renormalised parameters are known, the impurity spin and charge susceptibility, the specific heat coefficient and the induced impurity magnetisation at  $T = 0$  for arbitrary magnetic field can be expressed by substituting into the relevant exact formulae derived from a renormalised perturbation theory. The leading temperature dependent corrections to the susceptibility, magnetisation, the finite conductivity due to scattering from an impurity in a metallic host, and for the conductance through a quantum dot will also be calculated in a later section. It is interesting to see how the response coefficients behave when the field strength is increased. A number of physical properties are found to change qualitatively in the strongly correlated case for magnetic field strengths in the range  $0 < g\mu_B H < T_K$ , where  $T_K$  is the Kondo temperature. This should be a physically accessible magnetic field range for many systems. The  $T^2$  coefficient of the magnetic susceptibility, the conductivity from a magnetic impurity in the strong correlation regime, and the conductance through a quantum dot all change sign in this magnetic field range.

We also describe these systems beyond the low energy regime with the NRG and RPT method in section 3.4. The approach developed here is a general one and is equally applicable to other impurity models (Hewson et al. 2004) and to lattice models as will be seen in chapter 6. For lattice models, for which dynamical mean field theory is applicable, similar NRG methods to those employed here can be used. It is important to bear in mind that the approach is not restricted to the NRG method, the relevant renormalised parameters could also be estimated using other theoretical techniques, variational methods for example.

### 3.2 Field dependent renormalised parameters

For the characterisation of the low energy fixpoints of the AIM we had introduced renormalised parameters  $\tilde{\varepsilon}_d$ ,  $\tilde{\Delta}$  and  $\tilde{U}$  in section 1.1. In section 2.2.1 we defined them more rigorously in terms of the self-energy including an explicit dependence on the magnetic field  $h$ . As first demonstrated by Hewson et al. (2004) the field dependent parameters can be deduced from the low energy excitations in an NRG calculation. The details of how this

is achieved are given in appendix B. In this section we want to discuss the behaviour of these parameters, as the magnetic field  $h$  is varied, focusing on the particle-hole symmetric case. Before discussing the field dependence of the parameters let us give the generalisation of some of the equations from the first chapter to the case with magnetic field. The low energy scale  $T^*$  is defined by  $4T^* = \pi\tilde{\Delta}(0)$  in the following, such that in the Kondo regime  $T^* = T_K$ . The Friedel sum rule (Friedel 1956, Langreth 1966) is applicable to each spin component, and in terms of the renormalised parameters (2.34) it reads

$$n_{d,\sigma} = \frac{1}{2} - \frac{1}{\pi} \tan^{-1} \left( \frac{\tilde{\varepsilon}_{d,\sigma}(h)}{\tilde{\Delta}(h)} \right). \quad (3.1)$$

For particle hole symmetry we can write  $\tilde{\varepsilon}_{d,\sigma}(h) = -\sigma\tilde{\varepsilon}_d(h)$ . Thus from (3.1), we can deduce the induced impurity magnetisation  $M(h) = m(h)/g\mu_B$  at  $T = 0$ ,

$$m(h) = \frac{1}{2}(n_{d,\uparrow} - n_{d,\downarrow}) = \frac{1}{\pi} \tan^{-1} \left( \frac{\tilde{\varepsilon}_d(h)}{\tilde{\Delta}(h)} \right). \quad (3.2)$$

It is therefore specified by the two parameters  $\tilde{\varepsilon}_d(h)$  and  $\tilde{\Delta}(h)$  that characterise the non-interacting quasiparticles. The free quasiparticle density of states (1.13) generalises to

$$\tilde{\rho}_{d,\sigma}^0(\omega, h) = \frac{\tilde{\Delta}(h)/\pi}{(\omega - \sigma\tilde{\varepsilon}_d(h))^2 + \tilde{\Delta}^2(h)}. \quad (3.3)$$

As  $\tilde{\rho}_{d,\sigma}^0(0, h)$  is independent of the spin state we can drop the spin index  $\sigma$  for  $\omega = 0$ . The field dependent spin susceptibility at  $T = 0$  from equation (1.14) becomes

$$\chi_s(h) = \frac{1}{2}\tilde{\rho}_d^0(0, h)[1 + \tilde{U}(h)\tilde{\rho}_d^0(0, h)], \quad (3.4)$$

whilst the charge susceptibilities reads

$$\chi_c(h) = \frac{1}{2}\tilde{\rho}_d^0(0, h)[1 - \tilde{U}(h)\tilde{\rho}_d^0(0, h)]. \quad (3.5)$$

The corresponding transverse spin susceptibility  $\chi_t(h)$  [zero applied field limit in the transverse direction, cf. equation (1.26)] is given by

$$\chi_t(h) = \frac{m(h)}{2h}. \quad (3.6)$$

For the symmetric model  $\tilde{\varepsilon}_d(h)$  is entirely magnetic field driven it is convenient to write it as  $\tilde{\varepsilon}_d(h) = \tilde{\eta}(h)h$ . Then  $2h\tilde{\eta}(h)$  is the Zeeman splitting of the impurity levels for the non-interacting quasiparticles, and  $\tilde{\eta}(h)$  can be given the interpretation of a field dependent enhancement factor.

Equation (3.4) for the susceptibility  $\chi_s(h)$  has a term in  $\tilde{U}(h)$ . However, the susceptibility  $\chi_s(h) = \frac{\partial m(h)}{\partial h}$  can also be derived by differentiating the expression (3.2) for the magnetisation which depends explicitly only on the variables  $\tilde{\varepsilon}_d(h)$  and  $\tilde{\Delta}(h)$ . Hence, the

## 44 Field dependent quasiparticle dynamics in the Anderson impurity model

value of  $\tilde{U}(h)$  is not independent of the other two parameters and we can derive a relation between them,

$$1 + \tilde{U}(h)\tilde{\rho}_d^0(0, h) = \frac{\partial \tilde{\varepsilon}_d(h)}{\partial h} - \frac{\tilde{\varepsilon}_d(h)}{\tilde{\Delta}(h)} \frac{\partial \tilde{\Delta}(h)}{\partial h}. \quad (3.7)$$

The proof that equation (3.4) for the susceptibility is exact depends on a Ward identity, so the relation (3.7) we have derived must be an alternative statement of this identity. In terms of  $\tilde{\eta}(h) = \tilde{\varepsilon}_d(h)/h$  it becomes

$$1 + \tilde{U}(h)\tilde{\rho}_d^0(0, h) = \tilde{\eta}(h) + h \frac{\partial \tilde{\eta}(h)}{\partial h} - \frac{h\tilde{\eta}(h)}{\tilde{\Delta}(h)} \frac{\partial \tilde{\Delta}(h)}{\partial h}. \quad (3.8)$$

In the system with magnetic field the expression of the Wilson ratio (1.16) in terms of the renormalised parameters reads

$$R(h) = 1 + \tilde{U}(h)\tilde{\rho}_d^0(0, h). \quad (3.9)$$

In figure 3.1 we give a plot of the renormalised parameters as a function of the natural logarithm of the magnetic field,  $\log(h/T^*)$ , for the strong coupling case  $U/\pi\Delta = 4$ .

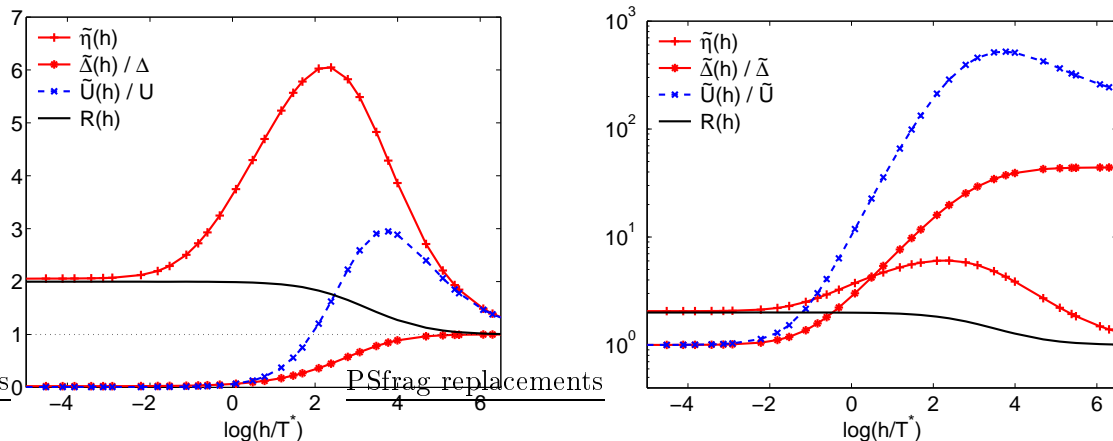


Figure 3.1: Left: The magnetic field dependence of the renormalised parameters  $\tilde{\Delta}(h)/\Delta$ ,  $\tilde{\varepsilon}_d(h)/\tilde{\varepsilon}_d (= \tilde{\eta}(h))$  and  $\tilde{U}(h)/U$ , and the Wilson ratio  $R(h)$ , for the symmetric Anderson model with  $U/\pi\Delta = 4.0$  plotted on a logarithmic scale. Right: The magnetic field dependence of the renormalised parameters  $\tilde{\Delta}(h)/\tilde{\Delta}$ ,  $\tilde{\eta}(h)$  and  $\tilde{U}(h)/\tilde{U}$ , and the Wilson ratio  $R(h)$  for the same parameters plotted on a logarithmic scale and with logarithmically scaled  $y$ -axis. In both cases the energy scale is set by  $T^* = \pi\tilde{\Delta}(0)/4 = T_K$ .

We give two different versions of this dependence, one scaled by the bare parameters (left), and one scaled by the renormalised parameters at zero field (right), which has a logarithmically scaled  $y$ -axis. We can follow the progressive decrease of renormalisation effects on the quasiparticles as the strong correlation effects are suppressed when magnetic field is increased. This can be seen directly from the ratio  $\tilde{\Delta}(h)/\Delta = z(h)$ , which after a

range with little variation increases steadily to one for large fields. For zero field in the Kondo regime  $z$  has a small value, but with increasing field the impurity spin is more and more polarised, leading to a suppression of the spin fluctuations and likewise the Kondo effect. The quasiparticles are therefore “de-renormalised” from the  $h = 0$  values by the magnetic field, and for very large field  $h > U$  essentially non-interacting behaviour ( $z = 1$ ) is found. The trend can also be seen in the field dependent Wilson ratio  $R(h)$  in (3.9). It is a combination of all the renormalised parameters and shows a smooth transition from  $R = 2$  for  $h = 0$  to  $R = 1$  for large field. It is known from Bethe ansatz calculations (Tsvelik and Wiegmann 1983) that  $R(h) = 2$  is independent of  $h$  in the Kondo model. This can be seen to be the case in the results for  $R(h)$  shown in figure 3.1 when the parameters correspond to the localised or Kondo regime. The localised model, however, is only valid when the charge fluctuations are completely suppressed. For very large field values  $h > U$  local charge fluctuations can be induced by the magnetic field and, as this regime is approached,  $R(h)$  makes a crossover to the value  $R = 1$  for non-interacting electrons.

In the limit  $h \rightarrow 0$ , the field dependent enhancement factor for the magnetic response of quasiparticles  $\tilde{\eta}(h)$  is equal to  $\tilde{\eta}(0) = R(0)$  due to (3.8) and (3.9). Therefore, in the Kondo regime,  $R(0) = 2$ , the quasiparticles have twice the non-interacting value for field dependent splitting showing the enhanced susceptibility towards exposure to a magnetic field. For very large  $h$ ,  $\tilde{\eta}(h)$  goes to one corresponding to a normal Zeeman splitting for non-interacting particles. In the intermediate field regime,  $h \simeq T^*$ ,  $\tilde{\eta}(h)$  becomes fairly large before going down to one. Coming from large fields this can be understood from mean field theory, where we can write

$$\tilde{\eta}^{\text{mf}} = \varepsilon_{d,\downarrow}(h)^{\text{mf}}/h = [\varepsilon_d + U(n_d/2 + m(h)) + h]/h = 1 + Um(h)/h, \quad (3.10)$$

where we have used particle hole symmetry. This term increases from one as  $h$  decreases as the magnetisation does not decrease much in this regime [see figure 3.2 (left)]. Coming from zero field the behaviour can be understood from the Friedel sum rule for the magnetisation (3.2) which gives

$$\tilde{\eta}(h) = \frac{\tilde{\Delta}(h)}{h} \tan(\pi m(h)) \quad (3.11)$$

As can be seen for the behaviour of the magnetisation in figure 3.2 (left) in this regime there is a sharp rise accompanied by a moderate increase of  $\tilde{\Delta}(h)$  which leads to the strong increase in  $\tilde{\eta}(h)$ .

It is not so straight forward to understand the behaviour of the renormalised quasiparticle interaction  $\tilde{U}(h)$ . At first sight it might seem surprising that in the intermediate field range  $\tilde{U}(h)$  is larger than the bare interaction of the model. This does not imply, however, that the interaction effects are becoming stronger. The effects of the interaction on the low energy scale depend upon the combination,  $\tilde{U}(h)\tilde{\rho}_d^0(0, h)$ , and  $\tilde{\rho}_d^0(0, h)$  falls off rapidly with  $h$  as  $\tilde{\varepsilon}_d(h)$  moves away from the Fermi level. The combination  $\tilde{U}(h)\tilde{\rho}_d^0(0, h)$  can be seen to

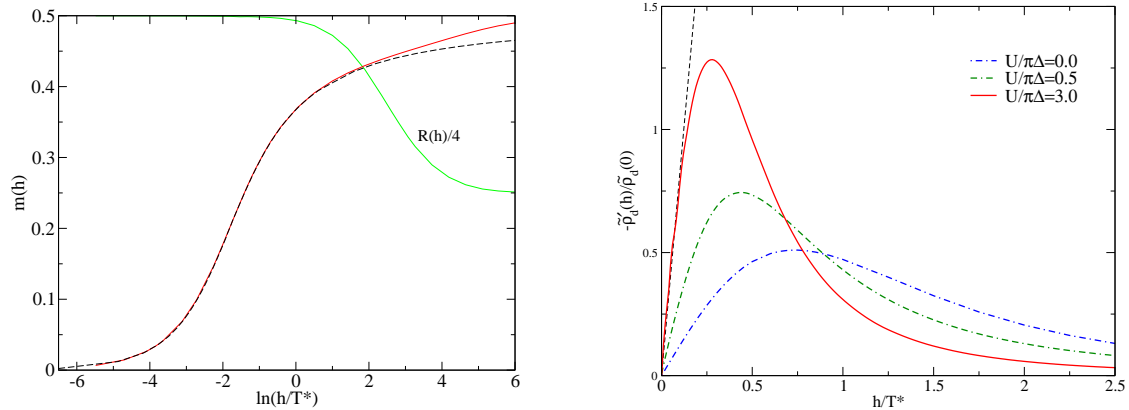


Figure 3.2: Left: The impurity magnetisation  $m(h)$  for the symmetric model with  $U/\pi\Delta = 3.0$ , together with  $R(h)/4$ , where  $R(h)$  is the Wilson ratio, plotted as a function of the logarithm of the magnetic field,  $\ln(h/T^*)$ . Also shown for comparison are the corresponding Bethe ansatz results Tselik and Wiegmann (1983) for the field induced magnetisation for the Kondo model. Right: The ratio  $-\tilde{\rho}_d^0(h)'/\tilde{\rho}_d^0(0)$ , where the prime indicates a derivative with respect to  $h/T^*$ , is shown for  $U/\pi\Delta = 0.0, 0.5, 3.0$  as a function of  $h/T^*$ . The dashed line shows the asymptotic result as  $h \rightarrow 0$ ,  $3h\pi\sqrt{3}/2T_K^2$ , for the Kondo model.

decrease monotonically with increase of  $h$ , as discussed above for  $R(h)$ . We can observe the enhancement of the effective interaction  $\tilde{U}(h)$ , as the magnetisation is reduced from the saturated value  $m_{\text{sat}} = 1/2$  for large field. As the applied magnetic field is reduced from the regime  $h > U$ , spin fluctuations increase and enhance the effective interaction  $\tilde{U}$ , as in the random phase approximation (RPA), above the bare value  $U$ ,

$$\tilde{U}^{\text{RPA}}(h) = \frac{U}{1 - U\rho_d(0, h)}. \quad (3.12)$$

This result corresponds to the enhancement of the susceptibility that one finds from the RPA. If the magnetic field is reduced from a large value then  $U\rho_d(0, h) > 0$  increases and so  $\tilde{U}^{\text{RPA}}(h)$  increases. This is precisely what is seen in the large  $h$  regime in the results in figure 3.1. As the magnetic field is further reduced the many-body correlations are increasingly effective in screening the impurity so that  $\tilde{U}(h)$  decreases from an enhanced value greater than  $U$  to a value  $4T_K$  as  $h \rightarrow 0$  when  $U > 2\pi\Delta$ . The increase as seen when coming from the other side, i.e. from small magnetic fields, can be understood as follows. The localised model gives  $R(h) = 2$  for all  $h$ , which implies that  $\tilde{U}(h) = 1/\tilde{\rho}_d^0(0, h)$ . From this result, and equations (3.3) and (3.2), the ratio  $\tilde{U}(h)/\pi\tilde{\Delta}(h)$  for the localised model can be expressed entirely in terms of the magnetisation and is such that  $\tilde{U}(h)/\pi\tilde{\Delta}(h) = 1/\cos^2(\pi m(h))$ . For  $h = 0$ , this corresponds to the strong correlation results  $\tilde{U}(0)/\pi\tilde{\Delta}(0) = 1$ , as  $m(0) = 0$ , and for very large fields where  $m(h) \rightarrow 1/2$  as  $h \rightarrow \infty$ , it gives  $\tilde{U}(h)/\pi\tilde{\Delta}(h) \rightarrow \infty$ , corresponding to the fact that charge fluctuations can only be completely suppressed if  $U$  is infinite. For a more extensive discussion we refer the

reader to the paper by Hewson, Bauer and Koller (2006).

The magnetisation in terms of the renormalised parameters (3.2) can be compared with exact results from Bethe ansatz calculations for the Kondo model (Tselik and Wiegmann 1983) as shown in figure 3.2 (left). It agrees with the the BA ansatz results over the field range, where charge fluctuations are not so important (Hewson, Bauer and Koller 2006), but starts to deviate for large  $h$ . Due to the charge fluctuations, the approach to saturation is much more rapid for the Anderson model than for the Kondo model, once  $h$  exceeds  $U$ .

### 3.3 Low temperature response

With the help of the field dependent parameters we can express the low order temperature dependence for response quantities and study the behaviour of the coefficients with magnetic field. We will consider the susceptibility and magnetisation first.

#### Magnetisation and Susceptibility

Using a thermodynamic identity one finds (Hewson, Bauer and Koller 2006)

$$\chi_s(T, h) = \chi_s(0, h) - c_\chi(h) \left( \frac{T}{T^*} \right)^2, \quad (3.13)$$

with

$$c_\chi(h) = -\frac{(\pi T^*)^2}{12} \frac{\partial^2 \tilde{\rho}_d^0(0, h)}{\partial h^2}. \quad (3.14)$$

On integrating these results with respect to  $h$  we can derive a similar relation for the induced magnetisation,

$$m(T, h) = m(0, h) - c_m(h) \left( \frac{T}{T^*} \right)^2 \quad (3.15)$$

where

$$c_m(h) = -\frac{(\pi T^*)^2}{6} \frac{\partial \tilde{\rho}_d^0(0, h)}{\partial h}. \quad (3.16)$$

In figure 3.2 (right) we plot the results for  $-\tilde{\rho}_d^0(h)'/\tilde{\rho}_d^0(0)$ , which is proportional to  $c_m(h)$ , for  $U/\pi\Delta = 3.0, 0.5, 0.0$  in the range  $0 < h/T^* < 2.5$ . It can be seen that all three curves have a maximum which implies that for a specific magnetic field  $h_{\text{mp}}$  the coefficient  $c_m(h)$  is maximal and therefore the magnetisation decreases most significantly with increasing temperature in this regime. For the strong coupling regime we see in figure 3.2 (right) that  $h_{\text{mp}} \lesssim 0.5T^*$  and that is the field region in figure 3.2 (left), where the magnetisation has the steepest rise. Another consequence of the fact that all three curves have a maximum is that  $c_\chi(h)$  in (3.14) becomes zero, and changes from positive to negative sign in this range. Hence, from this field  $h_{\text{mp}}$  on the low temperature susceptibility increases with the temperature. This occurs for  $h$  significantly smaller than  $T^* = T_K$  in the Kondo regime.

### Low Temperature Transport in an Arbitrary Magnetic Field

In order to determine the  $T^2$ -dependence of linear response transport coefficients we need to calculate the renormalised self-energy  $\tilde{\Sigma}_\sigma(\omega, T, h)$  both to order  $\omega^2$  and to order  $T^2$ . We calculate this from the renormalised perturbation expansion as explained in section 2.2.2 taken to order  $\tilde{U}^2(h)$ . This takes full account of the quasiparticle scattering and gives the exact result of Yamada (1975a) for  $h = 0$ . Note that no counter-terms have to be considered for the  $T^2$  and  $\omega^2$  coefficients. In order to deduce the  $\omega^2$  term we consider the second order diagram as given in figure 2.4 with  $\tilde{U} \rightarrow \tilde{U}(h)$ ,

$$\Sigma_\sigma^{r,(2)}(\omega) = \frac{\tilde{U}(h)^2}{(2\pi)^2} \iint d\omega_1 d\omega_2 \tilde{G}_\sigma^0(\omega - \omega_1) \tilde{G}_{-\sigma}^0(\omega_1 + \omega_2) \tilde{G}_{-\sigma}^0(\omega_2), \quad (3.17)$$

where the free causal Green's function for the symmetric model with magnetic field for  $T = 0$  in terms of renormalised parameters has the form

$$[\tilde{G}_\sigma^0(\omega)]^{-1} = \omega + \sigma \tilde{\varepsilon}_d(h) + \text{sgn}(\omega) i \tilde{\Delta}(h). \quad (3.18)$$

The corrections to order  $\omega^2$  can be deduced from the second derivative of the self-energy with respect to  $\omega$  evaluated at  $\omega = 0$  and  $T = 0$ . Using

$$\frac{\partial^2 \tilde{G}_\sigma^0(\omega)}{\partial \omega^2} = 2\tilde{G}_\sigma^0(\omega)^3 - 2\pi i \delta'(\omega) \tilde{\rho}_d^0(\omega, h) - \frac{8\pi^2 i}{\tilde{\Delta}(h)} \tilde{\rho}_d^0(\omega, h)^2 \delta(\omega) \sigma \tilde{\varepsilon}_d(h) \quad (3.19)$$

we find after some algebra

$$\tilde{\Sigma}_\sigma(\omega, 0, h) = -c(h)\omega^2 \left[ i - (2 + \tilde{\alpha}_\omega(h)) \sigma \tilde{\varepsilon}_d(h) / \tilde{\Delta}(h) \right], \quad (3.20)$$

where

$$c(h) = \frac{\pi \tilde{U}^2(h) [\tilde{\rho}_d^0(0, h)]^3}{2}, \quad \tilde{\alpha}_\omega(h) = \frac{2I(h) \tilde{\Delta}(h)}{\tilde{\xi}(h) [\tilde{\rho}_d^0(0, h)]^2}. \quad (3.21)$$

We have introduced  $\tilde{\xi}(h) = \pi \tilde{\rho}_d(0, h) \tilde{\varepsilon}_d(h)$  and  $I(h)$  is the integral

$$I(h) = \int_{-\infty}^{\infty} \int_{-\infty}^{\infty} \tilde{G}_\downarrow^0(\omega'') \tilde{G}_\downarrow^0(\omega'' + \omega') [\tilde{G}_\uparrow^0(\omega')]^3 \frac{d\omega''}{2\pi} \frac{d\omega'}{2\pi}, \quad (3.22)$$

which can conveniently be evaluated numerically.

The corresponding result for the renormalised self-energy to order  $T^2$  can be derived using the Sommerfeld expansion. The calculation can be performed by using for each internal propagator  $\tilde{G}_\sigma^0(\omega)$  in the  $T = 0$  diagrammatic expansion an additional correction term (Hewson 1993a, chapter 5),

$$- \frac{(\pi T)^2}{3} \frac{\delta'(\omega) \tilde{\Delta}(h)}{(\omega + \sigma \tilde{\varepsilon}_d(h))^2 + \tilde{\Delta}^2(h)}. \quad (3.23)$$

The result for the renormalised self-energy to order  $T^2$  for  $\omega = 0$  is

$$\tilde{\Sigma}_\sigma(T, 0, h) = -c(h)(\pi T)^2 \left[ i + (1 + \tilde{\alpha}_T(h))\sigma\tilde{\varepsilon}_d(h)/\tilde{\Delta}(h) \right], \quad (3.24)$$

where the parameter  $\tilde{\alpha}_T(h)$  is given by

$$\tilde{\alpha}_T(h) = \frac{\tilde{\Delta}(h)}{6\tilde{\xi}(h)\tilde{\varepsilon}_d(h)} \left[ 1 - \frac{\tilde{\varepsilon}_d(h)}{\tilde{\Delta}(h)} \tan^{-1} \left( \frac{\tilde{\varepsilon}_d(h)}{\tilde{\Delta}(h)} \right) \left( 4 + \frac{\tilde{\Delta}(h)}{\tilde{\xi}(h)\tilde{\varepsilon}_d(h)} \right) \right]. \quad (3.25)$$

We can now apply these results to the calculation of transport coefficients.

### Application to magnetic impurities

The contribution to the conductivity  $\sigma(T, h)$  from the scattering of isolated impurities described by an AIM is given by (Yamada 1975a)

$$\sigma(T, h) = \sigma_0 \sum_\sigma \int_{-\infty}^{\infty} \frac{1}{\rho_{d,\sigma}(\omega, T, h)} \left( -\frac{\partial f(\omega)}{\partial \omega} \right) d\omega, \quad (3.26)$$

where  $\rho_d(\omega, T, h) = \tilde{\Delta}(h)\tilde{\rho}_d(\omega, T, h)/\Delta$ , and  $\tilde{\rho}_d(\omega, T, h)$  is the spectral density of the quasiparticle Green function  $\tilde{G}_d(\omega, T, h)$  including the renormalised self-energy. The Sommerfeld expansion gives for (3.26) to second order in  $T$  on using the renormalised self-energy to calculate the quasiparticle spectral density  $\tilde{\rho}_d(\omega, T, h)$  (Hewson, Bauer and Koller 2006),

$$\sigma(h, T) = \sigma(h, 0) \left\{ 1 + \sigma_2(h) \left( \frac{\pi T}{\tilde{\Delta}(h)} \right)^2 + \mathcal{O}(T^4) \right\}, \quad (3.27)$$

where  $\sigma(h, 0) = 2\sigma_0/\cos^2(\pi m(h))$  and  $\sigma_2(h)$  is given by

$$\sigma_2(h) = \frac{\cos^2 \pi m(h)}{3} [1 + C(h)(R(h) - 1)^2]. \quad (3.28)$$

The coefficient  $C(h)$  reads

$$C(h) = 2\cos^2(\pi m(h)) - \sin^2(\pi m(h)) [1 - 3\tilde{\alpha}_T(h) + \tilde{\alpha}_\omega(h)]. \quad (3.29)$$

In figure 3.3 (left) we show the second order coefficient  $\sigma_2(h)$  plotted over  $\log(h/T^*)$  for a range of parameters ( $U/\pi\Delta = 0.5 - 4$ ).

For zero field the conductivity due to impurity scattering rises with temperature as is well known (Yamada 1975a). When  $h$  is increased,  $\sigma_2(h)$  decreases and tends to zero for very high fields, so that the low temperature conductivity becomes temperature independent. The impurity level is then shifted out of the range of the thermally excited states in the conduction band so that there is negligible impurity scattering. We note for the strong coupling cases, where there is a local moment ( $U/\pi\Delta = 2, 4$ ), that the coefficient  $\sigma_2(h)$  changes sign for a certain critical field  $h_c$ , with  $h_c \simeq 0.5T^*$ . The mathematical reason for this behaviour is discussed in Hewson, Bauer and Koller (2006). Physically, when coming

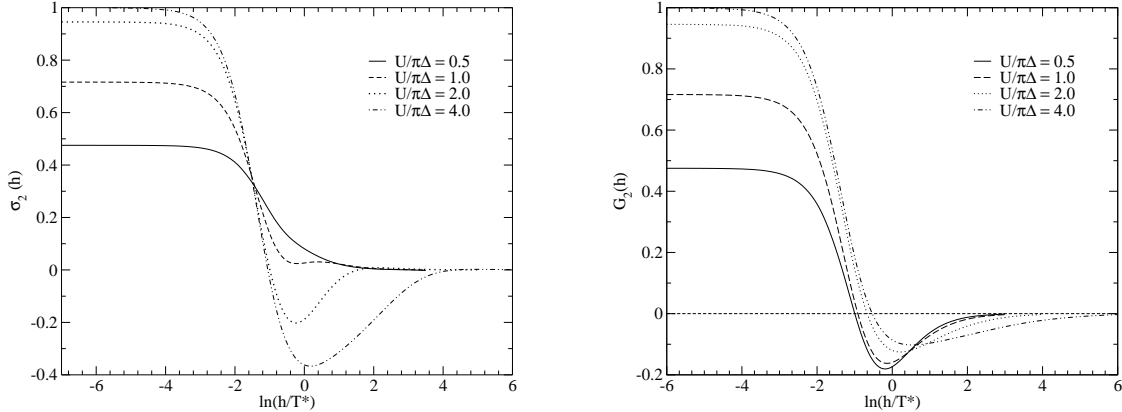


Figure 3.3: Left: Field dependent coefficient  $\sigma_2(h)$  from (3.28) for the second order temperature expansion of the conductivity. Right: Field dependent coefficient  $G_2(h)$  for the second order temperature expansion of the conductance (3.32). Weak coupling ( $U/\pi\Delta = 0.5$ ) up to strong coupling ( $U/\pi\Delta = 4$ ) is considered.

from larger temperatures it is the spin flip scattering of the local moment that causes the resistivity  $\rho(T) = 1/\sigma(T)$  to rise as the temperature is lowered, leading to a resistance minimum and the Kondo effect. Perturbation theory shows that spin-flip scattering gives a diverging amplitude for  $T \simeq T^*$ . The behaviour (characteristic for zero field) is then starting from  $T = 0$  a (quadratic) increase in the conductivity with rising temperature to a maximum (around  $T^*$ ) and from there on a decrease, when other processes like phonon scattering are taken into account. Likewise the resistivity decreases quadratically from  $T = 0$  to the famous minimum and then increases again. The situation changes for a strong field, since for a mainly polarised impurity spin spin-flip scattering processes are strongly suppressed, and therefore a minimum in the resistivity  $\rho(T) = 1/\sigma(T)$  might not occur anymore. The change in sign of the temperature dependence for a certain magnetic field for the behaviour starting from  $T = 0$  might therefore be connected to the fact that the resistivity in the strong field directly increases with temperature. As a consequence we would not observe a Kondo minimum anymore. To our knowledge, this effect has not been seen experimentally, but for magnetic impurities systems with a very low Kondo temperature it might be feasible to put the result to an experimental test.

### Application to quantum dots

In the limit of linear response the equilibrium value of the one-electron Green function can be used to calculate the differential conductance  $G = dI/dV$  through a quantum dot (Ferry and Goodnick 1997),

$$G(T, h) = \frac{G_0\Delta}{2} \sum_{\sigma} \int d\omega \pi \rho_{d,\sigma}(\omega, T, h) \left( -\frac{\partial n_{\text{F}}(\omega)}{\partial \omega} \right), \quad (3.30)$$

where  $n_F$  is the Fermi function and  $G_0 = e^2/\pi\hbar$  with Planck's constant  $\hbar$ . In the low temperature regime we can again apply the Sommerfeld expansion to obtain the leading order finite temperature corrections to order  $T^2$  (Hewson, Bauer and Koller 2006),

$$G(T, h) = G(0, h) \left( 1 - G_2(h) \left( \frac{\pi T}{\tilde{\Delta}(h)} \right)^2 \right), \quad G(0, h) = G_0 \cos^2(\pi m(h)), \quad (3.31)$$

and

$$G_2(h) = \frac{\cos^2(\pi m(h))}{3} \left\{ \cos^2(\pi m(h)) [1 + 2(R(h) - 1)^2] - \sin^2(\pi m(h)) [3 + (R(h) - 1)^2 (1 + 2\alpha_\omega(h) - 6\alpha_T(h))] \right\}.$$

In figure 3.3 (right) the field dependence of  $G_2(h)$  is shown. Note that we have included a minus sign before the  $T^2$  term in (3.31), so that the similar behaviour in figures 3.3 and 3.3 (right) actually corresponds to opposite temperature dependence. This is due to the approximate inverse relation between the two systems, if the hybridisation  $V = 0$  for an impurity, there is no scattering and hence infinite conductivity, whereas if  $V = 0$  for the quantum dot there is no current and hence infinite resistivity.

The temperature dependence and its scaling with  $T_K$  for zero magnetic field has been observed experimentally by Goldhaber-Gordon et al. (1998a). In finite field there is a sign change in this leading temperature dependence at a values of the magnetic field  $0 < h < T^*$ . A sign change in the second term in the Sommerfeld expansion of equation (3.30) occurs when  $\rho_d$  changes from a local maximum to a minimum (Hewson, Bauer and Koller 2006). Note that this effect, in contrast to the case discussed in the last section, is not unique to the Kondo regime and can also occur for weak coupling. A qualitative explanation of this sign change is that the local spectral density at the Fermi level is suppressed with increasing magnetic field. At higher fields when the spectral density develops two peaks then there are more thermally excited states which can contribute to an increase of the conductance. This temperature dependence could be experimentally observable, since estimates of the Kondo temperature are of the order  $300mK$  corresponding to magnetic fields in the experimental range (Kogan et al. 2004). A difficulty might be that the overall response is reduced by the  $\cos^2(\pi m(h))$  factor in equation (3.31).

## 3.4 Beyond the Low Energy Regime

### 3.4.1 NRG method

We can use the extension of the NRG method to calculate the dynamic response functions, as explained in section 2.1.2, to look at the behaviour of the model in an arbitrary magnetic field on higher energy scales. In doing so it is important to use one of the density matrix extensions as the standard NRG approach gives results which considerably underestimate the shift of the high energy spectral weight with the variation of

## 52 Field dependent quasiparticle dynamics in the Anderson impurity model

magnetic field. We also use the approach, in which the self-energy is deduced from the calculation of higher  $F$ -Green's functions. It can be shown in detail that the magnetisation obtained from integrating the density matrix improved spectra up to the Fermi energy agrees very well with results obtained from static NRG expectation values or the expression using renormalised parameters (3.2) in the weak and strong coupling regime (Hewson, Bauer and Koller 2006). In figure 3.4 (left) we give results for the spin up part of the  $d$ -site spectral density  $\rho_{d,\uparrow}(\omega) = -\frac{1}{\pi}\text{Im}G_{d,\uparrow}(\omega^+)$  for a strong coupling situation ( $U/\pi\Delta = 4$ ) for various values of the magnetic field  $h$ .

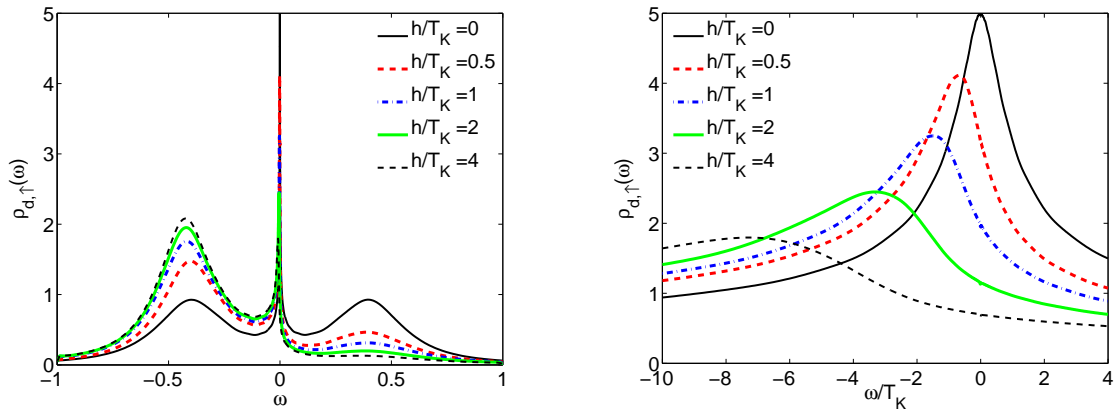


Figure 3.4: Left: Strong coupling ( $U/\pi\Delta = 4$ ) spectral density of the  $d$ -site Green function  $\rho_{d,\uparrow}(\omega)$  for various magnetic fields  $h$ . The energy scale is given by  $4T_K = \pi\tilde{\Delta}$ . Right: Quasiparticle peak for the spectral density of the  $d$ -site Green function  $\rho_{d,\uparrow}(\omega)$ . The energy scale on the left side is set by half the bandwidth  $D = 1$  and on the right  $\omega$ -axis is scaled with  $T_K$ .

The shift of the spin-up Kondo resonance from the Fermi level with increase of magnetic field, which is almost imperceptible on the plot on the left hand side, is accompanied by large shifts of the spectral weight on the higher energy scales as the impurity is magnetically polarised. In figure 3.4 (right), we focus on the effect of the magnetic field on the the quasiparticle (Kondo) resonance. The shift of the resonance from the Fermi level ( $\omega = 0$ ) with increasing magnetic field values is clearly seen on this higher resolution energy scale used for this plot. As the peak shifts, its height decreases and the resonance becomes broader. For even larger fields than shown here the peak merges with the lower atomic limit peak seen in figure 3.4 (left). Note that the peak form is asymmetric with logarithmic tails, similar to the results of Rosch et al. (2003), obtained using the perturbative RG for the Kondo model for large magnetic fields. However, some of the asymmetry in the results must be attributed to the logarithmic broadening scheme (2.12).

If  $-\varepsilon_p(h)$  denotes the position of the quasiparticle peak in the spectral density for a spin up electron, then the corresponding value for non-interacting electrons ( $U = 0$ ) is half the Zeeman splitting,  $\Delta_Z = 2h$ . An exact expression for  $\varepsilon_p(h)/h$  in the limit  $h \rightarrow 0$  has

been derived by Logan and Dickens (2001),

$$\lim_{h \rightarrow 0} \frac{\varepsilon_p(h)}{h} = \frac{R}{1 + b\Delta z^2}, \quad (3.32)$$

where  $R$  is the Wilson ratio and  $b$  is the curvature of the imaginary part of the self-energy at  $\omega = 0$ . The value of  $b$  can be calculated from the renormalised perturbation expansion (Hewson 2001) and the result (3.32) written as

$$\lim_{h \rightarrow 0} \frac{\varepsilon_p(h)}{h} = \frac{R}{1 + (R - 1)^2/2}. \quad (3.33)$$

This ratio, therefore, varies from one in the non-interacting case ( $R = 1$ ) to  $4/3$  in the Kondo limit ( $R = 2$ ). Note that this is a substantial reduction from the free quasiparticle values  $\tilde{\eta}(0) = 2$ . It is not straight forward to obtain a precise estimate of  $b$  or the value of  $\varepsilon_p(h)$  from the NRG spectra as they are sensitive to parameters of the logarithmic scale Gaussian broadening (2.12) which is used to obtain a continuous spectrum on all energy scales from the discrete results. However, if the broadening is modified to Lorentzian peaks with constant width for the very low energy scales the asymptotic results can be confirmed.

We have estimated the ratio  $\varepsilon_p(h)/h$  from the NRG spectra for higher magnetic field values and find that it increases monotonically with  $h$  and exceeds the value of 2 before the peak merges at high field values into the atomic limit peaks. There have been other estimates of the  $h$ -dependence of this ratio (Moore and Wen 2000, Costi 2000, Logan and Dickens 2001), but these differ markedly according to the method of calculation. On the basis of a Bethe ansatz calculation of the spinon spectrum for the Kondo model, Moore and Wen (2000) find that  $\varepsilon_p(h)/h < 2$  in all cases and conjecture that the value of 2 is the high field asymptotic limit. It is possible that this is a feature of the localised model, when charge fluctuations are completely suppressed. There is some evidence in support of this in our results in that, as we suppress the charge fluctuations on increasing the value of  $U$  through the values  $U/\pi\Delta = 2, 3, 4$ , the ratio  $\varepsilon_p(h)/h$  increases less rapidly with increase of  $h$ . The ratio only begins to exceed the value of 2 roughly at the point when charge fluctuations set in and  $R(h)$  begins to differ significantly from the value of  $R(h)$  for the localised model,  $R(h) = 2$ . Costi (2000) has also done NRG calculations for a localised model and finds a ratio close to but always less than 2. Using the local moment approximation Logan and Dickens (2001) have also estimated the ratio  $\varepsilon_p(h)/h$  and find an even more marked increase in the ratio with increase of  $h$  to values such that  $\varepsilon_p(h)/h > 2$ . The scaling of the ratio  $\varepsilon_p(h)/h$  with the Kondo temperature has also quantitatively been studied (Hewson, Bauer and Koller 2006).

### 3.4.2 RPT method

As seen in the last section we could give accurate results for the spectral functions with the NRG method. In this section we would like to use the renormalised perturbation theory

## 54 Field dependent quasiparticle dynamics in the Anderson impurity model

to calculate dynamic response functions. The theory gives asymptotically exact results for the  $\omega$  dependence for the self-energy, when we consider a second order expansion in  $\tilde{U}$ . Here we would like to see to what frequencies we can extend the description by calculating the relevant diagrams in the RPT expansion. The quality of the approximation can be gauged with the NRG results. We will start by considering calculations for the dynamic spin susceptibilities, where it has been shown that the RPT can give very accurate results (Hewson 2006).

### Dynamic Susceptibilities

We calculate the RPT approximation for the dynamic transverse spin susceptibility in a series of repeated quasiparticle scattering as described in section 2.2.3 and discussed by Hewson (2006). This is reminiscent of an RPA approximation, the propagators, however, are expressed in terms of renormalised parameters. Here, we focus on the transverse spin susceptibility  $\chi_t(\omega, h)$ , although the method is also applicable for other susceptibilities (Hewson 2006). The diagrammatic expression was given in figure 2.7, and we want to generalise these earlier results to the case with a magnetic field. Hence, we define the field dependent the pair propagator  $\Pi_{p-\sigma}^{h\sigma}(\omega, h)$  as in equation (2.61),

$$\Pi_{p-\sigma}^{h\sigma}(\omega, h) = - \int \frac{d\omega_1}{2\pi i} \tilde{G}_\sigma^0(\omega + \omega_1) \tilde{G}_{-\sigma}^0(\omega_1). \quad (3.34)$$

The analytic solution is

$$\Pi_{p-\sigma}^{h\sigma}(\omega, h) = \begin{cases} -\text{sgn}(\omega) \left( \frac{1}{i\pi} \frac{1}{\sigma\tilde{\eta}h + i\tilde{\Delta}\text{sgn}(\omega)} + \frac{1}{2\pi\tilde{\Delta}} \log \left( \frac{\sigma\tilde{\eta}h + i\text{sgn}(\omega)\tilde{\Delta}}{-\sigma\tilde{\eta}h + i\text{sgn}(\omega)\tilde{\Delta}} \right) \right) & \text{for } \omega = 2\tilde{\eta}h \\ -\frac{\text{sgn}(\omega)}{i\pi} \left[ \frac{\log \left( \frac{\omega - \sigma\tilde{\eta}h + i\text{sgn}(\omega)\tilde{\Delta}}{\sigma\tilde{\eta}h + i\text{sgn}(\omega)\tilde{\Delta}} \right)}{\omega - 2\sigma\tilde{\eta}h} - \frac{\log \left( \frac{\omega - \sigma\tilde{\eta}h + i\text{sgn}(\omega)\tilde{\Delta}}{-\sigma\tilde{\eta}h + i\text{sgn}(\omega)\tilde{\Delta}} \right)}{\omega - 2\sigma\tilde{\eta}h + 2i\text{sgn}(\omega)\tilde{\Delta}} \right] & \text{otherwise.} \end{cases}$$

Note that  $\Pi_{p\sigma}^{h-\sigma}(\omega, h) = \Pi_{p-\sigma}^{h\sigma}(-\omega, h)$  as can be easily seen, also that for  $\omega = 0$  we find

$$\Pi_{p-\sigma}^{h\sigma}(0, h) = \frac{\tan^{-1} \left( \frac{\tilde{\varepsilon}_{d,\sigma}}{\tilde{\Delta}} \right)}{\pi \tilde{\varepsilon}_{d,\sigma}}, \quad (3.35)$$

where we use  $\tilde{\varepsilon}_{d,\sigma} = \sigma\tilde{\eta}h$ . The full series for  $\chi_t(\omega, h)$  is obtained as

$$\chi_t(\omega, h) = \frac{1}{2} \frac{\Pi_{p-\sigma}^{h\sigma}(\omega, h)}{1 - \tilde{U}_{p-\sigma}^{h\sigma}(h) \Pi_{p-\sigma}^{h\sigma}(\omega, h)}. \quad (3.36)$$

The effective, renormalised vertex  $\tilde{U}_{p-\sigma}^{h\sigma}(h)$  can be determined as described in section 2.2.3 with the help of the exact static result. In the case with finite field we have as in (3.6),

$$\chi_t(0, h) = \frac{m(h)}{2h} = \frac{1}{2\pi h} \tan^{-1}(\tilde{\eta}h/\tilde{\Delta}(h)), \quad (3.37)$$

where we have used the expression for the magnetisation (3.2) in terms of the quasiparticle parameters. This yields for the effective interaction

$$\tilde{U}_{p-\sigma}^{h\sigma}(h) = \frac{\pi h(\tilde{\eta} - 1)}{\tan^{-1}(\tilde{\eta}h/\tilde{\Delta}(h))}. \quad (3.38)$$

Note that there is no explicit dependence on  $\tilde{U}(h)$  in this case. Since, however, the field dependent renormalised parameters are not independent as seen in equation (3.8), the dependence on  $\tilde{U}(h)$  can enter explicitly. In the limit  $h \rightarrow 0$  we find with

$$\lim_{h \rightarrow 0} \tilde{\eta}(h) - 1 = \tilde{U} \tilde{\rho}_d^0(0, 0) \quad (3.39)$$

that

$$\tilde{U}_{p-\sigma}^{h\sigma}(0) = \frac{\tilde{U}}{1 + \tilde{U} \tilde{\rho}_d^0(0, 0)}, \quad (3.40)$$

as before in equation (2.62).

In figure 3.5 we show RPT results for the case  $U/\pi\Delta = 4$  for the imaginary part of  $\chi_t(\omega, h)$  (ph-RPT) in comparison with corresponding results from an NRG calculation.

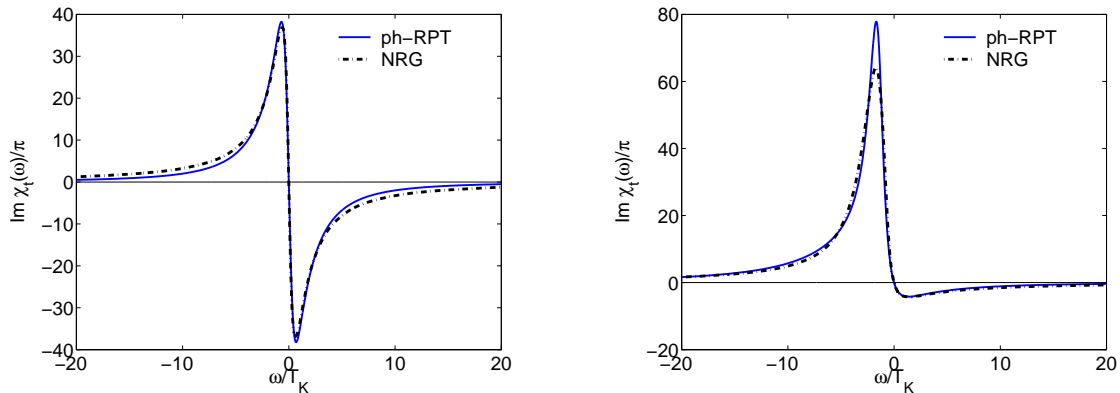


Figure 3.5: The imaginary part of the transverse susceptibility  $h = 0$  (left) and  $h = T_K$  (right). The renormalised perturbation theory results (ph-RPT) are in good agreement with NRG results over the whole frequency range.

We can see in the plots that for zero field (left) that the results agree remarkably well over the full frequency range shown. Also in the case of finite field,  $h = T_K$ , which is shown on the right hand side the curves agree very well apart from the discrepancy in the peak height. The NRG calculation for the susceptibility is based on the complete Anders-Schiller basis. One finds that both the RPT result and the NRG results satisfies the sum rule relating the integral over  $\text{Im}\chi_t(\omega, h)$  to the magnetisation.

In the article by Hewson (2006) it is shown that the RPT results give an accurate description of the spin and charge susceptibilities for zero and finite arbitrary magnetic field values  $H$ , and for frequencies  $\omega$  extending over a range significantly larger than the Kondo temperature  $T_K$ .

### Approximations for the renormalised self-energy

We would like to give a description of the Kondo resonance in magnetic field such as in figure 3.4 (right) in terms of the RPT. A first approximation for the low energy spectrum is given by free the quasiparticle spectrum  $\tilde{\rho}_d^0(\omega)$  as given in equation (1.13). As explained in section 2.2 corrections can be included via a renormalised self-energy  $\tilde{\Sigma}_\sigma(\omega)$ . In order to compare the quality of the RPT approximation for  $\tilde{\Sigma}_\sigma(\omega)$  we would like to compare it with a different result. If the original self-energy of the problem  $\Sigma_\sigma(\omega, h)$  is known,  $\tilde{\Sigma}_\sigma(\omega)$  can be expressed as

$$\tilde{\Sigma}_\sigma(\omega) = z_\sigma(h) \left( \Sigma_\sigma(\omega, h) - \Sigma_\sigma^R(0, h) - \omega \frac{\partial}{\partial \omega} \Sigma_\sigma^R(0, h) \right). \quad (3.41)$$

In the following we will use results for  $\Sigma_\sigma(\omega, h)$  deduced from NRG calculation and equation (3.41) to compare with RPT results.

In figure 3.6 (left) we show the full NRG spectrum (dot-dashed line) for a strong coupling case  $U/\pi\Delta = 4$  for zero field. To see that the RPT approach is in principal valid on all energy scales we have dressed the non-interacting quasiparticles  $\tilde{\rho}_d^0(\omega)$  with a renormalised self-energy as given in (3.41) and added as ‘‘RPT’’ in figure 3.6 (left).

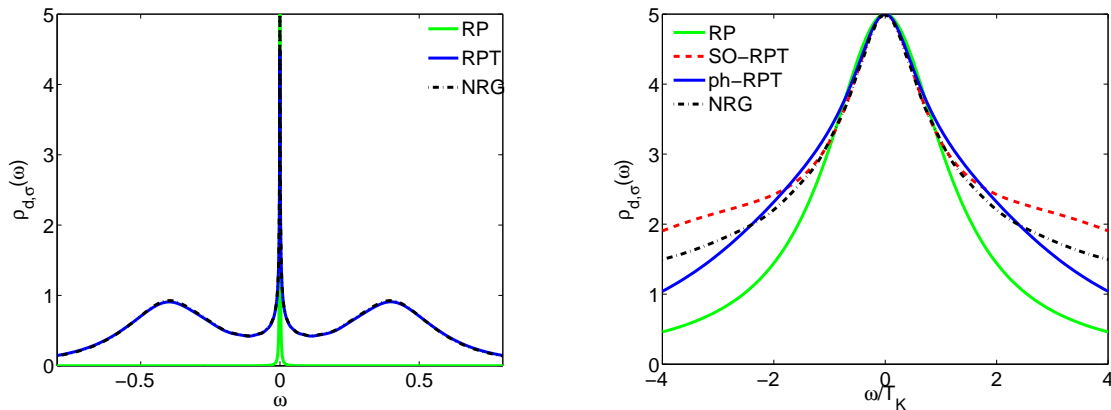


Figure 3.6: Left: Comparison of strong coupling spectra: Renormalised parameters (RP) and spectrum (1.13), Renormalised perturbation theory with full renormalised self-energy (RPT) (3.41) and Numerical Renormalisation Group (NRG). Right: Comparison of the low energy behaviour of the one-particle spectral density for particle hole symmetric case and  $U/\pi\Delta = 4$  calculated in different RPT approximations and the NRG result.

We can see that full agreement with the NRG curve is found. Note that this is not just a trivial rewriting of the propagator, since the renormalised parameters are not calculated from the self-energy, but from the low lying excitations at the fixed point. We have also included the free quasiparticle spectrum  $\tilde{\rho}_d^0(\omega)$  (3.3) in terms of the renormalised parameters (RP), which is seen to describe the very lowest energy behaviour, namely the Kondo resonance.

The simplest dynamic correction to the free quasiparticles from an RPT calculation comes from the second order (SO) diagram [see fig. 2.4 (right)],

$$\Sigma_{\sigma}^{r,(2)}(\omega) = -\tilde{U}^2 \int \frac{d\omega_2}{2\pi i} \Pi_{p-\sigma}^{h\sigma}(\omega_2, h) \tilde{G}_{\sigma}^0(\omega - \omega_2). \quad (3.42)$$

The pair propagator  $\Pi_{p-\sigma}^{h\sigma}(\omega, h)$  is given as in (3.34). As mentioned before this gives the asymptotically exact  $\omega^2$  behaviour for the imaginary part. The corresponding renormalised self-energy is obtained by including the counter-terms, as well. As explained in section 2.2.2 to this order we only need to take into account the trivial counter-terms  $\Sigma_{\sigma}^{ct}(\omega) = -[\lambda_{1,\sigma} + \lambda_{2,\sigma}\omega]$ . In the field dependent case we actually get a finite contribution to  $\lambda_3$  from the vertex diagrams as shown in figure 2.6. This gives, however, no dynamic contribution to the renormalised self-energy as  $\lambda_3 = \mathcal{O}(\tilde{U}(h)^2)$ . The renormalised self-energy to second order is then given by

$$\tilde{\Sigma}_{\sigma}^{(2)}(\omega) = \Sigma_{\sigma}^{r,(2)}(\omega) - [\lambda_{1,\sigma} + \lambda_{2,\sigma}\omega], \quad (3.43)$$

where  $\lambda_{1,\sigma}$  and  $\lambda_{2,\sigma}$  are determined by equation (2.40). Finite order expansions to higher order extend the frequency range where the renormalised self-energy gives an accurate description. A different way of extending the perturbative corrections is to include a certain class of diagrams. As illustrated in the last section this gave accurate RPT results for the transverse spin susceptibility in terms of a repeated quasiparticle scattering series. As well known from the study of metals near a magnetic transition and the analysis of the Kondo problem, spin fluctuations are the crucial processes in this regime. Mathematically, the simplest formulation for that is an RPA-like repeated scattering series, where a typical term for the self-energy is diagrammatically depicted in figure 2.7. The renormalised self-energy corresponding to this process is given by (Bauer et al. 2007a)

$$\Sigma_{\sigma}^{r,\text{ph}}(\omega) = \tilde{U}_1^2 \int \frac{d\omega_2}{2\pi i} 2\chi_t^{\sigma}(\omega - \omega_2, h) \tilde{G}_{-\sigma}^0(\omega_2), \quad (3.44)$$

with  $\chi_t^{\sigma}(\omega, h)$  as given in equation (3.36) with  $\tilde{U}_{p-\sigma}^{h\sigma}$  replaced by  $\tilde{U}_1$ . It is not directly clear for this approach where an infinite series of diagrams is considered what counter-terms have to be included. For the most straight forward expression for the renormalised self-energy  $\tilde{\Sigma}_{\sigma}^{\text{ph}}(\omega)$  in this case we only include the trivial counter-terms  $\Sigma_{\sigma}^{ct}(\omega)$ . The renormalised self-energy in this approximation of repeated particle-hole scattering  $\tilde{\Sigma}_{\sigma}^{\text{ph}}(\omega)$  is then given by an equation like (3.43) and again the parameters  $\lambda_{i,\sigma}$  are determined by the renormalisation conditions (2.40). Such a procedure is not rigorous, but it is adopted here as a first strategy to test this kind of ph-RPT approximation. A formally more satisfactory scheme for calculations with infinite series of diagrams can be given in terms of a self-consistent theory derived from a Luttinger Ward functional. This is described in appendix C.3 and remains for future research to be investigated.

We still have not specified the effective interaction  $\tilde{U}_1$ . This can be done by calculating the full renormalised vertex and using the renormalisation condition (2.41). We proceed

here as outlined in section 2.2.3, where it is argued that for this simple RPA like approximation the full vertex is just a sum of the terms shown in figure 2.7. From this we find with (3.35) and the condition (2.41) that

$$\tilde{U}_1(h) = \frac{\tilde{U}(h)}{1 + \frac{\tilde{U}(h)}{\pi\tilde{\epsilon}_{d,\sigma}} \tan^{-1}(\tilde{\epsilon}_{d,\sigma}/\tilde{\Delta}_\sigma(h))}. \quad (3.45)$$

This reduces to the earlier result (2.64) in the limit  $h \rightarrow 0$ . Note that this expression (3.45) is in general different from expression (3.38) used for the dynamic susceptibilities. The numerical comparison, however, shows that the corresponding values are very similar.

### Results for the dynamics

In the following we compare

- results derived from the renormalised self energy of the second order diagram (SO-RPT), cf. equation (3.43),
- results derived from the renormalised self energy and the repeated quasiparticle scattering (ph-RPT), cf. equation (3.44),
- the renormalised self-energy deduced from an NRG calculation and equation (3.41).

We consider the strong coupling case  $U/\pi\Delta = 4$  first for zero magnetic field,  $h = 0$ . In figure 3.7 (left) we compare the results for the real part of the renormalised self energy for the calculations specified above.

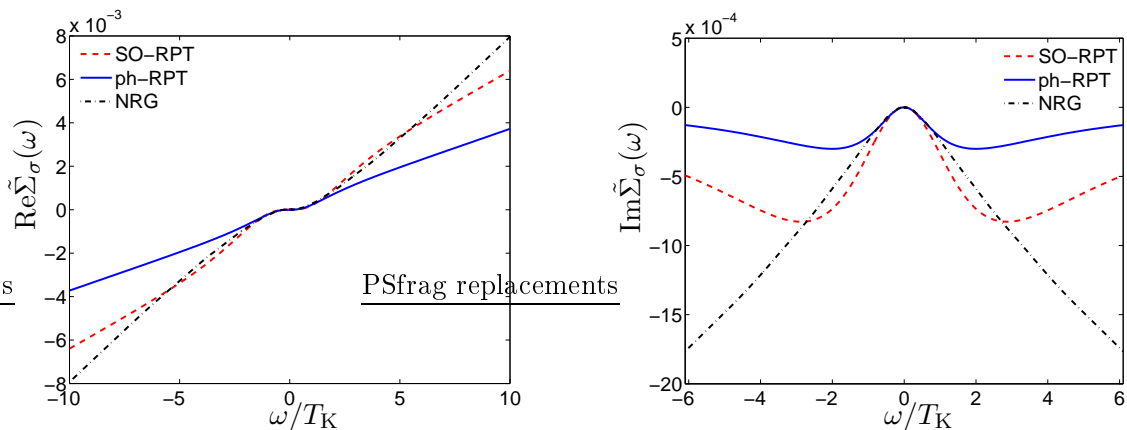


Figure 3.7: Comparison of the dynamics behaviour of the real part (left) and imaginary part (right) of the renormalised self-energy calculated with second order RPT (SO-RPT), repeated particle hole scattering RPT (ph-RPT) and NRG.

We find that that for small  $\omega$  the two perturbative approximations agree, but start to deviate for  $\omega > 2T_K$ . The slope for the real part of the second-order perturbation theory

(SO-RPT) is larger than the repeated particle hole series (ph-RPT); the exact asymptotic behaviour,  $(1 - z)\omega$ , found by the NRG calculated  $\text{Re}\tilde{\Sigma}_\sigma(\omega)$  is not reached by either. Similarly, we compare the imaginary part of the renormalised self-energy as shown in figure 3.7 (right). For small  $\omega$  we find a good agreement for the SO-RPT self-energy the ph-RPT self-energy and the one calculated from (3.41) and the NRG. However, as soon as the Kondo scale is reached the approaches give contributions of quite different magnitude, where the smallest one is found for the repeated scattering diagrams.

In the earlier figure 3.6 on the right, we compare the resulting low energy spectra for free quasiparticles based purely on the renormalised parameters (RP), the two RPT approximations and the direct NRG result. For small  $\omega$  all results agree well. The free quasiparticle spectrum (RP) falls off too rapidly as compared with the NRG result. Both of the two RPT approximations give corrections towards higher energies, but it remains inconclusive which of the two is the better approximation for larger  $\omega$ . It is useful, therefore, to study the situation with a magnetic symmetry breaking in which each component of the spectral density departs from the Fermi energy.

Therefore, we turn our attention now, for the same strong coupling situation with  $U/\pi\Delta = 4$ , to the finite field case. For  $h/T_K = 1$  we can see the results for the spectral density calculated with the different RPT approximations in figure 3.8 (left).

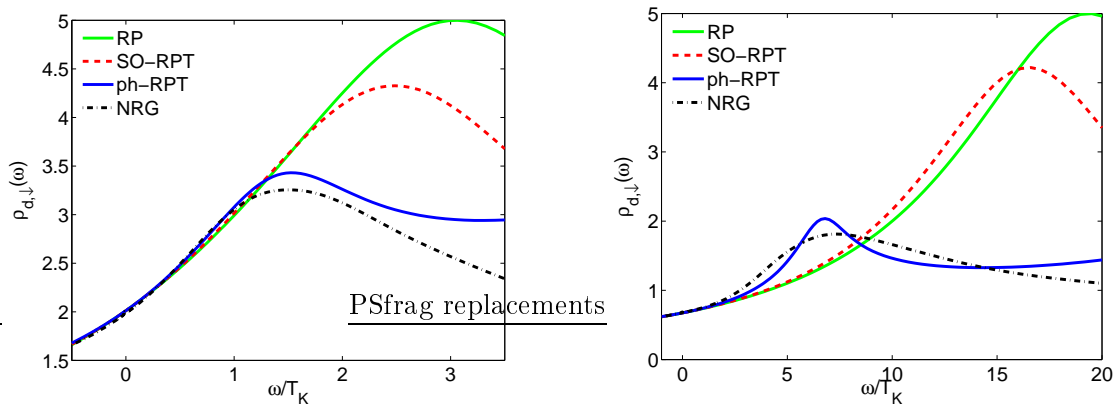


Figure 3.8: Strong coupling spectra in comparison for  $h/T_K = 1$  (left) and for  $h/T_K = 4$  (right).

Unlike in the case of zero field the results for the free quasiparticle propagator (RP) is not at all in agreement with the NRG spectrum. It does not include any suppression of the peak height typical for finite magnetic field. In contrast, one can see that the second order perturbation theory (SO-RPT) gives a dynamic correction in the right direction, albeit too small, whereas the repeated process (ph-RPT) renders a dynamic correction of the right magnitude. Differences in the peak height are visible, but they are rather small. We can see that, whilst for the low energy flank of the peak the agreement is very good, for the

high energy side the RPT results become inaccurate. This, however, is expected, since for higher energies other processes, such as charge fluctuations, will start to play an important role and need to be included in the renormalised self-energy.

In order to understand the discrepancy between the different approximations in terms of the corresponding renormalised self-energy, we plot them in the case  $h/T_K = 1$  in figure 3.9.

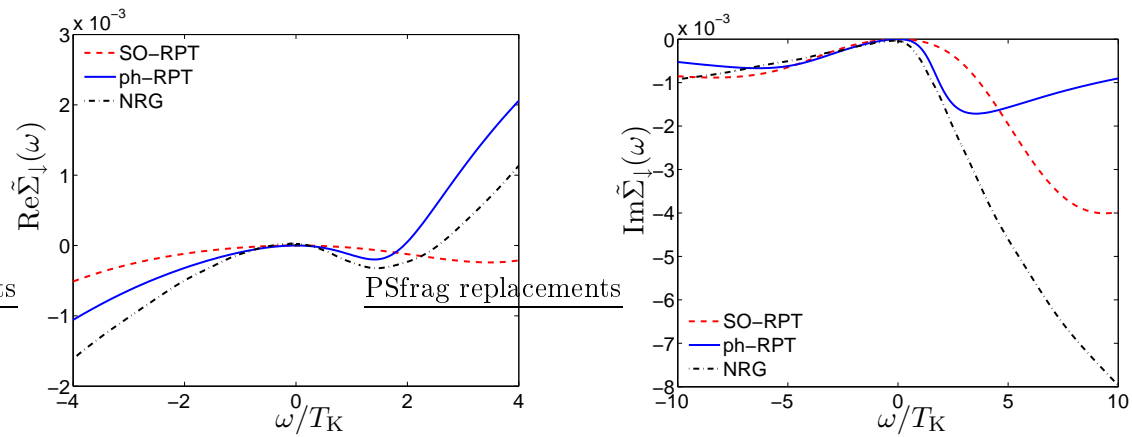


Figure 3.9: Frequency dependence of the real part (left) and imaginary (right) of the renormalised self-energy for  $h/T_K = 1$ .

Generally, we find that whilst the SO-RPT self-energy assumes greater values for higher energies, for small energies,  $\omega < 2T_K$ , there are larger contributions from the ph-RPT series, which are also found in  $\tilde{\Sigma}_\sigma(\omega)$  as computed from (3.41) with the NRG. This effect is seen more pronounced in the imaginary part in figure 3.9 (right). These contributions are important for the correction of the position and width of the Kondo resonance in a finite field starting with field dependent renormalised parameters. Since we find good agreement between the ph-RPT and the NRG result we conclude that up to these energies the chosen repeated quasiparticle series includes the most important contributions for energies up to  $T_K$  (Bauer et al. 2007a).

It is interesting to see up to what magnitudes of field strength the RPT approximation agrees well with the NRG results. For a quite large field,  $h/T_K = 4$ , we display results for the spectral density in figure 3.8 (right). One can see that the ph-RPT agrees quite well with the NRG result. Differences in the peak form of RPT and NRG can be attributed to broadening effects. The interpretation of this behaviour can in a similar way be understood as in the above case for  $h/T_K = 1$ . At higher fields such good agreement is not achieved anymore, and the RPT description is less satisfactory. At such field strengths, however, the Kondo resonance is already suppressed substantially.

Our conclusion from these considerations is, that for the low energy behaviour and not too large magnetic fields  $h \lesssim 4T_K$ , the most important contributions to the renormalised

self-energy are included in the repeated scattering processes shown in figure 2.7. In the presentation here we have deliberately focused on these processes, although other series, such as the ones representing longitudinal spin fluctuations or charge fluctuations could be calculated in a similar way. Such calculations have been carried out and analysed, but it was found that the effect of including these does not alter the results much.

Both the NRG as well as the RPT calculations can be extended to the non-symmetric AIM with magnetic field. The main differences for the case of a magnetic field in situations without particle-hole symmetry is that the wavefunction renormalisation factor  $z_\sigma(h)$  depends on the spin index  $\sigma$ , and as a consequence so does the effective resonance width  $\tilde{\Delta}_\sigma(h)$ , so the equations given earlier for the particle-hole symmetric model have to be generalised. The details for this are given in reference Bauer and Hewson (2007a).

In summary, we have shown in this chapter that the methods of NRG and RPT can be used for the description of the AIM in a magnetic field. We showed that the magnetisation and the static response functions can be well described in terms of the field dependent renormalised parameters. We have used these parameters to calculate the dynamic transverse spin susceptibilities in the RPT formulae and we find excellent results when compared with those obtained from a direct NRG calculation. It was also shown that a good approximation for the renormalised self-energy for frequencies up to the order of the Kondo temperature could be deduced by focusing on the transverse spin fluctuations part in terms of renormalised quasiparticles. The comparison of resulting spectral function for one spin component in a field with NRG gave good agreement for magnetic fields  $h$  up to the order of a few  $T_K$ .



*If there is not complete agreement between the results of one's work and experiment, one should not allow oneself to be too discouraged, because the discrepancy may well be due to minor features that are not properly taken into account and that will get cleared up with further development of the theory.*

Paul A.M. Dirac

## Chapter 4

# The Anderson impurity model in magnetic field in non-equilibrium

In this chapter we extend the RPT calculation for the AIM in magnetic field to the non-equilibrium case. We first discuss the relevant experimental situation and recent results of measurements of the field dependent differential conductance through a quantum dot in the Kondo regime. We analyse how well these results can be understood with theoretical estimates based on equilibrium theory. Then we introduce the non-equilibrium theory for the two-channel AIM and the corresponding RPT. We present asymptotically exact results in the low voltage regime and finite field regime, and also results for the dynamics at higher voltages. All calculations are based on the non-equilibrium RPT with field dependent renormalised parameters.

### 4.1 Transport through a quantum dot

Tunable mesoscopic systems, such as quantum dots, have attracted much attention from experimentalists as well as theorists in recent years. One reason is that they have proved to be extremely useful to study strong correlation physics, such as the Kondo effect (Kouwenhoven and Glazman 2001). This development was stimulated by the extraordinary progress in fabricating, probing and experimentally handling these nanoscale systems, which lead to many accurate measurements of the Kondo behaviour in such structures (Ralph and Buhrman 1994, Cronenwett et al. 1998, Goldhaber-Gordon et al. 1998b, De Franceschi et al. 2002, Kogan et al. 2004, Amasha et al. 2005). As shown by Goldhaber-Gordon et al. (1998a) the equilibrium Kondo effect in quantum dots, such as the scaling of the temperature dependence of the zero bias differential conductance with the Kondo temperature  $T_K$  can be understood quantitatively with the theoretical methods at hand (Hewson 1993a, Costi et al. 1994). In the last chapter we studied in detail the behaviour of quantum dot like system in a magnetic field. Experimentally, this behaviour

is investigated by measurements of the finite bias differential conductance, which really represent a non-equilibrium situation. To understand the experimental results properly it is therefore necessary to establish a full theoretical understanding of the out of equilibrium Kondo physics. We have to distinguish two types of non-equilibrium behaviour here: (a) relaxation from an out of equilibrium state, such as studied in time-dependent reduced density matrix NRG approach (Anders and Schiller 2005) and (b) the voltage  $V$  induced steady state current transport situation. Here we will focus on the latter case. First we will study how well measurements on quantum dots in a magnetic field can be described by equilibrium quantities as calculated in the last chapter.

A general expression for the current through a quantum dot derived in non-equilibrium theory (Hershfield et al. 1991, Meir and Wingreen 1992) reads

$$I = \frac{G_0}{2e} \sum_{\sigma} \int_{-\infty}^{\infty} d\omega [f_L(\omega) - f_R(\omega)] \frac{4\Gamma_L\Gamma_R}{\Gamma_L + \Gamma_R} [-\text{Im}G_{d\sigma}^{\text{ret}}(\omega, eV_{ds})], \quad (4.1)$$

where  $G_{d\sigma}^{\text{ret}}(\omega, eV_{ds})$  is the steady state retarded Green's function on the dot site, and  $f_L(\omega)$ ,  $f_R(\omega)$  are Fermi distribution functions for the electrons in the left and right reservoirs, respectively,  $f_{\alpha}(\omega) = n_{\text{F}}(\omega - \mu_{\alpha})$ ,  $n_{\text{F}}(\omega) = [1 + e^{\beta\omega}]^{-1}$ . Usually the chemical potentials are given by  $\mu_L = \mu_d + eV/2$  and  $\mu_R = \mu_d - eV/2$ , where  $V_{\text{ds}} = V$  is the source drain voltage and  $\mu_d$  is the chemical potential on the quantum dot.  $\Gamma_L$  and  $\Gamma_R$  describe the coupling to the left and right lead, respectively, and  $G_0 = e^2/\pi\hbar$  is the quantum conductance limit in mesoscopic transport with Planck's constant  $\hbar$ . All these quantities relate to the formulation of the two channel Anderson model, which is depicted in figure 4.3. For symmetric coupling to the leads we have  $\Gamma_L = \Gamma_R = \Delta/2$ .

Equation (4.1) is a generalisation of the earlier expression (3.30) for the linear response differential conductance  $G = dI/dV$ . The differential conductance is the quantity which can be accessed experimentally and therefore (4.1) provides the connection between the theoretically obtained Green's function  $G_{d\sigma}^{\text{ret}}(\omega, eV)$  and the measured current through a quantum dot.

Quantum dot experiments (Kogan et al. 2004, Amasha et al. 2005) in the presence of a magnetic field have been performed in non-equilibrium situations with a finite source-drain voltage  $V$ . In the last chapter we had seen that in a magnetic field the Kondo resonance is shifted from the position at the Fermi level. Therefore, for field strengths larger than a critical value  $h_c$  two peaks can be observed in the differential conductance as a function of the voltage  $V$ . There have been several interpretations (Moore and Wen 2000, Logan and Dickens 2001) of these results based on the approximation of using the equilibrium Green's function to evaluate  $G_{d\sigma}^{\text{ret}}(\omega, eV)$  in (4.1). With this approximation at  $T = 0$  we get an expression for the differential conductance  $G(V)$  as a function of the voltage  $V$ ,

$$G(V) = \frac{dI}{dV} = \frac{G_0\pi\Delta}{2} \rho_d(eV/2). \quad (4.2)$$

In this approximation  $G(V)$  is directly proportional to the total equilibrium spectral density  $\rho_d = \rho_{d,\uparrow} + \rho_{d,\downarrow}$  evaluated at  $\omega = eV/2$ , which is shown in figure 4.1 for the parameters used earlier ( $U/\pi\Delta = 4$ ) and a range of magnetic fields. The peak splits above a critical field,  $h_c \gtrsim 0.5T_K$ , which in agreement with results for the Kondo model (Costi 2000). A

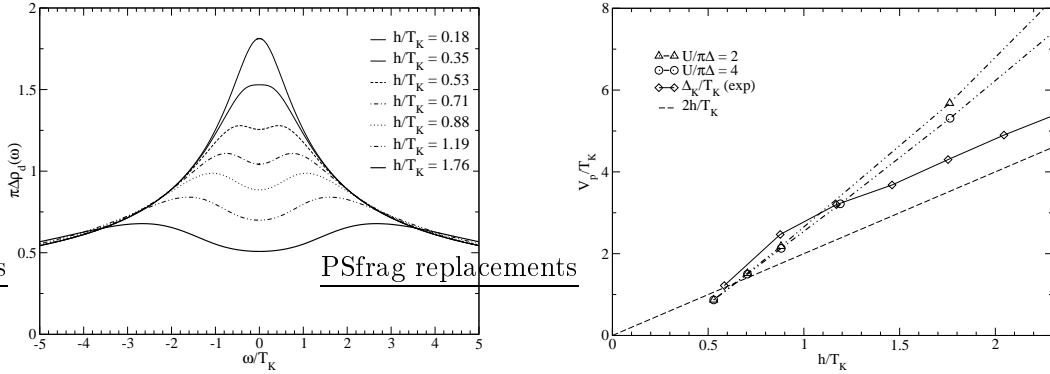


Figure 4.1: Left: Total spectral density of the d-site  $\rho_d(\omega)$  for various fields  $h$ . One can see that the peak splitting becomes visible only for fields  $h \gtrsim 0.5T_K$ . Right: We compare the peak position in the differential conductivity  $V_p$ , as deduced from equation (4.2) and the NRG results for  $\rho_d(\omega)$ , with  $V_{p,\text{exp}} = \Delta_K$  deduced from experiment Kogan et al. (2004). The Kondo temperature is inferred from the critical field for the peak splitting to be observed,  $B_c^{(\text{exp})} \approx 2\text{T}$  and the strong coupling result  $h_c \approx 0.584T_K$ , which is derived later in this chapter.

maximum of the differential conductance, occurs when one of the quasiparticle peaks in the spectral density is coincident with the left Fermi level at  $\mu_d + eV_{ds}/2$  and at the same time the other peak coincides with the right Fermi level,  $\mu_d - eV_{ds}/2$ . This is illustrated schematically in figure 4.2.

It is important to be careful when quantifying the magnitude of the splitting of the Kondo resonance for fields larger than the critical field,  $h > h_c$ . In the interpretation of the experimental results of  $dI/dV_{ds}$  the splitting of the Kondo resonance  $\Delta_{\text{Kondo}}^{(\text{exp})}$  was identified with the voltage splitting seen in the differential conductance  $e(V_{ds}^+ - V_{ds}^-) = \Delta_{\text{Kondo}}^{(\text{exp}),V}$  (Kogan et al. 2004, Amasha et al. 2005). We had denoted the peak position of one spin component of the Kondo resonance in the spectral density by  $\varepsilon_p(h)$  in the last chapter. The splitting between the up and down peaks in the total spectrum is  $\Delta_{\text{Kondo}}^{(\text{theo}),\omega} = 2\varepsilon_p(h)f_c(h)$ , where  $f_c(h)$  is a correction factor due to the overlap of the resonances (Hewson et al. 2005). It is common to compare the Kondo splitting with the Zeeman splitting  $\Delta_Z = 2h$ . It should be noted that results based on equation (4.2) include the change in the chemical potential on the dot  $\mu_d$  with the applied voltage  $V$ ,<sup>1</sup> and the Kondo resonance, being a many-body

<sup>1</sup>It is assumed that  $\mu_d$  always is at the average position of  $\mu_L$  and  $\mu_R$ , which for  $\Gamma_L = \Gamma_R$  is most reasonable.

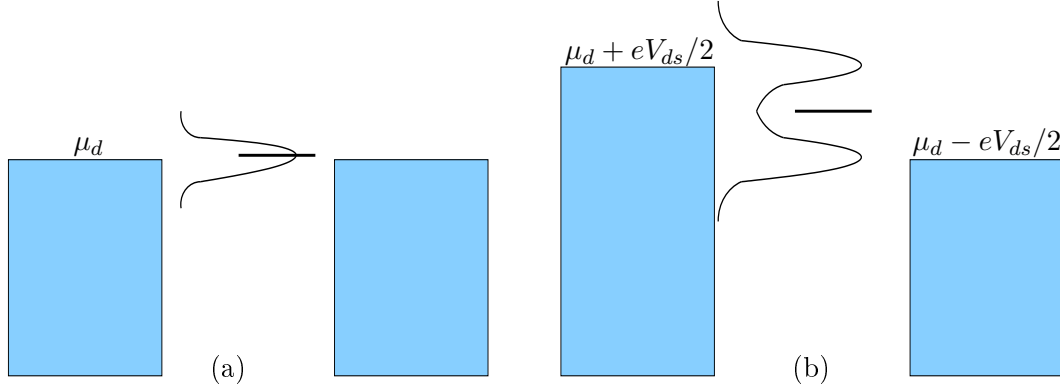


Figure 4.2: A schematic plot of the spectrum on the dot and chemical potentials for left/right lead ( $\mu_d \pm eV/2$ ) and dot ( $\mu_d$ ) for (a) zero bias and zero magnetic field and (b) finite voltage and finite field.

resonance is tied to this chemical potential (Hewson et al. 2005), as illustrated in figures 4.2. Therefore, as seen in equation (4.2) voltage and frequency arguments,  $eV$  and  $\omega$ , respectively, are related by a factor of two, hence  $\Delta_{\text{Kondo}}^{(\text{exp}),V} = 2\Delta_{\text{Kondo}}^{(\text{exp}),\omega}$  for Kondo splitting in the spectral density. Therefore, if experimentally a splitting in the differential conductance is identified as larger than twice the Zeeman splitting,  $\Delta_{\text{Kondo}}^{(\text{exp}),V} > 2\Delta_Z$ , based on (4.2) it implies that the corresponding Kondo splitting in the spectral density is merely larger than the Zeeman splitting,  $\Delta_{\text{Kondo}}^{(\text{exp}),\omega} > \Delta_Z$ , differing by a factor of 2 from the conclusion in reference Kogan et al. (2004).

To test whether the experimental results can be explained on the basis of equation (4.2), we have extracted the voltage peak position  $V_p$  which corresponds to half the magnitude of the peak splitting for  $U/\pi\Delta = 2, 4$  and a range of fields. The comparison with experimental results (Kogan et al. 2004) is displayed in figure 4.1 (right). We can see there that, whilst there is an agreement in the range  $h/T_K \simeq 0.5 - 1$ , in general there does not appear to be a satisfactory quantitative explanation of the experimental results based on approximating the non-equilibrium Green's function by the equilibrium one as the splitting of the Kondo resonance is overestimated like this. We conclude that an agreement of experimental and theoretical results rests on an accurate description of the steady state situation out of equilibrium. In fact, one must stress that source drain voltage sweeps for the differential conductance in quantum dot systems do not give direct information about the equilibrium density of states as sometimes assumed. We will therefore in the remainder of this chapter extend our analysis to the non-equilibrium transport situation and start by giving the formal setup for the two channel AIM.

## 4.2 Formal setup for the non-equilibrium theory

### 4.2.1 The two channel Anderson model and Keldysh formalism

In this section we consider a transport situation through a local interacting system, like a quantum dot (QD). The Hamiltonian has the general form corresponding to the sketch in figure 4.3,

$$H = H_L + H_{TL} + H_D + H_{TR} + H_R. \quad (4.3)$$

$H_\alpha$  ( $\alpha = L, R$ ) describes the left and right lead, respectively,

$$H_\alpha = \sum_{\mathbf{k}, \sigma} \varepsilon_{\mathbf{k}\alpha} c_{\mathbf{k}, \sigma, \alpha}^\dagger c_{\mathbf{k}, \sigma, \alpha} = - \sum_{i, j, \sigma} t_{ij}^\alpha c_{i, \sigma}^\dagger c_{j, \sigma}. \quad (4.4)$$

We assume  $i, j < 0$  for the operators in the left lead  $\alpha = L$  and  $i, j > 0$  for  $\alpha = R$ .  $\varepsilon_{\mathbf{k}\alpha} = \varepsilon_{\mathbf{k}} + \mu_\alpha$  includes the left and right chemical potential and gives the dispersion for the tight-binding chain form in (4.4).

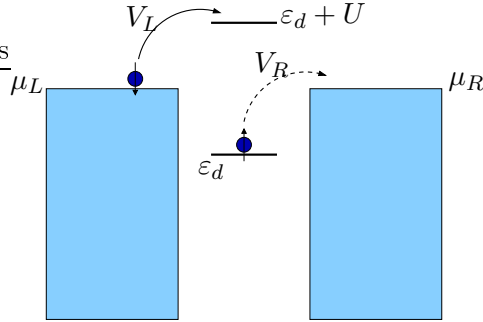


Figure 4.3: A schematic picture of the two channel Anderson model.

$H_{T\alpha}$  is the tunnelling term between lead  $\alpha$  and the dot. We can collect the left and right contribution to a mixing term of the form

$$H_{\text{mix}} = - \sum_{\sigma} V_L (c_{d, \sigma}^\dagger c_{-1, \sigma} + \text{h.c.}) - \sum_{\sigma} V_R (c_{1, \sigma}^\dagger c_{d, \sigma} + \text{h.c.}). \quad (4.5)$$

$H_D$  describes the isolated local system, which will in our case be an interacting Anderson s-level impurity,

$$H_D = \sum_{\sigma} \varepsilon_{d, \sigma} c_{d, \sigma}^\dagger c_{d, \sigma} + U c_{d, \uparrow}^\dagger c_{d, \uparrow} c_{d, \downarrow}^\dagger c_{d, \downarrow} \equiv H_{D, 0} + H_{D, U}. \quad (4.6)$$

We have allowed for a local magnetic field  $h = g\mu_B H/2$ . To consider the transport problem we employ the Keldysh formalism (Keldysh 1965, Rammer and Smith 1986) and follow the formulation of Caroli et al. (1971). Thus,  $H_1 = H_L + H_R + H_{D, 0}$  is the equilibrium starting point and the term  $H_2(t) = e^{-\delta|t|} (H_{\text{mix}} + H_{D, U})$  is adiabatically switched on. The main aim is to calculate the on-site retarded non-equilibrium Green's function  $G_{d\sigma}^{\text{ret}}(\omega, eV)$ , which

determines the current through the interacting quantum dot as seen in equation (4.1). This can be done by a perturbation theory, which is set up in analogy to the equilibrium case. In order to avoid the unknown ground state at  $t = \infty$ , one has to work with additional Green's function on the Keldysh contour  $C_K$  as depicted in figure 4.4. This is conveniently done by introducing  $2 \times 2$  matrices in Keldysh space (Keldysh 1965, Rammer and Smith 1986, Zagoskin 1998, Oguri 2006).



Figure 4.4: Keldysh Contour

The non-interacting two-channel problem can be dealt with explicitly. We assume wide conduction bands and the mixing of quantum dot with the leads is described by the hybridisation constants  $\Gamma_\alpha(\omega) = -V_\alpha^2 \text{Im}g_\alpha^{\text{ret}}(\omega) \equiv \Gamma_\alpha$  (Oguri 2006). Here, the retarded left and right lead Green's functions are  $g_{-1-1}^{\text{ret}}(\omega) = g_L^{\text{ret}}(\omega)$  and  $g_{11}^{\text{ret}}(\omega) = g_R^{\text{ret}}(\omega)$ . One finds the local unperturbed Green's function

$$\underline{G}_{d,\sigma}^{(0)}(\omega) = \begin{pmatrix} G_{d,\sigma}^{(0),--}(\omega) & G_{d,\sigma}^{(0),-+}(\omega) \\ G_{d,\sigma}^{(0),+-}(\omega) & G_{d,\sigma}^{(0),++}(\omega) \end{pmatrix}, \quad (4.7)$$

where the  $-/+$  index corresponds to the first/second part of the Keldysh contour  $C_K$ , respectively. The matrix elements, which include the voltage dependence explicitly, are given by

$$G_{d,\sigma}^{(0),--}(\omega) = \frac{\omega - \varepsilon_{d,\sigma} - i\Delta(1 - 2f_{\text{eff}}(\omega))}{(\omega - \varepsilon_{d,\sigma})^2 + \Delta^2}, \quad (4.8)$$

$$G_{d,\sigma}^{(0),-+}(\omega) = \frac{2i\Delta f_{\text{eff}}(\omega)}{(\omega - \varepsilon_{d,\sigma})^2 + \Delta^2}, \quad (4.9)$$

$$G_{d,\sigma}^{(0),+-}(\omega) = \frac{-2i\Delta(1 - f_{\text{eff}}(\omega))}{(\omega - \varepsilon_{d,\sigma})^2 + \Delta^2}, \quad (4.10)$$

and  $G_{d,\sigma}^{(0),++}(\omega) = -G_{d,\sigma}^{(0),--}(\omega)^*$ . We have defined  $\Delta = \Gamma_L + \Gamma_R$  and introduced the function

$$f_{\text{eff}}(\omega) = \frac{\Gamma_L f_L(\omega) + \Gamma_R f_R(\omega)}{\Gamma_L + \Gamma_R}. \quad (4.11)$$

We will assume in the following  $\mu_d = 0$  such that  $\mu_L = eV/2$  and  $\mu_R = -eV/2$ . The emphasis for the calculation in this chapter is laid on zero temperature, such that  $n_F(\omega) = 1 - \theta(\omega)$ .

In the interacting theory the full Green's function is given by the Dyson matrix equation

$$\underline{G}_{d,\sigma}(\omega)^{-1} = \underline{G}_{d,\sigma}^{(0)}(\omega)^{-1} - \underline{\Sigma}_{d,\sigma}(\omega). \quad (4.12)$$

The components of this self-energy  $\underline{\Sigma}_{d,\sigma}(\omega)$  can be determined in perturbation theory, which is conveniently described in the path integral formalism (Oguri 2005, 2006). Thus

the Anderson model for transport through a quantum dot in the Keldysh formalism is characterised by the effective action  $S = S_0 + S_U$  with

$$S_0 = \sum_{\sigma} \int_{-\infty}^{\infty} dt \int_{-\infty}^{\infty} dt' \bar{\mathbf{d}}_{\sigma}(t) \underline{G}_{d,\sigma}^{(0)}(t-t')^{-1} \mathbf{d}_{\sigma}(t') \quad (4.13)$$

where  $\mathbf{d}_{\sigma}(t) := {}^t(d_{\sigma,-}(t), d_{\sigma,+}(t))$  and

$$\underline{G}_{d,\sigma}^{(0)}(t-t')^{-1} = \frac{1}{2\pi} \int d\omega \underline{G}_{d,\sigma}^{(0)}(\omega)^{-1} e^{-i\omega(t-t')}.$$

$\underline{G}_{d,\sigma}^{(0)}(\omega)$  is given in (4.7). The interaction term reads

$$S_U = -U \int_{-\infty}^{\infty} dt (n_{d,\uparrow,-}(t)n_{d,\downarrow,-}(t) - n_{d,\uparrow,+}(t)n_{d,\downarrow,+}(t)). \quad (4.14)$$

The partition function of the model is given by

$$\mathcal{Z} = \int \mathcal{D}(\mathbf{d}_{\sigma}, \bar{\mathbf{d}}_{\sigma}) e^{iS[\mathbf{d}_{\sigma}, \bar{\mathbf{d}}_{\sigma}]}. \quad (4.15)$$

Comparing this with the results in section 2.2.1, we can see that the theory has the same structure as in equilibrium with the only difference that we have to take into account the additional degrees of freedom in matrix form.

### Non-equilibrium renormalised perturbation theory

We also have to generalise the setup of the renormalised perturbation theory from chapter 2 to the non-equilibrium case. The details for this are given in appendix C.4. The renormalised parameters are defined for zero temperature and in the equilibrium limit,  $eV \rightarrow 0$ , and we can therefore for their definition focus on the equilibrium retarded self-energy  $\Sigma_{\sigma}^{\text{ret}}(\omega)$ . In the Keldysh formalism it is generally given by

$$\Sigma_{\sigma}^{\text{ret}}(\omega) = \Sigma_{\sigma}^{-}(\omega) + \Sigma_{\sigma}^{-+}(\omega). \quad (4.16)$$

As seen in chapters 2 and 3 for the equilibrium RPT it is useful to include the magnetic field dependence in the self-energy, and then the definition of the parameters essentially coincide with (2.33) and (2.34) with  $\Sigma_{\sigma}(\omega) \rightarrow \Sigma_{\sigma}^{\text{ret}}(\omega)$ . The renormalised interaction  $\tilde{U}(h)$  is defined as before by the effective quasiparticle interaction of the problem, which is given by the full renormalised four point vertex function at zero frequency (2.37). Note that the renormalisation conditions (2.40) and (2.41) only have to be satisfied in the equilibrium limit. The matrix for the non-interacting Green's function in terms of the renormalised parameters is

$$\tilde{\underline{G}}_{d,\sigma}^{(0)}(\omega) = \begin{pmatrix} \tilde{G}_{d,\sigma}^{(0),--}(\omega) & \tilde{G}_{d,\sigma}^{(0),-+}(\omega) \\ \tilde{G}_{d,\sigma}^{(0),+-}(\omega) & \tilde{G}_{d,\sigma}^{(0),++}(\omega) \end{pmatrix}, \quad (4.17)$$

where the matrix elements are given by [cf. (4.8)-(4.10)]

$$\tilde{G}_{d,\sigma}^{(0),--}(\omega) = \frac{\omega - \tilde{\varepsilon}_{d,\sigma} - i\tilde{\Delta}_\sigma(1 - 2f_{\text{eff}}(\omega))}{(\omega - \tilde{\varepsilon}_{d,\sigma})^2 + \tilde{\Delta}_\sigma^2}, \quad (4.18)$$

$$G_{d,\sigma}^{(0),-+}(\omega) = \frac{2i\tilde{\Delta}_\sigma f_{\text{eff}}(\omega)}{(\omega - \tilde{\varepsilon}_{d,\sigma})^2 + \tilde{\Delta}_\sigma^2}, \quad (4.19)$$

$$G_{d,\sigma}^{(0),+-}(\omega) = \frac{-2i\tilde{\Delta}_\sigma(1 - f_{\text{eff}}(\omega))}{(\omega - \tilde{\varepsilon}_{d,\sigma})^2 + \tilde{\Delta}_\sigma^2}, \quad (4.20)$$

and  $\tilde{G}_{d,\sigma}^{(0),++}(\omega) = -\tilde{G}_{d,\sigma}^{(0),--}(\omega)^*$ . The renormalised perturbation theory can be set up in the one-particle irreducible scheme as described in section 2.2.2 and we only have to respect the matrix structure (see appendix C.4). We will be mainly interested in calculating the retarded renormalised self-energy (4.16). Therefore, we can focus on the combinations  $\lambda_i^{\text{ret}} \equiv \lambda_i^{--} + \lambda_i^{+-}$  for the counter-terms, and in the simplest case determine the value directly by the renormalisation condition (2.40), such that

$$\lambda_1^{\text{ret}} = \Sigma_\sigma^{r,--}(0) + \Sigma_\sigma^{r,+}(0) \quad (4.21)$$

and

$$\lambda_2^{\text{ret}} = \frac{\partial}{\partial \omega} (\Sigma_\sigma^{r,--}(\omega) + \Sigma_\sigma^{r,+}(\omega))|_{\omega=0}. \quad (4.22)$$

$\Sigma_\sigma^{r,\alpha\beta}$  is the self-energy calculated perturbatively, and in the above equations we take the limit  $eV \rightarrow 0$ . The voltage dependent renormalised retarded self-energy is then given by

$$\tilde{\Sigma}_\sigma^{\text{ret}}(\omega, eV) = \Sigma_\sigma^{r,--}(\omega, eV) + \Sigma_\sigma^{r,+}(\omega, eV) - \lambda_2^{\text{ret}}\omega - \lambda_1^{\text{ret}}. \quad (4.23)$$

We will give an example for the diagrammatic expansion for the second order diagrams for  $T = 0$ . The diagrams are of the same form as the one sketched in figure 2.4 (right), however, the vertices can enter with different sign  $\pm$  depending on which part of the contour they corresponds to. The convention here for the Feynman rules is a “+”-sign for the vertex on the lower contour (−) and a “−”-sign for the vertex on the upper contour (+). The earlier introduced pair propagator (2.61) becomes a matrix in Keldysh space  $\mathbf{\Pi}_{p-\sigma}^{h\sigma}$ ,

$$\mathbf{\Pi}_{p-\sigma}^{h\sigma} = \begin{pmatrix} \Pi_{p-\sigma}^{h\sigma,(-)} & \Pi_{p-\sigma}^{h\sigma,(-+)} \\ \Pi_{p-\sigma}^{h\sigma,(+-)} & \Pi_{p-\sigma}^{h\sigma,(+)} \end{pmatrix}, \quad (4.24)$$

whose matrix elements are given by

$$\Pi_{p-\sigma}^{h\sigma,(-)}(\omega) = i \int \frac{d\omega_1}{2\pi} \tilde{G}_{d,\sigma}^{(0),--}(\omega + \omega_1) \tilde{G}_{d,-\sigma}^{(0),--}(\omega_1), \quad (4.25)$$

$$\Pi_{p-\sigma}^{h\sigma,(-+)}(\omega) = i \int \frac{d\omega_1}{2\pi} \tilde{G}_{d,\sigma}^{(0),-+}(\omega + \omega_1) \tilde{G}_{d,-\sigma}^{(0),+-}(\omega_1), \quad (4.26)$$

$$\Pi_{p-\sigma}^{h\sigma,(+-)}(\omega) = i \int \frac{d\omega_1}{2\pi} \tilde{G}_{d,\sigma}^{(0),+-}(\omega + \omega_1) \tilde{G}_{d,-\sigma}^{(0),-+}(\omega_1) \quad (4.27)$$

and  $\Pi_{p-\sigma}^{h\sigma,(++)}(\omega) = -[\Pi_{p-\sigma}^{h\sigma,(--)}(\omega)]^*$ . All four pair propagators can be calculated analytically for finite voltage and magnetic field. The resulting expressions are, however, long and not very instructive. The negative spin expressions for the Green's functions yield

$$\Pi_{p\sigma}^{h-\sigma,(--)}(\omega, h) = \Pi_{p-\sigma}^{h\sigma,(--)}(-\omega, h) \quad (4.28)$$

and  $\Pi_{p\sigma}^{h-\sigma,(+-)}(\omega, h) = \Pi_{p-\sigma}^{h\sigma,(+-)}(-\omega, h)$ . The matrix elements of the second order self-energy read ( $\alpha, \beta = \pm$ )

$$\Sigma_{\sigma}^{r(2)\alpha\beta}(\omega) = -(\alpha\beta) \frac{\tilde{U}^2}{2\pi i} \int d\omega_2 \Pi_{p-\sigma}^{h\sigma,(\alpha\beta)}(\omega - \omega_2) \tilde{G}_{d,-\sigma}^{(0)\alpha\beta}(\omega_2). \quad (4.29)$$

For the symmetric AIM and symmetric coupling to the dot  $\Gamma_L = \Gamma_R = \Delta/2$ , and we have  $f_{\text{eff}}(\omega) = [f(\omega - eV/2) + f(\omega + eV/2)]/2$ , which is symmetric for  $V \rightarrow -V$ . Since the only dependence in the free Green's functions comes from this factor, the self-energies satisfy

$$\Sigma_{\sigma}^{r(2)\alpha\beta}(\omega, -eV) = \Sigma_{\sigma}^{r(2)\alpha\beta}(\omega, eV). \quad (4.30)$$

By examining the specific expressions for the Green's function (4.18)-(4.20) we also find for the retarded renormalised self-energy (4.16) in the second order expansion that

$$\tilde{\Sigma}_{-\sigma}^{(2)\text{ret}}(\omega) = -\tilde{\Sigma}_{\sigma}^{(2)\text{ret}}(-\omega)^*. \quad (4.31)$$

Hence, to second order it is enough to calculate, say, the spin up retarded Green's function and the other one can be inferred from (4.31).

### 4.2.2 Low voltage asymptotics for the self-energy

Asymptotically exact results for the small voltage dependence of the self-energy have been derived by Oguri (2001, 2005). His arguments are based on Ward identities and relate the derivative of the self-energy to the equilibrium vertex function. The considerations can be viewed as an extension of the exact results by Yamada (1975b) for the  $\omega$  dependence. These exact results are reproduced by a second order renormalised perturbation expansion in  $\tilde{U}$  in the Keldysh formalism (Oguri 2005) which yields

$$\tilde{\Sigma}(\omega, V_{ds}) = -ic \left[ \omega^2 + \frac{3}{4}(eV_{ds})^2 \right], \quad \text{with } c = \frac{1}{2\Delta} \left( \frac{\tilde{U}}{\pi\tilde{\Delta}} \right)^2. \quad (4.32)$$

When a magnetic field is included this result can be generalised in the renormalised perturbation theory framework (Hewson et al. 2005). Starting point is equation (4.29) for the second order self-energy diagram. The retarded self-energy is given by the combination in equation (4.16).  $\Sigma^{-}$  is purely imaginary, and therefore for the real part contribution we only have to consider  $\Sigma^{--}$  as given in (4.29). For  $T = 0$  we can expand

$$f_{\text{eff}} = \frac{1}{2}(f_L(\omega) + f_R(\omega)) = 1 - \theta(\omega) - \frac{(eV)^2}{8} \delta'(\omega). \quad (4.33)$$

The Green's function  $\tilde{G}_{d,\sigma}^{(0),--}$  can thus be expressed as

$$G_{d,\sigma}^{(0),--}(\omega) = \frac{\omega - \tilde{\varepsilon}_{d,\sigma} - i\tilde{\Delta}(2\theta(\omega) - 1)}{(\omega - \tilde{\varepsilon}_{d,\sigma})^2 + \tilde{\Delta}^2} - \frac{i\tilde{\Delta}\delta'(\omega)(eV)^2/4}{(\omega - \tilde{\varepsilon}_{d,\sigma})^2 + \tilde{\Delta}^2}, \quad (4.34)$$

where the first term is identical to the equilibrium  $T = 0$  causal Green's function. This means that the  $(eV)^2$ -term is found by three terms where in each of them one Green's function is replaced by the second term in (4.34) and the other two are equilibrium Green's functions. Comparing this with equation (3.23) we see that this expansion is apart from the prefactor completely analogous to the low order temperature expansion in the last chapter. We find that the renormalised self-energy for finite field  $h$  to order  $\omega^2$  and  $V_{ds}^2$  can be expressed in the form,

$$\tilde{\Sigma}_\sigma(\omega, V_{ds}) = -c(h) \left[ i \left( \omega^2 + 3 \left( \frac{eV_{ds}}{2} \right)^2 \right) + \frac{\tilde{\varepsilon}_{d,\sigma}(h)}{\tilde{\Delta}(h)} \left( \alpha_\omega(h)\omega^2 + \alpha_V(h) \left( \frac{eV_{ds}}{2} \right)^2 \right) \right], \quad (4.35)$$

where

$$c(h) = \frac{\pi\tilde{U}^2(h)[\tilde{\rho}_d^0(0, h)]^3}{2}. \quad (4.36)$$

The quasiparticle density of states  $\tilde{\rho}_{d,\sigma}^0(\omega, h)$  is given in equation (3.3). The coefficient  $\alpha_\omega(h)$  for the expansion of the real part of  $\tilde{\Sigma}_\sigma(\omega, V_{ds})$  is given as in equation (3.21). The result for  $\tilde{\alpha}_V(h)$  is

$$\alpha_V(h) = 3 + \frac{\tilde{\Delta}(h)}{2\tilde{\rho}_d^0(0, h)\pi\tilde{\varepsilon}_{d,\sigma}(h)^2} \left[ 1 - \frac{\tilde{\varepsilon}_{d,\sigma}(h)}{\tilde{\Delta}(h)} \tan^{-1} \left( \frac{\tilde{\varepsilon}_{d,\sigma}(h)}{\tilde{\Delta}(h)} \right) \left( 4 + \frac{\tilde{\Delta}(h)}{\tilde{\rho}_d^0(0, h)\pi\tilde{\varepsilon}_{d,\sigma}(h)^2} \right) \right]. \quad (4.37)$$

In the limit  $h \rightarrow 0$  equation (4.35) reduces to (4.32). For a certain magnetic field  $h$  the coefficient  $\alpha_V(h)$  changes sign and thus the asymptotics of the real part of the voltage dependence. In a generic strong coupling situation  $U/\pi\Delta = 4$  this happens for  $h_c \simeq 0.46T_K$ . Also in the large voltage limit asymptotic exact results can be derived (Oguri 2002).

### 4.3 Differential conductance for low voltage

In this section we will employ the asymptotically exact results for small voltage to study the behaviour of the differential conductance. Starting from (4.1), for particle hole symmetry we can express the differential conductance for zero temperature as

$$\frac{dI}{dV} = \frac{G_0\Delta}{2} \sum_\sigma \left( -\text{Im}G_{d\sigma}^{\text{ret}}(eV/2, eV) \right) + \frac{G_0\Delta}{e} \sum_\sigma \int_0^{eV/2} d\omega \left[ -\text{Im} \frac{\partial G_{d,\sigma}^{\text{ret}}(\omega, eV)}{\partial eV} \right]. \quad (4.38)$$

If the voltage dependence of  $G_{d\sigma}^{\text{ret}}(\omega, eV)$  was not important, the differential conductance would be given directly by the first term in (4.38) without the voltage dependence in

the second argument. This was discussed in equation (4.2), and as a consequence the differential conductance is identified with the spectral density on the quantum dot. In general, the voltage dependence can not be neglected, and for the correct non-equilibrium description for the differential conduction in equation (4.38), we need to calculate the voltage dependence of the local Green's function, which is incorporated in the renormalised self-energy as shown in the last section.

### 4.3.1 Effect of the voltage on the differential conductance for small field

In this section we focus on the situation with a small magnetic field. Then we can use the asymptotic result for the renormalised self-energy (4.35) to calculate the differential conductance in equation (4.38). To clarify the effect of the finite voltage we consider different approximations. The simplest situation is to ignore the renormalised self-energy term completely, but use the renormalised parameters. The differential conductance at  $T = 0$  then takes the simple form,

$$\frac{dI}{dV} = \frac{G_0}{2} \sum_{\sigma} \frac{\tilde{\Delta}^2}{(eV/2 - \tilde{\varepsilon}_{d,\sigma})^2 + \tilde{\Delta}^2}. \quad (4.39)$$

We refer to this as (a) in the following. As (b) we refer to the case where the  $\omega^2$  term in the renormalised self-energy in (4.35) is included for the calculation of  $dI/dV$ . For small  $\omega$  this corresponds to (4.2), where the equilibrium spectral density is used, and no non-equilibrium voltage dependence is included. By (c) we denote the full first term in equation (4.38) with the voltage dependence in the second argument of the Green's function which comes from the self-energy in (4.35), but neglecting the second term in (4.38). (d) takes into account the full expression (4.38) with the self-energy asymptotics (4.35).

We would like to analyse these expressions for a small magnetic field. If we plot both the contributions ( $\sigma = 1$  and  $\sigma = -1$ ) to  $dI/dV_{ds}$  in the very weak field regime then, due to overlap, no magnetic field splitting can be observed. We can calculate, however, the shifts in the component resonance for  $\sigma = \nu = \pm 1$ . In figure 4.5 we plot the terms in the differential conductance (in units of  $G_0$ ) given by equation (4.38) as a function of  $eV/\tilde{\Delta}$ , where we use  $\sigma = \uparrow$  in (4.38).

We take values corresponding to the Kondo regime, with  $R = \tilde{\eta} = 2$  ( $\tilde{\varepsilon}_{d,\sigma}(h) = \sigma\tilde{\eta}h$ ), and a small field  $h/\tilde{\Delta} = 0.05$  ( $\pi\tilde{\Delta} = 4T_K$ ). As explained above we have distinguished the different contributions from (a) the case for the non-interacting quasiparticles as in equation (4.39) to (d) which takes into account the full expression (4.38) with the self-energy asymptotics (4.35). As different contributions in (4.38) are included going from (a) to (c) we see that the peak position and width is reduced. We also see that the integral term arising from the voltage dependence of  $G_{d,\sigma}^{\text{ret}}(\omega, eV)$  causes a significant further reduction (d) of the magnetic shift beyond that estimated from the first term (c) in equation (4.38), such that it cannot be neglected. In an experimental conductance measurement, the component conductance for small field is not observable, however, due to the overlap of the two components. The

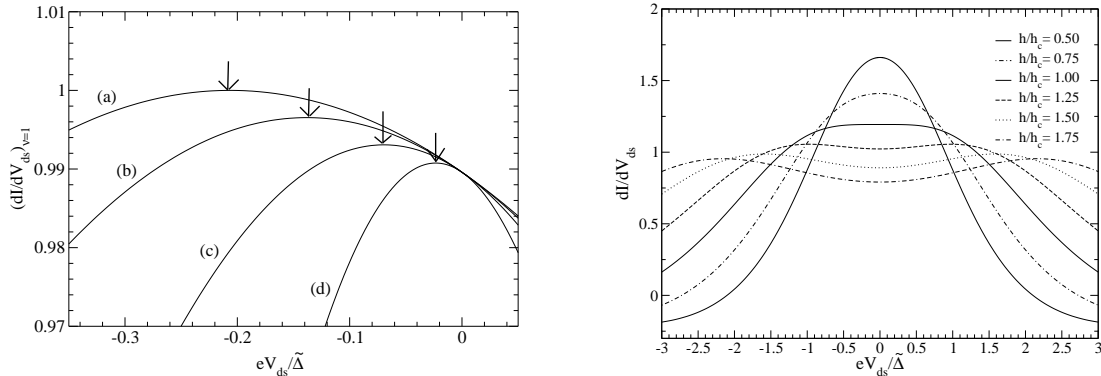


Figure 4.5: Left: The shift of the component resonance ( $\nu = \sigma = 1$ ) in the differential conductance (in units of  $G_0$ ) in a magnetic field for  $h/\tilde{\Delta} = 0.05$  as a function of the bias voltage  $eV_{ds}/\tilde{\Delta}$ , according to the inclusion of different contributions as described in the text. The arrows indicate the respective maxima. Right: The total differential conductance (in units of  $e^2/h$ ) in the Kondo regime for larger magnetic field values, calculated using equation (4.38) taking into account the full self-energy expansion from (4.35). These results are asymptotically exact for  $eV_{ds}/\tilde{\Delta} \ll 1$  and approximate, based on a second order expansion in  $eV_{ds}$  for larger values.

results for the different cases in figure 4.5 leave no doubt that the finite voltage has an important effect on the peak form and position of the Kondo resonance in a magnetic field - at least for small fields. We expect that at larger fields  $h \sim T_K$  the effect will also not be negligible.

### 4.3.2 Critical field for peak splitting

The arguments for the voltage dependence in this section are restricted to the regime where  $eV$  is small compared to  $\tilde{\Delta}$ . These results are, however, sufficient for us to deduce the critical value of the magnetic field  $h_c$  at which two distinct peaks begin to appear in the total differential response. For values of  $h < h_c$  the differential conductance will have a maximum at  $eV = 0$ , and for  $h > h_c$  this will become a minimum. Thus, we can write the differential conductance as

$$\frac{dI}{dV} = G^{(0)}(h) + G_2(h) (eV)^2 + \mathcal{O}((eV)^4) \quad (4.40)$$

and from the coefficient  $G_2(h)$  we can determine the point at which the sign change occurs as a function of  $h$ , and hence we can determine  $h_c$ . In the first term in (4.38) we have to expand the denominator up to second order in  $(eV)$ . The contribution to the real part of the self-energy to order  $\omega^2$  and  $(eV)^2$  is proportional to  $\sigma\tilde{\eta}(h)h$ . It might be thought that such a term should cancel out in taking the sum over the two spin components. However, there is a  $\sigma$ -independent contribution from a cross term with the effective Zeeman term  $\sigma h\eta(h)$ ,

which has to be included. The contribution from the second integral term in equation (4.38) to order  $(eV)^2$  can be easily be evaluated, as it is sufficient to put  $\omega = eV = 0$  in the integrand after the differentiation. As a first estimate using the above results the value of  $h_c$  can be calculated analytically by dropping the  $h$  dependence of the parameters and without the real part contribution to the self-energy expansion. The result,  $G_2(h_c) = 0$ , can be expressed entirely in terms of  $\tilde{\Delta}$  and the Wilson ratio  $R = \tilde{\eta}(0) = 1 + \tilde{U}/\pi\tilde{\Delta}$ ,

$$\frac{h_c^2}{\tilde{\Delta}^2} = \frac{\sqrt{9 + 20(R-1)^2(1 + 5(R-1)^2)} - 3}{10R^2(R-1)^2}. \quad (4.41)$$

In the non-interacting case,  $R = 1$  and  $h_c/\Delta = 1/\sqrt{3} = 0.577$  and in the Kondo regime,  $R = 2$ ,  $\tilde{\Delta} = 4T_K/\pi$ , and  $h_c/T_K = 0.582$ , with  $T_K$  given by (1.10). If the voltage dependence of the Green's function is neglected the result in the Kondo regime is  $h_c/T_K = 0.491$ , significantly smaller than if this term is included. This is in line with the observation in figure 4.5 that the peak position is reduced to smaller voltages when non-equilibrium effects are included.

The estimated critical magnetic field is comparable with  $\tilde{\Delta}$ , and for  $U \neq 0$  it may not be sufficient to work to linear order in  $h$ . It is possible to work with an arbitrary magnetic field, but in this case we have to use the field dependent renormalised parameters and the full expansion of the self-energy to order  $\omega^2$  and  $(eV)^2$  as given in (4.35). The equation for the critical field  $h_c$  becomes

$$\frac{h^2}{\tilde{\Delta}^2(h)} = \frac{\sqrt{(3 - \alpha(h)\gamma(h))^2 + 4\gamma(h)(5 - \alpha(h))(1 + 5\gamma(h))} - 3 + \alpha(h)\gamma(h)}{2\gamma(h)(5 - \alpha(h))\tilde{\eta}(h)^2}, \quad (4.42)$$

where  $\alpha(h) = \alpha_\omega(h) + \alpha_V(h)$ , and

$$\gamma(h) = \pi\tilde{\Delta}(h)\tilde{U}^2(h)[\tilde{\rho}_d^0(0, h)]^3 = \pi\tilde{\Delta}(h)\tilde{\rho}_d^0(0, h)(R(h) - 1)^2. \quad (4.43)$$

Equation (4.42) is an implicit equation for  $h_c$  which can be solved by iteration starting from the much simpler result (4.41), obtained within the linear approximation. Of course, (4.42) reduces to (4.41) if we drop the field dependence of the parameters and take  $\alpha = 0$ .

For a strong coupling situation ( $U/\pi\Delta = 4$ ) the result for the critical field obtained by iterating equation (4.42) and using the  $h$ -dependent renormalised parameters is  $h_c \simeq 0.459\tilde{\Delta} = 0.584T_K$ . This differs only by 0.3% from the value obtained from (4.41). The small difference is due to the fact that the various correction terms due to the  $h$  dependence of the parameters in the more general formula (4.42) tend to cancel giving only a small resultant change.

Plots of the total differential conductance for various fields above and below the critical field are displayed in figure 4.5 (right). We have taken the full self-energy expansion as given in (4.35) into account, including the field dependence of the renormalised parameters. The results are asymptotically exact only for small  $eV$  and a more complete theory is required to calculate the magnitude of the splitting at larger bias voltages. The major problem to

be solved is the dependence of the self-energy on the voltage bias term, when  $eV$  is of the order of the Kondo temperature  $T_K$ , so that a detailed comparison with experiment can be made with the experimental results in this regime. In the next section we present RPT calculations for larger values of  $eV$ .

## 4.4 Higher voltages and non-equilibrium RPT calculations

In the last chapter in section 3.4.2 we have seen that in the equilibrium AIM with magnetic field the spectral density could be described well in the RPT framework, up to energies and fields of the order of the Kondo temperature  $T_K$ . We saw that it was not enough to consider the second order diagram, but a class of repeated particle hole scattering diagrams had to be taken into account. In this section we present results for the extension of these calculations to the non-equilibrium. In order to calculate a good approximation for the renormalised self-energy we adopt a similar strategy as the one, which has proven to be successful in the equilibrium case. Therefore, the self-energy will be calculated by taking into account repeated quasiparticle scattering. Before we consider these calculations for the one-particle spectral function we look at the transverse spin susceptibility, in order to get a first impression what the effect of the non-equilibrium situation and finite voltage on the dynamic response functions is.

### 4.4.1 Non-equilibrium repeated quasiparticle scattering

When we sum up the repeated scattering series for the transverse spin susceptibility we have to be careful that the signs at the vertex are taken into account correctly (convention “-”-sign for +-vertex). Hence, in addition to the matrix for the pair propagator  $\mathbf{\Pi}_{p-\sigma}^{h\sigma}$  (4.24) we define

$$\hat{\mathbf{\Pi}}_{p-\sigma}^{h\sigma} = \begin{pmatrix} \Pi_{p-\sigma}^{h\sigma,(-)} & \Pi_{p-\sigma}^{h\sigma,(-+)} \\ -\Pi_{p-\sigma}^{h\sigma,(+-)} & -\Pi_{p-\sigma}^{h\sigma,(++)} \end{pmatrix}. \quad (4.44)$$

Then the series corresponding to the diagrams in figure 2.7 for the matrix for the transverse spin susceptibility  $\chi_t$  takes the form

$$\chi_t = \mathbf{\Pi}_{p-\sigma}^{h\sigma} \sum_{k=0}^{\infty} [\tilde{U}_{p-\sigma}^{h\sigma} \hat{\mathbf{\Pi}}_{p-\sigma}^{h\sigma}]^k = \mathbf{\Pi}_{p-\sigma}^{h\sigma} [\mathbb{1} - \tilde{U}_{p-\sigma}^{h\sigma} \hat{\mathbf{\Pi}}_{p-\sigma}^{h\sigma}]^{-1}. \quad (4.45)$$

The renormalised vertex  $\tilde{U}_{p-\sigma}^{h\sigma}$  is given as in the equilibrium theory in equation (3.38). The explicit result for  $\chi_t(\omega, eV)$  is obtained by matrix inversion, where the determinant is given by

$$D = (1 - \tilde{U}\Pi^{(-)}) (1 + \tilde{U}\Pi^{(++)}) + \tilde{U}^2 \Pi^{(-+)} \Pi^{(+-)}. \quad (4.46)$$

We have dropped the redundant  $ph, \sigma$  indices in the last equations. Similar series expressions can be derived for other RPA like series in the Keldysh formalism.

We consider the retarded, dynamic, transverse spin susceptibility and think of the voltage like an external field,

$$\chi_t(\omega, eV) = \chi_t^{(--)}(\omega, eV) - \chi_t^{(-+)}(\omega, eV). \quad (4.47)$$

This result is similar to the earlier one in equation (3.36), which is valid in equilibrium case and finite magnetic field. In figure 3.5 we found excellent agreement of the ph-RPT results with the NRG results for  $\chi_t(\omega, eV = 0)$  and arbitrary field;  $h = 0$  and  $h = T_K$  was shown there. Here we study the effect of the finite voltage and plot  $\text{Im}\chi_t(\omega, eV)$  for  $h = 0$  (left) and  $h = T_K$  (right) and various values of the voltage in figure 4.6.

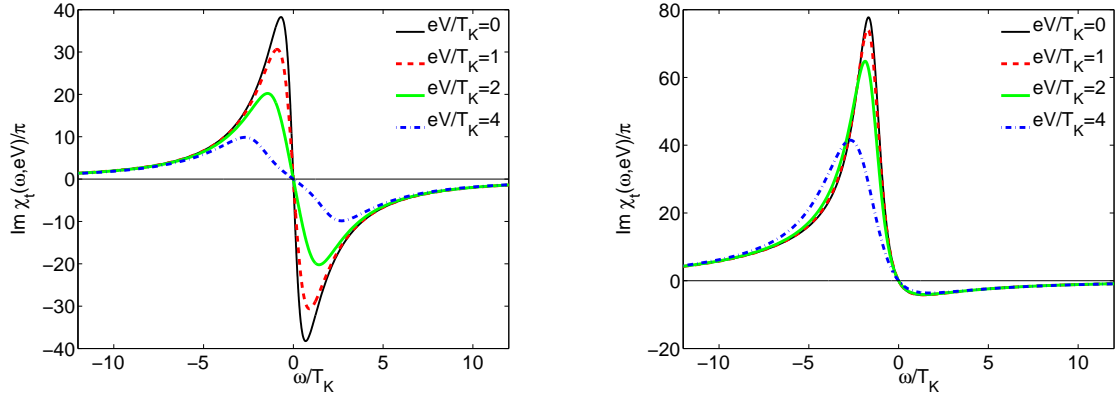


Figure 4.6: The imaginary part of the retarded, dynamic, transverse spin susceptibility  $\chi_t(\omega, eV)$  for  $h = 0$  (left) and  $h = T_K$  (right) and various values of the voltage.

The results for  $h = 0$  and  $h = T_K$  and zero voltage are identical with the ones of figure 3.5. In the case of finite voltage of the order of the Kondo temperature we find that the peaks in the susceptibility are suppressed, both in the zero and finite field case. The effect is visible more strongly for smaller magnetic fields. Generally, the results seem to give a sound representation for the system in finite voltage, and although we have no results from an alternative calculation to compare to, the behaviour seems on general grounds to give a reasonable approximation for the quantity.

Having derived expressions for the susceptibility we can now consider the matrix elements of the to the repeated scattering corresponding self-energy  $\Sigma^{\text{ph}}$ , which have the same structure as for the second order diagram (4.29),

$$\Sigma_{\sigma}^{r,\text{ph},\alpha\beta}(\omega) = \frac{\tilde{U}_1^2}{2\pi i} \int d\omega_2 \chi_t^{(\alpha\beta)}(\omega - \omega_2) \tilde{G}_{d,-\sigma}^{(0),\alpha\beta}(\omega_2). \quad (4.48)$$

$\chi_t^{(\alpha\beta)}(\omega)$  was given in equation (4.45), and we only have to replace  $\tilde{U}_{p-\sigma}^{h\sigma}$  by  $\tilde{U}_1$ . This effective interaction  $\tilde{U}_1$  is found in the equilibrium limit and given as in (3.45). The

retarded self-energy is given by the combination in equation (4.16). With the identity

$$2\text{Im}\Sigma_{\sigma}^{--}(\omega) = -\text{Im}\Sigma_{\sigma}^{-+}(\omega) - \text{Im}\Sigma_{\sigma}^{+-}(\omega) \quad (4.49)$$

and relations for the susceptibility, we obtain as in (4.31),

$$\tilde{\Sigma}_{-\sigma}^{\text{ph}}(\omega) = -\tilde{\Sigma}_{\sigma}^{\text{ph}}(-\omega)^*. \quad (4.50)$$

Therefore also here the negative spin part can be obtained from the positive one (particle hole symmetric case). This implies for the imaginary part of the retarded Green's function

$$\text{Im}G_{d,-\sigma}^{\text{ret}}(\omega, eV) = \text{Im}G_{d,\sigma}^{\text{ret}}(-\omega, eV). \quad (4.51)$$

The appropriate renormalised retarded self-energy  $\tilde{\Sigma}_{\sigma}^{\text{ph,ret}}(\omega)$  is obtained in the equilibrium limit by including the counter-terms as in equation (4.23).

#### 4.4.2 Single particle dynamics in zero magnetic field

Before considering the field *and* voltage dependent case, we investigate purely the effect of the finite voltage on the Kondo resonance with the second order RPT approximation. Namely, we first study the splitting of the Kondo resonance with finite voltage in the RPT framework in zero magnetic field. From the asymptotic behaviour to order  $(eV)^2$  and  $\omega^2$  in equation (4.35) we immediately see that no splitting can occur due to the absence of a mixed term. Rather than carrying out higher order asymptotic expansions, we analyse the situation by numerically evaluating the second order diagrams (4.29). In figure 4.7 (left) we display the  $\omega$ -dependence of the imaginary part of the renormalised self-energy for a number of voltages and a generic strong coupling situation ( $U/\pi\Delta = 4$ ).

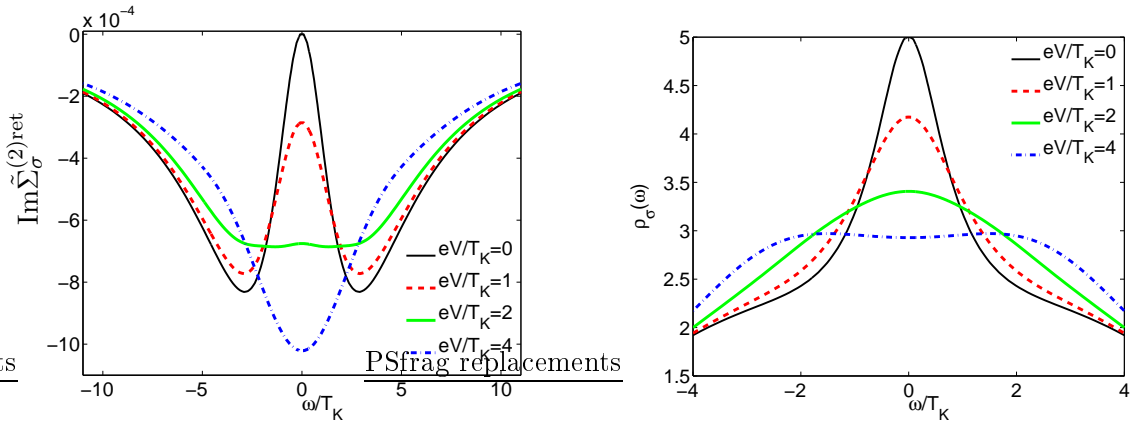


Figure 4.7: Left: The imaginary part of the the renormalised self-energy  $\tilde{\Sigma}_{\sigma}^{(2)\text{ret}}(\omega, eV)$  for different voltages. Right: Spectra for the shown renormalised self-energy for different voltages.

We can see that for finite voltage the imaginary part at  $\omega = 0$  becomes finite, something visible from the asymptotic expansion (4.35). For increasing voltages the value  $|\text{Im}\tilde{\Sigma}_\sigma^{(2)\text{ret}}(0, eV)|$  goes over from a minimum to a maximum in the  $\omega$ -dependence. The effect of this behaviour of the renormalised self-energy on the spectral density in finite voltage is shown in figure 4.7 (right). We find that for increasing voltage the peak height of the Kondo resonance is reduced from its equilibrium value. For values of  $eV$  between  $2 - 4T_K$  the curvature at zero frequency changes sign and the peak is seen to split in the finite voltage. The numerical analysis shows a splitting to occur at  $eV_{\text{sp}} \simeq 3.3T_K$ . We can see that the broadened peaks are a bit less than the voltage difference apart. Therefore one is tempted to connect the physical origin of the peak splitting with the two chemical potentials and the tendency of the Kondo resonance to be pinned to a Fermi level.

To our knowledge up to now no precise prediction about the splitting of the Kondo resonance in finite voltage has been made. Fuji and Ueda (2003, 2005) find a splitting in a 4th order perturbation expansion in the bare  $U$ , but their values for  $eV$  are rather large, and it is not easy to compare to their results. Experimentally, it is difficult to access the voltage dependence of the spectral density directly. De Franceschi et al. (2002) claim to have observed such a splitting in a three terminal experimental setup at voltages of the order of the Kondo temperature. Thus the results are in qualitative agreement. If this experimental setup actually corresponds to the two channel Anderson model is, however, not completely clear.

In conclusion, we find in the non-equilibrium RPT scheme for strong coupling a splitting of the Kondo resonance when the voltage exceeds a critical  $eV_{\text{sp}}$  of the order of the Kondo temperature. We know that the theory presented is asymptotically correct for small voltage. If it is, however, quantitatively correct for voltages of the order of  $T_K$  is not clear. It would be interesting to compare this quantitative prediction with other non-equilibrium methods.

The quantity which is directly measured in most experiments is not the spectral density, but the differential conductance  $dI/dV$ , (4.38). In figure 4.8 we show the voltage dependence of  $dI/dV$  calculated from the second order RPT (left) and the repeated scattering series (right) for zero magnetic field.

We have included different contributions for comparison: the term with no non-equilibrium voltage dependence (“No V-dep.”) corresponds to the evaluation based on the equilibrium density of states as described in equation (4.2). The label “First term” refers to only the first term in equation (4.38) including the voltage dependence of the renormalised self-energy, whilst the thick lines (“Full expr.”) are calculated with the full expression (4.38). We can observe that in contrast to the spectral density no peak splitting can be observed in the plots for the differential conductance. This is in line with all experimental results for this quantity. We can also see that the width of the peak is reduced, when the finite voltage is taken into account. This can be traced back to the increasing self-energy contributions for finite voltage. It suggests that an experimental estimate of the Kondo temperature

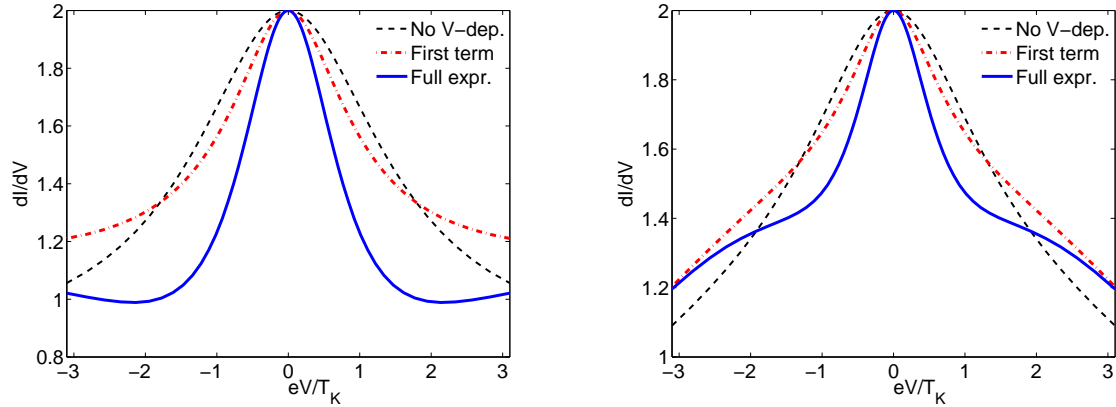


Figure 4.8: Different contributions to the differential conductance (in units of  $G_0$ ) for the second order calculation based on (4.29) (left) and the repeated scattering diagrams, (4.48), (right). The meaning of the different contributions is explained in the text.

from the peak width in  $dI/dV$  is likely to give a too small value. In both approximations (SO and ph-RPT) we see that for voltages of the order of  $T_K$  a shoulder develops in the voltage dependent calculations, and this is seen more pronounced in the results for the full expression (4.2). This behaviour can be explained from the fact that the approximations for the renormalised self-energies become inaccurate for these energy and voltage scales.

#### 4.4.3 Dynamics and differential conductance in finite magnetic field

In this subsection we present results for the extension of the equilibrium RPT calculations in section 3.4.2. There we had seen that in a finite magnetic field the repeated scattering results for the renormalised self-energy gave a correction to the free quasiparticles spectra such that the resulting low energy spectra agreed well with NRG results. We had also seen at the beginning of this chapter [cf. fig. 4.1] that the results for the differential conductance based on equilibrium spectra gave a larger estimate of the Kondo splitting in magnetic field as compared with experimental results. Further we found in section 4.3 that the inclusion of non-equilibrium effects resulted in a reduction of the peak position in small magnetic field. It is therefore reasonable to test whether the extension of the RPT calculation to the non-equilibrium case at higher magnetic fields gives results for the differential conductance which compare well with experimental ones. In figure 4.9 we show the differential conductance with the different contributions, as explained earlier, for a finite field case,  $h = T_K$ .

We can see that the peak in  $dI/dV$  is split since the field exceeds the critical value  $h_c$ . The value of  $dI/dV$  at  $eV = 0$  is reduced substantially as compared to the zero field case. By comparing the dashed line with the full line we can also observe that the magnitude of the peak splitting  $\Delta_{\text{Kondo}}^{(\text{theo}),V}$  in the voltage dependent expressions is reduced substantially when

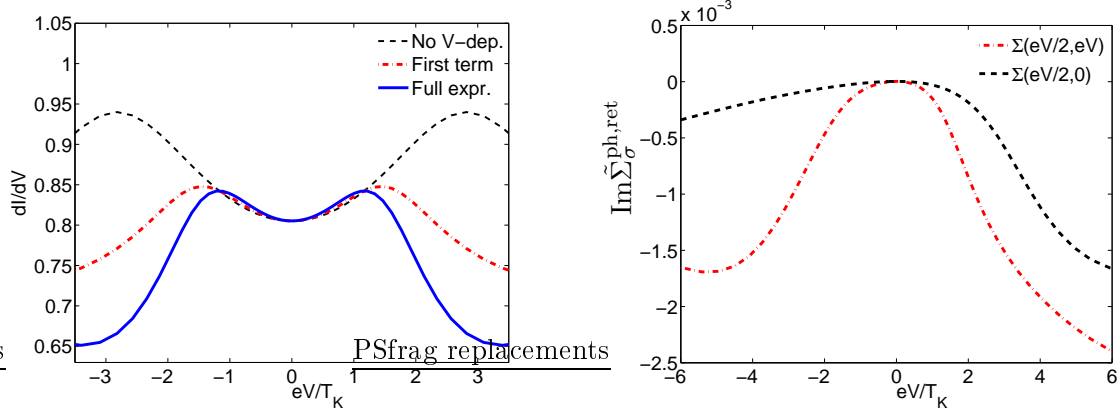


Figure 4.9: Left: Different contributions to the differential conductance (in units of  $G_0$ ) for the the repeated scattering diagrams for  $h = T_K$ . Right: Comparison of the imaginary part of the renormalised self-energy as a function of voltage illustrating the non-equilibrium effects for  $h = T_K$ .

compared with the result (4.2) corresponding to the equilibrium approximation (“No V-dep.”) for the differential conductance. Such an effect had been observed for one component of  $dI/dV$  in the asymptotic expansion in figure 4.5 for a smaller field. To illustrate the effect of the voltage dependence in the renormalised self-energy here we have included a plot on the left of figure 4.9, where the imaginary part of  $\tilde{\Sigma}_\sigma^{\text{ph,ret}}(\omega, eV)$  is shown as dependent on the voltage like  $\tilde{\Sigma}_\sigma^{\text{ph,ret}}(\omega = eV/2, eV)$ , which corresponds to the first term in (4.38) and without the voltage dependence in the second argument,  $\tilde{\Sigma}_\sigma^{\text{ph,ret}}(\omega = eV/2, 0)$ . It is visible that the imaginary part of the  $|\tilde{\Sigma}_\sigma^{\text{ph,ret}}(\omega = eV/2, eV)|$  is larger, when the full voltage dependence is included and thus the effect on the Kondo peak in the differential conductance can be understood. The closer inspection reveals that the reduction in the magnitude of the Kondo splitting in the non-equilibrium theory through the effect of finite voltage is substantial, as seen for example in figure 4.9 but also for other values of the field  $h$ . In fact the resulting values for  $\Delta_{\text{Kondo}}^{\text{(theo),V}}$  give a Kondo splitting which is substantially smaller than the experimental result  $\Delta_{\text{Kondo}}^{\text{(exp),V}}$  in figure 4.1 (right). In other words the non-equilibrium effects in the RPT calculation presented reduce the splitting too much from the equilibrium approximation as to give an agreement with the experimental values. At the time of writing it is not fully resolved why the ph-RPT approximation works well in the equilibrium in fields up to about  $4T_K$  (compared with NRG results), but does not explain the quantum dot measurements in finite voltage of the same order of magnitude. Generally, the non-equilibrium problem in finite field is clearly a difficult one since the non-equilibrium spectral function for fields  $h$ , frequencies  $\omega$  and voltages  $eV$ , all of the order of the Kondo temperature  $T_K$ , have to be determined. Future research on non-equilibrium Kondo physics will show if an agreement between experimental and theoretical results

for the differential conductance can be found, based on the equation (4.38), or if other effects have to be considered. Promising approaches include non-equilibrium Bethe ansatz calculations (Mehta and Andrei 2006) and reformulation of the non-equilibrium problem in terms of scattering states (Oguri 2007).

In summary, we have analysed the transport through a quantum dot in magnetic field in this chapter. The description is based on the two-channel AIM and a renormalised perturbation theory in the Keldysh formalism. We derived an asymptotically exact expression for the low voltage behaviour of the renormalised self-energy and used it to study the non-equilibrium effects on the differential conductance for a small magnetic field. We also presented results for dynamic susceptibilities, spectral densities and the differential conductance for higher voltages and fields (order of  $T_K$ ). These were based on second order and repeated scattering RPT. We established that the finite voltage plays an important role in the problem, and attempted to give a quantitative interpretation of the Kondo splitting observed experimentally in conductance measurements. Based on our calculation, however, no quantitative agreement was found, and it remains to be seen in future research, whether there are flaws in the calculation presented or additional features which have not been taken into account in the present approach play a role.

*The most important thing is to find out  
what is the most important thing.*

Shunryu Suzuki

## Chapter 5

# Locally correlated electrons in a superconducting bath

The subject of this chapter is the AIM with a superconducting bath. We start by outlining the NRG approach for this model, and introduce the basic features appearing, such as the singlet-doublet ground state transition and the bound states in the gaps. Then we present NRG results for the position and weight of the bound states, and also for the anomalous expectation values focusing on the symmetric model first. This is followed by a discussion of the spectral functions on all energy scales for different parameters. The last section is devoted to the situation away from particle hole symmetry, where we give a global phase diagram for parameter regimes with singlet and doublet ground states.

### 5.1 Kondo physics and BCS superconductors

So far in this part of the thesis we have studied the Anderson impurity model in a metallic medium, focusing on the effect of a local symmetry breaking in the spin channel induced by a magnetic field. In this section we will investigate a situation where a symmetry breaking in the bath rather than on the impurity site is included. Specifically, we will look at a symmetry breaking in the charge channel and study the case where the bath is in a BCS superconducting state. This situation is of interest for understanding the effect of magnetic impurities in superconductors and recent experiments with quantum dots with superconducting leads. Due to the proximity effect there is induced symmetry breaking on the impurity site. As a consequence localised excited state (LES) with an energy within the superconducting gap can be induced at the impurity site. Such states are well known from superconductor-normal-superconductor (SNS) junctions and are usually called Andreev bound states. For a weak on-site interaction the ground state of the system is usually a superconducting singlet ( $S = 0$ ) and the LES is an  $S = 1/2$  excitation. If there is a strong repulsion on the impurity site, such that single occupation is favoured, we have a situation

where a single spin is coupled to the superconducting medium. Similar to the case with a normal, metallic bath the Kondo effect plays a role here. The ground state can be a singlet, more specifically a Kondo singlet, when both the local interaction and the superconducting gap are not too large. Physically, one can think of a situation where enough continuum states are available to screen the impurity spin. If the local interaction is, however, increased beyond a critical value  $U_c$  the ground state becomes a doublet ( $S = 1/2$ ) with an unscreened spin at the impurity site. In this situation the LES is an  $S = 0$  excitation. This ground state transition at zero temperature is an example of a quantum phase transition which occurs for a level crossing that depends on a system parameter (Sachdev 1999). The relevant energy scales for this singlet-doublet transition to occur in the Kondo regime are the Kondo temperature  $T_K$  and the superconducting gap  $\Delta_{sc}$ . In early work by Matsuura (1979) the effects of impurities on superconductors in an interpolation theory were studied. For a single impurity it was found that the singlet-doublet transition occurs at  $4T_K \simeq \pi\Delta_{sc}$  ( $\pi/4 \simeq 0.78$ ). There have also been NRG studies for a spin coupled to a superconducting bath (Kondo model) by Satori et al. (1992) and subsequent work by Sakai et al. (1993). In this work a more accurate estimate for the transition is given,  $T_K/\Delta_{sc} \simeq 0.3$ , i.e. for  $T_K/\Delta_{sc} > 0.3$  we have a singlet ground state whilst for  $T_K/\Delta_{sc} < 0.3$  the ground state is a doublet. It is also found there that at the transition,  $T_K/\Delta_{sc} \simeq 0.3$ , where the bound state energy of the LES becomes zero. Yoshioka and Ohashi (2000) presented another NRG study, for the Anderson impurity model with superconducting bath, where a larger parameter space is accessible. A more extensive comparison with mean field results is given there and the behaviour of the LES is analysed in detail. Many of the more recent papers (Rozhkov and Arovas 1999, Matsumoto 2001, Vecino et al. 2003, Siano and Egger 2004, Choi et al. 2004, Oguri et al. 2004) (theoretically), (Buitelaar et al. 2002, van Dam et al. 2006) (experimentally) focus on the impurity (quantum dot) embedded in two superconducting baths with different (complex) superconducting order parameters. There a phase shift dependent Josephson current can be observed which varies with the model parameters. Situations with two channels with Josephson or nonequilibrium currents are not covered in this chapter. The analysis presented here focuses on the spectral properties of an impurity in a superconducting bath. For low energies within the superconducting gap we calculate the position and weight of the LES and also give the values for the induced anomalous on-site correlation. We also present results for the spectral density for the diagonal and offdiagonal correlations functions on all energy scales and present singlet-doublet ground state phase diagrams for the symmetric and non-symmetric case. We start by outlining some of the details for the NRG calculation with a superconducting medium. Many aspects discussed in this chapter are published in reference Bauer et al. (2007b).

## 5.2 The Anderson model with superconducting medium

### 5.2.1 NRG approach

Starting point is the Anderson impurity model in the form

$$H = H_d + H_{\text{mix}} + H_{\text{sc}}. \quad (5.1)$$

The local interacting part is given as before in equation (1.1) and also the mixing term has the usual form,

$$H_{\text{mix}} = \sum_{\mathbf{k}, \sigma} V_{\mathbf{k}} (c_{\mathbf{k}, \sigma}^\dagger c_{d, \sigma} + \text{h.c.}). \quad (5.2)$$

In order to avoid confusion in the notation with the superconducting gap we define for this chapter  $\Gamma = \pi V^2 \rho_c(0)$  as the energy scale for hybridisation ( $\rho_c(0) = 1/2D$  as before). The superconducting medium is given in a BCS meanfield form

$$H_{\text{sc}} = \sum_{\mathbf{k}, \sigma} \varepsilon_{\mathbf{k}} c_{\mathbf{k}, \sigma}^\dagger c_{\mathbf{k}, \sigma} - \Delta_{\text{sc}} \sum_{\mathbf{k}} [c_{\mathbf{k}, \uparrow}^\dagger c_{-\mathbf{k}, \downarrow}^\dagger + \text{h.c.}], \quad (5.3)$$

where  $\Delta_{\text{sc}}$  is the superconducting gap, which is taken to be real for simplicity. In (5.3) we let the summations run over all  $\mathbf{k}$  in a wide band. Another energy scale  $\omega_D$ , the Debye cutoff in BCS theory, could enter at this stage to restrict the summation. As shown by Satori et al. (1992) with a scaling argument, this effect does not alter the results substantially. We will keep it in mind for some of the following arguments, but neglect it later (see below).

For the NRG approach we have to derive a discrete form of the Hamiltonian, which can be diagonalised conveniently in a renormalisation group scheme descending to lower energies. This is done in an analogous fashion as for a metallic medium, which was described in section 2.1. Essentially, there are three steps which only affect  $H_{\text{mix}}$  and  $H_{\text{sc}}$ :

(1) Mapping to a one-dimensional problem, (2) logarithmic discretisation, (3) Basis transformation. We obtain finally [cf. (2.1)]

$$H_{\text{mix}}/D = \sqrt{\frac{\Gamma}{\pi D}} \sum_{\sigma} (f_{0\sigma}^\dagger c_{d, \sigma} + \text{h.c.}), \quad (5.4)$$

and

$$H_{\text{sc}}/D = \sum_{\sigma, n=0}^{\infty} \gamma_{n+1} (f_{n\sigma}^\dagger f_{n+1, \sigma} + \text{h.c.}) - \frac{\Delta_{\text{sc}}}{D} \sum_{n=m_0}^{\infty} (f_{n\uparrow}^\dagger f_{n, \downarrow}^\dagger + \text{h.c.}) \quad (5.5)$$

where  $\gamma_n$  has the usual form (Hewson 1993a).  $m_0$  corresponds to the site on the chain, at which the energy scale has reached  $\omega_D$ , and it is explicitly given by

$$m_0 = -\frac{\log(\omega_D/D)}{\log \Lambda}. \quad (5.6)$$

We follow earlier works (Satori et al. 1992, Yoshioka and Ohashi 2000) and restrict our calculations to the case  $m_0 = 0$ , which corresponds to  $\omega_D = D$ . As mentioned above details about the justification for this in the NRG approach have been discussed by Satori et al. (1992).

The iterative diagonalisation scheme is set up in the same way as in the normal case. Due to the anomalous term in the superconducting band the charge  $Q$  is not a good quantum number of the system any longer, i.e. the charge operator does not commute with the Hamiltonian. Thus eigenstates are characterised only in terms of the spin quantum number  $S$ . The numerical RG transformation is defined by

$$H_{N+1} = \mathcal{R}(H_N) = \sqrt{\Lambda}H_N + \xi'_{N+1}(f_{N\sigma}^\dagger f_{N+1,\sigma} + \text{h.c.}) - \Delta_{N+1}(f_{N+1,\uparrow}^\dagger f_{N+1,\downarrow}^\dagger + \text{h.c.}) \Big|_{N \geq m_0}, \quad (5.7)$$

with  $\xi'_N$  as in chapter 2 and

$$\Delta_N = \begin{cases} \Lambda^{(N-1)/2} \Delta_{\text{sc}} & \text{for } N \geq m_0 \\ 0 & \text{otherwise.} \end{cases} \quad (5.8)$$

We can see that the superconducting gap becomes a dominating energy scale for large  $N$  and a relevant perturbation. It does not make sense to continue NRG iterations down to energies much below this scale as there are no continuum states anymore in the gap. Therefore, we stop the NRG procedure at an  $N_{\text{max}}$ , such that the typical energy scale  $\Lambda^{-(N_{\text{max}}-1)/2}$  is not too much smaller than the superconducting gap  $\Delta_{\text{sc}}$ . More details for the iterative diagonalisation are given elsewhere (Bauer 2007).

### 5.2.2 Relevant Green's functions

For the Green's functions it is convenient to work in Nambu space,  $\mathbf{C}_d^\dagger = (c_{d,\uparrow}^\dagger, c_{d,\downarrow})$ , with  $2 \times 2$  matrices. The relevant retarded Green's functions are then

$$\underline{G}_d(\omega) = \langle\langle \mathbf{C}_d; \mathbf{C}_d^\dagger \rangle\rangle_\omega = \begin{pmatrix} \langle\langle c_{d,\uparrow}; c_{d,\uparrow}^\dagger \rangle\rangle_\omega & \langle\langle c_{d,\uparrow}; c_{d,\downarrow} \rangle\rangle_\omega \\ \langle\langle c_{d,\downarrow}^\dagger; c_{d,\uparrow}^\dagger \rangle\rangle_\omega & \langle\langle c_{d,\downarrow}^\dagger; c_{d,\downarrow} \rangle\rangle_\omega \end{pmatrix} = \begin{pmatrix} G_{11}(\omega) & G_{12}(\omega) \\ G_{21}(\omega) & G_{22}(\omega) \end{pmatrix}. \quad (5.9)$$

In the NRG approach we calculate  $G_{11}$  and  $G_{21}$  directly and infer  $G_{22}(\omega) = -G_{11}(-\omega)^*$ , which follows from  $G_{A,B}^{\text{ret}}(\omega) = -G_{B,A}^{\text{adv}}(-\omega)$  and  $G_{A,B}^{\text{ret/adv}}(\omega) = -G_{A^\dagger, B^\dagger}^{\text{ret/adv}}(-\omega)^*$  for fermionic operators  $A, B$ . Similarly, we can find  $G_{12}(\omega) = G_{21}(-\omega)^*$ . In the derivation one has to be careful and include a sign change for up down spin interchange in the corresponding operator combination.

In the non-interacting case we can work out the Green's function matrix exactly. To do so rewrite the term  $H_{\text{sc}}$  by introducing the vector of operators and the symmetric matrix

$$\mathbf{C}_{\mathbf{k}} := \begin{pmatrix} c_{\mathbf{k},\uparrow} \\ c_{-\mathbf{k},\downarrow}^\dagger \end{pmatrix}, \quad \mathbf{A}_{\mathbf{k}} := \begin{pmatrix} \varepsilon_{\mathbf{k}} & -\Delta_{\text{sc}} \\ -\Delta_{\text{sc}} & -\varepsilon_{\mathbf{k}} \end{pmatrix}. \quad (5.10)$$

Then  $H_{\text{sc}}$  can be written as

$$H_{\text{sc}} = \sum_{\mathbf{k}} C_{\mathbf{k}}^\dagger A_{\mathbf{k}} C_{\mathbf{k}}.$$

The matrix Green's function in the superconducting lead is then given by  $\underline{g}_{\mathbf{k}}(i\omega_n) = (i\omega_n \mathbb{1}_2 - A_{\mathbf{k}})^{-1}$ ,

$$\underline{g}_{\mathbf{k}}(i\omega_n)^{-1} = i\omega_n \mathbb{1}_2 - \varepsilon_{\mathbf{k}} \tau_3 + \Delta_{\text{sc}} \tau_1, \quad (5.11)$$

where  $\tau_i$  are Pauli matrices. Note that for a three component vector  $\mathbf{b}$

$$(a \mathbb{1}_2 + \mathbf{b} \cdot \boldsymbol{\tau})^{-1} = \frac{\mathbb{1}_2}{a^2 - \mathbf{b}^2} (a \mathbb{1}_2 - \mathbf{b} \cdot \boldsymbol{\tau}), \quad (5.12)$$

and hence

$$\underline{g}_{\mathbf{k}}(i\omega_n) = \frac{i\omega_n \mathbb{1}_2 + \varepsilon_{\mathbf{k}} \tau_3 - \Delta_{\text{sc}} \tau_1}{(i\omega_n)^2 - (\varepsilon_{\mathbf{k}}^2 + \Delta_{\text{sc}}^2)}. \quad (5.13)$$

In the wide band limit with a constant density of states the hybridisation term takes the form

$$V^2 \frac{1}{N} \sum_{\mathbf{k}} \underline{g}_{\mathbf{k}}(i\omega_n) = -\Gamma \frac{i\omega_n \mathbb{1}_2 + \Delta_{\text{sc}} \tau_1}{E(i\omega_n)}. \quad (5.14)$$

We are mostly interested in the limit of zero temperature ( $i\omega_n \rightarrow \omega \in \mathbb{R}$ ) here, and the function in the denominator  $E(z)$  after analytic continuation reads

$$E(\omega) = \begin{cases} -i \operatorname{sgn}(\omega) \sqrt{\omega^2 - \Delta_{\text{sc}}^2} & \text{for } |\omega| > \Delta_{\text{sc}} \\ \sqrt{\Delta_{\text{sc}}^2 - \omega^2} & \text{for } |\omega| < \Delta_{\text{sc}} \end{cases}. \quad (5.15)$$

In the non-interacting case for  $T = 0$ , we have therefore

$$\underline{G}_d^0(\omega)^{-1} = \omega \mathbb{1}_2 - \varepsilon_d \tau_3 + \Gamma \frac{\omega \mathbb{1}_2 + \Delta_{\text{sc}} \tau_1}{E(\omega)}. \quad (5.16)$$

The Green's function is obtained by matrix inversion, which yields with (5.12)

$$\underline{G}_d^0(\omega) = \frac{1}{D(\omega)} \left[ \omega \left( 1 + \frac{\Gamma}{E(\omega)} \right) \mathbb{1}_2 - \frac{\Gamma \Delta_{\text{sc}}}{E(\omega)} \tau_1 + \varepsilon_d \tau_3 \right], \quad (5.17)$$

where the determinant,  $D(\omega) := \det(\underline{G}_d^0(\omega)^{-1})$  is given by

$$D(\omega) = \omega^2 \left[ 1 + \frac{\Gamma}{E(\omega)} \right]^2 - \frac{\Gamma^2 \Delta_{\text{sc}}^2}{E(\omega)^2} - \varepsilon_d^2. \quad (5.18)$$

The full Green's function matrix  $\underline{G}_d(\omega)^{-1}$  at the impurity site is given by the Dyson matrix equation

$$\underline{G}_d(\omega)^{-1} = \underline{G}_0^{-1}(\omega) - \underline{\Sigma}(\omega), \quad (5.19)$$

where we have introduced the self-energy matrix  $\underline{\Sigma}(\omega)$ .

### Self-energy using the higher $F$ -Green's function

As described earlier in chapter 2 there is a method to calculate the self-energy employing a higher  $F$ -Green's function, and it can also be used for the superconducting case. In order to derive the equations of motions for the correlation functions, the identity

$$\omega \langle\langle A; B \rangle\rangle_\omega + \langle\langle [H, A], B \rangle\rangle_\omega = \langle [A, B]_\eta \rangle \quad (5.20)$$

( $\eta = +$  for fermions) is useful. The calculation taking into account all offdiagonal terms yields the following matrix equation

$$\underline{G}_0^{-1}(\omega) \underline{G}_d(\omega) - U \underline{F}(\omega) = \mathbb{1}_2, \quad (5.21)$$

with the matrix of higher Green's functions  $\underline{F}(\omega)$ ,

$$\underline{F}(\omega) = \begin{pmatrix} F_{11}(\omega) & F_{12}(\omega) \\ F_{21}(\omega) & F_{22}(\omega) \end{pmatrix}. \quad (5.22)$$

We have introduced the matrix elements  $F_{11}(\omega) = \langle\langle c_{d,\uparrow} n_\downarrow; c_{d,\uparrow}^\dagger \rangle\rangle_\omega$ ,  $F_{12}(\omega) = \langle\langle c_{d,\uparrow} n_\downarrow; c_{d,\downarrow} \rangle\rangle_\omega$ ,  $F_{21}(\omega) = -\langle\langle c_{d,\downarrow}^\dagger n_\uparrow; c_{d,\uparrow}^\dagger \rangle\rangle_\omega$  and  $F_{22}(\omega) = -\langle\langle c_{d,\downarrow}^\dagger n_\uparrow; c_{d,\downarrow} \rangle\rangle_\omega$ . In the NRG we calculate  $F_{11}$  and  $F_{21}$  and the others follow from  $F_{12}(\omega) = -F_{21}(-\omega)^*$  and  $F_{22}(\omega) = F_{11}(-\omega)^*$ . We can define the self-energy matrix by

$$\underline{\Sigma}(\omega) = U \underline{F}(\omega) \underline{G}_d(\omega)^{-1}. \quad (5.23)$$

The properties of the Green's function and the higher  $F$ -Green's function lead to the relations  $\Sigma_{12}(\omega) = \Sigma_{21}(-\omega)^*$  and  $\Sigma_{22}(\omega) = -\Sigma_{11}(-\omega)^*$  for the self-energies. We can therefore calculate the diagonal self-energy  $\Sigma(\omega) = \Sigma_{11}(\omega)$  and the offdiagonal self-energy  $\Sigma^{\text{off}}(\omega) = \Sigma_{21}(\omega)$  and deduce the other two matrix elements from them. With the relation (5.23) between  $\underline{G}$ ,  $\underline{F}$  and  $\underline{\Sigma}$  the Dyson equation is recovered in (5.21),

$$\underline{G}_d(\omega)^{-1} = \underline{G}_0^{-1}(\omega) - \underline{\Sigma}(\omega). \quad (5.24)$$

Therefore, the Green's function can be calculated from the free Green's function as given in (5.17) and the self-energy as calculated from (5.23). Details for the matrix elements for the actual calculation are given elsewhere (Bauer 2007).

### 5.2.3 Andreev bound states

The denominator of the Green's function in equation (5.19) can vanish inside the gap  $|\omega| < \Delta_{\text{sc}}$ . As the imaginary part of the self-energy is zero in the gap this leads to excitations with infinite lifetime there. They correspond to the localised excited states (LES) or Andreev bound states. For the non-interacting case they are determined by the equation  $D(\omega) = 0$  [cf. eq. (5.18)],

$$\omega^2 - \varepsilon_d^2 - \Gamma^2 + \frac{2\omega^2\Gamma}{E(\omega)} = 0. \quad (5.25)$$

This is an equation in  $\omega^2$ , thus if  $E_b^0$  is a solution so is  $-E_b^0$ . In general, in the interacting case we have to analyse the equation

$$\left[\omega - \varepsilon_d + \frac{\omega\Gamma}{E(\omega)} - \Sigma(\omega)\right] \left[\omega + \varepsilon_d + \frac{\omega\Gamma}{E(\omega)} + \Sigma(-\omega)^*\right] - \left[\frac{\Gamma\Delta_{\text{sc}}}{E(\omega)} - \Sigma^{\text{off}}(\omega)\right] \left[\frac{\Gamma\Delta_{\text{sc}}}{E(\omega)} - \Sigma^{\text{off}}(-\omega)^*\right] = 0. \quad (5.26)$$

Once the self-energies are calculated it is possible to solve this equation iteratively. We will develop a simplified description by using an approximate form of the self-energy. First note that in the gap,  $|\omega| < \Delta_{\text{sc}}$ ,  $\text{Im}\Sigma(\omega) = \text{Im}\Sigma^{\text{off}}(\omega) = 0$ . We expand the real part of the diagonal self-energy  $\Sigma(\omega)$  to first order around  $\omega = 0$ , which is motivated by the Fermi liquid expansions for the normal case and the numerical results for the behaviour in this regime. The offdiagonal self-energy is approximated by the real constant  $\Sigma^{\text{off}}(0)$ , as it does not vary much for small  $\omega$ . This approximation for the self-energy is easy to justify if the gap is small parameter, such that it only covers small values of  $\omega$ , but also works reasonably well for larger gap parameters. Hence, we find instead of (5.26) the equation

$$\omega^2 - \tilde{\varepsilon}_d^2 - \tilde{\Gamma}^2 - z^2\Sigma^{\text{off}}(0)^2 + \frac{2\tilde{\Gamma}[\omega^2 + \Delta_{\text{sc}}z\Sigma^{\text{off}}(0)]}{E(\omega)} = 0, \quad (5.27)$$

where renormalised parameters  $\tilde{\varepsilon}_d = z[\varepsilon_d + \Sigma(0)]$  and  $\tilde{\Gamma} = z\Gamma$  were introduced. As usual  $z^{-1} = 1 - \Sigma'(0)$ . The form of the equations (5.25) and (5.27) is very similar and both can be easily solved numerically to give the bound state solutions  $\omega = E_b^\alpha = \alpha E_b$ ,  $\alpha = \pm$ . Due to the offdiagonal self-energy term  $\Sigma^{\text{off}}(0)$  a simple interpretation of the interacting theory based on using renormalised parameters  $\tilde{\varepsilon}_d$ ,  $\tilde{\Gamma}$  in equation (5.25) for the non-interacting theory is, however, not possible.

Based on the same idea we can give approximate expressions for the weights of the bound states  $w_b^\alpha$  by expanding the diagonal part of the Green's function around  $\omega = E_b^\alpha$ . We can write the Green's function in the gap near the bound states  $\omega \simeq \pm E_b$  as

$$G(\omega) = \frac{w_b^-}{\omega - E_b^- + i\eta} + \frac{w_b^+}{\omega - E_b^+ + i\eta}. \quad (5.28)$$

Using the above approximation for the self-energy the weights are found to be

$$w_b^\alpha = \frac{z}{2} E(E_b)^2 \frac{E(E_b)(1 + \alpha \frac{\tilde{\varepsilon}_d}{E_b}) + \tilde{\Gamma}}{E(E_b)^2(E(E_b) + 2\tilde{\Gamma}) + \tilde{\Gamma}(E_b^2 + \Delta_{\text{sc}}z\Sigma^{\text{off}}(0))}. \quad (5.29)$$

In a more sophisticated approximation one could consider an expansion of the self-energies around the bound state energies  $E_b$  rather than  $\omega = 0$ . Various things can be seen from the expression (5.29). First we note that in the particle hole symmetric case,  $\tilde{\varepsilon}_d = 0$ ,  $w_b^+ = w_b^- = w_b$ . As the weights are proportional to the renormalisation factor  $z$  they are expected to decrease with increasing interaction  $U$ . One can also easily see that for bound states close to the gap,  $|E_b| \rightarrow \Delta_{\text{sc}}$ , the weights go to zero,  $w_b^\alpha \rightarrow 0$ .

A useful limit to obtain analytical results is to consider the case where the superconducting gap is a large parameter,  $\Delta_{\text{sc}} \rightarrow \infty$  (Oguri et al. 2004). Then one can show that

the problem essentially reduces to a localised model with an anomalous on-site term which is of the order of the hybridisation  $\Gamma$ . We will write it in the form

$$H_d = \sum_{\sigma} \xi_d (c_{d,\sigma}^{\dagger} c_{d,\sigma} - 1) - \Gamma [c_{d,\uparrow}^{\dagger} c_{d,\downarrow}^{\dagger} + \text{h.c.}] + \frac{U}{2} \left( \sum_{\sigma} n_{d,\sigma} - 1 \right)^2, \quad (5.30)$$

where  $\xi_d = \varepsilon_d + U/2$ . Without interaction this Hamiltonian can be diagonalised by a Bogoliubov transformation and the excitation energies  $E_d = \sqrt{\xi_d^2 + \Gamma^2}$  are found, which usually lie in the gap as  $\Gamma \ll \Delta_{\text{sc}}$  as assumed initially. This gives a direct picture of the emergence of the Andreev bound states for large  $\Delta_{\text{sc}}$ .

We can discuss the ground state crossover from the singlet to the doublet state in terms of the single site Hamiltonian (5.30). First note that the  $S = 1/2$  (doublet) states,  $|\uparrow\rangle$  and  $|\downarrow\rangle$ , are eigenstates of (5.30) with energy 0. The  $S = 0$  singlet states, empty site  $|0\rangle$  and doubly occupied site  $|\uparrow\downarrow\rangle$ , are not eigenstates of (5.30). However, the linear combinations in the BCS-form,

$$|\Psi_1\rangle = u_d |0\rangle + v_d |\uparrow\downarrow\rangle, \quad |\Psi_2\rangle = v_d |0\rangle - u_d |\uparrow\downarrow\rangle, \quad (5.31)$$

are eigenstates with eigenvalues  $E_1 = -E_d + U/2$  and  $E_2 = E_d + U/2$ , respectively. The coefficients  $u_d, v_d$  are given by

$$u_d^2 = \frac{1}{2} \left( 1 + \frac{\xi_d}{E_d} \right), \quad v_d^2 = \frac{1}{2} \left( 1 - \frac{\xi_d}{E_d} \right). \quad (5.32)$$

The ground-state is therefore a singlet as long as  $E_1 < 0$  and a doublet otherwise. The condition  $E_1 = 0$  or

$$\frac{\xi_d^2}{U^2} + \frac{\Gamma^2}{U^2} = \frac{1}{4} \quad (5.33)$$

defines therefore the phase boundary for the transition. It is a semicircle in the  $(\xi_d/U)$ - $(\Gamma/U)$ -plane with radius  $1/2$ , which is shown in figure 5.11. How this phase boundary looks like for finite gap  $\Delta_{\text{sc}}$  will be investigated later in section 5.5, when we look at the situation away from particle hole symmetry. In the case of particle hole symmetry  $\xi_d = 0$  and the condition reduces to  $\Gamma = U/2$ .

Having established the most important relations we will in the next section present results for behaviour of the bound state in the symmetric AIM with superconducting bath with a finite gap parameter.

### 5.3 Bound state behaviour for the symmetric model

The position and weight of the Andreev bound states in the gap can be calculated from the NRG routine for spectral functions as the lowest spectral excitation (SE). The bound states correspond to a single excitation with energy  $E_b^{\pm} = \pm E_b$ ,  $|E_b| < \Delta_{\text{sc}}$ , and carry a certain weight  $w_b$ . In figure 5.1 we show the bound state energies  $\pm E_b$  for a series of values

of the on-site interaction  $U$  and different values for the gap in the medium  $\Delta_{\text{sc}}$ . Here and in the following we take a fixed value for the hybridisation,  $\pi\Gamma = 0.2$ . All quantities can be thought of as being scaled by half the band width  $D = 1$ .

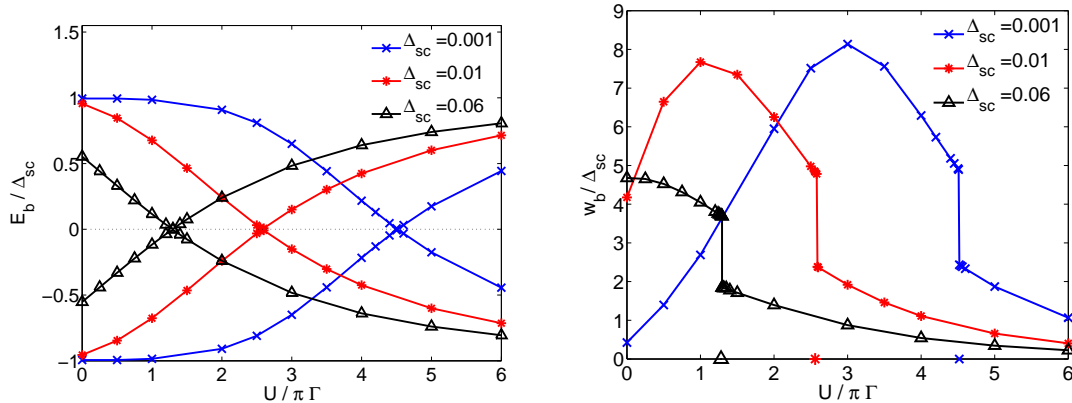


Figure 5.1: Bound state energies  $E_b$  (left) and weights  $w_b$  (right) for various  $U/\pi\Gamma$  and  $\Delta_{\text{sc}}$ . Both quantities have been scaled by the corresponding value of  $\Delta_{\text{sc}}$ .

We can see that in the non-interacting case the bound state energy for the cases with small gap ( $\Delta_{\text{sc}} = 0.001, 0.01$ ) is very close to  $\pm\Delta_{\text{sc}}$  and decreases to zero with increasing interaction. For a critical value  $U_c$  the nature of the ground-state changes from a singlet ( $S = 0$ ) to a doublet ( $S = 1/2$ ) and at this point  $E_b = 0$ . For this transition we can think of the positive  $E_b^+$  and negative solution  $E_b^-$  for the bound states as crossing at  $\omega = 0$ . If the interaction is increased further,  $|E_b^\pm|$  becomes finite again and increases with  $U$ . The larger the gap  $\Delta_{\text{sc}}$  the smaller critical value  $U_c$  for this ground state transition becomes. In the case where  $\Delta_{\text{sc}}$  is of the order of  $\Gamma$  - as can be seen for the case  $\Delta_{\text{sc}} = 0.06$  - the bound state energy  $E_b$  lies within the gap, detached from the continuum part at  $\Delta_{\text{sc}}$ , already for the non-interacting case, but otherwise shows a similar behaviour as described above.

On the right hand side of figure 5.1 the weight  $w_b$  of these bound states is plotted. We have marked the position  $U_c$  of the singlet-doublet crossover point by a symbol on the  $x$ -axis. The two curves for a value of the gap  $\Delta_{\text{sc}} = 0.001$  and  $\Delta_{\text{sc}} = 0.01$  have a maximum for some intermediate value of  $U$  which is smaller than the critical  $U_c$  for the ground state transition. For the other curve ( $\Delta_{\text{sc}} = 0.06$ ) the weight is maximal for the non-interacting case. In all cases the weight becomes very small for large  $U$ . Note that we plot the weight scaled by the gap,  $w_b/\Delta_{\text{sc}}$ , and therefore the absolute values are larger for the cases with larger superconducting gap. At the singlet-doublet transition we can see discontinuous behaviour as the weight changes sharply. This is a feature of the zero temperature calculation, where the matrix elements change their values when the levels cross on increasing  $U$ , such that the nature of the ground state changes. It will be seen for the anomalous correlations as well. For finite temperature this discontinuity becomes smooth.

In the last section we discussed how the bound state energy, which so far we have deduced from the spectral excitations (SE), could also be calculated from the bound state equation (BE) (5.26). The latter was derived by expanding the self-energy to first order. It involves the renormalised parameters  $\tilde{\varepsilon}_d$ ,  $\tilde{\Gamma}$  and the constant value of the offdiagonal self-energy  $\Sigma^{\text{off}}(0)$ . In figure 5.2 we compare the bound state energies calculated by these two methods for two values of the gap  $\Delta_{\text{sc}} = 0.005$  (left) and  $\Delta_{\text{sc}} = 0.06$  (right).

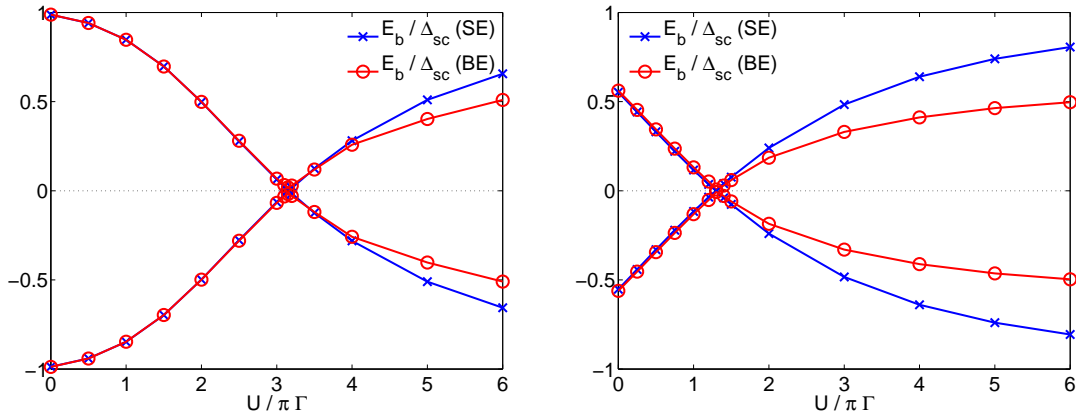


Figure 5.2: Bound state energies  $E_b$  as calculated from the spectral excitations (SE) and from the bound state equation (BE) (5.26) with renormalised parameters for  $\Delta_{\text{sc}} = 0.005$  (left) and for  $\Delta_{\text{sc}} = 0.06$  (right) for various  $U/\pi\Gamma$ .

We can see that for values of  $U < U_c$  the agreement is excellent in both cases. However, when  $U \geq U_c$  we find less accurate values with the method based on bound state equation (BE) with renormalised parameters. Since the method to calculate the bound state energy from the spectral excitations (SE) is very accurate there must be some problem with the BE method. The closer inspection of the numerical results for the diagonal and off-diagonal self-energies reveals that the linear and constant approximation made to derive the bound state equation with renormalised parameters (5.26) becomes less valid for  $U \geq U_c$ .

In the last section we also derived an expression (5.29) for the weights  $w_b$  of the bound states in the gap. It can be expressed in terms of the renormalised parameters  $\tilde{\varepsilon}_d$ ,  $\tilde{\Gamma}$ , the offdiagonal self-energy  $\Sigma^{\text{off}}(0)$  and the bound states energy  $E_b$ . In figure 5.3 we compare the weights calculated from the spectral excitations (SE) with the ones from the bound state equation (BE) analysis with renormalised parameters. We show the results for the same parameters  $\Delta_{\text{sc}} = 0.005$  (left) and  $\Delta_{\text{sc}} = 0.06$  (right). We can see for both cases that the overall behaviour of the weights as a function of  $U$  is described reasonably well by equation (5.29). It is, however, clearly visible that the agreement between the SE and BE values is much better in the singlet regime for  $U < U_c$ . This is similar as observed for the values of the bound states energies  $E_b$  in figure 5.2, and the reason for this is the same. The discontinuity for the weight is not reproduced by the approximation based on equation (5.29). As can be seen from that equation this would require a sudden change in the self-energy as function of  $U$ , which was not found with sufficient accuracy in the

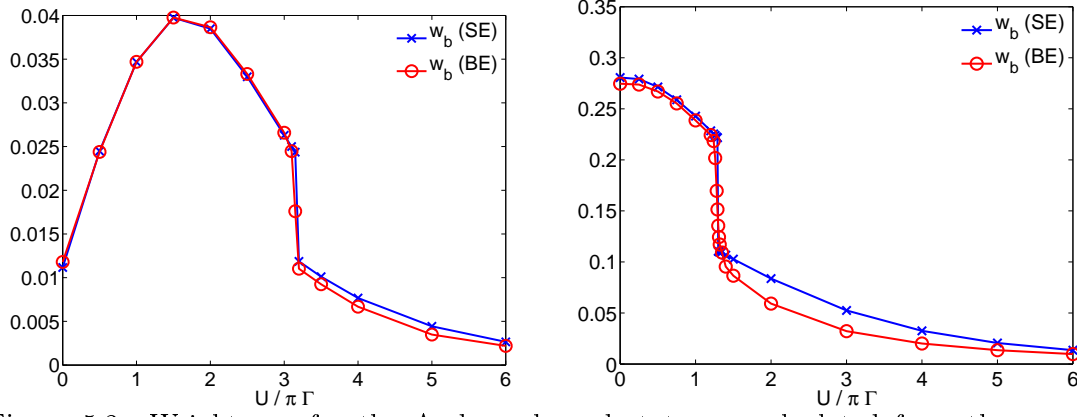


Figure 5.3: Weights  $w_b$  for the Andreev bound states as calculated from the spectral excitations (SE) and from the equation (5.29) with renormalised parameters for  $\Delta_{\text{sc}} = 0.005$  (left) and for  $\Delta_{\text{sc}} = 0.06$  (right) for various  $U/\pi\Gamma$ .

present calculation. This can partly be attributed to the broadening procedure involved and to the inaccuracies when calculating the numerical derivative.

The anomalous expectation value  $\langle d_{\uparrow}d_{\downarrow} \rangle$  is an indicator for the strength of the proximity effect of the superconducting medium at the impurity site and quantifies the induced on-site superconducting correlations. In the following figure 5.4 we show the dependence of  $\langle d_{\uparrow}d_{\downarrow} \rangle$  on the interaction  $U/\pi\Gamma$  for the same values of  $\Delta_{\text{sc}}$  as in figure 5.1. The values are scaled by the gap  $\Delta_{\text{sc}}$ .

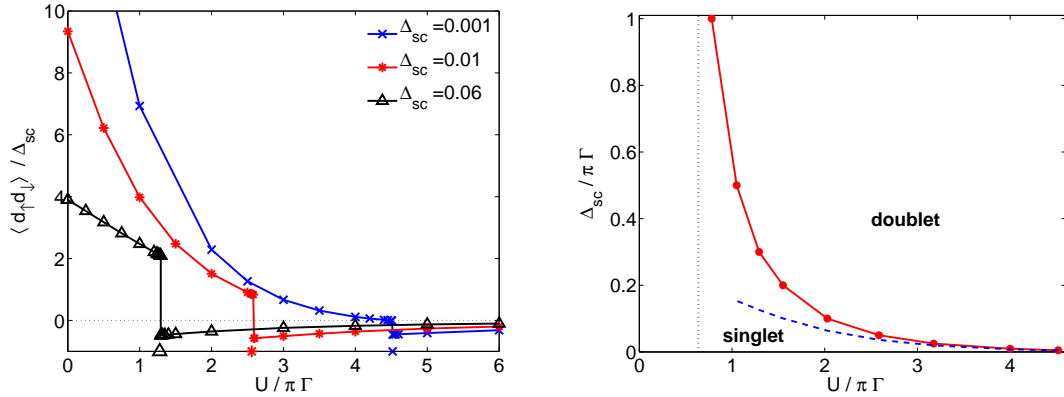


Figure 5.4: Left: Anomalous expectation values as a function of  $U/\pi\Gamma$  for various  $\Delta_{\text{sc}}$ . The values are scaled by the gap  $\Delta_{\text{sc}}$ . Right: Phase diagram for singlet and doublet ground-state as a function of  $\Delta_{\text{sc}}/\pi\Gamma$  and  $U/\pi\Gamma$ . The dotted line corresponds to  $U/\Gamma = 2$ , which gives the singlet doublet transition for  $\Delta_{\text{sc}} \rightarrow \infty$ . The dashed line gives the transition as  $T_{\text{K}}/\Delta_{\text{sc}} \simeq 0.3$  with  $T_{\text{K}}$  given in equation (5.34).

We see that as a general trend  $\langle d_{\uparrow}d_{\downarrow} \rangle$  decreases for increasing on-site interaction. This is expected since the superconducting correlations are suppressed by the repulsive interaction. We have marked the ground state transition with a symbol on the  $x$ -axis, and we see that

$\langle d_\uparrow d_\downarrow \rangle$  changes discontinuously in magnitude and sign there. The sign change is due to a phase change of  $\pi$  of the local order parameter which occurs at the transition as discussed in reference Balatsky et al. (2006). It is characteristic for this zero temperature quantum phase transition. At finite temperature this behaviour becomes continuous. In the situation of infinite gap in the medium, as discussed above, at the transition point  $\langle d_\uparrow d_\downarrow \rangle$  drops to zero for the singlet ground state.

On the right hand side of figure 5.4 we present a phase diagram for singlet and doublet state for the symmetric model. For small  $U$  the ground state is always a singlet. It can become a doublet when  $U/\pi\Gamma$  is increased. The critical  $U_c$  for the transition decreases with increasing value of the gap  $\Delta_{sc}$  as can be seen in the diagram. In the limit  $\Delta_{sc} \rightarrow \infty$ , the critical interaction is given by  $U_c/\pi\Gamma = 2/\pi$ , which is shown with a dotted vertical line in the figure. As mentioned earlier there have been estimates of the boundary between singlet and doublet in the strong coupling regime (Satori et al. 1992, Yoshioka and Ohashi 2000) as  $T_K/\Delta_{sc} \simeq 0.3$ . In this case the Kondo temperature is given as by Yoshioka and Ohashi (2000) (eq. 3.9),

$$T_K = 0.182U \sqrt{\frac{8\Gamma}{\pi U}} e^{-\pi U/8\Gamma}. \quad (5.34)$$

We have added a dashed line representing this result which agrees with the ones presented here in the strong coupling regime, but starts to deviate for smaller values of  $U$ . In the limit  $\Delta_{sc} \rightarrow 0$  the ground-state is a singlet for any value of  $U$  as the Kondo effect always leads to a screened impurity spin in a singlet formation. For finite gap the nature of the singlet ground state can differ depending on the magnitude of  $U$ . We expect a ‘‘superconducting singlet’’ for small  $U$  and a Kondo singlet for larger  $U$ . We will comment on this again at the end of the next section.

## 5.4 Spectral functions

In this section we present results for the behaviour of the spectral functions. The diagonal and offdiagonal Green’s function can be calculated directly from the Lehman representation as illustrated in chapter 2 and we use the method based on the Anders-Schiller basis. As in this procedure the excitations for the spectral peaks in the Green’s function have to be broadened, it is difficult like this to obtain a sharp spectral gap at  $|\omega| = \Delta_{sc}$ . We can, however, determine the self-energy components from the Green’s function and the higher  $F$ -Green’s function [cf. eq. (5.23)] as explained earlier. We use the exact expression for the non-interacting Green’s function  $\underline{G}_d^0(\omega)$  in equation (5.17), which includes a sharp spectral gap, and the Dyson matrix equation (5.24) to calculate the diagonal and offdiagonal Green’s function. This is the way the Green’s function are calculated for the region outside the gap,  $|\omega| > \Delta_{sc}$ . Inside the gap,  $|\omega| < \Delta_{sc}$ , we have extracted the delta-function peaks for the Andreev bound states energies  $E_b$  and weights  $w_b$  from the NRG excitation data for the Green’s function. The delta-functions are represented by an arrow. Altogether the

diagonal spectral function  $\rho(\omega) = -\text{Im}G(\omega)/\pi$  can then be written in the form

$$\rho(\omega) = \sum_{\alpha=\pm} w_b \delta(\omega - E_b^\alpha) + \rho_{\text{cont}}(\omega), \quad (5.35)$$

where  $\rho_{\text{cont}}(\omega)$  is the continuum part for  $|\omega| > \Delta_{\text{sc}}$ .

In figure 5.5 we show the resulting spectral function (5.35) for  $\Delta_{\text{sc}} = 0.005$  for the diagonal Green's function at the impurity site for a number of different values of  $U$ . As before  $\pi\Gamma = 0.2$  throughout the section.

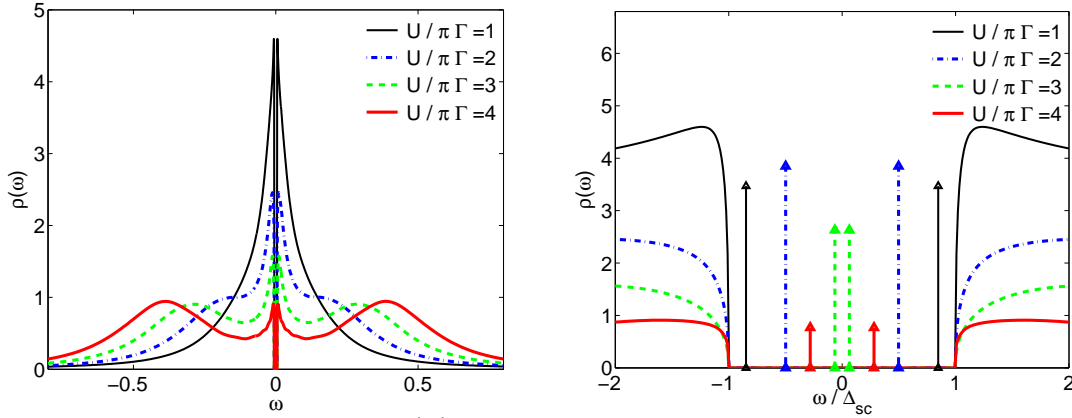


Figure 5.5: The spectral density  $\rho(\omega)$  for various values of  $U$  for the whole energy regime (left) and the region in the gap (right);  $\Delta_{\text{sc}} = 0.005$ .

In the plot on the left hand side we give the spectrum over the full energy range. One can see the development of the atomic limit peaks at  $\pm U/2$  as the interaction is increased, and also the beginning of the formation of a Kondo resonance at low frequencies. As  $U$  increases the Kondo resonance becomes narrower, its formation, however, is suppressed, since in the gap region the continuum part of the spectrum vanishes. In the gap there are only the delta function contributions from the Andreev bound states. These are shown in an enlarged plot in figure 5.5 on the right, where the arrows give the position of the bound state  $E_b^\pm$  and their height indicates the spectral weight  $w_b$ . It can be seen that the position of the bound state changes when we increase the interaction. The weight first increases and then decreases as a function of  $U$ , which corresponds to the features which was discussed explicitly in the last section in figure 5.1. Note that the largest value of  $U$  shown, is greater than the critical  $U_c$  for the singlet-doublet transition ( $U_c/\pi\Gamma \simeq 3.2$ ). In the high energy spectrum there is no significant change to be seen in the behaviour, however at low energies we observe the crossing of the bound state energies at  $\omega = 0$  at  $U_c$ .

The offdiagonal part of the spectrum  $\rho^{\text{off}}(\omega) = -\text{Im}G^{\text{off}}(\omega)/\pi$  has a similar general form as the diagonal part,

$$\rho^{\text{off}}(\omega) = \sum_{\alpha=\pm} \bar{w}_b^\alpha \delta(\omega - E_b^\alpha) + \rho_{\text{cont}}^{\text{off}}(\omega), \quad (5.36)$$

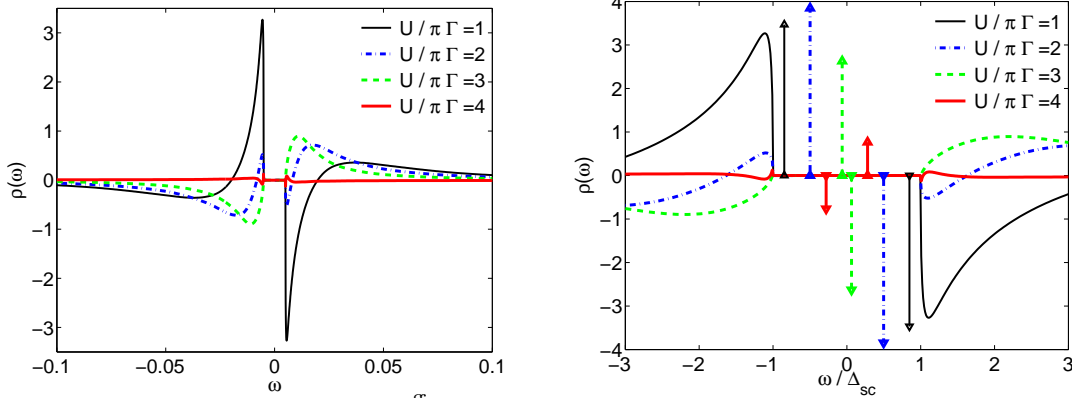


Figure 5.6: The spectral density  $\rho^{\text{off}}(\omega)$  for various values of  $U$  for the whole energy regime (left) and the region in the gap (right);  $\Delta_{\text{sc}} = 0.005$ .

where the weights  $\bar{w}_b^\alpha$  can have positive and negative values. For half filling the spectrum  $\rho^{\text{off}}(\omega)$  is an asymmetric function of  $\omega$ . In figure 5.6 we show the spectral function (5.36) for  $\Delta_{\text{sc}} = 0.005$  for the offdiagonal Green's function at the impurity site for a number of different values of  $U$ . In the plot on the left hand side we can see the behaviour for the continuum part outside the gap. Notice that the frequency range only extends up to  $\omega = \pm 0.1$ . We can see a peak close to  $\omega = \pm \Delta_{\text{sc}}$ , which is suppressed for larger  $U$  and changes sign towards the singlet-doublet transition. The behaviour of the bound state peaks in the offdiagonal spectrum is displayed on the right hand side of the figure. We can see similar features as observed before in the diagonal part, i.e. the weight first increases with  $U$  and then decreases. If we follow the excitations with the weight of the same sign we can see, that at the singlet-doublet transition the bound state levels cross at  $\omega = 0$ .

In figure 5.7 we show the diagonal spectral function for a larger gap  $\Delta_{\text{sc}} = 0.02$  for the diagonal Green's function at the impurity site for a number of different values of  $U$ .

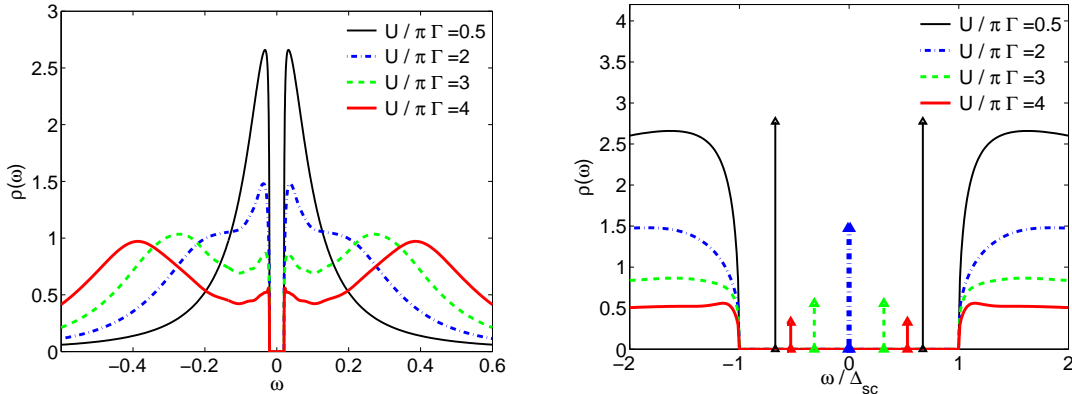


Figure 5.7: The spectral density  $\rho(\omega)$  for various values of  $U$  for the whole energy regime (left) and the region in the gap (right);  $\Delta_{\text{sc}} = 0.02$ .

The overall picture on the left is similar to the case in figure 5.5 with the smaller gap. Due

to the larger gap the formation of the central Kondo resonance is completely suppressed, but the high energy spectrum is as before. From the behaviour within the gap (right side in figure 5.7) we can see that the bound state position  $E_b^\pm$  goes to zero for smaller  $U$  than in the case  $\Delta_{\text{sc}} = 0.005$ , and hence the ground state transition occurs for smaller  $U_c$  for the larger gap ( $U_c/\pi\Gamma \simeq 2.03$ ). This was discussed in the last section. For the values of  $U$  shown the spectral weight of the bound states  $w_b$  decreases with increasing  $U$ . Note that the weights  $w_b$  of the peaks in the gap have been scaled differently in figures 5.5 and 5.7, so that their height should not be compared directly.

The spectral function of the offdiagonal Green's function at the impurity site (5.36) for this value of the gap,  $\Delta_{\text{sc}} = 0.02$ , is shown in figure 5.8 for a number of different values of  $U$ .

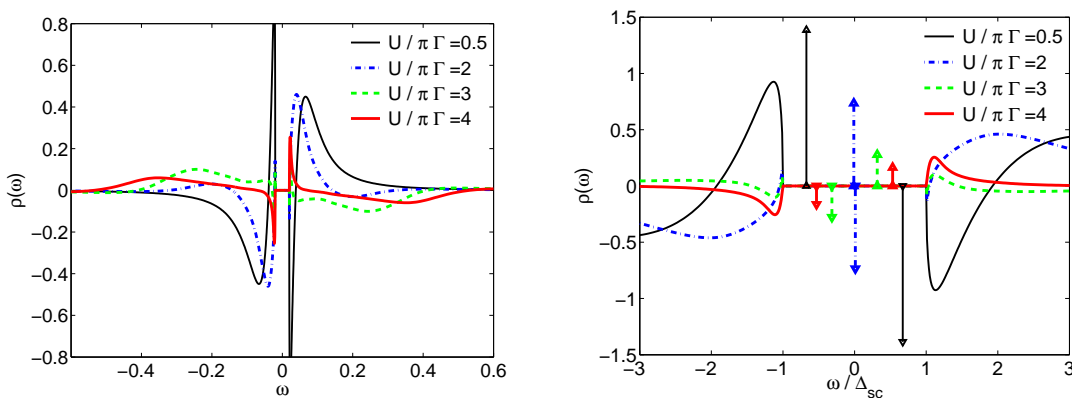


Figure 5.8: The spectral density  $\rho^{\text{off}}(\omega)$  for various values of  $U$  for the whole energy regime (left) and the region in the gap (right);  $\Delta_{\text{sc}} = 0.02$ .

For larger frequencies outside of the gap (left) we can see a peak near  $\omega = \Delta_{\text{sc}}$ , whose height is reduced due to the larger interaction. At larger frequencies we find that the tails develop a broad peak for larger values of  $U$ . This has not been observed in the case with the smaller gap shown in figure 5.6. Also a sign change of the low energy peak can be observed as before. The behaviour near and in the gap (right) can be understood as before for the bound states, where in this case we have two bound states for the singlet ground state and two for the doublet ground state.

We have analysed the transition from a singlet to a doublet ground state in detail in the spectral excitations. Within the parameter regime for the singlet ground state there are two possibilities for the nature of the ground state. It can be a singlet corresponding to an s-wave pair like in the wave function given in equation (5.31), which is a superposition of zero and double occupation. This is the natural singlet ground state for a BCS superconductor. In the strong coupling regime  $U/\pi\Gamma > 2$  we can, however, also have a screened local spin, i.e. a Kondo singlet. The wave function has a different form then and consists rather of a singly occupied impurity state coupled to the spins of the medium as many-body singlet. In our NRG calculations it is not easy to distinguish these different natures of the singlet

ground states. We can, however, get an indication for what is favoured from the two particle response functions in the spin and in the charge channel. In figure 5.9 we show the imaginary part of the dynamic charge and spin susceptibility,  $\chi_c(\omega)$  [cf. eq. (1.25)] and  $\chi_s(\omega)$  [cf. eq. (1.24)], for  $\Delta_{sc} = 0.005$  and a series of values for the interaction  $U$ .

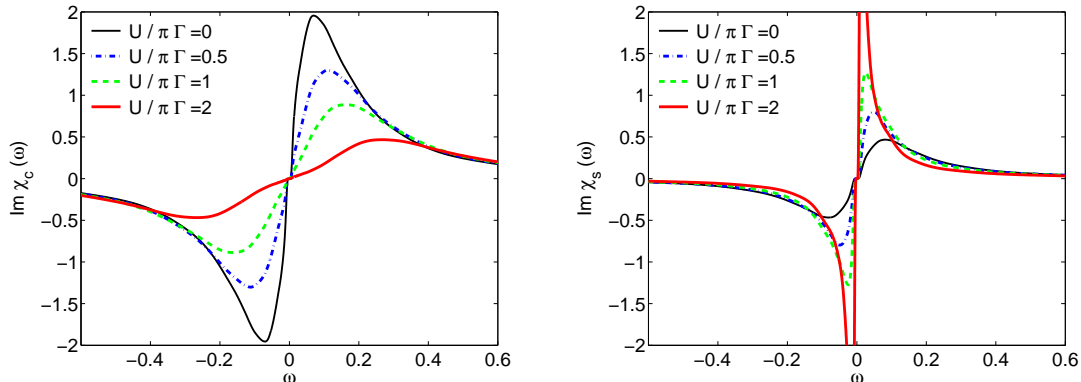


Figure 5.9: The imaginary part of the dynamic charge (left) and spin (right) susceptibility various values of  $U$  and  $\Delta_{sc} = 0.005$ . The scale on both axes is the same such that the results can be compared well.

We can see that the peaks in the charge susceptibility exceed the ones in the spin susceptibility for zero and weak interaction indicating the dominance of the symmetry breaking in the charge channel, and a ground state of superconducting singlet nature. However, for  $U/\pi\Gamma > 1$  the spin susceptibility develops large and narrow peaks at low frequency. This signals the importance of the spin fluctuations and low energy spin excitations and indicates a ground states of a screened spin. In contrast the decreasing peaks in the charge susceptibility for large  $U$  represent the effect of suppressing the superconducting on-site correlations.

## 5.5 Away from particle hole symmetry

So far we have considered the situation at particle-hole symmetry,  $\varepsilon_d = -U/2$ . In this section we will briefly discuss a few aspects that change in the situation away from particle hole symmetry. Let us consider the case where for a given gap  $\Delta_{sc}$ , on-site interaction  $U$ , and hybridisation  $\Gamma$ , the ground-state of the system is a doublet at half filling,  $\xi_d = 0$ . When  $\xi_d$  is increased, we find that a transition to a singlet state can occur at a certain value  $\xi_d^c$ . Similar to the cases shown for the symmetric model the ground state change is accompanied by vanishing energy of the bound state  $E_b$ . This is illustrated in the following figure 5.10, where we have plotted the bound state energy  $E_b$  for fixed  $\Delta_{sc} = 0.01$ , two values of  $U/\pi\Gamma = 3, 5$  and a series of values of the on-site energy scaled by  $U$ ,  $\xi_d/U$ . As before we have  $\pi\Gamma = 0.2$ .

The critical interaction for the ground state transition for this case at half filling is  $U_c/\pi\Gamma \simeq$

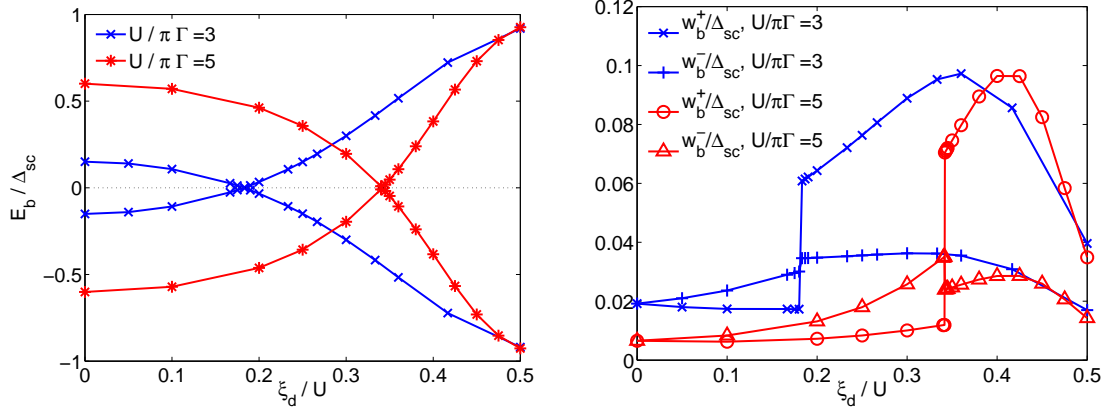


Figure 5.10: The dependence of the bound state energies  $E_b$  (left) and weights  $w_b$  (right) on  $\xi_d/U$  for  $\Delta_{sc} = 0.01$  and  $U/\pi\Gamma = 3, 5$ .

2.6, such that both cases have a doublet ground state for  $\xi_d = 0$ . We can see that with increasing asymmetry  $\xi_d$  the bound state energy  $|E_b|$  first decreases towards zero and then increases again in the singlet regime for  $\xi_d > \xi_d^c$ . As in the symmetric case the singlet-doublet transition is accompanied by  $|E_b| \rightarrow 0$ . The weights for these bound states are shown on the right hand side of figure 5.10. Away from particle hole symmetry the weight  $w_b^+$  for the positive energy  $E_b^+$  and  $w_b^-$  the one for the negative bound state  $E_b^-$  are not equal, as was already visible in equation (5.29). We can see that the weights  $w_b^\pm$  start to assume different values when  $\xi_d$  is increased from 0. At the ground state transition the values change discontinuously similar as observed in the half filled case. If we follow the both the positive weight  $w_b^+$  and the negative  $w_b^-$  separately the weights cross at the transition point. If, however, we think of the bound states as crossing at zero, i.e.  $w_b^+ \leftrightarrow w_b^-$  at the transition, a more direct connection can be deduced from the results shown. In the singlet phase there is a maximum for both the positive and the negative bound state weight, more pronounced for  $w_b^+$ .

Also in the asymmetric case it is possible to calculate the bound state position  $E_b$  from equation (5.27) and the weights from equation (5.29) employing the renormalised parameters. We abstain from showing explicit plots here, but note that the results resemble figures 5.2 and 5.3 in the respect that they give good agreement in the singlet regime, but deviations for parameters where the ground state is a doublet.

In the following figure 5.11 (left) we show the dependence of the anomalous expectation value  $\langle d_\uparrow d_\downarrow \rangle$  on the asymmetry scaled by the interaction  $\xi_d/U$  for the same value of  $\Delta_{sc}$  as in figure 5.10. The values for  $\langle d_\uparrow d_\downarrow \rangle$  are scaled by the gap  $\Delta_{sc}$ . For the values of  $U$  shown, at half filling the system has a doublet ground state and  $\langle d_\uparrow d_\downarrow \rangle$  is negative. First it does not vary much when  $\xi_d$  is increased, but at the transition to the singlet ground state we find, as in the half filled case, a jump to a positive value and  $\langle d_\uparrow d_\downarrow \rangle$  increases to a saturation value on further increasing  $\xi_d$ . This value is smaller for larger  $U$ , similar to what has been found in the symmetric case.

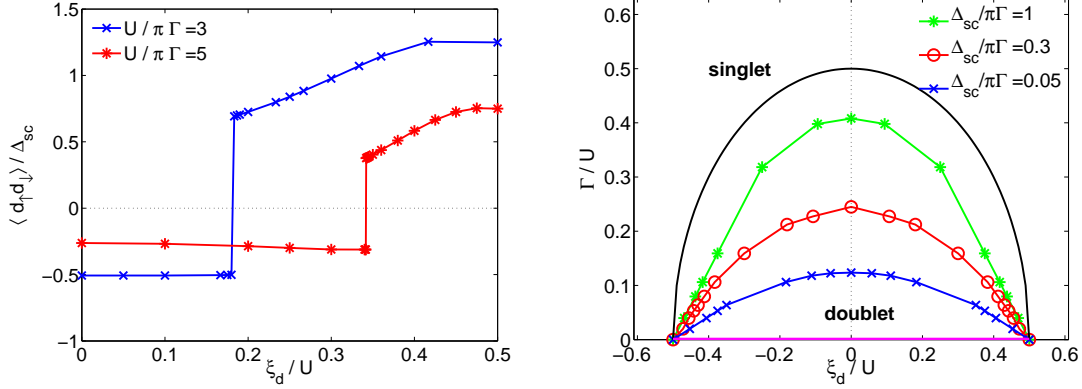


Figure 5.11: Left: Anomalous expectation values for various  $U/\pi\Gamma$  and  $\Delta_{\text{sc}} = 0.01$ . Right: Phase diagram showing the regions for singlet and doublet ground state as dependent on  $\Gamma/U$  and  $\xi_d/U$  for different values of the gap  $\Delta_{\text{sc}}$ . The full semicircular line corresponds to the phase boundary for  $\Delta_{\text{sc}} = \infty$  as discussed in equation (5.33).

On the right hand side of figure 5.11 we present a global phase diagram of parameter regimes for singlet and doublet ground states for the non-symmetric case. This representation in the  $\Gamma/U$ - $\xi_d/U$ -plane is motivated by the result for the phase boundary for the case  $\Delta_{\text{sc}} \rightarrow \infty$  derived in equation (5.33). The corresponding semicircle is shown in the figure accompanied by the phase boundaries for finite values of the gap  $\Delta_{\text{sc}}$ . Note that the line on the  $x$ -axis, to which the phase boundary is contracted in the limit  $\Gamma \rightarrow 0$  or  $U \rightarrow \infty$ , possess a doublet ground state for  $|\xi_d|/U < 1/2$ .

In summary, we have discussed the behaviour of an interacting impurity site in a medium with symmetry breaking in the charge channel. This situation is motivated by the situation of magnetic impurities in superconductors and nanoscale quantum dot systems with superconducting leads. As an additional parameter, the magnitude of the gap  $\Delta_{\text{sc}}$  enters the problem. The low energy spectrum is dominated by the gap, and we saw that the lowest excitations in these cases are Andreev bound states within the gap region, which change position and weight according to the other parameters. These have been analysed in detail in both the symmetric and the asymmetric model. We have shown that a renormalised parameter description for the position of the weights of the bound states is possible. We have presented spectral functions for both the low energy regime and the full frequency range. The behaviour of the ground state, which can be a singlet or doublet, is summarised in the two phase diagrams in figures 5.4 and 5.11.

## Part III

# Correlated Lattice Systems



*Everything should be as simple as it is, but not simpler.*

Albert Einstein

## Chapter 6

# The Hubbard model in magnetic field

In the third part of this thesis we study correlated electrons in the lattice model subject to a certain symmetry breaking. In this chapter we describe the response of the interacting electrons to a homogeneous magnetic field. We first briefly describe the DMFT-NRG formalism with magnetic symmetry breaking and explain how the field dependent renormalised parameter and RPT description from chapter 3 can be generalised. Then we present results for different parameter regimes at half filling and away from half filling.

### 6.1 Magnetic states in the Hubbard model

The Hubbard model (1.29) had originally been proposed to study magnetic ordering and ferromagnetism, based on an a microscopic theory of itinerant correlated electrons. Mean field theory, indeed, predicts spontaneous magnetic order in the Hubbard model when the Stoner criterion

$$\rho_0(\varepsilon_F)U > 1 \tag{6.1}$$

is satisfied. More careful studies have revealed, however, that it is not so easy to find a ferromagnetic ground state in the Hubbard model and corresponding region of the parameters in the phase diagram is not so large (Kotliar and Ruckenstein 1986, von der Linden and Edwards 1991) [for a review see Tasaki (1995)]. The criterion (6.1) although not accurate gives the right tendency for the onset of magnetism, i.e. large  $U$  and large density of states at the Fermi level. A rigorous result for ferromagnetic ordering by Nagaoka (1966) for infinite  $U$  and one hole exist, but it has not been easy to extend this result (von der Linden and Edwards 1991). A more recent DMFT study found ferromagnetism for very large  $U$  and moderate doping (Zitzler et al. 2002). It has also be found in flat band models with an infinite density of states (Mielke 1993). One reason that ferromagnetism is not found for an ordinary DOS and at smaller values  $U$ , say of order of the bandwidth, is that the tendency to antiferromagnetic ordering by the induced by the inter-site spin coupling  $J$ , (1.31), is dominant. Antiferromagnetic ordering is discussed in the next chapter.

In this chapter, rather than studying spontaneous ferromagnetic ordering we want to focus on the paramagnetic response of the correlated lattice electrons towards an external magnetic field. We have seen for the impurity model in section 3.2 that the susceptibility towards the exposure to a magnetic field increases with the degree of correlation and similar effects will be found here. We also saw there that the corresponding quasiparticle behaviour could be characterised in terms of field dependent renormalised parameters. In this section we want to extend these methods to the study of the effect of a magnetic field on the lattice system of correlated electrons. We will find quite distinct behaviour depending on the on-site interaction  $U$ . The extreme limits can easily be understood without any calculation. In the non-interacting limit, we deal with a free Fermi gas and only have to consider the competition of the magnetic field energy of order  $h$  with the kinetic energy which is of order of the hopping  $t$ . The system therefore only shows a strong polarisation when  $h \gtrsim t$ , which - as  $t$  is of the order of electron volts - in practice is a very large field. In the limit of very strong local interaction,  $U \rightarrow \infty$ , the situation is completely different. In the half filled case every site is singly occupied and thus possess a local moment as charge fluctuations are completely frozen. These uncoupled spins, polarise completely even for a very small field and thus the susceptibility of the system diverges in the zero temperature limit (Curie law). The intermediate regime between these extreme limits is more interesting, but needs a more careful consideration, which is carried out here in the DMFT framework.

To study the Hubbard model with an induced magnetic symmetry breaking is not only of interest for theoretical reasons. A number of materials, such as heavy fermions, vanadium oxide, liquid  $^3\text{He}$  can be understood as a strongly correlated Fermi liquid and their response to a magnetic field has been investigated in great detail. For instance, phenomena like field and spin dependent effective masses and metamagnetic behaviour have been observed experimentally in several heavy fermion compounds (Aoki et al. 1993, Goodrich et al. 1999, Manekar et al. 2000, Dordevic et al. 2006). The Hubbard model, however, being a one band model is not an appropriate starting point to make a quantitative comparison with the heavy fermion class of materials. A periodic Anderson model with a two band structure and including the degeneracy of the f electrons would be a better model to describe these materials. Field dependent effects in this model have been studied by several techniques, modified perturbation theory (Meyer and Nolting 2001), exact diagonalisation (Saso and Itoh 1996),  $1/N$  expansion (Ono 1998) and variational approach (Edwards and Green 1997).

## 6.2 Setup for the DMFT with a magnetic field symmetry breaking

We consider the Hubbard model (1.29) in a magnetic field,

$$H = - \sum_{i,j,\sigma} (t_{ij} c_{i,\sigma}^\dagger c_{j,\sigma} + \text{h.c.}) - \sum_{i\sigma} \mu_\sigma n_{i\sigma} + U \sum_i n_{i,\uparrow} n_{i,\downarrow}, \quad (6.2)$$

where  $\mu_\sigma = \mu + \sigma h$  with the field  $h$  as introduced earlier and the chemical potential  $\mu$ . We will treat (6.2) in the DMFT approximation and due to the symmetry breaking term all relevant quantities introduced in section 2.3 now become spin dependent. The generalisation of the equations in section 2.3 is, however, completely straightforward. The effective Weiss field  $\mathcal{G}_{0,\sigma}^{-1}(\tau)$  carries a spin index, and equation (2.71) generalises to two equations for each spin component,

$$\mathcal{G}_{0,\sigma}^{-1}(\omega) = G_\sigma^{\text{loc}}(\omega)^{-1} + \Sigma_\sigma(\omega), \quad (6.3)$$

which form the two self-consistency equations for the approach. Once the spin dependent self-energy  $\Sigma_\sigma(\omega)$  is obtained in the effective impurity problem the local lattice Green's function  $G_\sigma^{\text{loc}}(\omega)$  can be calculated from

$$G_\sigma^{\text{loc}}(\omega) = \sum_{\mathbf{k}} G_{\mathbf{k},\sigma}(\omega) = \int d\varepsilon \frac{\rho_0(\varepsilon)}{\omega + \mu_\sigma - \Sigma_\sigma(\omega) - \varepsilon}, \quad (6.4)$$

where  $\rho_0(\varepsilon)$  is the density of states for the non-interacting model ( $U = 0$ ).  $G_\sigma^{\text{loc}}(\omega)$  can be identified with the Green's function  $G_\sigma(\omega)$  of an effective AIM, by re-expressing  $\mathcal{G}_{0,\sigma}^{-1}(\omega)$  as

$$\mathcal{G}_{0,\sigma}^{-1}(\omega) = \omega + \mu_\sigma - K_\sigma(\omega), \quad (6.5)$$

such that

$$G_\sigma(\omega) = \frac{1}{\omega - \varepsilon_{d,\sigma} - K_\sigma(\omega) - \Sigma_\sigma(\omega)}, \quad (6.6)$$

with  $\varepsilon_{d,\sigma} = -\mu_\sigma$ . The dynamical mean field  $K_\sigma(\omega)$ , describing the effective medium surrounding the impurity, is also spin dependent now. As illustrated in section 2.3 quite generally, starting from an initial form for  $K_\sigma(\omega)$ ,  $\Sigma_\sigma(\omega)$  is calculated using an appropriate impurity solver from which  $G_\sigma^{\text{loc}}(\omega)$  can be calculated using equation (6.4). A new result for  $K_\sigma(\omega)$  is then obtained from equations (6.3) and (6.5). This  $K_\sigma(\omega)$  serves as an input for the effective impurity problem and the process is repeated until it converges to give a self-consistent solution. As impurity solver we use the NRG in this thesis, which is most accurate for calculations at  $T = 0$  and for the low energy excitations. There has been a DMFT study of the static properties of a half-filled Hubbard model in a magnetic field using the exact diagonalisation (ED) method by Laloux et al. (1994).

The density of states  $\rho_0(\varepsilon)$  of the non-interacting infinite dimensional model here is chosen as the semi-elliptical form corresponding to a Bethe lattice (2.75)

$$\rho_0(\varepsilon) = \frac{2}{\pi D^2} \sqrt{D^2 - (\varepsilon + \mu_0)^2} \quad (6.7)$$

where  $2D$  is the band width, with  $D = 2t$  for the Hubbard model, and  $\mu_0$  the chemical potential of the free electrons. We choose this form, rather than the Gaussian density of states of the hypercubic lattice, as it has a definite finite bandwidth.

Before considering in detail the methods of solving these equations, we look at the form of these equations in the low energy regime, where we can give them an interpretation in

terms of renormalised quasiparticles. We assume that we can expand  $\Sigma_\sigma(\omega)$  in powers of  $\omega$  for small  $\omega$ , and retain terms to first order in  $\omega$  only. Substituting this expansion into the equation for the local Green's function gives

$$G_\sigma^{\text{loc}}(\omega) = z_\sigma \int d\varepsilon \frac{\rho_0(\varepsilon/z_\sigma)}{\omega + \tilde{\mu}_{0,\sigma} + \mathcal{O}(\omega^2) - \varepsilon}, \quad (6.8)$$

where

$$\tilde{\mu}_{0,\sigma} = z_\sigma(\mu_\sigma - \Sigma_\sigma(0)), \quad \text{and} \quad z_\sigma = 1/[1 - \Sigma'_\sigma(0)]. \quad (6.9)$$

We have assumed the Luttinger result that the imaginary part of the self-energy vanishes at  $\omega = 0$  (Luttinger 1961). As the Green's function in equation (6.8) has the same form of that of the non-interacting system, apart from the weight factor  $z_\sigma$ , we can use it to define a free quasiparticle propagator,  $\tilde{G}_{0,\sigma}^{\text{loc}}(\omega)$ ,

$$\tilde{G}_{0,\sigma}^{\text{loc}}(\omega) = \int d\varepsilon \frac{\rho_0(\varepsilon/z_\sigma)}{\omega + \tilde{\mu}_{0,\sigma} - \varepsilon}. \quad (6.10)$$

We then interpret  $z_\sigma$  as the quasiparticle weight. We will refer to  $\tilde{\rho}_{0,\sigma}(\omega)$  derived from this Green's function via  $\tilde{\rho}_{0,\sigma}(\omega) = -\text{Im}\tilde{G}_{0,\sigma}(\omega + i\delta)/\pi$  as the free quasiparticle density of states (DOS). For the Bethe lattice (6.7), the quasiparticle DOS takes the form of a band with renormalised parameters,

$$\tilde{\rho}_{0,\sigma}(\omega) = \frac{2}{\pi\tilde{D}_\sigma^2} \sqrt{\tilde{D}_\sigma^2 - (\omega + \tilde{\mu}_{0,\sigma})^2}. \quad (6.11)$$

where  $\tilde{D}_\sigma = z_\sigma D$ . We can also define a quasiparticle occupation number  $\tilde{n}_\sigma^0$  by integrating this density of states up to the Fermi level,

$$\tilde{n}_\sigma^0 = \int_{-\infty}^0 d\omega \tilde{\rho}_{0,\sigma}(\omega). \quad (6.12)$$

It is possible to relate this free quasiparticle occupation number  $\tilde{n}_\sigma^0$  to the expectation value of the occupation number  $n_\sigma$  in the interacting system at  $T = 0$ . Using the quasiparticle density of states in equation (6.11), we can rewrite equation (6.12) as

$$\tilde{n}_\sigma^0 = \int_{-\infty}^0 d\varepsilon \rho_0(\varepsilon) \theta(\mu_\sigma - \Sigma_\sigma(0) - \varepsilon), \quad (6.13)$$

where  $\rho_0(\varepsilon)$  as given in equation (6.7). Then assuming a generalisation of Luttinger's theorem (Luttinger 1960) for each spin component, the right-hand side of equation (6.13) is equal to  $n_\sigma$ . We then have the result,

$$\tilde{n}_\sigma^0 = n_\sigma, \quad (6.14)$$

that the occupation for electrons of spin  $\sigma$  is equal to the number of free quasiparticle of spin  $\sigma$ , as calculated from equation (6.12). It should be noted that there is no simple generalisation of the  $h = 0$  DMFT result (Koller et al. 2005),  $\mu_0 = \mu - \Sigma(0)$ , in the spin polarised case to  $\mu_{0,\sigma} = \mu_0 + \sigma h = \mu_\sigma - \Sigma_\sigma(0)$ . The latter would imply the same occupation number for each spin species of free electrons and interacting electrons in a magnetic field, and thus identical magnetisation. Since, however, non-interacting electrons are less susceptible to a magnetic field, this is obviously wrong.

To evaluate the renormalised parameters,  $z_\sigma$  and  $\mu_{0,\sigma}$ , which specify the form of the quasiparticle DOS, we use two different methods. The first method is a direct one, where we use the NRG determined self-energy  $\Sigma_\sigma(\omega)$  and the chemical potential  $\mu_\sigma$ , and then substitute into equation (6.9) for  $z_\sigma$  and  $\tilde{\mu}_{0,\sigma}$ . The second method is indirect, and makes no reference to the self-energy. It is based on the quasiparticle interpretation of the NRG low energy fixed point of the effective impurity. It is analogous to what has been done for the impurity model in chapter 3, and the details are given in appendix B. In such an approach we have  $K_\sigma(\omega) = |V_\sigma|^2 g_{0,\sigma}(\omega)$ , where  $g_{0,\sigma}(\omega)$  is the one-electron Green's function for the first site of the isolated conduction electron chain. As earlier, we expand the self-energy  $\Sigma_\sigma(\omega)$  to first order in  $\omega$ , and then substitute the result into equation (6.6). We can define a free quasiparticle propagator,  $\tilde{G}_{0,\sigma}(\omega)$ , for the impurity site as

$$\tilde{G}_{0,\sigma}(\omega) = \frac{1}{\omega - \tilde{\varepsilon}_{d,\sigma} - |\tilde{V}_\sigma|^2 g_{0,\sigma}(\omega)}, \quad (6.15)$$

where

$$\tilde{\varepsilon}_{d,\sigma} = z_\sigma(\varepsilon_{d,\sigma} + \Sigma_\sigma(0)), \quad |\tilde{V}_\sigma|^2 = z_\sigma |V_\sigma|^2, \quad (6.16)$$

In the DMFT approach we identify  $\tilde{G}_{0,\sigma}(\omega)$  with the local quasiparticle Green's function for the lattice (6.10),

$$\tilde{G}_{0,\sigma}^{\text{loc}}(\omega) = \tilde{G}_{0,\sigma}(\omega), \quad (6.17)$$

which specifies the form of  $g_{0,\sigma}(\omega)$  in (6.15) and yields  $\tilde{\mu}_{0,\sigma} = -\tilde{\varepsilon}_{d,\sigma}$ . The quasiparticle weight  $z_\sigma$  is then obtained from the relation  $z_\sigma = |\tilde{V}_\sigma/V_\sigma|^2$  in equation (6.16), and  $\tilde{\mu}_{0,\sigma}$  from  $\tilde{\mu}_{0,\sigma} = -\tilde{\varepsilon}_{d,\sigma}$ .

As an extension of the RPT considerations in chapter 3 we can also calculate the local dynamic spin susceptibilities,  $\chi_{\text{loc}}(\omega) = \sum_{\mathbf{k}} \chi(\omega, \mathbf{k})$ . We focus on the transverse part  $\chi_t(\omega)$  for this model, which can be also obtained from a similar equation to (3.36). The details are described in Bauer and Hewson (2007b). We can calculate the local on-site quasiparticle interaction  $\tilde{U}$  as in the impurity case, but we do not have the simple formula relating  $\tilde{U}$  to  $\chi_t(0)$  that enabled us to deduce the irreducible quasiparticle interactions  $\tilde{U}_t$ ; the impurity formula we used earlier is only valid in the wide band limit. To determine  $\tilde{U}_t$  in the lattice case we use the condition that  $\text{Re}\chi_t(\omega)$  fits the NRG result at the single point  $\omega = 0$ . We can then compare the results based on these RPT formulae, which take into account the repeated quasiparticle scattering, with the NRG results over the whole frequency range. An analogous procedure applies for  $\chi_l(\omega)$  (Bauer and Hewson 2007b).

### 6.3 Results at Half-filling

We present results at half-filling for three main parameters regimes where we find qualitatively different behaviour (Laloux et al. 1994). The results in all cases will be for a Bethe lattice with a band width  $W = 2D = 4$ , such that  $t = 1$  sets the energy scale. In concentrating on the field induced polarisation, we do not include the possibility of anti-ferromagnetic ordering. The regimes are a relatively weak coupling regime (a) where  $U$  is smaller than the band width, an intermediate coupling regime (b) with  $W < U < U_c$ , where  $U_c$  is the value at which a Mott-Hubbard gap develops in the absence of a magnetic field [ $U_c \approx 5.88$ , Bulla (1999)], and (c) a strong coupling regime with  $U > U_c$ .

#### 6.3.1 Weakly correlated regime

The first plot in figure 6.1 (left) gives the spectral densities for the majority spin electrons  $\rho_{\uparrow}(\omega)$  for various magnetic field values in the weakly correlated regime,  $U = 2$ .

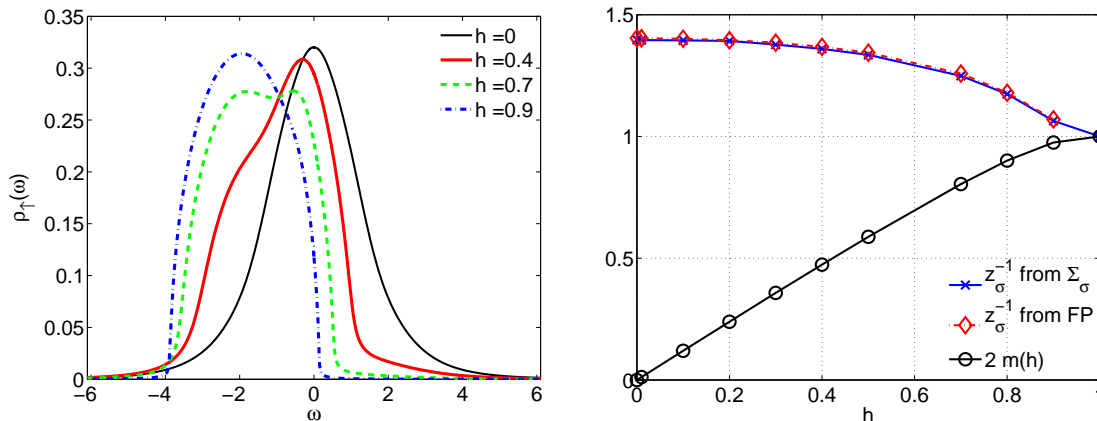


Figure 6.1: Left: The local spectral density for the majority spin  $\rho_{\uparrow}(\omega)$  for  $U = 2$  and various fields  $h$ . Right: The inverse of the quasiparticle weight  $z_{\sigma}(h)$  calculated from the impurity fixed point (FP) and directly from the self-energy and the magnetisation  $m(h)$  also for  $U = 2$ .

We can see clearly that, for increasing magnetic field, more and more spectral weight is shifted to lower energies (the opposite happens for the other spin component, which is not displayed here). Above  $h \simeq 1.0$  the system is completely polarised,  $2m = 1$ . This extreme high field limit corresponds to an insulator; there is a gap of the magnitude  $\Delta_g(h) = 2h + U - W$  between the upper (minority) and lower (majority) band, which both have the semi-elliptical form as for the non-interacting system with  $W = 4$ , as can be seen already in 6.1 (left) for  $h = 0.9$ . The inverse of the quasiparticle weight  $z_{\sigma}(h)$ , which in the DMFT corresponds to the enhancement of the effective mass  $m_{\sigma}^*(h) = m/z_{\sigma}(h)$ , is shown as a function of  $h$  in figure 6.1 (right). We calculated the values of  $z_{\sigma}(h)$  using the two methods described earlier, i.e. directly from the numerical derivative of the NRG self-energy at  $\omega = 0$  and from the impurity fixed point (FP) (see appendix B), where

$z_\sigma = |\tilde{V}_\sigma/V_\sigma|^2$ . At half filling we have  $z_\uparrow(h) = z_\downarrow(h)$  and we have plotted the average of the values for  $\sigma = \uparrow$  and  $\sigma = \downarrow$ , which is compared for the two methods. The deviation for the values for the different spins is only due to small numerical inaccuracies and is less than 2%. The method based on analysing the excitation of the impurity fixed point (FP) is only applicable in the metallic regime, when the system is not completely polarised.

The values of  $z_\sigma(h)$  increase from about 0.75 to 1, which corresponds to a progressive “de-renormalisation” of the quasiparticles with increasing field, as observed earlier for the impurity model in section 3.2. Since the interaction term in the Hubbard model acts only for opposite spins it is clear that there is no renormalisation when the system is completely polarised with one band fully occupied and the other empty. We have also calculated, but do not display the expectation value of the double occupancy  $\langle n_\uparrow n_\downarrow \rangle$ . It is found that it decreases with increasing field, which further illustrates why the interaction term becomes less important for larger fields.

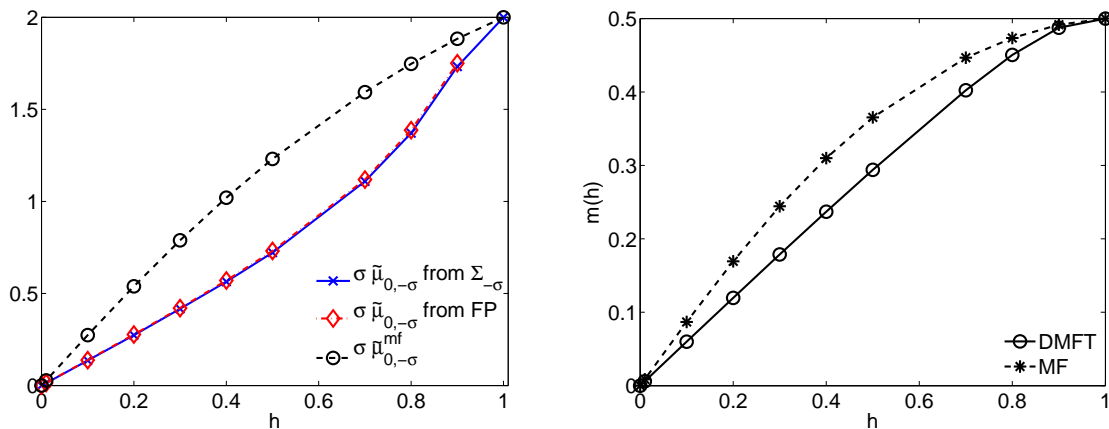


Figure 6.2: Left: The renormalised chemical potential  $\tilde{\mu}_{0,\sigma}(h)$  calculated from the impurity fixed point (FP) and directly from the self-energy for  $U = 2$  and various fields  $h$ . Right: The magnetisation in the mean field approximation compared with the DMFT result for  $U = 2$  and for the full range of magnetic fields  $h$ .

We can also follow the field dependence of the renormalised chemical potential  $\tilde{\mu}_{0,\sigma}(h)$  as shown in figure 6.2 (left). It is shown deduced from the renormalised parameter (RP)  $\tilde{\epsilon}_{d,\sigma}$  and as calculated directly from the self-energy. The agreement is very good over the full range of magnetic fields. Mean field theory is valid for very weak interactions, so we compare our results for  $\tilde{\mu}_{0,\sigma}(h)$  for  $U = 2$ , with the mean field value  $\tilde{\mu}_{0,\sigma}^{\text{mf}} = \mu + \sigma h - U n_{-\sigma}^{\text{mf}}$  in figure 6.2 (left). The results coincide for  $h = 0$ , when  $\tilde{\mu}_{0,\sigma}^{\text{mf}} = 0$  and when the system becomes fully polarised at large field values,  $\tilde{\mu}_{0,\sigma}^{\text{mf}} = -\sigma(U/2 + h)$ , but in general  $\tilde{\mu}_{0,\sigma}^{\text{mf}} > \tilde{\mu}_{0,\sigma}(h)$ . We also compare the mean field (MF) result for the field dependence of the magnetisation  $m(h)$  with the one obtained in the DMFT calculation in figure 6.2 (right). The general behaviour is similar, but the mean field theory without quantum fluctuations overestimates the magnetisation, as one would expect.

### 6.3.2 Intermediate coupling regime

In the next plot in figure 6.3 (left), where  $U = 5$ , we show typical behaviour of the majority spin density of states in the intermediate coupling regime.

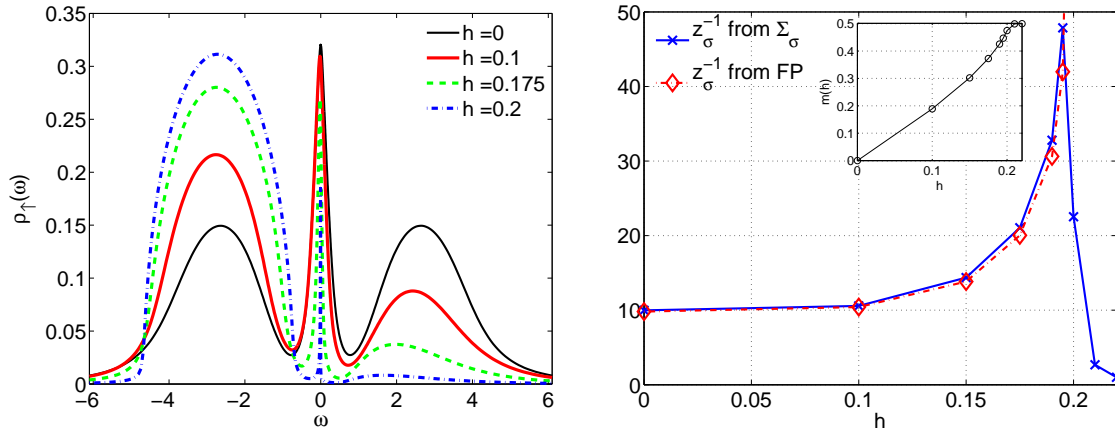


Figure 6.3: Left: The local spectral density for the majority spin  $\rho_{\uparrow}(\omega)$  for  $U = 5$  and various fields  $h$ . Right: The inverse of the quasiparticle weight  $z_{\sigma}(h)$  calculated from the impurity fixed point (FP) and directly from the self-energy also for  $U = 5$ . The inset shows the magnetisation  $m(h)$ .

Similar to the weak coupling regime, we find a shift of spectral weight towards lower energy for the majority spin. There is, however, a difference in the way this happens due to the initial three peak structure, namely the quasiparticle peak in the middle gets narrower for increasing field and finally vanishes in the polarised phase. This gives rise to metamagnetic behaviour in this parameter regime. The quasiparticle weight, which is shown in figure 6.3 (right), reflects this behaviour by decreasing to zero with increasing field signalling heavy quasiparticles. Here, as in the weak coupling case, we plot the average of the spin up and down results for each method. The deviations can be larger here, especially close to the metamagnetic transition. When the material is polarised the  $z_{\sigma}(h)$  reverts to 1, which corresponds to the band insulator as before. This approach to the fully polarised localised state in high fields contrasts with that found in the weak coupling regime.

To illustrate further this different response to a magnetic field, the real part of the local longitudinal dynamic spin susceptibility  $\chi_l(\omega, h)$  as a function of  $\omega$  is shown for various values of  $h$  in figure 6.4 (left). It can be seen that the local susceptibility  $\chi^{loc}(h) = \text{Re} \chi_l(0, h)$  in this regime increases with  $h$  so that  $\partial \chi^{loc}(h) / \partial h > 0$ . Such a feature can also be seen in the curvature of the magnetisation shown in the inset of figure 6.3 (right). This is behaviour characteristic of a metamagnetic transition and related to the magnetic field induced metal-insulator transition.

We can also check the Luttinger theorem in a magnetic field (6.14), as discussed in the previous section, by comparing the values of  $\tilde{n}_{\sigma}^0$ , deduced from integrating the quasiparticle density of states with the value of  $n_{\sigma}$  calculated from the direct NRG evaluation in the

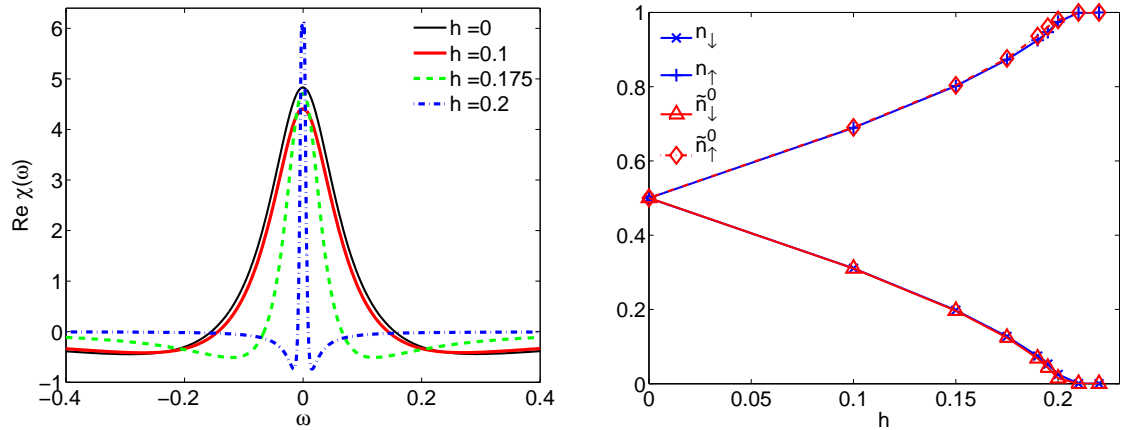


Figure 6.4: Left: The real part of the local longitudinal dynamic spin susceptibility for  $U = 5$  and various fields  $h$ . Right: The comparison of the spin dependent occupation numbers  $\tilde{n}_\sigma^0$  and  $n_\sigma$  corresponding to Luttinger's theorem in a magnetic field (6.14) also for  $U = 5$ .

ground state. These results are shown in figure 6.4 (right). It can be seen that there is excellent agreement between the results of these two different calculations,  $\tilde{n}_\sigma^0 = n_\sigma$ , so that Luttinger's theorem is satisfied for all values of the magnetic field in this intermediate coupling regime.

Having deduced the renormalised parameters of the quasiparticles from the NRG results, we are now in a position to test how well we can describe the low energy dynamics of this model in a magnetic field in terms of a renormalised perturbation theory. It is of interest first of all to see how the free quasiparticle density of states  $\tilde{\rho}_{0,\sigma}(\omega)$  from equation (6.11) multiplied by  $z_\sigma(h)$  compares with the low energy spectral density  $\rho_\sigma(\omega)$ . In figure 6.5 we make a comparison in the zero magnetic field case for  $U = 5$ .

We see that the quasiparticle band gives a good representation of the low energy peak in  $\rho_\sigma(\omega)$  and, as expected, does not reproduce the high energy features. These, however, to a fair approximation can be described by the mean field solution  $\rho_{\text{mf}}(\omega)$  weighted with a factor  $1 - z_\sigma$  as can be seen in figure 6.5 (left). A case with a finite magnetic field  $h = 0.15$ , where the peaks in the density of states of the two spin species are shifted due to the induced polarisation relative to the Fermi level, is shown in figure 6.5 (right). The figure focuses on the region at the Fermi level and one can see the the free quasiparticle density of states describes well the form of  $\rho_\sigma(\omega)$  in the immediate vicinity of the Fermi level. It is to be expected that the frequency range for this agreement can be extended if self-energy corrections are included in the quasiparticle density of states using the renormalised perturbation theory as shown in chapter 3 in the impurity case.

We now compare the NRG results for the transverse local dynamic spin susceptibilities for the same value  $U = 5$  and a similar range of magnetic field values with those based on the RPT formula as explained at the end of section 6.2. In figure 6.6 we show the imaginary

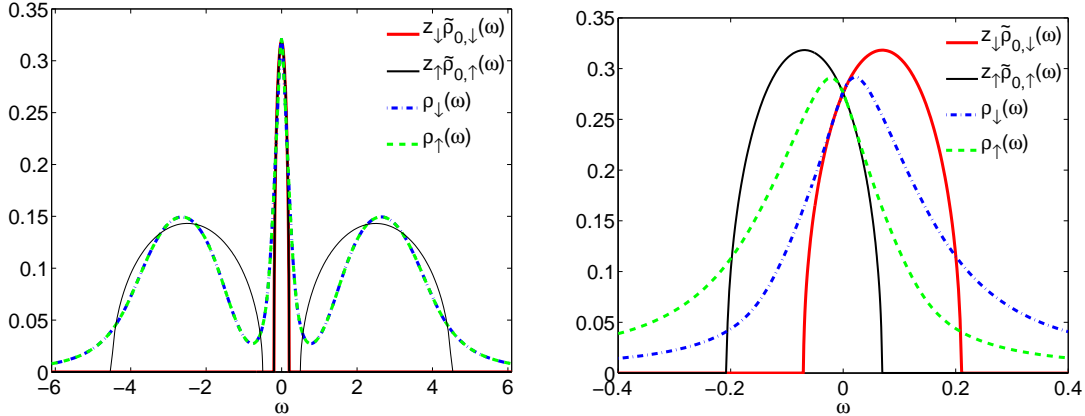


Figure 6.5: Left: The free quasiparticle density of states  $\tilde{\rho}_{0,\sigma}(\omega)$  in comparison with interacting local spectral density for  $U = 5$  and  $h = 0$ . We have also plotted a thin black line for  $\rho_{\text{mf}}(\omega) = [\rho_0(\omega + U/2) + \rho_0(\omega - U/2)]/2$  which describes the non-magnetic mean field solution and weighted with  $1 - z_\sigma$ . Right: The free quasiparticle density of states in comparison with interacting the local spectral density for  $U = 5$  and  $h = 0.15$ .

part of the transverse spin susceptibility calculated with the two different methods.

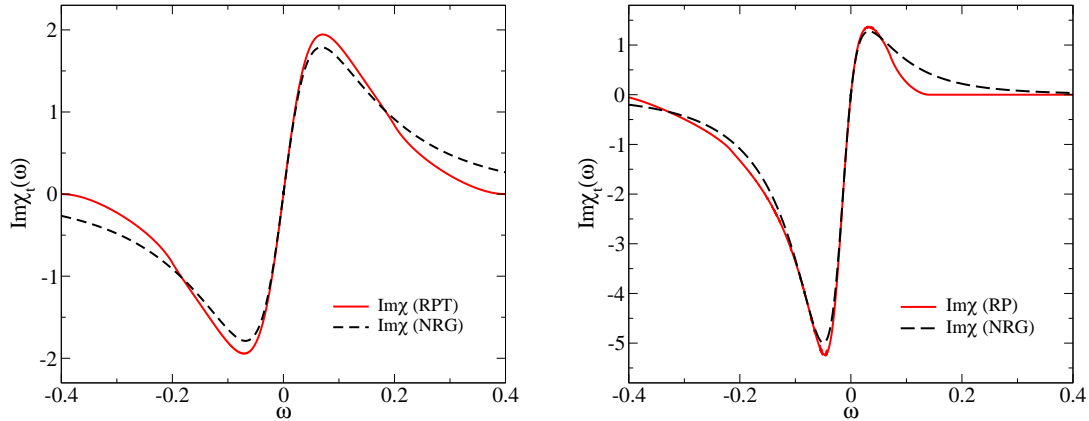


Figure 6.6: A comparison of the imaginary parts of the transverse dynamic spin susceptibility for  $U = 5$  and  $h = 0.0$  (left) and  $h = 0.15$  (right) calculated using renormalised perturbation theory (RPT, full line) and from a direct NRG calculation (dashed line).

It can be seen that the RPT formula gives the overall form of the NRG results, and precisely fits the gradient of the NRG curve at  $\omega = 0$ . Some of the relatively small differences between the results might be attributed to the broadening factor used in the NRG results which gives a slower fall off with  $\omega$  in the higher frequency range, and a slightly reduced peak. We get similar good agreement between the two sets of results for the same quantity for the case with a magnetic field  $h = 0.15$ , shown in figure 6.6 (right).

In figure 6.7, where we give both the real and imaginary parts of the transverse susceptibility for  $h = 0.19$ , we see that this overall agreement is maintained in the large field

regime where we get metamagnetic behaviour. The shapes of the low energy peaks for both quantities are well reproduced by the RPT formulae. Note that the peak in the real part is not at  $\omega = 0$ , so it is not fixed by the condition that determines  $\tilde{U}_t$ , but nevertheless is in good agreement with the NRG results. Due to their very small values it becomes difficult to calculate  $z_\sigma(h)$  as the system approaches localisation for larger fields. In this regime as  $z_\sigma(h) \rightarrow 0$  the free quasiparticle density of states will converge to a delta-function. Self-energy corrections to the free quasiparticle propagators will become increasingly important as this limit is approached. Once the system has localised and is completely polarised, however, we find that the values  $\tilde{\mu}_\sigma(z_\sigma(h) = 1)$  deduced from the self-energy give a quasiparticle density of states coinciding with the DMFT-NRG result of an upper and lower semi-circular bands.

### 6.3.3 Strong coupling regime

Finally we consider the strong coupling regime with  $U > U_c$ , where for  $h = 0$  the spectral density has a Mott-Hubbard gap so that for half-filling the system is an insulator [see dashed line in fig. 6.7 (right)]. The electrons will be localised with free magnetic moments coupled by an effective antiferromagnetic exchange  $J \sim t^2/U$  as in (1.31). In fields such that  $h > J$ , the system polarises completely as can be seen in figure 6.7 (right), where we show the total density of states  $\rho(\omega) = \rho_\uparrow(\omega) + \rho_\downarrow(\omega)$  for  $h = 0$  and  $h = 0.2$ .

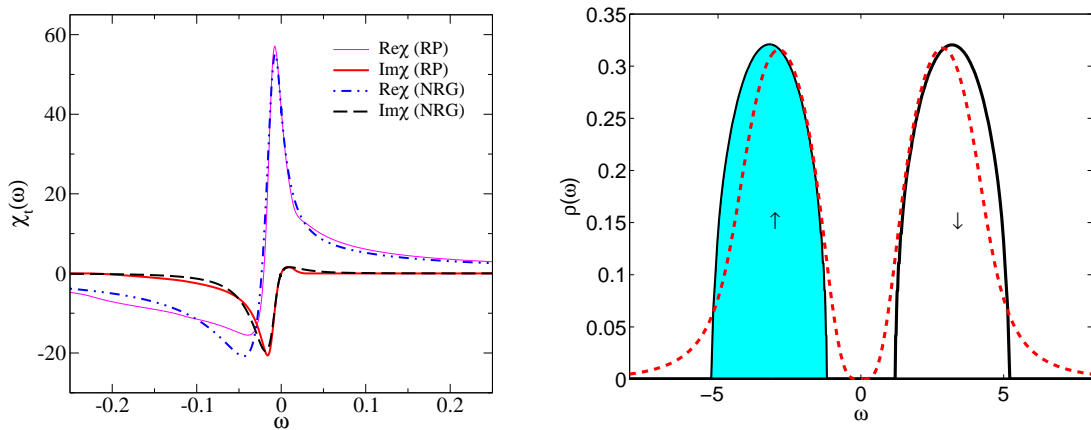


Figure 6.7: Left: Plots of the imaginary part of the transverse dynamic spin susceptibility for  $U = 5$  and  $h = 0.19$ . Right: The total local spectral density  $\rho(\omega)$  for  $U = 6$  for  $h = 0$  (dashed line), Mott insulator, and  $h = 0.2$  (full line), fully polarised band insulator.

For smaller fields, such that  $h < J$ , we do not find a convergent solution to the DMFT equations, and the iterations oscillate between local states which are either completely full or empty. We interpret this as due to the tendency to antiferromagnetic order which in a weak field, due to the absence of anisotropy, will be almost perpendicular to the applied field in the  $x$ - $y$  plane with a slight canting of the spins in the  $z$ -direction (spin flopped

phase). In this calculation no allowance has been made for this type of ordering, but this state can be well described using an effective Heisenberg model for the localised moments.

## 6.4 Results away from half filling

### 6.4.1 Quarter Filled Case

We now compare the results in the intermediate coupling regime with  $U = 5$  at half-filling with those at quarter filling,  $x = 0.5$ , where the Fermi level falls in the lower Hubbard peak in the spectral density. To see how the band changes with increasing magnetic field we plot the density of states for both spin types in figure 6.8, for the majority spin electrons (left) and for the minority spin electrons (right), for various values of the magnetic field.

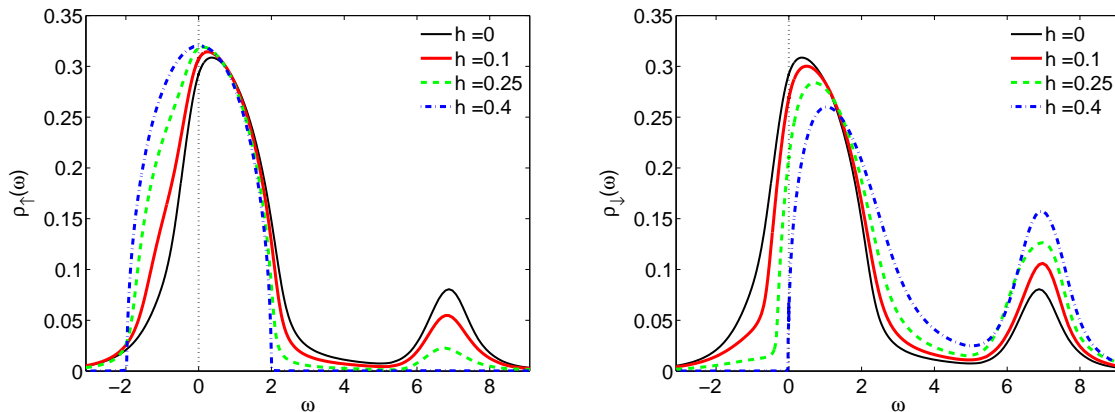


Figure 6.8: The local spectral density for the majority spin  $\rho_{\uparrow}(\omega)$  (left) and for the minority spin  $\rho_{\downarrow}(\omega)$  (right) for  $U = 5$ ,  $x = 0.5$  and various fields  $h$ . The dotted vertical line marks the position of the Fermi level.

In the majority spin case (left) the lower peak gains spectral weight on the low energy side and the weight in the upper peaks decreases with increase of the field. The opposite features can be seen in the minority spin case (right), with the spectral weight in the lower peak below the Fermi level decreasing and the weight in the upper peak increasing. Thus the increase of spectral weight below the Fermi level for the majority spin electrons, and the decrease for the minority spin electrons, can be seen to be due to a change of band shape rather than a simple relative shift of the two bands, which would be the case in mean field theory. In the fully polarised state there are no minority states below the Fermi level and the upper peak in the majority state density of states has disappeared. Note that the magnetic field necessary for polarisation  $h_{\text{pol}}$  is more than twice as large this case,  $h_{\text{pol}} \simeq 0.4$ , as in the half filled case, where  $h_{\text{pol}} \simeq 0.2$ .

The corresponding values for the inverse of the quasiparticle weight  $1/z_{\sigma}(h)$  are shown in figure 6.9 (left) for a range of fields.

As noted in the impurity case, the quasiparticle weights differ for the two spin types with

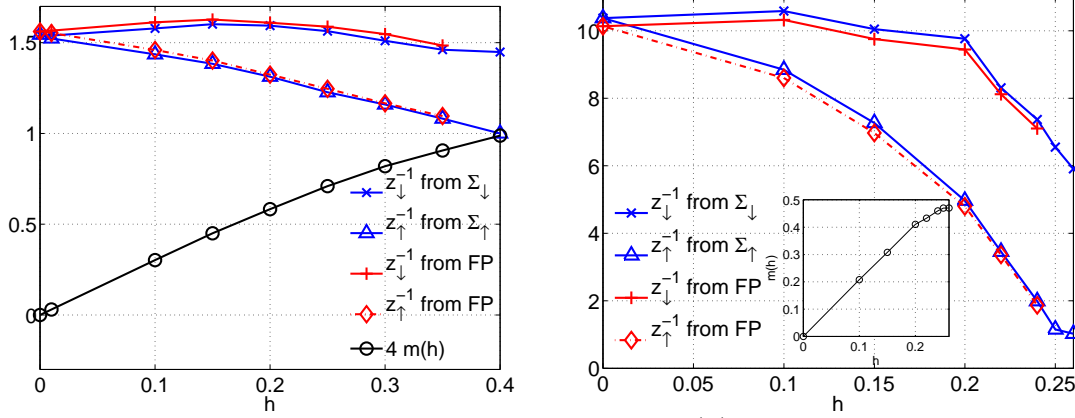


Figure 6.9: The inverse of the quasiparticle weight  $z_{\sigma}(h)$  calculated from the impurity fixed point (FP) and directly from the self-energy for  $U = 5$ ,  $x = 0.5$  (left) and for  $U = 6$ ,  $x = 0.95$  (right) for various fields  $h$ . The magnetisation  $m(h)$  is also displayed.

$z_{\uparrow}(h) > z_{\downarrow}(h)$ . The values of  $z_{\sigma}(h)$  have been calculated, as described earlier, both from the energy levels (RP) and from a numerical derivative of the NRG derived self-energy. There is reasonable agreement between the two sets of results, and the small differences to be seen be attributed to the uncertainty due to the broadening in the numerical derivative of the NRG self-energy. As in the impurity case without particle hole symmetry (Bauer and Hewson 2007a), there is an initial decrease of  $z_{\downarrow}(h)$  with increase of  $h$ , whereas  $z_{\uparrow}(h)$  increases monotonically. Note that  $z_{\downarrow}(h)$  does not revert to one in the polarised case as an additional down spin electrons just above the Fermi level interacts with the other up polarised electrons. This will be seen even more pronounced in the case near half filling discussed below. The field dependence of the magnetisation is also shown in figure 6.9, and is similar to the half-filled case with a weak interaction ( $U = 2$ ). We have calculated, but do not show, the corresponding occupation values for  $\tilde{n}_{\sigma}^0$  which again agree well with the values of  $\tilde{n}_{\sigma}$ , verifying Luttinger's theorem.

Our conclusion from these results, and from calculations with other values of intermediate and large  $U$ , is that when there is significant doping, the behaviour in the field corresponds to a weakly correlated Fermi liquid, very similar to that at half-filling in the weak interaction regime. The only remarkable difference in the field is the spin dependence of the effective masses as shown in figure 6.9, which is also found similarly in the impurity case (Bauer and Hewson 2007a).

### 6.4.2 Near half filling

Very close to half-filling and for large values of  $U$  we have a qualitatively different parameter regime. Here the system is metallic but we can expect strong correlation effects when  $U$  is of the order or greater than  $U_c$ , due to the much reduced phase space for quasiparticle scattering. We look at the case with 5% hole doping from half-filling and a value  $U = 6$ ,

which is just greater than the critical value for the metal-insulator transition. In figure 6.10 we show the spectral density of states for both the majority (left) and minority (right) spins states and various values of the magnetic field.

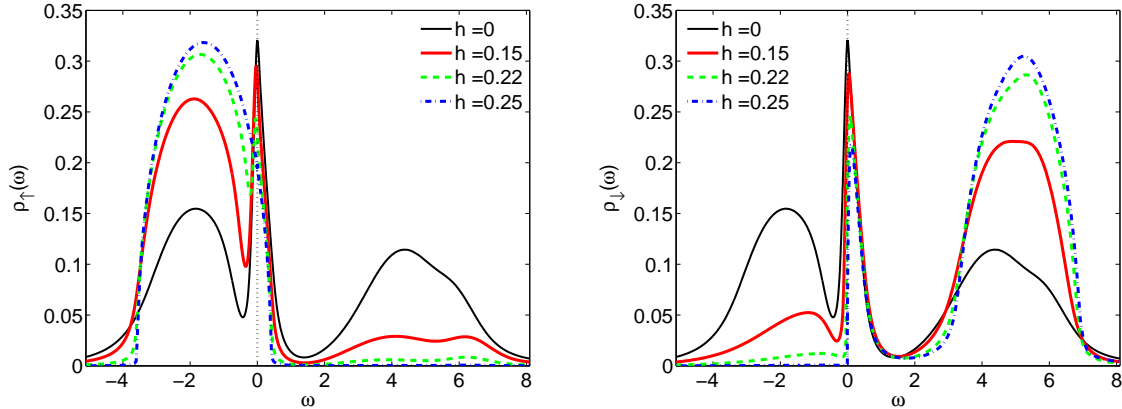


Figure 6.10: The local spectral density for the majority spin  $\rho_{\uparrow}(\omega)$  (left) and the minority spin  $\rho_{\downarrow}(\omega)$  (right) for  $U = 6$ ,  $x = 0.95$  and various fields  $h$ .

There is a clear sharp quasiparticle peak for  $h = 0$  at the Fermi level at the top of the lower Hubbard band. As in the quarter filling case with  $U = 5$  we see a similar transfer of spectral weight with increasing field to below the Fermi level for the majority spin case, and above the Fermi level for the minority spins. For large fields,  $h > 0.26$ , when the system is completely polarised there is still a sharp narrow peak in the spectral density of the minority spin states (right) above the Fermi level, though the spectrum for the majority states (left) below the Fermi level is that of the non-interacting system. A spin up electron added above the Fermi level feels no interaction as the system is completely spin up polarised so these electrons see the non-interacting density of states. On the other hand a spin down electron above the Fermi level interacts strongly with the sea of up spin electrons. The self-energy due to scattering with particle-hole pairs in the sea creates a distinct resonance in the down spin density of states just above the Fermi level. Just such a resonance was predicted by Hertz and Edwards (1972) for a Hubbard model in a strong ferromagnetic (fully polarised) state.

The field dependence of the inverse of the quasiparticle weight is presented in the earlier figure 6.9 (right). Again we find reasonable agreement between the two methods of calculation for these quantities. The magnetisation as a function of  $h$  is shown as an inset in the same figure. The behaviour of  $z_{\uparrow}(h)$  and  $z_{\downarrow}(h)$  as a function of  $h$  contrasts sharply with the behaviour found for the metallic state at half-filling with  $U = 5$  shown in figure 6.3 (right). Notice comparing with figure 6.3 that for zero field the quasiparticle weight has a very similar value in both cases. At half-filling the tendency of the magnetic field to induce localisation resulted in values of  $z_{\sigma}^{-1}(h)$  ( $z_{\uparrow}(h) = z_{\downarrow}(h)$ ) which increase sharply as a function of  $h$ . In the 5% doped case with  $U = 6$ , the system remains metallic and the inverse quasiparticles weights,  $z_{\uparrow}^{-1}(h)$  and  $z_{\downarrow}^{-1}(h)$ , both decrease in large fields

though their values differ significantly. The quasiparticle weight for the minority spin electrons decreases initially with increase of  $h$ , whereas that for the majority spins  $z_{\uparrow}(h)$  increases monotonically and quite dramatically with  $h$ . For a field  $h = h_{\text{pol}}$  when the system becomes fully polarised the up spin electrons become essentially non-interacting,  $z_{\uparrow}(h_{\text{pol}}) = 1$ , whereas there is a strong renormalisation for a down spin electron and we find in this case  $z_{\downarrow}(h_{\text{pol}}) \simeq 0.15$ . The interpretation for this is as given in the previous paragraph for the spectral densities. For very large fields,  $h \gg h_{\text{pol}}$ , also the minority renormalisation factor  $z_{\downarrow}(h)$  tends to one.

In figure 6.11 (left) we compare the free quasiparticle DOS  $z_{\sigma}\tilde{\rho}_{0,\sigma}(\omega)$  with the full one  $\rho_{\sigma}(\omega)$  for the fully polarised case ( $h_{\text{pol}} = 0.26$ ) near half filling,  $x = 0.95$ ,  $U = 6$ . Note that the parameters,  $\tilde{\mu}_{0,\sigma}$  and  $z_{\sigma}$ , used in  $\tilde{\rho}_{0,\sigma}(\omega)$  are purely derived from the NRG self-energy in this case.

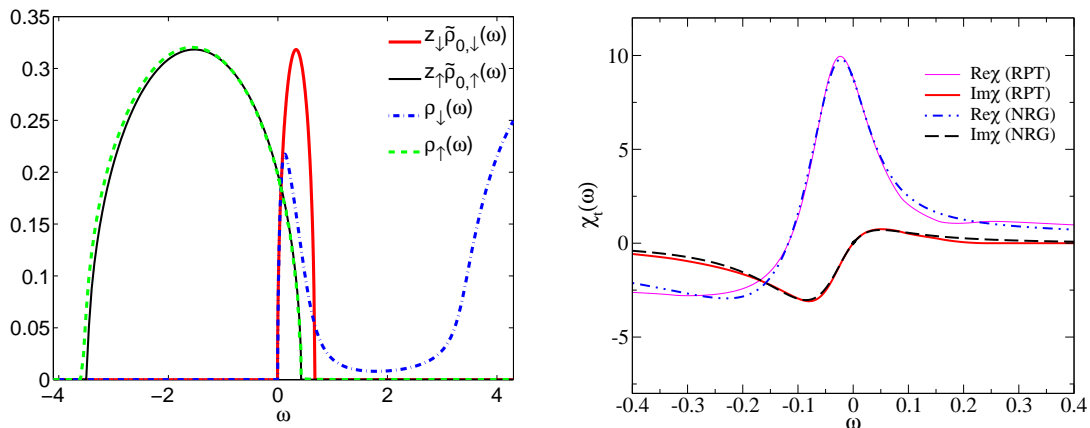


Figure 6.11: Left: The free quasiparticle density of states in comparison with interacting local spectral density for  $U = 6$ ,  $x = 0.95$  and  $h = 0.26$ . Right: The real and imaginary parts of the transverse dynamic spin susceptibility (upper panel) and of the longitudinal dynamic spin susceptibility (lower panel) for  $U = 6$ ,  $x = 0.95$  and  $h = 0.15$ .

We can see that the different values for the field dependent quasiparticle weight for up and down spin  $z_{\sigma}(h)$  lead to remarkably different quasiparticle band shapes. With  $z_{\uparrow}(h_{\text{pol}}) \simeq 1$  the majority spin quasiparticle band is essentially that of the non-interacting density of states. The very much smaller value  $z_{\downarrow}(h_{\text{pol}})$  leads to a narrow quasiparticle band above the Fermi level. The low energy flank of this quasiparticle band describes well the narrow peak seen in the spectral density just above the Fermi level. To describe these strong asymmetries in the spectral densities near half filling, we need  $z_{\uparrow} \gg z_{\downarrow}$ , which contrasts with the cases at half filling such as in figures 6.5 (right) where always  $z_{\uparrow} = z_{\downarrow}$ . This suggests a discontinuous behaviour of the renormalisation factors  $z_{\sigma}$  as a function of doping on the approach to half filling.

Also for this case we display results for the real and imaginary part for the transverse susceptibility for a field of  $h = 0.15$ , shown in figure 6.11 (right). The low energy features are seen on an  $\omega$ -scale an order of magnitude smaller than that for quarter filling due to

the much stronger renormalisation effects in this regime. There is excellent agreement both with the peak positions and shapes between the NRG and RPT results for both quantities. More examples of how the dynamic (transverse and longitudinal part) susceptibility compares to NRG results can be found in reference Bauer and Hewson (2007b).

We conclude that already a small doping of the system is enough to maintain a metallic character even for very strong interaction. Although the zero field spectra of the half filled case for  $U = 5$  and the small doping case with  $U = 6$  display very similar zero field behaviour, i.e. a strongly renormalised quasiparticle band with similar  $z_\sigma$ , no field induced localisation transition occurs for finite doping and no metamagnetic behaviour is observed in the latter case.

To summarise, in this chapter we have used the DMFT-NRG method to calculate the spectral densities for one-particle and two-particle response functions for the infinite dimensional Hubbard model in a magnetic field, for the qualitatively different filling regimes and interaction strengths. The results extend earlier calculations of Laloux et al. (1994) using the ED method, which were restricted to the case of half-filling. The results are on the whole consistent with this earlier work, except in the insulating regime for weak fields, where we could not find a convergent solution of the DMFT equations. We have also extended the method for calculating the field dependent quasiparticle parameters (chapter 3) to infinite dimensional lattice models where the self-energy, as in the impurity case, is a function of frequency only. Using the field dependent renormalised parameters  $z_\sigma(h)$  and  $\tilde{\mu}_{0,\sigma}(h)$  in the RPT formulae for the dynamic transverse spin susceptibilities we found agreement with the overall features to be seen in the DMFT-NRG results for these quantities. In all metallic parameter regimes a spin dependent Luttinger theorem in the form  $n_\sigma = \tilde{n}_\sigma^0$ , the number of particles equals the number of quasiparticles, was found to be satisfied for all strengths of the magnetic field.

Well away from half filling we find a magnetic response similar to the weakly correlated case even for large values of  $U$ . The large phase space for quasiparticle scattering in this regime leads to modest renormalisation effects. Here, as in the impurity case, we find spin dependent quasiparticle weights,  $z_\uparrow(h) \neq z_\downarrow(h)$ . This implies spin dependent as well as field dependent effective masses, which have been discussed earlier in work by Spalek and Gopalan (1990), Korbelt et al. (1995) and Riseborough (2006). A qualitative comparison with the results there can be found in Bauer and Hewson (2007b).

*Wie sich Verdienst und Glück verketten,  
Das fällt den Toren niemals ein,  
Wenn sie den Stein der Weisen hätten,  
Der Weise mangelte dem Stein.*

Johann W. von Goethe

## Chapter 7

# Renormalised quasiparticles in metallic Antiferromagnets

In this chapter we discuss spontaneous antiferromagnetic order in the Hubbard model. We focus on the case away from half filling. First we discuss the general situation and the phase diagram, before explaining the details necessary for the DMFT-NRG approach. This is followed by a detailed analysis of the quasiparticle parameters, which are obtained with two different methods. Finally we discuss local and  $\mathbf{k}$ -resolved spectral functions and give a detailed analysis of the renormalised quasiparticle excitations including their effective mass and spectral weight.

### 7.1 Antiferromagnetic order in the Hubbard model

In the last section we analysed the behaviour of the Hubbard model subject to a homogeneous magnetic field and we saw qualitatively different responses in certain regimes for the interaction  $U$  and the doping  $\delta$ . We did not find a spontaneously broken symmetry state, i.e. a ferromagnetic ordered state, in the parameter space under consideration. A more natural symmetry breaking than the ferromagnetic ordering for the Hubbard model is the antiferromagnetic ground state. The easiest way to see this is to consider large  $U$  and half-filling, where the model can be mapped to a Heisenberg model of antiferromagnetically coupled spins on a lattice. The spin coupling term was given in equation (1.31) and the coupling constant is  $J = 4t^2/U$ . With (1.31) as an effective model we can directly see the antiferromagnetic ordering tendency in the limit of large  $U$ . Also for small values of the interaction, where mean field theory is valid, one finds an antiferromagnetic solution. In fact it is generally accepted at present that for  $\delta = 0$  and finite  $U$  the ground state of the Hubbard model with a bipartite lattice is antiferromagnetically ordered. The situation can be compared with the formally analogous situation in a superconductor (cf. mapping in section 1.2.2), where any finite attraction leads to an instability of the Fermi sea. We

will deal with this situation in more detail in the next chapter. An extensive study by Zitzler et al. (2002) used the DMFT-NRG method to describe the antiferromagnetic solutions and phase separation in the Hubbard model. The results presented here are in agreement with these earlier predictions, but this study has a different emphasis as will be explained below.

Anticipating some of the results of this chapter we show a global antiferromagnetic/paramagnetic phase diagram as a function of the doping  $\delta$  and the on-site interaction  $U$  in figure 7.1. It has been obtained with DMFT-NRG calculation. The value of the corresponding sublattice magnetisation  $m_A$  is shown in a false colour plot. We have added a dashed line separating the spontaneously ordered and paramagnetic regimes.

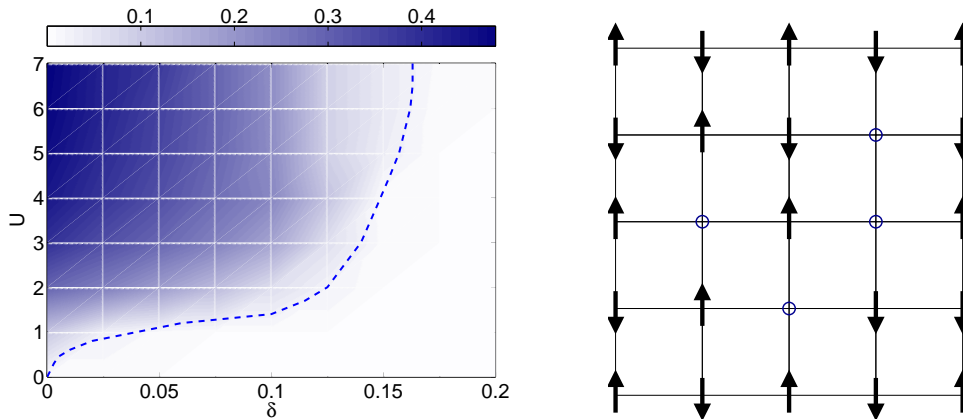


Figure 7.1: Left: Phase diagram showing the doping and the  $U$  dependence of the sublattice magnetisation  $m_A$  as deduced from the DMFT-NRG calculations. Right: Schematic plot of an antiferromagnetically ordered state with a few additional holes.

At half filling ( $\delta = 0$  axis) the spontaneous magnetisation increases with  $U$ . We can see that the antiferromagnetic order from the half filled case persists when holes are added. The value of the critical doping  $\delta_c$  at which the antiferromagnetism disappears depends on the on-site interaction  $U$ . We expect that for small  $U$  the critical doping  $\delta_c$  will increase with  $U$  since a tendency to order only appears when an on-site interaction is present. From the mapping to the  $t - J$  model we also expect that for large  $U$  the antiferromagnetic coupling  $J$  decreases and therefore the order is destroyed more easily. The values of  $U$  are, however, not large enough to display this trend.

If we compare these results with the phase diagram given by Zitzler et al. (2002) we see that they are in very good agreement. In their case the antiferromagnetic region was mapped out to values of  $U \simeq 4.5$ . A picture illustrating the antiferromagnetic lattice in a Néel state (arrows symbolise electrons with certain spin direction) and some added holes is shown in figure 7.1 (right). It is a two-dimensional  $5 \times 5$  cluster with 4 holes, hence  $\delta = 0.16$  which corresponds to the maximal values we have found for the critical doping  $\delta_c$ . The picture is reminiscent of numerous numerical studies for cluster of this size with exact diagonalisation and Quantum Monte Carlo (for a review see Dagotto (1994) and references

therein).

Here in this chapter, we focus on the metallic antiferromagnetism, the doped state with long range antiferromagnetic order. Our interest is to examine how well the low energy excitations in this ordered state can be described in terms of renormalised quasiparticles. Since the motion of a hole in an antiferromagnetic lattice is accompanied with the generation of spin excitations [see schematic picture in figure 7.1 (right)] its mobility will be inhibited and the effective mass enhanced. Due to a similar effect for charge carrier coupling to lattice phonons with the corresponding quasiparticle excitations called polarons, the quasiparticle excitations are sometimes referred to as magnetic polarons. Here, we will mainly refer to them with the generic term of renormalised quasiparticles. To tackle this problem of studying the nature of this renormalised quasiparticle excitations in the system with spontaneous antiferromagnetic symmetry breaking, we use the infinite dimensional Hubbard model and the DMFT-NRG approach.

## 7.2 General setup and DMFT approach

In considering the response of the Hubbard model (1.29) to a staggered magnetic field and antiferromagnetic order, we take the case of a bipartite lattice, which consists of two sublattices  $A$  and  $B$  such that the nearest neighbours of a site in the  $A$  sublattice are on the  $B$  sublattice and vice versa. The Hamiltonian for the Hubbard model can be written in the form,

$$H_\mu = - \sum_{i,j,\sigma} (t_{ij} c_{A,i,\sigma}^\dagger c_{B,j,\sigma} + \text{h.c.}) - \sum_{i,\sigma} (\mu_\sigma c_{A,i,\sigma}^\dagger c_{A,i,\sigma} + \mu_{-\sigma} c_{B,i,\sigma}^\dagger c_{B,i,\sigma}) + U \sum_{i,\alpha} n_{\alpha,i,\uparrow} n_{\alpha,i,\downarrow} \quad (7.1)$$

where the hopping matrix element is taken as  $t_{ij} = t$  between nearest sites  $i$  and  $j$  only, and zero otherwise, and  $\alpha = A, B$ . A staggered field  $H_s^i$

$$H_s^i = \begin{cases} H & \text{for } i \in A \text{ sublattice} \\ -H & \text{for } i \in B \text{ sublattice} \end{cases} \quad (7.2)$$

has been included so that  $\mu_\sigma = \mu + \sigma h$ . The non-interacting part of the Hamiltonian  $H_{0,\mu}$  can be diagonalised in terms of Bloch states and then expressed in the form,

$$H_{0,\mu} = \sum_{\mathbf{k},\sigma} C_{\mathbf{k},\sigma}^\dagger M_{\mathbf{k},\sigma} C_{\mathbf{k},\sigma}. \quad (7.3)$$

where  $C_{\mathbf{k},\sigma}^\dagger = (c_{A,\mathbf{k},\sigma}^\dagger, c_{B,\mathbf{k},\sigma}^\dagger)$ , and the matrix  $M_{\mathbf{k},\sigma}$  is given by

$$M_{\mathbf{k},\sigma} = \begin{pmatrix} -\mu_\sigma & \varepsilon_{\mathbf{k}} \\ \varepsilon_{\mathbf{k}} & -\mu_{-\sigma} \end{pmatrix}. \quad (7.4)$$

The  $\mathbf{k}$  sums run over a reduced Brillouin zone as we have doubled the Wigner-Seitz cell in position space including two lattice sites. The free Green's function matrix  $\underline{G}_{\mathbf{k},\sigma}^0(\omega)$  is

given by  $(\omega - M_{\mathbf{k},\sigma})^{-1}$ . The poles of the free Green's function give the elementary single particle excitations, which are given by

$$E_{\mathbf{k},\pm}^0(U=0) = -\mu_0(h) \pm \sqrt{h^2 + \varepsilon_{\mathbf{k}}^2}, \quad (7.5)$$

where  $\mu_0(h)$  is the chemical potential of the noninteracting system in a staggered field. This illustrates that the electronic excitations are split into two sub-bands for a finite staggered field.

Notice that we have adopted a special choice of basis  $\{c_{A,\mathbf{k},\sigma}, c_{B,\mathbf{k},\sigma}\}$  here (Georges et al. 1996, Zitzler et al. 2002). Another common basis to study antiferromagnetic and spin density wave symmetry (SDW) breaking is  $\{c_{\mathbf{k},\sigma}, c_{\mathbf{k}+\mathbf{q}_0,\sigma}\}$ , where  $\mathbf{q}_0$  is the reciprocal lattice vector for commensurate SDW ordering. The bases can be related by a linear transformation,

$$\begin{pmatrix} c_{\mathbf{k},\sigma} \\ c_{\mathbf{k}+\mathbf{q}_0,\sigma} \end{pmatrix} = \frac{1}{\sqrt{2}} \begin{pmatrix} 1 & -1 \\ 1 & 1 \end{pmatrix} \begin{pmatrix} c_{A,\mathbf{k},\sigma} \\ c_{B,\mathbf{k},\sigma} \end{pmatrix}. \quad (7.6)$$

For the latter basis the matrix  $M_{\mathbf{k},\sigma}$  would be diagonal in the kinetic energy term and the symmetry breaking is offdiagonal. For our study in the DMFT framework the  $A - B$ -sublattice basis is, however, more convenient and we will use it throughout the rest of this chapter. It is possible, of course, to relate the quantities obtained with the help of (7.6) to the  $\{c_{\mathbf{k},\sigma}, c_{\mathbf{k}+\mathbf{q}_0,\sigma}\}$  basis.

We can generalise the equations to the interacting problem by introducing a self-energy  $\Sigma_{\alpha,\mathbf{k},\sigma}(\omega)$ , so that the matrix Green's function can be written in the form

$$\underline{G}_{\mathbf{k},\sigma}(\omega) = \frac{1}{\zeta_{A,\mathbf{k},\sigma}(\omega)\zeta_{B,\mathbf{k},\sigma}(\omega) - \varepsilon_{\mathbf{k}}^2} \begin{pmatrix} \zeta_{B,\mathbf{k},\sigma}(\omega) & -\varepsilon_{\mathbf{k}} \\ -\varepsilon_{\mathbf{k}} & \zeta_{A,\mathbf{k},\sigma}(\omega) \end{pmatrix}, \quad (7.7)$$

where  $\zeta_{\alpha,\mathbf{k},\sigma}(\omega) = \omega + \mu_{\sigma} - \Sigma_{\alpha,\mathbf{k},\sigma}(\omega)$ . As we are dealing with the infinite dimensional limit of the model, we take the self-energy to be local so we can drop the  $\mathbf{k}$  index. This is the reason why the self-energy has a single site index  $\alpha = A, B$  and no offdiagonal terms appear in equation (7.7). The symmetry of the bipartite lattice gives  $\Sigma_{B,\sigma}(\omega) = \Sigma_{A,-\sigma}(\omega) \equiv \Sigma_{-\sigma}(\omega)$  and hence

$$\zeta_{B,-\sigma}(\omega) = \zeta_{A,\sigma}(\omega) \equiv \zeta_{\sigma}(\omega),$$

where we have simplified the notation. To determine these quantities  $\Sigma_{\sigma}(\omega)$  it is sufficient to focus on the  $A$  sublattice only. Summing the first component in the Green's function in equation (7.7) over  $\mathbf{k}$  we obtain the Green's function for a site on the  $A$  sublattice,  $G_{\sigma}^{\text{loc}}(\omega)$ ,

$$G_{\sigma}^{\text{loc}}(\omega) = \frac{\zeta_{-\sigma}(\omega)}{\sqrt{\zeta_{\sigma}(\omega)\zeta_{-\sigma}(\omega)}} \int d\varepsilon \frac{\rho_0(\varepsilon)}{\sqrt{\zeta_{\sigma}(\omega)\zeta_{-\sigma}(\omega)} - \varepsilon}, \quad (7.8)$$

where  $\rho_0(\varepsilon)$  is the density of states of the non-interacting system in the absence of the staggered field.

In the DMFT this local Green's function, and the self-energy  $\Sigma_\sigma(\omega)$ , are identified with the corresponding quantities for an effective impurity model. This implies that the Green's function  $\mathcal{G}_{0,\sigma}(\omega)$  for the effective impurity in the absence of an interaction at the impurity site is given by the same self-consistency equation (6.3) as in the last chapter. The iterative scheme to find self-consistent solution can be carried out in the same way as described there, we only need to take into account the different form of the local Green's function (7.8).

To find antiferromagnetic solutions, we calculated self-consistent solutions for a decreasing sequence of staggered magnetic fields to see if broken symmetry solutions of this type exist as the staggered field is reduced to zero. For the non-interacting density of states  $\rho_0(\varepsilon)$  we take the Gaussian form  $\rho_0(\varepsilon) = e^{-(\varepsilon/t^*)^2}/\sqrt{\pi}t^*$ , corresponding to an infinite dimensional hypercubic lattice. It is useful to define an effective bandwidth  $W = 2D$  for this density of states via  $D$ , the point at which  $\rho_0(D) = \rho_0(0)/e^2$ , giving  $D = \sqrt{2}t^*$  corresponding to the choice in reference Bulla (1999). In all the results we present here we take the value  $W = 4$ . In the NRG calculations we have used the improved method of evaluating the response functions with the complete Anders-Schiller basis, and also determine the self-energy from a higher order Green's function. The staggered magnetic field induces a sublattice magnetisation,

$$m_A = \frac{1}{2}(n_{A,\uparrow} - n_{A,\downarrow}), \quad (7.9)$$

and the spectra for both spin components differ. For certain parameters, this difference persists as the staggered field is reduced to zero so that one has a spontaneous sublattice magnetisation corresponding to spontaneous antiferromagnetic order. For the case away from half filling,  $\delta \neq 0$ , we have to keep adjusting the chemical potential when iterating for a self-consistent solution. It shows a slightly oscillatory behaviour when iterating for a specific filling  $x$ , and we follow the procedure of stabilising the calculations by averaging the effective medium over a number of iterations as described in reference Zitzler et al. (2002). This feature is related to the fact that the calculations are for a metastable ground state and instabilities to more complicated ground states for antiferromagnetic ordering than the homogeneous, commensurate Néel state, which forms the basis for these DMFT calculations, can occur (Shraiman and Siggia 1989, Kato et al. 1990, Emery et al. 1990, van Dongen 1995, 1996, Schulz 1990, Freericks and Jarrell 1995, Emery et al. 1999, Zitzler et al. 2002). As far as phase separation in the ground state is concerned, the results of our calculations are generally in line with the conclusions in Zitzler et al. (2002) as they are carried out within the same framework. The focus of this work is, however, the analysis of generic quasiparticle properties in a doped antiferromagnetic state. We consider the approach as a valid, approximate starting point for this endeavour, but modifications to the results presented here can occur for calculations based on a more complicated ground states not accessible within the DMFT framework. For a more extensive discussion of the applicability of the DMFT in this situation we refer to the earlier work (Zitzler et al. 2002).

### 7.3 Quasiparticle analysis

To examine the nature of the low energy excitations, we will assume that the self-energy  $\Sigma_\sigma(\omega)$  is non-singular at  $\omega = 0$  so that, at least asymptotically, it can be expanded in powers of  $\omega$ . This assumption is not expected to be valid close to the quantum critical point when the magnetic order sets in, but to be a reasonable assumption otherwise. We also assume that the imaginary part of the self-energy vanishes which is confirmed by the numerical results of the DMFT-NRG calculations. We will retain terms to order  $\omega$  only for the moment. The higher order corrections will be considered later. We then find for  $\zeta_\sigma(\omega)$ ,

$$\zeta_\sigma(\omega) = \omega(1 - \Sigma'_\sigma(0)) + \mu_\sigma - \Sigma_\sigma(0) \quad (7.10)$$

$$= z_\sigma^{-1}(\omega + \tilde{\mu}_{0,\sigma}), \quad (7.11)$$

where

$$\tilde{\mu}_{0,\sigma} = z_\sigma(\mu - \Sigma_\sigma(0)), \quad \text{and} \quad z_\sigma^{-1} = 1 - \Sigma'_\sigma(0). \quad (7.12)$$

The interacting Green's function (7.7) has poles at the roots of the quadratic equation,

$$\zeta_\sigma(\omega)\zeta_{-\sigma}(\omega) - \varepsilon_{\mathbf{k}}^2 = 0. \quad (7.13)$$

The solutions of this equation are

$$E_{\mathbf{k},\pm}^0 = -\tilde{\mu} \pm \sqrt{\tilde{\varepsilon}_{\mathbf{k}}^2 + \Delta\tilde{\mu}^2}, \quad (7.14)$$

where  $\tilde{\varepsilon}_{\mathbf{k}} = \sqrt{z_\uparrow z_\downarrow} \varepsilon_{\mathbf{k}}$ ,  $\Delta\tilde{\mu} = (\tilde{\mu}_{0,\uparrow} - \tilde{\mu}_{0,\downarrow})/2$ , and  $\tilde{\mu} = (\tilde{\mu}_{0,\uparrow} + \tilde{\mu}_{0,\downarrow})/2$ . This has the same form as for the non-interacting system in a staggered field (7.5), so we can interpret these excitations as quasiparticles coupled to an effective staggered magnetic field  $\tilde{h}_s = \Delta\tilde{\mu}/g\mu_B$ , with  $\tilde{\mu}$  playing the role of a quasiparticle chemical potential. This equation gives the dispersion relation for these single particle excitations, which can be regarded as constituting a renormalised band, or bands as there are two branches. The term magnetic polaron is sometimes used to describe these single particle excitations in states of magnetic order, because of the analogy with the motion of a particle in a lattice to which it is strongly coupled, where the excitation is termed a polaron.

The corresponding density of states of these free quasiparticles on the sublattice is

$$\tilde{\rho}_{0,\sigma}(\omega) = \frac{1}{\sqrt{z_\uparrow z_\downarrow}} \sqrt{\frac{\omega + \tilde{\mu} - \sigma\Delta\tilde{\mu}}{\omega + \tilde{\mu} + \sigma\Delta\tilde{\mu}}} \rho_0 \left( \frac{\sqrt{(\omega + \tilde{\mu})^2 - \Delta\tilde{\mu}^2}}{\sqrt{z_\uparrow z_\downarrow}} \right), \quad (7.15)$$

for  $|\omega + \tilde{\mu}| > |\Delta\tilde{\mu}|$ , and is zero otherwise. In the case of a half-filled band  $\tilde{\mu} = 0$  and there is a gap at the Fermi level  $\varepsilon_F = 0$ .

To determine this quasiparticle density of states in the presence of the symmetry breaking staggered magnetic field we need to calculate  $z_\sigma$  and  $\tilde{\mu}_{0,\sigma}$  for each spin type. Using the

NRG we can do this in two ways. As the DMFT-NRG calculations give us the self-energy  $\Sigma_\sigma(\omega)$  directly, we only need its value, and that of its first derivative at  $\omega = 0$ , to deduce both  $z_\sigma$  and  $\tilde{\mu}_{0,\sigma}$  using equation (7.12). However, because the model is solved using an effective impurity model, we can also deduce these quantities indirectly from the many-body energy levels of the impurity on approaching the low energy fixed point, as was done in the last chapter and is described in appendix B. This second method gives us not only a check on the results of the direct method, but also allows to deduce some information about the quasiparticle interactions  $\tilde{U}$ .

### 7.3.1 Quasiparticle weight

We first consider the values of the local quasiparticle weight factor  $z_\sigma$ , commonly known also as the wavefunction renormalisation factor. This is an important factor in determining the parameters needed to describe the low energy behaviour of the system. When there is no  $\mathbf{k}$ -dependence of the self-energy, as is the case for infinite dimensional models and DMFT, the effective mass of the quasiparticles in the paramagnetic state is proportional to  $1/z_\sigma$ . We show later that in the antiferromagnetic state the expression is more complicated and depends both on  $z_\sigma$  and the renormalised chemical potential  $\tilde{\mu}_{0,\sigma}$ . We have determined this quantity from the NRG results by the two methods described and give the values of  $z_\sigma$  deduced for both spin types as a function of doping in figure 7.2. The results are for the case  $U = 3$  (left) and  $U = 6$  (right), where there is antiferromagnetic order and the external staggered field has been set to zero.

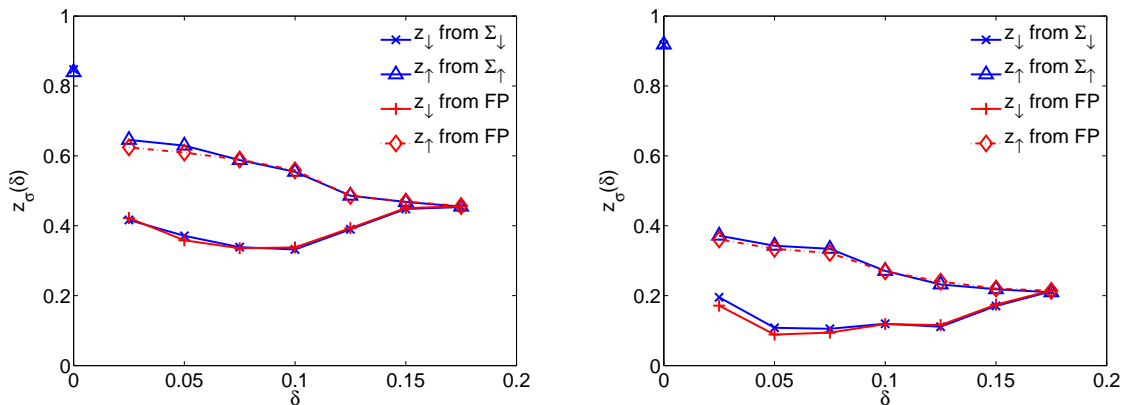


Figure 7.2: The quasiparticle weight  $z_\sigma$  as deduced directly from the self-energy and also from the impurity fixed point (FP) for  $U = 3$  (left) and  $U = 6$  (right) for various dopings.

It can be seen that there is a reasonable agreement between the values obtained by the two different methods of calculation. For the half filled case  $\delta = 0$ , the system has a gap and there is no unique value for the Fermi energy. We have in this case taken values  $z_\sigma$  only from the derivative of the self-energy at  $\omega = 0$ . Here due to particle-hole symmetry  $z_\uparrow = z_\downarrow$ . When the system is doped but still ordered, however,  $z_\uparrow \neq z_\downarrow$ , and the local

quasiparticle weights have smaller values especially the minority (down) spin particles on the sublattice. This is similar to the results we found for a doped Hubbard model in a paramagnetic state in the presence of a strong uniform magnetic field in the last chapter. For certain range of dopings the values of  $z_\uparrow$  and  $z_\downarrow$  do not vary much. The tendency is that  $z_\downarrow$  first decreases and later increases, whereas  $z_\uparrow$  decreases over the whole range until both of them merge at the doping point where the antiferromagnetic order disappears. On the whole the behaviour for  $U = 6$  is quite similar to that for the case  $U = 3$ , only that the values of the local quasiparticle weights are further reduced.

### 7.3.2 Renormalised chemical potential

In figure 7.3 we give the results for the renormalised chemical potential,  $\tilde{\mu}_{0,\sigma}$  [defined in equation (7.12)], for the two spin types in the spontaneously ordered antiferromagnetic states for  $U = 3$  (left) and  $U = 6$  (right) for a range of dopings.

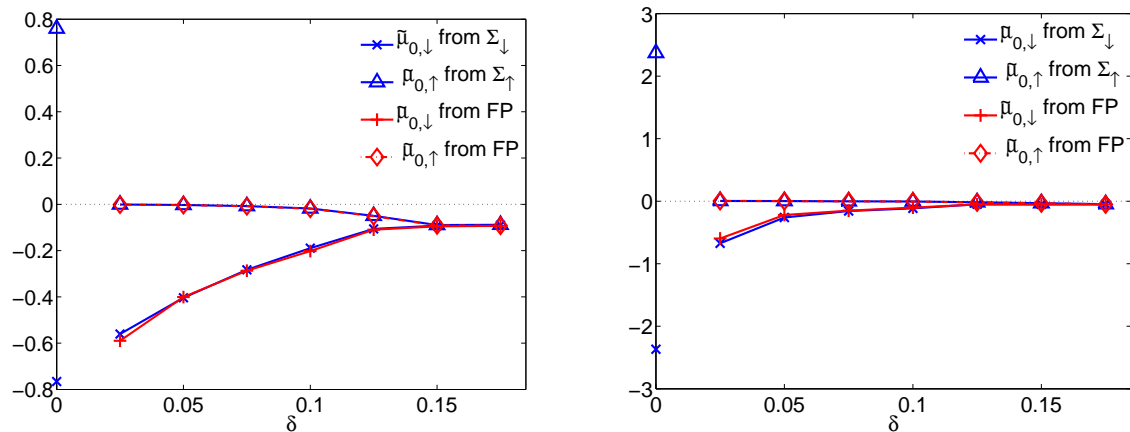


Figure 7.3: The renormalised chemical potential  $\tilde{\mu}_{0,\sigma}$  as deduced directly from the self-energy and from the impurity fixed point (FP) for various dopings for  $U = 3$  (left) and  $U = 6$  (right).

The values calculated by the two different methods can be seen to be in good agreement here, as well. We have added the values for the half filled case. These were calculated from the self-energy in the gap at  $\omega = 0$ . We can see that the value for renormalised chemical potential for the majority spin,  $\tilde{\mu}_{0,\uparrow}$ , drops from a finite value at half filling to small negative value when the system is doped. This corresponds to the fact that the chemical potential for the hole doped system falls into the lower band and will be seen in more detail later. The general behaviour of the values for  $\tilde{\mu}_{0,\sigma}$  for the case with  $U = 6$  is very similar to the case with smaller  $U$ , with again good agreement between the two sets determined by the different methods.

The renormalised chemical potential  $\tilde{\mu}_{0,\sigma}$  is an important parameter in specifying the form of the sublattice quasiparticle spectral density  $\tilde{\rho}_\sigma^0(\omega)$ . From equation (7.15) it can be

seen that, as  $\omega \rightarrow -\tilde{\mu}_{0,\sigma}$ ,  $\tilde{\rho}_{0,\sigma}(\omega)$  behaves asymptotically as

$$\tilde{\rho}_{0,\sigma}(\omega) \sim \frac{1}{\sqrt{\omega + \tilde{\mu}_{0,\sigma}}}, \quad (7.16)$$

so the quasiparticle density of states has a square root singularity at  $\omega = -\tilde{\mu}_{0,\sigma}$ . On the other hand, however, as  $\omega \rightarrow -\tilde{\mu}_{0,-\sigma}$ ,  $\tilde{\rho}_{0,\sigma}(\omega)$  behaves as

$$\tilde{\rho}_{0,\sigma}(\omega) \sim \sqrt{\omega + \tilde{\mu}_{0,-\sigma}}, \quad (7.17)$$

so the quasiparticle density of states goes to zero at  $\omega = -\tilde{\mu}_{0,-\sigma}$ . Between the two points,  $\omega = -\tilde{\mu}_{0,\sigma}$  and  $\omega = -\tilde{\mu}_{0,-\sigma}$ , the quasiparticle density of states has a gap of magnitude  $2\Delta\tilde{\mu}$ . As can be seen in figure 7.3 this free quasiparticle gap decreases with the doping and closes in the paramagnetic state. If we take into account the values at half filling we see a strong reduction of  $2\Delta\tilde{\mu}$ , when doping the system. We also see that  $\tilde{\mu}_{0,\uparrow}$  drops to small negative values for finite hole doping, which corresponds to the fact that the Fermi level then lies within the lower band. These features will be seen clearly in the figures presented in the next section, where we compare the quasiparticle densities of states with the full local spectral densities calculated from the DMFT-NRG.

### 7.3.3 The quasiparticle interaction

When two or more quasiparticles are excited from the interacting ground state, there is an interaction between them. For the Anderson impurity model this interaction is local and can be expressed as  $\tilde{U}$ , a renormalised value of the original interaction of the ‘bare’ particles. The value of  $\tilde{U}$  can be deduced by looking at lowest lying two-particle excitations derived from NRG calculation as described in the appendix B in detail. In figure 7.4 (left) we give the values of  $\tilde{U}_{pp}^{\uparrow,\downarrow}(N)$ ,  $\tilde{U}_{hh}^{\downarrow,\uparrow}(N)$  and  $\tilde{U}_{ph}^{\uparrow,\downarrow}(N)$  as deduced from DMFT-NRG calculation for the Hubbard model in an antiferromagnetic state with  $U = 6$ , 10% doping and  $\Lambda = 1.8$ . It can be seen that the three sets of results settle down to common value  $\tilde{U}$ .

Hence, we can go further and identify  $\tilde{U}$  with the local quasiparticle 4-vertex interaction for the effective impurity model as in equation (2.37), where  $\Gamma_{\uparrow,\downarrow,\downarrow,\uparrow}(\omega_1, \omega_2, \omega_3, \omega_4)$  is the total 4-vertex at the impurity site, which is equal to the same quantity for a site in the lattice model. With this interpretation it is possible to identify these parameters with those used in a renormalised perturbation expansion.

In figure 7.4 (right) we plot the doping dependence of the renormalised interaction over a range of dopings and  $U = 3$  and  $U = 6$ . We can see that in both cases the values decrease with increasing doping. Hence, the effective quasiparticle interaction is stronger for a smaller hole density. For a certain range of dopings  $\tilde{U}$  does, however, not vary much. We can also see that the ratio  $\tilde{U}/U$  for the effective interaction assume smaller values the larger the bare  $U$  becomes. Also the absolute value of  $\tilde{U}$ , i.e. without the scaling with  $U$  as in figure 7.4, is smaller for larger bare  $U$  for the full range of dopings. We will see in the next section that the fact that for larger bare  $U$  the quasiparticle interactions is smaller leads to sharper quasiparticle peaks in the strong coupling case.

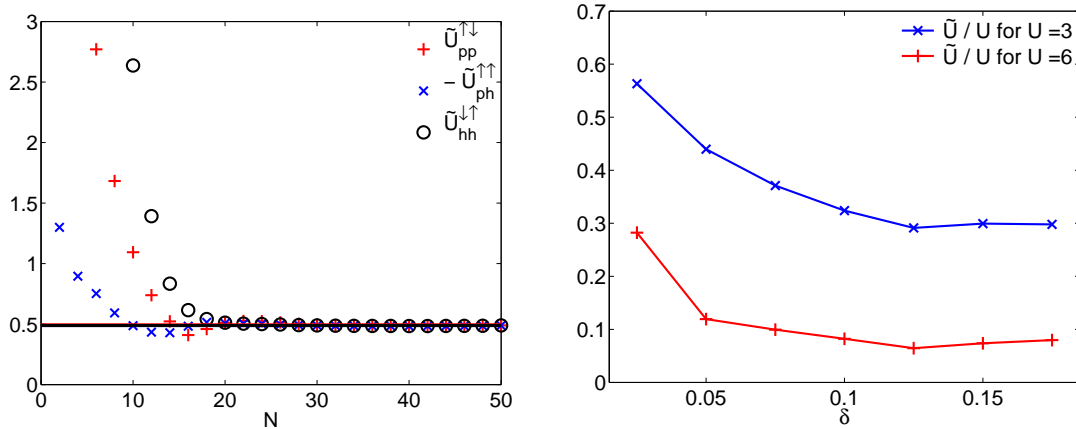


Figure 7.4: Left: The  $N$ -dependence of the renormalised particle-particle, particle-hole and hole-hole interactions for  $U = 6$  and  $x = 0.9$ , showing that they converge to a unique value  $\tilde{U}$ . Right: The renormalised quasiparticle interaction  $\tilde{U}/U$  as deduced from the impurity fixed point for various dopings and  $U = 3, 6$ .

## 7.4 Spectra

### 7.4.1 Local Spectra

The sublattice quasiparticle density of states  $\tilde{\rho}_{0,\sigma}(\omega)$ , evaluated from equation (7.15) with the renormalised parameters, describes the low energy features seen in the local spectral density  $\rho_\sigma(\omega)$  calculated from the DMFT-NRG (Bauer and Hewson 2007c). At half filling there is a gap at the Fermi level, so there are no single particle excitations in the immediate neighbourhood of the Fermi level, and this is not a very interesting case to consider. But for finite hole doping the Fermi level lies at the top of the lower band. We look in detail at the case of 10% doping where the Fermi level lies at the top of the lower band, and consider the case  $U = 3$ . In the upper panel of figure 7.5 we compare the spectral density  $\rho_\uparrow(\omega)$  with the corresponding quantity  $z_\uparrow \tilde{\rho}_{0,\uparrow}(\omega)$ , from the quasiparticle density of states.

The behaviour near the Fermi level ( $\omega = 0$ ), and the singular feature seen in the lower branch of  $\rho_\uparrow(\omega)$ , are well reproduced by the quasiparticle density of states. Above the Fermi level there is a peak in the quasiparticle density of states similar to that in the full spectrum but somewhat more pronounced. Above the Fermi level and below the upper peak there is a pseudo-gap region. In the free quasiparticle spectrum it is a definite gap. In the spectrum calculated from the direct NRG evaluation it appears as a pseudo-gap, with rather small spectral weight just above the Fermi level. From the direct DMFT-NRG calculations, due to the broadening features introduced to obtain a continuous spectrum, it is not always possible to say definitively whether there is a true gap above the Fermi level or not. To resolve this question we can appeal to the renormalised perturbation theory to look at the corrections to the quasiparticle density of states arising from the quasiparticle

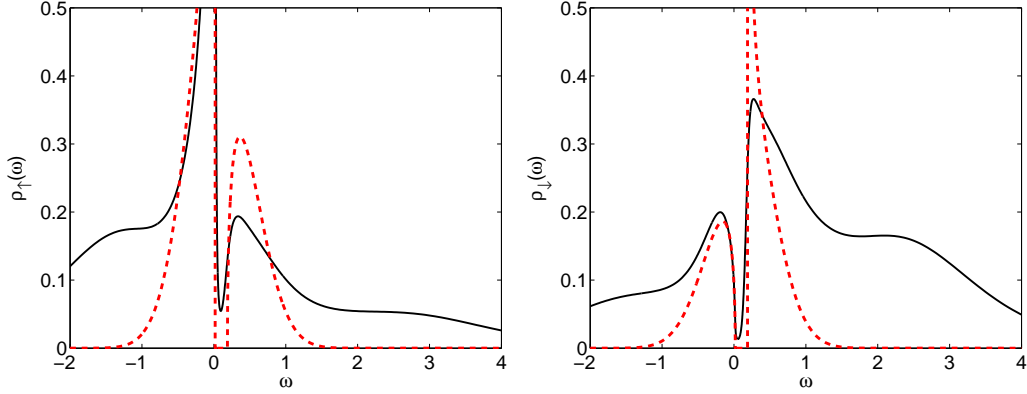


Figure 7.5: The free quasiparticle spectrum (dashed line) in comparison with DMFT-NRG spectrum for  $x = 0.9$  and  $U = 3$  for the spin-up electrons (majority, upper panel) and spin-down electrons (minority, lower panel).

interactions. A calculation of the imaginary part of the renormalised self-energy  $\tilde{\Sigma}_\sigma(\omega)$  to order  $\tilde{U}^2$  is sufficient to settle this issue. One finds that there is a small, but finite imaginary part of the self-energy in the free quasiparticle gap  $2\Delta\tilde{\mu}$ , when it lies above the Fermi level, giving rise to a finite spectral weight there. However, this spectral weight is very small close to the lower edge of the free quasiparticle density of states, when this edge lies only just above the Fermi level (Bauer and Hewson 2007c).

#### 7.4.2 $\mathbf{k}$ -resolved Spectra

We can learn more about the low energy single particle excitations by looking at the spectral density of the Green's function  $\underline{G}_{\mathbf{k},\sigma}(\omega)$  in equation (7.7) for a given wave-vector  $\mathbf{k}$ . With the self-energies  $\Sigma_\sigma(\omega)$  calculated within the DMFT-NRG approach all elements of this matrix can be evaluated. The local spectra and self-energies are spin-dependent in the doped broken symmetry state, however, the free quasiparticle bands  $E_{\mathbf{k},\pm}^0$  [equation (7.14)] do not depend on the spin. Here, we focus on the diagonal part of  $\underline{G}_{\mathbf{k},\sigma}(\omega)$  corresponding to the  $A$  sublattice,

$$G_{\mathbf{k},\sigma}(\omega) = \frac{\zeta_{-\sigma}(\omega)}{\zeta_\sigma(\omega)\zeta_{-\sigma}(\omega) - \varepsilon_{\mathbf{k}}^2}. \quad (7.18)$$

The weights of the quasiparticle excitations in this case depend on the spin corresponding to the sublattice properties. We note that one can also analyse the quasiparticle bands differently, for instance, from the  $\mathbf{k}$ -resolved spectra and the diagonal form of  $\underline{G}_{\mathbf{k},\sigma}(\omega)$ . The form of the quasiparticle bands remains unchanged then, but the weights differ and do not depend on the spin  $\sigma$  in that case.

We first of all look at the Fermi surface which is the locus of the  $\mathbf{k}$ -points at the Fermi level ( $\omega = 0$ ) where the Green's function has poles. The conduction electron energy  $\varepsilon_{\mathbf{k}_F}$  at

these point is given by

$$\varepsilon_{\mathbf{k}_F}^2 = (\mu_\uparrow - \Sigma_\uparrow(0))(\mu_\downarrow - \Sigma_\downarrow(0)). \quad (7.19)$$

By Luttinger's theorem, the volume of the Fermi surface for the interacting system must equal that of the non-interacting system with the same density. As the self-energy depends only on  $\omega$ , the two Fermi surfaces must also have the same shape, and therefore must be identical. The Fermi surface of the non-interacting system is given by  $\varepsilon_{\mathbf{k}_F} = \mu_0$ , where  $\mu_0$  is the chemical potential of the non-interacting system in the absence of any applied field for the given density. For this to be identical with that given in equation (7.19),

$$(\mu_\uparrow - \Sigma_\uparrow(0))(\mu_\downarrow - \Sigma_\downarrow(0)) = \mu_0^2. \quad (7.20)$$

We can check that this relation indeed holds from our results for  $\Sigma_\sigma(\omega)$  and  $\mu_\sigma$ , independent of the value of  $U$ , or in the case of an applied staggered field, independent of the field value. This relation implies that the total number of electrons per site  $n$  can be calculated from an integral over the non-interacting density of states,

$$n = 2 \int_{-\infty}^{\mu_0} \rho_0(\omega) d\omega, \quad (7.21)$$

where in the hole doped case  $\mu_0 = -\sqrt{\bar{\mu}_\uparrow \bar{\mu}_\downarrow}$  and  $\bar{\mu}_\sigma = \mu_\sigma - \Sigma_\sigma(0)$ .

To relate this result to the quasiparticle picture, we expand the self-energy in equation (7.18) to first order in  $\omega$ , but retain the remainder term. The Green's function can be rewritten in the form,

$$\tilde{G}_{\mathbf{k},\sigma}(\omega) = \frac{\tilde{\zeta}_{-\sigma}(\omega)}{\tilde{\zeta}_\sigma(\omega)\tilde{\zeta}_{-\sigma}(\omega) - \tilde{\varepsilon}_{\mathbf{k}}^2}, \quad (7.22)$$

where  $\tilde{\zeta}_\sigma(\omega) = \omega + \tilde{\mu}_{0,\sigma} - \tilde{\Sigma}_\sigma(\omega)$ . We define a quasiparticle Green's function  $\tilde{G}_{\mathbf{k},\sigma}(\omega)$  via  $z_\sigma \tilde{G}_{\mathbf{k},\sigma}(\omega) = G_{\mathbf{k},\sigma}(\omega)$ . The renormalised self-energy vanishes,  $\tilde{\Sigma}_\sigma(\omega) = 0$ , for the free quasiparticle Green's function  $\tilde{G}_{\mathbf{k},\sigma}^{(0)}(\omega)$ , which can be separated into two independent branches of free quasiparticles,

$$\tilde{G}_{\mathbf{k},\sigma}^{(0)}(\omega) = \frac{u_+^\sigma(\varepsilon_{\mathbf{k}})}{\omega - E_{\mathbf{k},+}^0} + \frac{u_-^\sigma(\varepsilon_{\mathbf{k}})}{\omega - E_{\mathbf{k},-}^0}, \quad (7.23)$$

where  $E_{\mathbf{k},\pm}^0$  was defined in equation (7.14) and the weights are given by

$$u_\pm^\sigma(\varepsilon_{\mathbf{k}}) = \frac{1}{2} \left( 1 \mp \sigma \frac{\Delta \tilde{\mu}}{\sqrt{\Delta \tilde{\mu}^2 + \tilde{\varepsilon}_{\mathbf{k}}^2}} \right). \quad (7.24)$$

This is similar in form to mean field theory, which would correspond to putting  $z_\sigma = 1$ , and  $\Delta \tilde{\mu} = U m_{\text{mf}}$ , where  $m_{\text{mf}}$  is the mean field sublattice magnetisation. The spin dependent contribution in (7.24) which arises from the second term is most marked in the region near

the Fermi level. It should be noted that the quasiparticle excitations  $E_{\mathbf{k},\pm}^0$  and weights  $u_{\pm}^{\sigma}(\varepsilon_{\mathbf{k}})$  here are defined by expanding the self-energy at  $\omega = 0$ . This is so that they correspond to the free quasiparticles in the renormalised perturbation theory which have an infinite lifetime.

The spectral density  $\tilde{\rho}_{\mathbf{k}}^{(0)}(\omega)$  for this free quasiparticle Green's function is a set of delta-functions,

$$\tilde{\rho}_{\mathbf{k},\sigma}^{(0)}(\omega) = u_{+}^{\sigma}(\varepsilon_{\mathbf{k}})\delta(\omega - E_{\mathbf{k},+}^0) + u_{-}^{\sigma}(\varepsilon_{\mathbf{k}})\delta(\omega - E_{\mathbf{k},-}^0). \quad (7.25)$$

On the Fermi surface  $E_{\mathbf{k},-}^0 = 0$ , which is consistent with the result for the Fermi surface given in equation (7.19). Summing over  $\mathbf{k}$  gives the local quasiparticle density of states in equation (7.15). We define the quasiparticle number  $\tilde{n}$  as the integral of the sum of the spin up and spin down quasiparticle density of states up to the Fermi level,

$$\tilde{n} = \frac{2}{\sqrt{z_{\uparrow}z_{\downarrow}}} \int_{-\infty}^0 \frac{d\omega(\omega + \tilde{\mu})}{\sqrt{(\omega + \tilde{\mu})^2 - \Delta\tilde{\mu}^2}} \rho_0 \left( \frac{\sqrt{(\omega + \tilde{\mu})^2 - \Delta\tilde{\mu}^2}}{\sqrt{z_{\uparrow}z_{\downarrow}}} \right). \quad (7.26)$$

If we change the variable of integration to  $\omega'$ , where  $\omega' \sqrt{z_{\uparrow}z_{\downarrow}} = \sqrt{(\omega + \tilde{\mu})^2 - \Delta\tilde{\mu}^2}$ , the integration can be shown to be identical with that in equation (7.21), using the fact that  $\mu_0 = -\sqrt{\tilde{\mu}_{\uparrow}\tilde{\mu}_{\downarrow}}$ . We then have an alternative statement of Luttinger's theorem in the form  $\tilde{n} = n$ . This can also be found by summing both spin components in (7.25), integrating over  $\omega$  and then converting the  $\mathbf{k}$ -summation to an integral over the free electron density of states  $\rho_0(\omega)$ . We can check in our numerical results that the relation in this form holds. The occupation number  $n$  can be calculated both from a direct evaluation of the number operator in the ground state, and also by integrating the sum of the spectral densities  $\rho_{\sigma}(\omega)$  of the full local Green's function to the Fermi level. The value of  $\tilde{n}$  is similarly determined from the integral over the total quasiparticle density of states,  $\tilde{\rho}_{\sigma}(\omega)$ . All three results were found to be in good agreement, to within one or two percent deviation at the most.

Before discussing the  $\mathbf{k}$ -resolved spectra in detail we would like to ask what the spectral weight  $w_{\text{qp}}$  of a quasiparticle excitation at the Fermi level in the lower band is,

$$G_{\text{qp}}(\omega) = \frac{w_{\text{qp}}}{\omega - E_{\mathbf{k}_{\text{F}},-}^0}. \quad (7.27)$$

For this we can not focus on the spin dependent sublattice quantities, but have to sum over both sublattices or equivalently the two spin components. The reason for this is that the antiferromagnetically ordered state does not possess any net magnetisation and has on average as many spin up polarised as spin down electrons. The division in the  $A$  and  $B$  sublattices is convenient for the DMFT calculations but somewhat artificial. In our case with hole doping the Fermi level lies within the lower band, which for the free quasiparticles is denoted by  $E_{\mathbf{k},-}^0$ . The corresponding weight on the Fermi surface defined by (7.19) is then given by

$$w_{\text{qp}} = \sum_{\sigma} z_{\sigma} u_{-}^{\sigma}(\varepsilon_{\mathbf{k}_{\text{F}}}) = \frac{z_{\uparrow} + z_{\downarrow}}{2} + \frac{(z_{\uparrow} - z_{\downarrow})\Delta\tilde{\mu}}{2|\tilde{\mu}|}, \quad (7.28)$$

where the average of the renormalised chemical potential  $\tilde{\mu}$  and the difference  $\Delta\tilde{\mu}$  were defined below equation (7.14). From the definition of  $\Delta\tilde{\mu}$  we see that the second term in (7.28) is spin rotation invariant. The spectral quasiparticle weight  $w_{\text{qp}}$  on the Fermi surface depends not only on the renormalisation factors  $z_{\sigma}$ , but also on the renormalised chemical potentials  $\tilde{\mu}_{0,\sigma}$ . The same result for the weight (7.28) can be obtained from the diagonal form of  $\underline{G}_{\mathbf{k},\sigma}(\omega)$  and the spectral weight of the lower band. The weight  $w_{\text{qp}}$  corresponds to the spectral weight  $Z$  at the Fermi level as for example given in references Dagotto (1994), Sangiovanni et al. (2006b,a). The first term of the result for  $w_{\text{qp}}$  is like the arithmetic average of  $z_{\sigma}$ . From figure 7.2 we can see that  $z_{\uparrow} > z_{\downarrow}$  and from figure 7.3 that  $\tilde{\mu}_{0,\downarrow} < \tilde{\mu}_{0,\uparrow} < 0$ . Therefore the second term in (7.28) gives a positive contribution to the spectral weight. At the end of the chapter in figure 7.10 we show values of  $w_{\text{qp}}$  in comparison with the arithmetic average of  $z_{\sigma}$ .

In order to understand better the properties of the quasiparticle bands, we now compare the quasiparticle spectrum with the  $\mathbf{k}$ -resolved spectral density  $\rho_{\mathbf{k},\sigma}(\omega)$  derived from the DMFT-NRG results. In figure 7.6 we make a comparison for the case of 12.5% doping with  $U = 3$  for the Green's function  $G_{\mathbf{k},\sigma}(\omega)$  given in equation (7.18),  $\rho_{\mathbf{k},\sigma}(\omega) = -\text{Im}G_{\mathbf{k},\sigma}(\omega^+)/\pi$ , where  $\omega^+ = \omega + i\eta$ , with  $\eta \rightarrow 0$ , with that derived for the free quasiparticles,  $z_{\sigma}\tilde{\rho}_{\mathbf{k},\sigma}^{(0)}(\omega)$  from equation (7.25).

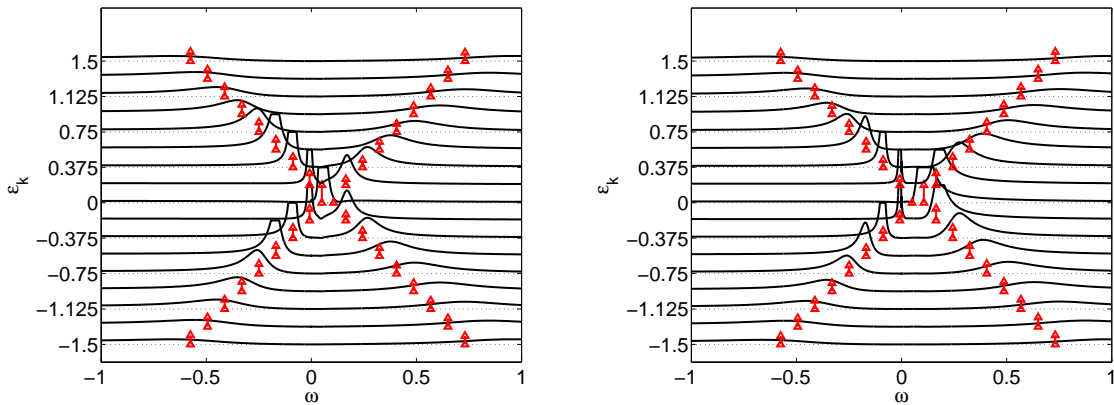


Figure 7.6: The spectral density  $\rho_{\mathbf{k},\sigma}(\omega)$  for the spin-up electrons (upper panel) and spin-down (lower panel) plotted as a function of  $\omega$  and a sequence of values of  $\varepsilon_{\mathbf{k}}$  for  $U = 3$  and 12.5% doping. Also shown with arrows are the positions of the free quasiparticle excitations, with the height of the arrow indicating the corresponding weight.

The delta-functions of the free quasiparticle results are indicated by arrows with the height of the arrow indicating the value of the corresponding spectral weight. The plots as a function of  $\omega$  are shown for a sequence values of  $\varepsilon_{\mathbf{k}}$  and, where the peaks in  $\rho_{\mathbf{k},\sigma}(\omega)$  get very narrow and high in the vicinity of the Fermi level, they have been truncated. It can be seen that the free quasiparticle results give a reasonable picture of the form of  $\rho_{\mathbf{k},\sigma}(\omega)$ , particularly in the immediate region of the Fermi level. There is considerable

variation along the curves in the way the overall spectral weight is distributed between the excitations below and above the pseudo-gap as a function of  $\varepsilon_{\mathbf{k}}$ . This is most marked in the region near the Fermi level for the spin-up electrons where most of the spectral weight is in the lower band and it is much reduced in the upper band, whereas the opposite is the case for the spin-down electrons. This is reflected in the analytic form of the weights  $u_{\pm}^{\sigma}(\varepsilon_{\mathbf{k}})$ , equation (7.24). For instance, the majority spin weight  $u_{-}^{\uparrow}(\varepsilon_{\mathbf{k}})$  for the lower band  $E_{\mathbf{k},-}^0$  becomes maximal near the Fermi energy, whereas  $u_{+}^{\uparrow}(\varepsilon_{\mathbf{k}})$  goes to zero there. The finite width of the quasiparticle peaks in  $\rho_{\mathbf{k},\sigma}(\omega)$  can be described by a RPT, when we take into account the renormalised self-energy  $\tilde{\Sigma}_{\sigma}(\omega)$  in equation (7.22). If we, for instance, use the second order approximation in  $\tilde{U}$ , which was mentioned in the last section, we get a similar behaviour for small  $\omega$  as seen for  $\rho_{\mathbf{k},\sigma}(\omega)$  in figure 7.6.

From the positions of the peaks in the  $\rho_{\mathbf{k},\sigma}(\omega)$  spectra we can deduce two branches of an effective dispersion  $E_{\mathbf{k},\pm}$  for single particle excitations and compare it with the ones for the free quasiparticles  $E_{\mathbf{k},\pm}^0$ . We give the results for  $U = 3$  in figure 7.7.

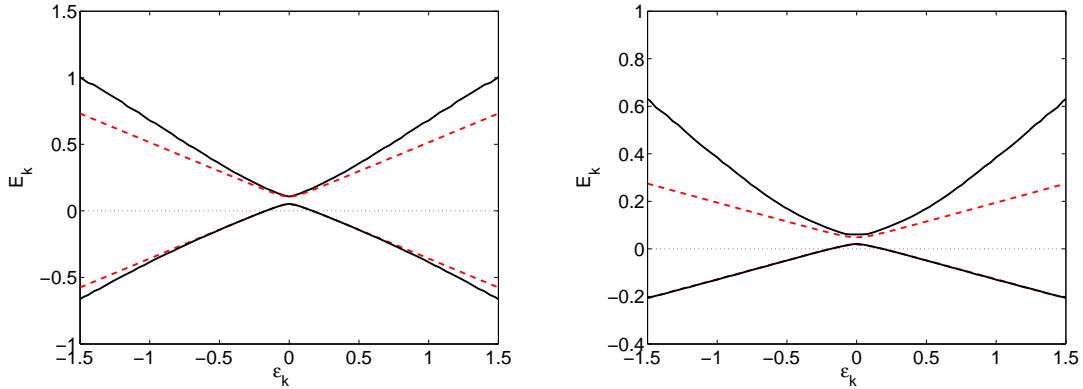


Figure 7.7: A plot of the peaks in the spectral density  $\rho_{\mathbf{k},\sigma}(\omega)$  (full line) as a function of  $\varepsilon_{\mathbf{k}}$  for  $U = 3$  (left) and  $U = 6$  (right) and 12.5% doping compared with the free quasiparticle dispersion  $E_{\mathbf{k}}^0$  (dashed line). For  $U = 6$  on the range shown the lower band  $E_{\mathbf{k},-}$  completely coincides with the free quasiparticle band  $E_{\mathbf{k},-}^0$ .

It can be seen that  $E_{\mathbf{k},-}^0$  tracks the peak in the lower band closely over a wide range of  $\varepsilon_{\mathbf{k}}$ ,  $-1.5 < \varepsilon_{\mathbf{k}} < 1.5$  (note the bandwidth  $W = 4$ ). This is not the case in the upper band, where  $E_{\mathbf{k},+}^0$  tracks the peak closely only in the lowest section that lies closest to the Fermi level. As one can see from the dotted line the Fermi level lies in the lower band and intersects the lower band twice. This corresponds to the two values with opposite sign  $\varepsilon_{\mathbf{k}_F}^{\pm}$  as can be seen from equation (7.19).

The corresponding results for  $\mathbf{k}$  resolved spectra for  $U = 6$  and also 12.5% doping are shown in figure 7.8. In order to compare well with the case  $U = 3$  we have chosen an identical range for  $\omega$  and  $\varepsilon_{\mathbf{k}}$ , although the large spectral peaks near the energy are very close together in this presentation. It can be seen that the overall features are very similar to those seen for  $U = 3$ . For the spin up spectrum (upper panel) the peaks for

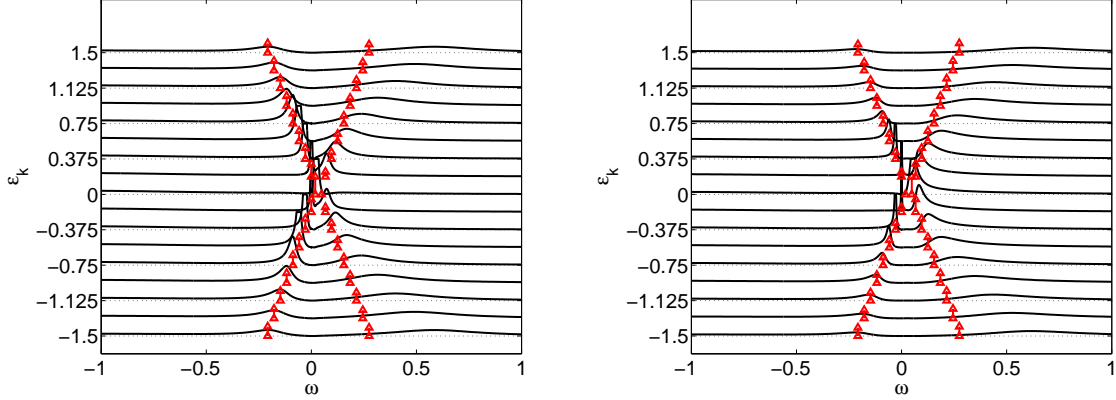


Figure 7.8: The spectral density  $\rho_{\mathbf{k},\sigma}(\omega)$  for the spin-up electrons (upper panel) and spin-down (lower panel) plotted as a function of  $\omega$  and a sequence of values of  $\varepsilon_{\mathbf{k}}$  for  $U = 6$  and 12.5% doping. Also shown with arrows are the positions of the free quasiparticle excitations, with the height of the arrow indicating the corresponding weight.

the lower band have most of the weight near the Fermi energy, whereas the upper band is suppressed there, and vice versa for the opposite spin direction. The lower bands are tracked well by the free quasiparticles, and we can see that the bands for the larger value of  $U$  are significantly flatter. This is also clearly visible in figure 7.7 (right), where we again compare the quasiparticle band with the peak position of the full spectra. On the range shown the lower band  $E_{\mathbf{k},-}$  completely coincides with the free quasiparticle band  $E_{\mathbf{k},-}^0$ .

From the  $\mathbf{k}$ -resolved spectra in figures 7.6 and 7.8 we can also extract the width of the quasiparticle peak  $\Delta_{\text{qp}}$  in the spectral density  $\rho_{\mathbf{k},\sigma}(\omega)$ . Its inverse  $1/\Delta_{\text{qp}}$  gives a measure of the quasiparticle lifetime. The results for  $\Delta_{\text{qp}}$  for the lower band  $E_{\mathbf{k},-}$  for the two cases  $U = 3, 6$  and 12.5% doping are shown in figure 7.9 as function of  $\varepsilon_{\mathbf{k}}$ . This plot brings out more clearly the feature that can be seen already in figures 7.6 and 7.8 (upper panel) that the width increases sharply when we move away from the Fermi level and the values for the width  $\Delta_{\text{qp}}$  for  $U = 6$  are significantly smaller than those for  $U = 3$ . This is in line with the fact that the local quasiparticle interaction  $\tilde{U}$  is smaller for the larger value of the bare interaction  $U$  as commented on earlier. The free quasiparticle picture is therefore even more appropriate in the case with stronger interaction. To numerical accuracy the width vanishes at  $\varepsilon_{\mathbf{k}_F}^{\pm}$  and is finite for the interval  $\varepsilon_{\mathbf{k}_F}^{-} < \varepsilon_{\mathbf{k}} < \varepsilon_{\mathbf{k}_F}^{+}$  which lies within the lower band but above the Fermi level.

Another quasiparticle property that can be extracted from our calculations is the enhancement of the effective mass  $m^*/m$ . In a Fermi liquid it is reasonable to define  $m^*/m$  as the ratio of the linear expansion coefficients of the non-interacting and interacting dispersion relation evaluated on the Fermi surface (7.19)<sup>1</sup>. If we use the free quasiparticle

<sup>1</sup>In DMFT the Fermi surface of the non-interacting and interacting system have the same form and we do not need to specify the  $\mathbf{k}$ -vector for the effective mass.

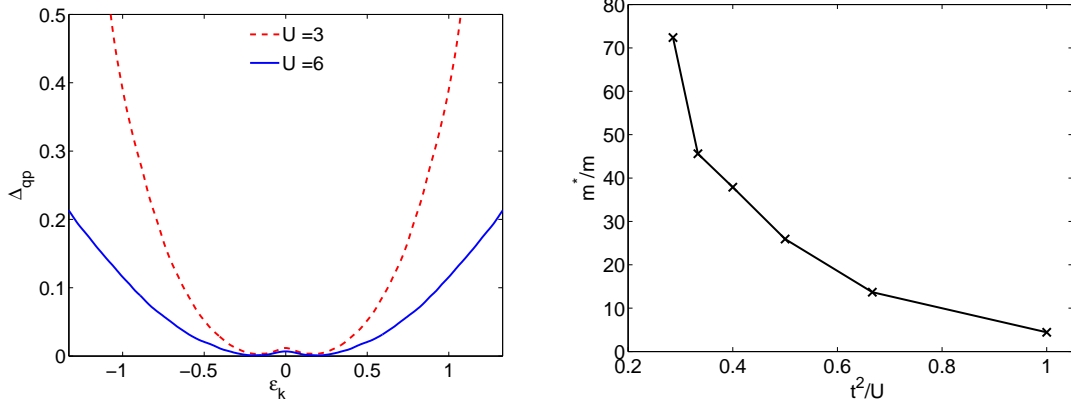


Figure 7.9: Left: A plot of the width of the peaks  $\Delta_{\text{qp}}$  in the spectral density  $\rho_{\mathbf{k},\sigma}(\omega)$  as a function of  $\varepsilon_{\mathbf{k}}$  for  $U = 3$  (dashed line) and  $U = 6$  (full line) and 12.5% doping. Right: The ratio  $m^*/m$  plotted over a range of  $t^2/U$  for 7.5% doping. For the bare band bandwidth  $W = 4$  we have  $t = \sqrt{2}$  here.

form  $E_{\mathbf{k},-}^0$  from equation (7.14) for the interacting case, this yields

$$\frac{m^*}{m} = \left. \frac{|\nabla_{\mathbf{k}} \varepsilon_{\mathbf{k}}|}{|\nabla_{\mathbf{k}} E_{\mathbf{k},-}^0|} \right|_{\mathbf{k}_F} = \frac{1}{\sqrt{z_{\uparrow} z_{\downarrow}}} \frac{|\tilde{\mu}|}{\sqrt{\tilde{\mu}_{0,\uparrow} \tilde{\mu}_{0,\downarrow}}}. \quad (7.29)$$

The effective mass enhancement therefore does not only depend on  $z_{\sigma}$ , but also on the renormalised chemical potentials  $\tilde{\mu}_{0,\sigma}$ . The general trend for  $m^*/m$  calculated from (7.29) as function of  $t^2/U$  can be seen in figure 7.9 (right) for the case of 7.5% doping. The effective mass increases strongly for large  $U$  as the hole motion is energetically more costly in the ordered background. The fact that the lower band for  $U = 6$  seen in figure 7.7 (right) is flatter than in the case  $U = 3$  in figure 7.7 (left) can be clearly attributed to the larger effective mass. We find a similar behaviour for  $m^*/m$  as function of  $U$  for different filling factors from the ones shown in figure 7.9 (right). The trend is that the effective mass enhancement is less pronounced for larger doping, which is intuitively understandable by the quasiparticle motion in an ordered background. In the DMFT framework for the paramagnetic state as well as the case with homogenous magnetic field, the quasiparticle spectral weight  $w_{\text{qp}}$  and the inverse of the effective mass enhancement  $m/m^*$  can be described simply by the renormalisation factor  $z_{\sigma}$ . In figure 7.10 we compare the spectral quasiparticle weight  $w_{\text{qp}}$  (7.28) the arithmetic,  $(z_{\uparrow} + z_{\downarrow})/2$ , and geometric,  $\sqrt{z_{\uparrow} z_{\downarrow}}$ , average of the renormalisation factors, and the inverse of the effective mass,  $m/m^*$ , from equation (7.29) for  $U = 3$  for various dopings.

As seen in this case with antiferromagnetic symmetry breaking these quantities take a different form (7.28) and (7.29) and have distinct values. As a first approximation the quasiparticle spectral weight  $w_{\text{qp}}$  corresponds to the arithmetic average of the renormalisation factors  $z_{\sigma}$ , whilst  $m/m^*$  relates to the geometric average. In general, one can,

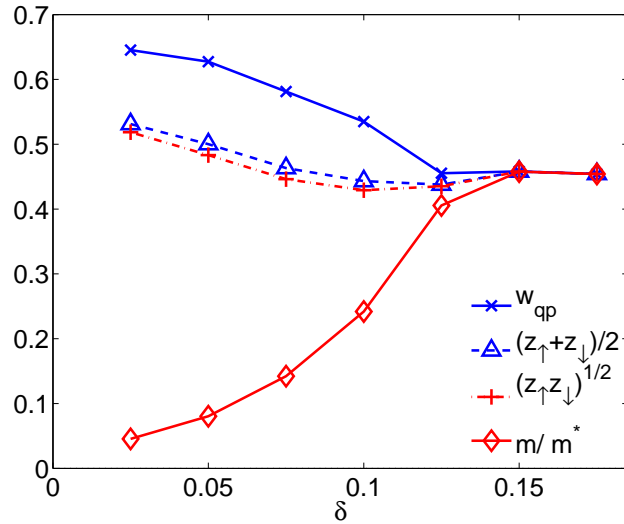


Figure 7.10: Comparison of the spectral quasiparticle weight  $w_{\text{qp}}$  (7.28) the arithmetic,  $(z_{\uparrow} + z_{\downarrow})/2$ , and geometric,  $\sqrt{z_{\uparrow} z_{\downarrow}}$ , average of the renormalisation factors, and the inverse of the effective mass,  $m/m^*$ , (7.29) for  $U = 3$  for various dopings.

however, not omit the dependence on the renormalised chemical potential as it gives a significant contribution as seen in figure 7.10. This can be understood for example for the limit of zero doping. The system then becomes an antiferromagnetically ordered insulator with a spectral gap. The weights  $z_{\sigma}$  tend to finite quite large values, but the effective mass must diverge. This is found in equation (7.29) since  $\tilde{\mu}_{0,\uparrow} \rightarrow 0$  for  $\delta \rightarrow 0$  and the trend can be seen in figure 7.10.

To summarise, we have given a detailed analysis of the properties of the renormalised quasiparticles in a metallic antiferromagnetic state in the Hubbard model. The calculations are based on a commensurate antiferromagnetic ordering in a bipartite lattice and carried out within the DMFT-NRG framework. It is shown that the relevant quasiparticle parameters can be deduced by two different methods, which give values which are in reasonable agreement. We have presented results for  $\mathbf{k}$ -resolved spectral functions, and analysed them in terms of quasiparticle bands. We also gave explicit expressions for the quasiparticle spectral weight and the effective mass in terms of the renormalised parameters. The results for the spectral quasiparticle weight  $w_{\text{qp}}$  are on the whole in agreement with earlier calculations (Dagotto 1994) and more recent ones (Sangiovanni et al. 2006b,a). In reference Dagotto (1994) the effective quasiparticle bandwidth  $W_{\text{eff}}$  in the  $t$ - $J$ -model is found to decrease with decreasing  $J$ . This is line with our results if we identify  $W_{\text{eff}} \sim m/m^*$  and  $J \sim t^2/U$  (see figure 7.9).

## Chapter 8

# The attractive Hubbard model

In this final chapter we present results of a preliminary study of the attractive Hubbard model within the DMFT-NRG approach. First we discuss the relevance of the model and in which situations it is applied. Then we outline the details for the DMFT approach. This is followed by a presentation of results for static expectation values, like the average pair density and the anomalous expectation value as function of the local attraction  $U$  and dynamic spectral functions.

### 8.1 The BCS-BEC crossover

Whilst in the foregoing chapters we have discussed impurity and lattice models with a local repulsion, we consider a system of fermions with local attraction in this last chapter of the thesis. As outlined in section 1.2.2 the attractive model and the repulsive model can be mapped onto one another by a spin-isospin transformation. Symmetry breaking fields in the spin channel then take the role of the corresponding symmetry breaking fields in the charge channel. Hence, for instance, the repulsive Hubbard model with the spontaneous antiferromagnetic symmetry breaking as discussed in the last chapter translates to a charge ordering symmetry breaking for the attractive model. At half filling charge order and superconductivity are degenerate as they form part of a larger symmetry group there. The focus here is on the superconducting state, which corresponds to an offdiagonal long range order in contrast to the diagonal long range order for the antiferromagnetic and charge ordered state. To study superconducting solutions it is therefore better to consider a situation with a different filling factor,  $x \neq 1$ . We will explore the superconducting phase both at half filling and also for quarter filling, where no degeneracy with the charge ordered state occurs. The problem is approached in a similar way as before with DMFT-NRG calculations.

There are various reasons why it is of interest to study the attractive Hubbard model. One of them is that it can be viewed as an effective model for superconductors for different coupling strength. In fact, in the famous theory of Bardeen, Cooper and Schrieffer (1957)

(BCS) an effective attractive model with a Debye cutoff is studied. The local attraction between the electrons can be thought of as mediated by a boson, a phonon or exciton for instance (Micnas et al. 1990). Retardation effects are neglected in such an approach. In the weak coupling limit,  $U \rightarrow 0$ , BCS mean field theory has been very successful. The resulting excitation gap  $\Delta_{\text{sc}}$  in the spectrum and the transition temperature  $T_c$  can be obtained from simple mean field equations (Micnas et al. 1990), and one finds that both depend exponentially on  $U$ , viz  $\Delta_{\text{sc}}, T_c \sim e^{-1/U\rho_0}$ . The general picture in this situation is that for any attractive interactions the Fermi-surface of the non-interacting electrons is unstable to the formation of Cooper pairs (Cooper 1956). These pairs extend over a large range in position space and are often referred to as momentum space pairs,  $c_{\mathbf{k},\uparrow}^\dagger c_{-\mathbf{k},\downarrow}^\dagger$ . The kinetic energy for the state with these pairs is a bit larger than in the normal phase, but the bound-state formation leads to a gain in potential energy. The Cooper pairs only begin to form at the transition temperature  $T_c$ .

In contrast, in the strong coupling limit, where  $|U|$  exceeds the other energy scales, the fermions are tightly bound to local pairs in position space already at a high temperature  $T_0$  of the order of  $U$ . These pairs behave like real bosons and can therefore undergo Bose-Einstein condensation (BEC) at a lower temperature  $T_c$ , which is proportional to the particle density and the inverse of the mass of the pairs  $m_B$ . In this limit the effective mass  $m_B$  of a boson (pair of fermions) can be related to the inverse of the pair hopping amplitude  $t_B$ . One finds  $t_B = 4t^2/U$  in the lattice model (Dupuis 2005), and thus  $m_B \sim U$ . As a consequence the critical temperature for condensation decreases with  $U$ ,  $T_c \sim t^2/U$  in the BEC limit. The transition here is driven by kinetic energy, which is lowered as fermion pairs join the condensate with the lowest energy. The single particle excitation gap  $\Delta_{\text{sc}}$  in this limit is proportional to the magnitude of the attraction,  $\Delta_{\text{sc}} \sim U$ , since the binding energy of the pair increases linearly with  $U$ . These two limiting cases, the weak coupling BCS limit and the strong coupling BEC limit, correspond to quite different situations and it is remarkable that as discovered over the years, they are connected by a smooth crossover (Eagles 1969, Nozières and Schmitt-Rink 1985, Randeria 1995, Leggett 2006). It was shown that the spectral gap  $\Delta_{\text{sc}}$  at zero temperature evolves smoothly from small to large  $U$ . Also the BCS wave-function from the weak coupling limit can be seen to go over continuously to a wave function of bosons as fermionic pairs in the strong coupling limit. Moreover, the transition temperature  $T_c$  to the superfluid state is a smooth function of the local attraction connecting the BCS and BEC limit. Here we will focus on the attractive Hubbard model to study this BCS-BEC crossover. It is worth mentioning that this problem has also been investigated by a continuum field theoretic model (Hausmann 1992, Dupuis 2005, Randeria 1995, for instance).

In the 1990s experimental groups were first able to realise BECs for laser cooled bosonic atoms, from which the field of cold atomic gases emerged. In recent years many groups have also focused on studying the properties of fermionic cold gas systems. When loaded into an optical trap their interaction can be tuned by means of a Feshbach resonance. One therefore

has a very clean and controllable system, which can be modelled by the Hubbard model. It has been possible to generate a BEC of tightly bound fermions (Greiner et al. 2003, Zwierlein et al. 2004), and experimental groups are working on detecting the full crossover to the BCS limit (Zwierlein et al. 2005). Apart from the cold gases the study of the BCS-BEC crossover had already been taken up by condensed matter researchers interested in understanding the strong coupling and high temperature superconductors (Micnas et al. 1990). The high temperature superconductors contain some properties, which are better understood in terms of local pairs, preformed above the transition temperature  $T_c$ , than in the BCS picture (Toschi et al. 2005). DMFT studies for the attractive Hubbard model have been carried out by Keller et al. (2001) and Capone et al. (2002) in the normal phase, and more recently by Garg et al. (2005) and Toschi et al. (2005) in the broken symmetry phase. Here we will also focus on describing the attractive Hubbard model for various  $U$  in the broken symmetry phase employing the DMFT-NRG method. The work presented in this chapter is still in progress and the results are at a preliminary stage. We will therefore keep the presentation very brief.

## 8.2 The DMFT setup

We want to study the attractive Hubbard model in the grand canonical formalism (1.35),

$$H = - \sum_{i,j,\sigma} (t_{ij} c_{i,\sigma}^\dagger c_{j,\sigma} + \text{h.c.}) - \mu \sum_{i\sigma} n_{i\sigma} - U \sum_i n_{i,\uparrow} n_{i,\downarrow}. \quad (8.1)$$

For convenience we take this form (8.1) with  $U > 0$ . To study superconducting order we include an explicit superconducting symmetry breaking term  $H_{\text{sc}}$  with a “field”  $\Delta_{\text{sc}}^0$ . After a lattice Fourier transform (8.1) then reads

$$H + H_{\text{sc}} = \sum_{\mathbf{k},\sigma} (\varepsilon_{\mathbf{k}} - \mu) c_{\mathbf{k},\sigma}^\dagger c_{\mathbf{k},\sigma} - \Delta_{\text{sc}}^0 \sum_{\mathbf{k}} [c_{\mathbf{k},\uparrow}^\dagger c_{-\mathbf{k},\downarrow}^\dagger + \text{h.c.}] - U \sum_i n_{i,\uparrow} n_{i,\downarrow}. \quad (8.2)$$

Note that we have not restricted the  $\mathbf{k}$ -summation in  $H_{\text{sc}}$ . The non-interacting Green’s function is best worked out in Nambu space like in (5.10), i.e.,

$$\underline{G}_{\mathbf{k}}^0(\omega)^{-1} = \begin{pmatrix} \omega - \xi_{\mathbf{k}} & \Delta_{\text{sc}}^0 \\ \Delta_{\text{sc}}^0 & \omega + \xi_{\mathbf{k}} \end{pmatrix}, \quad (8.3)$$

where we have introduced  $\xi_{\mathbf{k}} = \varepsilon_{\mathbf{k}} - \mu$ . The interacting problem can be treated by introducing the matrix self-energy  $\underline{\Sigma}_{\mathbf{k}}(\omega)$  such that the interacting Green’s function is given by the Dyson equation

$$\underline{G}_{\mathbf{k}}(\omega)^{-1} = \underline{G}_{\mathbf{k}}^0(\omega)^{-1} - \underline{\Sigma}_{\mathbf{k}}(\omega). \quad (8.4)$$

The DMFT formulation in the path integral formalism for this model is in analogy to what has been presented in chapter 2. Due to the symmetry breaking field it is, however,

suitable to work in Nambu space with

$$\mathbf{C}_i(\tau) := \begin{pmatrix} c_{i,\uparrow}(\tau) \\ c_{i,\downarrow}(\tau) \end{pmatrix}$$

and  $2 \times 2$  matrices. The effective Weiss field is now a  $2 \times 2$  matrix  $\underline{\mathcal{G}}_0^{-1}(\tau)$  and the effective action on the “0”-site reads

$$S_{\text{eff}} = - \int_0^\beta d\tau \int_0^\beta d\tau' \sum_\sigma \bar{\mathbf{C}}_0(\tau) \underline{\mathcal{G}}_0^{-1}(\tau - \tau') \mathbf{C}_0(\tau') - U \int_0^\beta d\tau \sum_i n_{0,\uparrow}(\tau) n_{0,\downarrow}(\tau). \quad (8.5)$$

As the effective impurity model we consider the attractive Anderson model in a superconducting medium (5.1) as discussed in the beginning of chapter 5 with an additional on-site symmetry breaking  $\Delta_{\text{sc}}^d$ . The non-interacting Green’s function matrix then has the form of equation (5.17),

$$\underline{\mathcal{G}}_0(\omega)^{-1} = \omega \mathbb{1}_2 - \varepsilon_d \tau_3 - \Delta_{\text{sc}}^d \tau_1 - \underline{\mathcal{K}}(\omega), \quad (8.6)$$

where  $\varepsilon_d = -\mu$  and the on-site symmetry breaking field  $\Delta_{\text{sc}}^d = \Delta_{\text{sc}}^0$ . The generalised matrix hybridisation for the medium  $\underline{\mathcal{K}}(\omega)$  has the form

$$\underline{\mathcal{K}}(\omega) = \tau_3 \frac{1}{N} \sum_{\mathbf{k}} V_{\mathbf{k}}^2 \underline{g}_{\mathbf{k}}(\omega) \tau_3, \quad (8.7)$$

where  $\underline{g}_{\mathbf{k}}(\omega)$  was given in (5.11).

The DMFT self-consistency equation (2.71) in this case with symmetry breaking is a matrix equation,

$$\underline{\mathcal{G}}_0^{-1}(\omega) = \underline{\mathcal{G}}(\omega)^{-1} + \underline{\Sigma}(\omega), \quad (8.8)$$

where we have dropped the  $\mathbf{k}$ -dependence of the self-energy. We use the NRG to solve the effective impurity problem for a given medium  $\underline{\mathcal{K}}(\omega)$  and calculate  $\underline{\Sigma}(\omega)$ . From this we can obtain the diagonal local lattice Green’s function which for the superconducting case takes the form [cf. (8.3) and (8.4)],

$$G(\omega) = \int d\varepsilon \frac{\rho_0(\varepsilon)(\zeta_2(\omega) + \varepsilon)}{(\zeta_1(\omega) - \varepsilon)(\zeta_2(\omega) + \varepsilon) - (\Delta_{\text{sc}}^0 - \Sigma_{21}(\omega))(\Delta_{\text{sc}}^0 - \Sigma_{12}(\omega))}, \quad (8.9)$$

where  $\zeta_1(\omega) = \omega + \mu - \Sigma_{11}(\omega)$  and  $\zeta_2(\omega) = \omega - \mu - \Sigma_{22}(\omega)$ . As before  $\rho_0(\varepsilon)$  is the density of states of non-interacting fermions. The offdiagonal local lattice Green’s function is given by

$$G^{\text{off}}(\omega) = -\Sigma_{21}(\omega) \int d\varepsilon \frac{\rho_0(\varepsilon)}{(\zeta_1(\omega) - \varepsilon)(\zeta_2(\omega) + \varepsilon) - (\Delta_{\text{sc}}^0 - \Sigma_{21}(\omega))(\Delta_{\text{sc}}^0 - \Sigma_{12}(\omega))}. \quad (8.10)$$

We denote  $G_{11} = G$ ,  $G_{21} = G^{\text{off}}$  and  $G_{21}(\omega) = G_{12}(-\omega)^*$ ,  $G_{22}(\omega) = -G_{11}(-\omega)^*$ . These Green’s functions can be collected to the matrix  $\underline{\mathcal{G}}$ . Having calculated the local Green’s function  $\underline{\mathcal{G}}$  the self-consistency equation (8.8) determines the new Weiss field and medium.

We take the impurity model in the form described in chapter 5, and identify  $\underline{G}_0(\omega) = \underline{\mathcal{G}}_0(\omega)$ . Then from equation (8.6) we obtain an equation for the effective medium matrix  $\underline{K}(\omega)$ . This has the general form (8.7), with diagonal,

$$K_{11}(\omega) = \frac{1}{N} \sum_{\mathbf{k}} V_{\mathbf{k}}^2 \frac{\omega + \varepsilon_{\mathbf{k}}}{\omega^2 - (\varepsilon_{\mathbf{k}}^2 + \Delta_{\text{sc}}^2)} \quad (8.11)$$

and offdiagonal part,

$$K_{21}(\omega) = \frac{1}{N} \sum_{\mathbf{k}} V_{\mathbf{k}}^2 \frac{-\Delta_{\text{sc}}}{\omega^2 - (\varepsilon_{\mathbf{k}}^2 + \Delta_{\text{sc}}^2)}. \quad (8.12)$$

Note that the parameter of the medium  $\Delta_{\text{sc}}$  is different from the “external field”  $\Delta_{\text{sc}}^0$ . In the calculations with spontaneous superconducting order we will always consider the limit  $\Delta_{\text{sc}}^0 \rightarrow 0$ , where a solution with superconducting symmetry breaking will have a bath parameter  $\Delta_{\text{sc}} \neq 0$ . Due to the symmetry broken form (8.11) and (8.12) it is not straight forward to extract the parameters  $\varepsilon_{\mathbf{k}}$ ,  $V_{\mathbf{k}}$  and  $\Delta_{\text{sc}}$  and the corresponding ones for the effective linear chain problem relevant in the NRG approach. To carry out the calculations here we have considered the diagonal part of the medium  $K_{11}(\omega)$  as the earlier scalar function  $K(\omega)$ , from which we can calculate the linear chain parameters by the standard method (Bulla et al. 1997, Bauer 2007). The medium parameter  $\Delta_{\text{sc}}$  (see chapter 5) is determined from the mean field criterion

$$\Delta_{\text{sc}} = U \langle c_{0,\uparrow} c_{0,\downarrow} \rangle = U \int_{-\infty}^0 d\omega \left( -\frac{1}{\pi} \text{Im} G^{\text{off}}(\omega) \right). \quad (8.13)$$

This procedure has the advantage that the same NRG program as for calculations for the local model in chapter 5 can be used. The obvious disadvantage is that we do not make full use of the self-consistency equation involving  $K_{21}(\omega)$ , and the mean field criterion (8.13) overestimates the size of the gap  $\Delta_{\text{sc}}$ . An improved approach needs to take into the full matrix structure of the self-consistency equation properly, and a more general form of medium for the Anderson model with for instance an energy dependent parameter  $\Delta_{\text{sc}}$  needs to be considered. One possible way for such a generalisation is described in Bauer (2007) section 1.4.3.

### 8.3 Renormalised quasiparticle description

The  $\mathbf{k}$ -dependent Green’s function is given as in equation (8.4),

$$\underline{G}_{\mathbf{k}}(\omega) = \frac{\begin{pmatrix} \omega + \xi_{\mathbf{k}} - \Sigma_{22}(\omega) & \Delta_{\text{sc}}^0 - \Sigma_{12}(\omega) \\ \Delta_{\text{sc}}^0 - \Sigma_{21}(\omega) & \omega - \xi_{\mathbf{k}} - \Sigma_{11}(\omega) \end{pmatrix}}{[\omega - \xi_{\mathbf{k}} - \Sigma_{11}(\omega)][\omega + \xi_{\mathbf{k}} - \Sigma_{22}(\omega)] - [\Delta_{\text{sc}}^0 - \Sigma_{12}(\omega)][\Delta_{\text{sc}}^0 - \Sigma_{21}(\omega)]}, \quad (8.14)$$

The excitations of the system can be analysed as usual as the poles of (8.14), which are given by the zeros of the denominator. In order to be able to develop a simple picture of

the quasiparticle excitation of the attractive Hubbard model we proceed in a similar way as in chapter 5, where we studied the bound state equation with renormalised parameters. We expand the diagonal self-energies to linear order and approximate the off-diagonal ones by a real constant at  $\omega = 0$ , similar as in (5.27). This is motivated by the fact that the imaginary part of the self-energy vanishes in the gap,  $\text{Im}\underline{\Sigma}(\omega) = 0$ , and the fact that numerical results for the real part show an approximately linear behaviour. In this approximation the excitations are given by

$$E_{\mathbf{k}}^{0,\pm} = \pm E_{\mathbf{k}}^0 = \pm \sqrt{\tilde{\xi}_{\mathbf{k}}^2 + \tilde{\Delta}_{\text{sc}}^2}, \quad (8.15)$$

where we have introduced  $\tilde{\xi}_{\mathbf{k}} = z[\xi_{\mathbf{k}} - \Sigma(0)]$  and  $\tilde{\Delta}_{\text{sc}} = z(\Delta_{\text{sc}}^0 - \Sigma^{\text{off}}(0))$ , with the usual definition  $z^{-1} = 1 - \Sigma(0)'$ . We can see that when we study spontaneous broken symmetry and take the limit  $\Delta_{\text{sc}}^0 \rightarrow 0$ , the superconducting gap is mainly given by the value  $z\Sigma^{\text{off}}(0)$ . Then the diagonal quasiparticle Green's function  $\tilde{G}_{\mathbf{k}}^0(\omega)$  and the offdiagonal part  $\tilde{G}_{\mathbf{k}}^{0,\text{off}}(\omega)$  can be written in the well-known form

$$\tilde{G}_{\mathbf{k}}^0(\omega) = \frac{u_{\mathbf{k}}^2}{\omega - E_{\mathbf{k}}^0} + \frac{v_{\mathbf{k}}^2}{\omega + E_{\mathbf{k}}^0}, \quad \tilde{G}_{\mathbf{k}}^{0,\text{off}}(\omega) = u_{\mathbf{k}}v_{\mathbf{k}} \left( \frac{1}{\omega - E_{\mathbf{k}}^0} - \frac{1}{\omega + E_{\mathbf{k}}^0} \right), \quad (8.16)$$

where

$$u_{\mathbf{k}}^2 = \frac{1}{2} \left( 1 + \frac{\tilde{\xi}_{\mathbf{k}}}{E_{\mathbf{k}}^0} \right), \quad v_{\mathbf{k}}^2 = \frac{1}{2} \left( 1 - \frac{\tilde{\xi}_{\mathbf{k}}}{E_{\mathbf{k}}^0} \right). \quad (8.17)$$

These expressions describe the two bands of quasiparticle excitations and their weights. They reduce the Bogoliubov mean field result for  $z \rightarrow 1$  and  $\Sigma(0) = Un/2$  and  $\Sigma^{\text{off}}(0) = U\langle c_{0,\uparrow}c_{0,\downarrow} \rangle$ . This result is most accurate in the weak coupling limit for small  $U$ . In the strong coupling limit, the spectral gap is large and therefore the expansion around  $\omega = 0$  is more questionable. We will show, however, that in the calculations presented the spectra can still be described well by the approximation (8.16). The spectral gap is then proportional to  $U$ .

In BCS theory the excitation gap  $\Delta_{\text{sc}}$  at  $T = 0$  can be found from the equation

$$\Delta_{\text{sc}} = U \sum_{\mathbf{k}} u_{\mathbf{k}}v_{\mathbf{k}} = \frac{U}{2} \sum_{\mathbf{k}} \frac{z\Delta_{\text{sc}}}{E_{\mathbf{k}}^0} = \frac{U}{2} \sum_{\mathbf{k}} \frac{\Delta_{\text{sc}}}{\sqrt{(\varepsilon_{\mathbf{k}} - \mu_0)^2 + \Delta_{\text{sc}}^2}}, \quad (8.18)$$

where  $\mu_0 = \mu - \Sigma(0)$  and the gap is defined as in equation (8.13),  $\Delta_{\text{sc}} = U\langle c_{0,\uparrow}c_{0,\downarrow} \rangle$ . Equation (8.18) is clearly applicable in the weak coupling limit, but also gives a reasonable result in the strong coupling limit, where  $\Delta_{\text{sc}} = U\sqrt{x(2-x)}/2$  (Micnas et al. 1990);  $x$  is the filling factor. As mentioned earlier the gap  $\Delta_{\text{sc}}$  given by (8.18) interpolates therefore smoothly between the BCS and BEC limit. From equation (8.18) we can also determine the anomalous expectation value  $\langle c_{0,\uparrow}c_{0,\downarrow} \rangle$ .

Another quantity of interest is the double occupancy  $\langle n_{\uparrow}n_{\downarrow} \rangle$  or average pair density. In the non-interaction limit it is given by  $(x/2)^2$ . The probability to find an electron with spin  $\sigma$  on site is  $x/2$  and as the particles are uncorrelated  $\langle n_{\uparrow}n_{\downarrow} \rangle = (x/2)^2$ . In the

strong coupling limit the probability to find an electron on site is still  $x/2$ , but since the attractive energy is large the probability to find another one there goes to one, and therefore  $\langle n_\uparrow n_\downarrow \rangle \rightarrow x/2$ . In other words, all particles are then bound to pairs and the pair density is given by half the filling factor,  $\langle n_\uparrow n_\downarrow \rangle = x/2$ . The double occupancy  $\langle n_\uparrow n_\downarrow \rangle$  multiplied by  $U$  is also of interest as it gives the expectation value of the potential energy. For a system in a coherent superfluid state another relevant quantity is the superfluid stiffness  $D_s$ . It is a measure for the energy required to twist the phase of the condensate. It is therefore related to the degree of phase coherence of the superconducting particles, and it is usually proportional to the superfluid density  $n_s$ . It can be found either from the weight of the delta-function in the optical conductivity or from the current-current correlation function. In the DMFT approach and for the Bethe lattice with semicircular density of states  $\rho_0(\varepsilon)$  (2.75) it can be calculated directly from the offdiagonal Green's function (Toschi et al. 2005). At zero temperature it takes the form,

$$D_s = -\frac{8}{\pi} \int d\varepsilon_{\mathbf{k}} \rho_0(\varepsilon_{\mathbf{k}}) V(\varepsilon_{\mathbf{k}}) \int_{-\infty}^0 d\omega \operatorname{Im} G_{\mathbf{k}}^{r,\text{off}}(\omega) \operatorname{Re} G_{\mathbf{k}}^{r,\text{off}}(\omega), \quad (8.19)$$

where  $G_{\mathbf{k}}^{r,\text{off}}(\omega)$  is the retarded offdiagonal Green's function (8.14) and  $V(\varepsilon_{\mathbf{k}}) = (4t^2 - \varepsilon_{\mathbf{k}}^2)/3$  is a square vertex (Toschi et al. 2005). We can evaluate the expression (8.19) using the renormalised quasiparticle Green's function  $z\tilde{G}_{\mathbf{k}}^{0,\text{off}}(\omega)$  (8.16), which yields the somewhat simpler expression

$$D_s^{\text{qp}} = 4z^2 \int_{-D}^D d\varepsilon_{\mathbf{k}} \rho_0(\varepsilon_{\mathbf{k}}) V(\varepsilon_{\mathbf{k}}) \frac{u_{\mathbf{k}}^2 v_{\mathbf{k}}^2}{E_{\mathbf{k}}^0}. \quad (8.20)$$

## 8.4 Results

We have carried out DMFT-NRG calculations for the attractive Hubbard model at half and quarter filling in the state with spontaneously broken symmetry,  $\Delta_{\text{sc}}^0 \rightarrow 0$ . For simplicity the semicircular density of states (2.75) was used. The energy scale is set by  $t = 1$  such that the bare bandwidth  $W = 4$ . In figure 8.1 we give results for the static expectation values double occupancy  $\langle n_\uparrow n_\downarrow \rangle$  and the anomalous expectation value  $\langle c_{0,\uparrow} c_{0,\downarrow} \rangle$  as a function of  $U$  for  $x = 1$  (left) and  $x = 0.5$  (right).

We can see that as discussed above the pair density or double occupancy increases continuously from the value  $(x/2)^2$  (1/4, left, and 1/16, right) at  $U = 0$  to the value  $(x/2)$  (1/2 and 1/4). The anomalous expectation value  $\langle c_{0,\uparrow} c_{0,\downarrow} \rangle$  is zero in the non-interacting case, and for small  $U$  it increases like  $e^{-1/U} \rho_0(0)$  as in BCS theory. For large  $U$  it tends to the value  $\sqrt{x(2-x)}/2$  (1/2, left, and 0.433, right) as discussed above. The gap  $\Delta_{\text{sc}}$  is then proportional to  $U$  as expected in the BEC limit (energy for pair breaking). The dashed line gives the result for  $\langle c_{0,\uparrow} c_{0,\downarrow} \rangle$  from the mean field equation (8.18), which fits the DMFT-NRG result very well for the full range of interactions  $U$ . Due to numerical

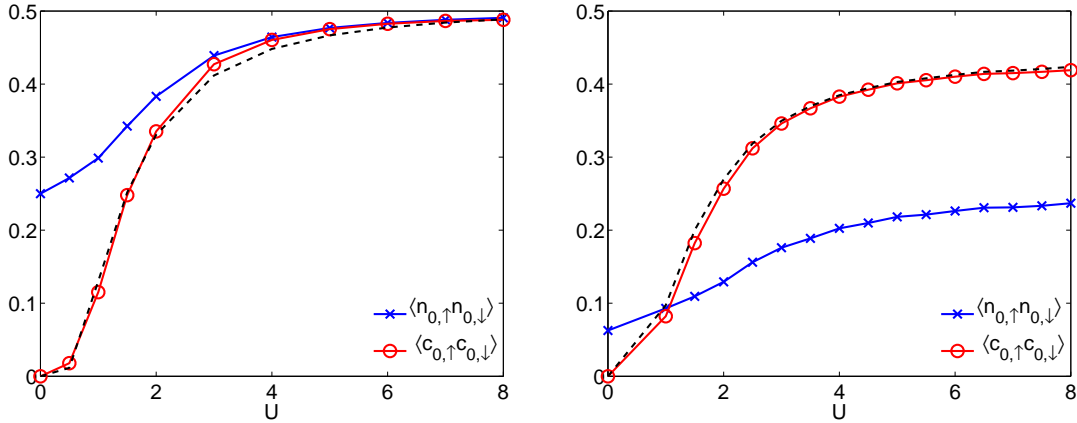


Figure 8.1: The static expectation values double occupancy  $\langle n_{\uparrow} n_{\downarrow} \rangle$  and the anomalous expectation value  $\langle c_{0,\uparrow} c_{0,\downarrow} \rangle$  as a function of  $U$  for half filling (left) and quarter filling (right). The dashed line gives the result for  $\langle c_{0,\uparrow} c_{0,\downarrow} \rangle$  from the mean field equation (8.18).

problems with the small gap and very sharp peaks the BCS limit was not investigated in great detail with the DMFT-NRG calculations.

In figure 8.2 the superfluid stiffness  $D_s$  calculated from equation (8.19) is shown as a function of  $U$  for half filling (left) and for quarter filling (right). The dashed line shows the result as obtained from equation (8.20), where the quasiparticle Green's functions are used to evaluate the integrals.

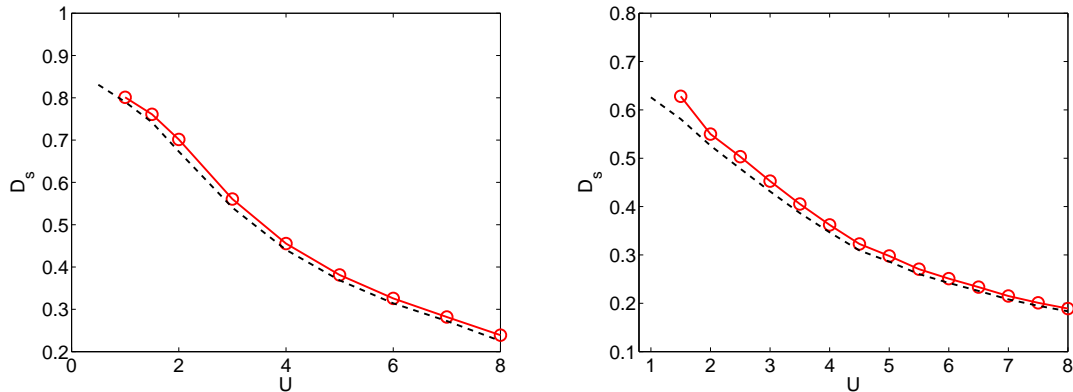


Figure 8.2: The superfluid stiffness  $D_s$  as calculated from the offdiagonal Green's function in equation (8.19) for  $x = 1$  (left) and  $x = 0.5$  (right). The dashed line gives the result for  $D_s$ , when evaluated with the quasiparticle Green's functions as in (8.20).

We can see that the results for  $D_s$  agree generally well, which shows that the approximation (8.20) is already quite good. In both cases for the filling the superfluid stiffness is maximal in the BCS limit and decreases to small values in the BEC limit.  $D_s$  is proportional to the inverse of the effective mass of the pairs  $m_B \sim U$ , and therefore expected to decrease like  $1/U$ . The system in this limit consists of heavy, weakly interacting bosons, with little phase coherence. The results shown are in agreement with the ones reported by

Toschi et al. (2005). At the time of writing it has not been possible to investigate the BCS limit,  $U \rightarrow 0$ , in more detail with the DMFT-NRG calculation in detail due to numerical problems when evaluating the integrals in (8.19). It can, however, be studied in BCS mean field theory based on (8.18) for the gap. One finds in the limit  $U \rightarrow 0$ , which implies that  $\Delta_{\text{sc}} \rightarrow 0$ , that the superfluid stiffness  $D_s$  goes to a constant value. The superfluid stiffness is therefore maximal in the BCS limit, when calculated with the approximations here.

We now turn to the spectral functions  $\rho_{\mathbf{k}}(\omega) = -\text{Im}G_{\mathbf{k}}(\omega)/\pi$ . In the BCS limit we expect that they can be described well by the free quasiparticle spectra  $z\tilde{\rho}_{\mathbf{k}}^0 = z[-\text{Im}\tilde{G}_{\mathbf{k}}^0(\omega)]/\pi$  (8.16). In figure 8.3 we plot the  $\mathbf{k}$ -resolved spectra in the two limiting cases for  $U = 1$  (BCS limit, left) and  $U = 6$  (BEC-limit, right) for quarter filling,  $x = 0.5$ .

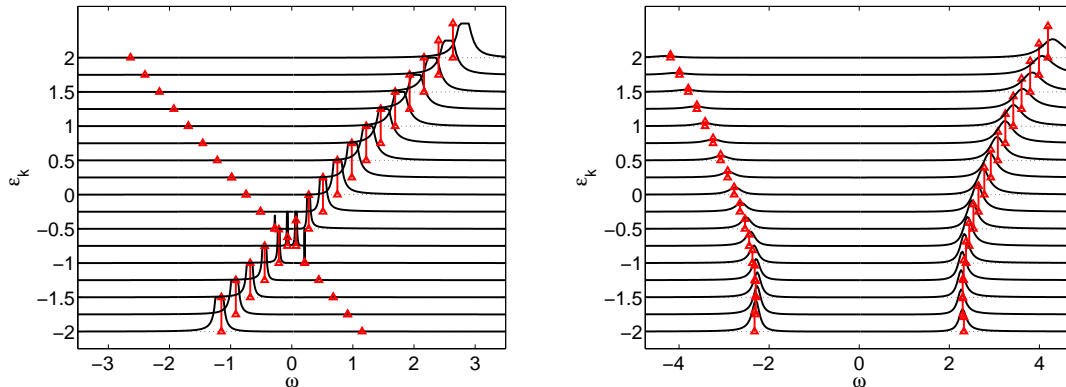


Figure 8.3: The  $\mathbf{k}$ -resolved spectral functions  $\rho_{\mathbf{k}}(\omega)$  for quarter filling in the BCS-limit,  $U = 1$  (left), and towards the BEC limit,  $U = 6$  (right). The arrows show the delta-function peaks of  $z\tilde{\rho}_{\mathbf{k}}^0(\omega)$ , where the height of the arrow indicates the weight of the peak.

We plots show a small spectral gap for  $U = 1$  and a large gap ( $E_g = 2\Delta_{\text{sc}}$ ) of the order of  $U$  for the strong coupling case. We can see a series of broadened quasiparticle peaks which are most narrow in the region  $\varepsilon_{\mathbf{k}} = \mu_0$ , where  $\mu_0 = \mu - \Sigma(0)$  (numerically  $\mu_0 \simeq -0.79$  for  $U = 1$  and  $\mu_0 \simeq -1.61$  for  $U = 6$ ). As can be seen  $\varepsilon_{\mathbf{k}} = \mu_0$  is also the point where the spectral gap is minimal. We have also added arrows corresponding to  $z\tilde{\rho}_{\mathbf{k}}^0(\omega)$ , which indicate the position of the quasiparticle peaks  $\pm E_{\mathbf{k}}^0$  and the height gives the spectral weight. We can see that they track very well the position of the real quasiparticle excitation  $E_{\mathbf{k}}$  in both cases. The width of the peaks comes from the imaginary part of the self-energies which lead to a finite life-time of these quasiparticles. These spectra can be compared with the ones presented by Garg et al. (2005). There the quasiparticle excitation delta peaks are disconnected from the continuum, which is however an artefact of the approximation for the self-energy there, whose imaginary part vanishes over too large a region in  $\omega$ . As mentioned, in the BEC limit (right) the effective mass  $m_B$  of a boson pair  $m_B \sim U$ . This can be seen reflected in the small effective band width for the case  $U = 6$ . In this case it is not related to the quasiparticle weight  $z$ , which assumes values close to one. The weight of the peaks in the full spectrum  $\rho_{\mathbf{k}}(\omega)$  is in accordance with the height of the arrows for

$z\tilde{\rho}_{\mathbf{k}}^0(\omega)$ . We can see that in the BCS limit (left) the weight in the lower band decreases rapidly to zero near  $\varepsilon_{\mathbf{k}} = \mu_0$ , whereas in the BEC limit (right) it spreads over a much larger region. This can be seen more clearly in figure 8.4, where we plot the momentum distribution  $n_{\mathbf{k}} = v_{\mathbf{k}}^2$  calculated from (8.17) for  $x = 1$  (left) and  $x = 0.5$  (right).

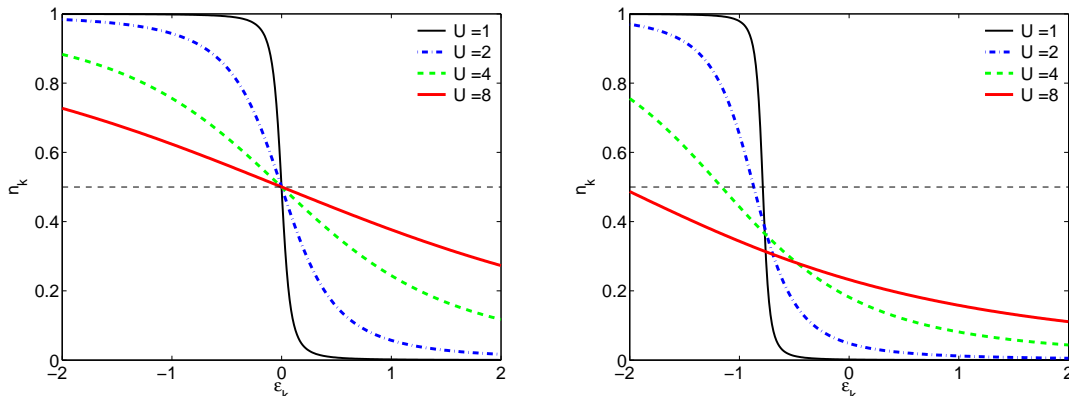


Figure 8.4: The momentum distribution  $n_{\mathbf{k}} = v_{\mathbf{k}}^2$  calculated from (8.17) for  $x = 1$  (left) and  $x = 0.5$  (right).

In both cases ( $x = 0.5, 1$ ) for small attraction ( $U = 1$ ) we can see that  $n_{\mathbf{k}}$  shows the typical form known from BCS theory dropping from one to zero in a small range around  $\varepsilon_{\mathbf{k}} = \mu_0$ . Therefore, some momentum states above  $\mu_0$  are occupied, but only in a small region of the order of the gap. When  $U$  is increased, the momentum distribution is spread over a larger range. In the BEC limit, where the fermions are tightly bound and therefore very localised in position space, we expect the momentum distribution to be spread due to the uncertainty principle. In all cases the sum rule  $1/N \sum_{\mathbf{k}} n_{\mathbf{k}} = x/2$  is satisfied numerically within an accuracy of about 1%.

To summarise, we have discussed the behaviour of attractive fermions in the Hubbard model from weak to strong coupling at  $T = 0$  with the DMFT-NRG approach. We found a smooth crossover of the relevant response quantities, expectation values and the spectral functions. The description in terms of non-interacting renormalised quasiparticles could on the whole represent the results of the full DMFT-NRG calculation well.

*Cuando estes triste, ponte a cantar,  
cuando estes alegre, ponte a llorar.  
Cuando estes vacio, de verdad va-  
cicio, ponte a mirar.*

Jaime Sabines

# Conclusions

A number of different topics in condensed matter theory have been addressed in this thesis, ranging from Kondo physics in quantum dot systems with normal and superconducting leads over magnetic order in lattice models to superfluidity for attractive fermions. Before putting the scientific contributions into perspective let us recapitulate on what has been presented.

After the description of the relevant models (AIM and Hubbard model) and methods (NRG, RPT and DMFT) in the first part, we have studied the AIM subject to certain types of symmetry breaking. We saw that the low energy quasiparticle excitations and the response of the AIM to a magnetic field could be characterised well in terms of field dependent renormalised parameters. In an RPT expansion based on these parameters dynamic correlation functions could be deduced, and they were in good agreement with NRG results for a significant range of frequencies. This approach was shown to be generalisable to the non-equilibrium situation where the RPT is carried out in the Keldysh-formalism. It could be used there to calculate the non-equilibrium differential conductance in quantum dot systems in a magnetic field. Thus, we have presented a reliable description of the AIM in magnetic field in equilibrium with NRG and RPT, and a promising possibility for the non-equilibrium situation in the RPT framework. For the one-particle quantities in both the equilibrium and non-equilibrium case, however, a more thorough analysis of the RPT approach is necessary to understand, what the most important processes are up to a certain scale, in frequency  $\omega$ , magnetic field  $h$ , and voltage  $eV$ . Also the treatment of the counter-terms for the renormalised self-energy, when summing diagrams to infinite order, has not been completely satisfactory from a formal perspective.

For the AIM with superconducting symmetry breaking in the bath we gave a thorough description of static and dynamic properties deduced from NRG calculations. This included the ground state transition from a singlet to a doublet state with varying interaction or level position. We presented detailed results for the position and weight of the localised excited state in the gap, the Andreev bound state. These quantities could also be calculated from a renormalised parameter analysis based on a low energy expansion of the self-energy. As the system is not a Fermi liquid we could not readily extend the method of extracting these renormalised parameters from the NRG low energy excitations. This might, however, be possible when a more general form of the excitation is considered and can be subject of

further research.

For the lattice model in a homogeneous magnetic field in the third part of the thesis, we showed that the methods applied to the local model could be extended. We were able to deduce renormalised parameters for the quasiparticle description and to calculate the dynamic susceptibilities in an RPT expansion. We also presented a thorough analysis of different types of qualitative behaviour of the strongly correlated electron system in a magnetic field. This includes the phenomenon of metamagnetism, which occurs at half filling and intermediate coupling strength. Away from half filling no metamagnetic behaviour was observed, but renormalisation effects near half filling are strong and the spin dependent effective masses of the quasiparticles differ markedly.

The last two chapters dealt with spontaneous symmetry breaking. We analysed in great detail the properties of the quasiparticle excitations in a metallic antiferromagnetic state. Renormalised parameters could be deduced as before, but the symmetry breaking nature leads to expressions for the spectral quasiparticle weight and the effective mass enhancement different from the ones in the normal state, where they are just given by the inverse of one another. Therefore, the quasiparticles in the doped antiferromagnetic system can have a rather large spectral weight and at the same time a large effective mass. This can be understood physically from the hole motion in an antiferromagnetically ordered state. For the corresponding attractive system we studied the broken symmetry state with superconducting order. We showed that the crossover of static quantities and spectral functions from the BCS superconducting regime at weak coupling to the BEC regime of tightly bound fermions at strong coupling occurs smoothly. We also saw at half and at quarter filling for any attraction that the static and dynamic properties of the system can be described in a good approximation by non-interacting, renormalised quasiparticle excitations. This is not surprising in the BCS limit, but it is remarkable in the BEC limit, where there is a large spectral gap.

With these diverse situations in mind we can return to the unifying question of the thesis posed in the introduction: what are the properties of quasiparticle excitations subject to certain symmetry breakings, and how can they be analysed. Clearly, the properties of the quasiparticle excitations in local and lattice models of strongly correlated fermions differ with the kind of symmetry breaking occurring. For instance, the local system remains a Fermi liquid for any magnetic field applied, whereas the ground state of the lattice model can be insulating. We have shown, however, that a description in terms of renormalised parameters, which can be obtained from the one-particle self-energy, and in some cases also directly from the low lying excitations, is possible in all cases dealt with here. This is very important as it allows us to formulate a simplified description in terms of non-interacting renormalised quasiparticles, which is valid as a first approximation. It is remarkable that this is not limited to the cases, where the system is strictly a Fermi liquid, but also works for cases with symmetry breaking. This suggests that the RPT approach is extendable to a larger class of systems, and it has already been proven to be useful for the lattice

---

models in chapters 6 and 7. This gives an exciting prospect, but we have to bear in mind that the work carried out for the lattice models is exact only in the infinite dimensional limit. Therefore, the work presented is only a piece in a much larger puzzle, which provides certain links and insights but requires future work in many directions. We will mention but a few in the following.

The NRG calculations for the AIM in magnetic field give a rather complete picture. More work is needed to understand the details of the RPT approach both in equilibrium and non-equilibrium. This includes finding good perturbative approximations as well as a satisfactory treatment of the counter-terms. A self-consistent approach with dressed quasiparticle propagators, as sketched in the appendix C.3, gives a promising route to follow. The AIM in a superconducting bath at and away from half filling is well understood from calculations with the NRG methods by this and other groups' work. A better understanding of the low energy excitations in terms of renormalised quasiparticles would be of interest. Moreover, an extension of the analysis to the situation with two leads with different complex gap parameters, Josephson currents and non-equilibrium transport, would be of considerable interest for theory and experiment.

As for the lattice models, many future avenues of research can be envisaged leading on from the work presented, and we can only hint towards a few. For instance, the effect of phonons in doped antiferromagnetically ordered state is of considerable interest in the condensed matter community as it can be relevant for the understanding of the behaviour of materials of strongly correlated electrons, for instance the cuprate superconductors. Also ordered states in more complicated models than the Hubbard model, e.g. with coupling to a localised magnetic moment, would be of great interest. The attractive model with superconducting order also deserves more attention. A DMFT-NRG treatment taking into account the full self-consistency equations needs to be carried out. Apart from the model with on-site attraction, strongly correlated models with a competition of on-site repulsion and a coupling to local phonon mode, like the Hubbard-Holstein model, with superconducting ordering could then also be addressed. This would be of considerable interest for the phenomenon of superconductivity in fullerenes. These suggestions do not comprise an exhaustive list, and many other studies could be proposed.

The final conclusion at this stage is the hope that in the same way as this work has built on and benefitted from many earlier studies, its insights may serve as a fruitful basis for future research on strong correlation effects in condensed matter physics. After all, as George Bernard Shaw puts it, it is in the nature of science that it *never solves a problem without creating ten more*.



# Appendix



# Appendix A

## Spectral functions in the full density matrix (FDM) approach

In this section of the appendix we give details for the full density matrix approach to calculate spectral functions in the NRG based on the Anders Schiller basis. We derive explicit expressions for the reduced density matrix and for dynamic response functions.

### A.1 General expressions

Before deriving the general expressions for a correlation function, let us first we establish a few general relations. The starting point for the following considerations is the complete Anders Schiller (AS) basis for the NRG chain (2.20),

$$\{|l, \mathbf{e}; m\rangle\}_{m=m_0, \dots, N}. \quad (\text{A.1})$$

The unit operator can be then expressed as follows

$$\mathbb{1} = \sum_{m=m_0}^N \sum_{l, \mathbf{e}} |l, \mathbf{e}; m\rangle \langle l, \mathbf{e}; m|. \quad (\text{A.2})$$

Also the following relation for discarded ( $l$ ) and kept part ( $k$ ) can be found (Peters et al. 2006),

$$\sum_{m=m_1+1}^N \sum_{l, \mathbf{e}} |l, \mathbf{e}; m\rangle \langle l, \mathbf{e}; m| = \sum_{k, \mathbf{e}} |k, \mathbf{e}; m_1\rangle \langle k, \mathbf{e}; m_1|. \quad (\text{A.3})$$

Our aim is now to express the one-particle Green's function in terms of the AS basis employing the concept of the reduced density matrix. First we consider generally for operators  $A, B$ ,

$$\text{tr}(\rho A(t)B) = \text{tr}(\rho e^{iHt} A e^{-iHt} B). \quad (\text{A.4})$$

This is evaluated as

$$\begin{aligned} \text{tr}(\rho e^{iHt} A e^{-iHt} B) &= \sum_{l, \mathbf{e}, m} \langle l, \mathbf{e}; m | e^{iHt} A e^{-iHt} B \rho | l, \mathbf{e}; m \rangle \\ &= \sum_{l_1, \mathbf{e}_1, m_1} \sum_{l_2, \mathbf{e}_2, m_2} \langle l_1, \mathbf{e}_1; m_1 | e^{iHt} A e^{-iHt} | l_2, \mathbf{e}_2; m_2 \rangle \langle l_2, \mathbf{e}_2; m_2 | B \rho | l_1, \mathbf{e}_1; m_1 \rangle \end{aligned}$$

Now we divide the sum over  $m_2$  into three parts:  $m_2 > m_1$ ,  $m_2 = m_1$  and  $m_2 < m_1$ . Equation (A.3) can be used to write the part  $m_2 > m_1$  as

$$\text{tr}(\rho e^{iHt} A e^{-iHt} B)_{m_2 > m_1} = \sum_m \sum_{l, \mathbf{e}_1, k, \mathbf{e}_2} \langle l, \mathbf{e}_1; m | e^{iHt} A e^{-iHt} | k, \mathbf{e}_2; m \rangle \langle k, \mathbf{e}_2; m | B \rho | l, \mathbf{e}_1; m \rangle. \quad (\text{A.5})$$

For  $m_2 < m_1$  we rearrange the summation according to

$$\sum_{m_1=m_0+1}^N \sum_{m_2=m_0}^{m_1-1} f(m_1, m_2) = \sum_{m_2=m_0}^{N-1} \sum_{m_1=m_2+1}^N f(m_1, m_2). \quad (\text{A.6})$$

Using (A.3) we find then a similar term as in equation (A.5), but kept and discarded states are interchanged,

$$\text{tr}(\rho e^{iHt} A e^{-iHt} B)_{m_2 < m_1} = \sum_m \sum_{l, \mathbf{e}_1, k, \mathbf{e}_2} \langle l, \mathbf{e}_2; m | B \rho | k, \mathbf{e}_1; m \rangle \langle k, \mathbf{e}_1; m | e^{iHt} A e^{-iHt} | l, \mathbf{e}_2; m \rangle. \quad (\text{A.7})$$

If we collect all these terms we obtain the following expression trace

$$\begin{aligned} \text{tr}(\rho e^{iHt} A e^{-iHt} B) &= \sum_m \sum_{l_1, \mathbf{e}_1, l_2, \mathbf{e}_2} \langle l_1, \mathbf{e}_1; m | e^{iHt} A e^{-iHt} | l_2, \mathbf{e}_2; m \rangle \langle l_2, \mathbf{e}_2; m | B \rho | l_1, \mathbf{e}_1; m \rangle \\ &+ \sum_m \sum_{l, \mathbf{e}_1, k, \mathbf{e}_2} \langle l, \mathbf{e}_2; m | B \rho | k, \mathbf{e}_1; m \rangle \langle k, \mathbf{e}_1; m | e^{iHt} A e^{-iHt} | l, \mathbf{e}_2; m \rangle \\ &+ \sum_m \sum_{l, \mathbf{e}_1, k, \mathbf{e}_2} \langle l, \mathbf{e}_1; m | e^{iHt} A e^{-iHt} | k, \mathbf{e}_2; m \rangle \langle k, \mathbf{e}_2; m | B \rho | l, \mathbf{e}_1; m \rangle. \end{aligned} \quad (\text{A.8})$$

By definition of the AS basis  $|k, e; m\rangle$  and  $|l, e; m\rangle$  are exact eigenstates of the Hamiltonian at stage  $m$ ,  $H_m | \alpha, e; m \rangle = E_m^\alpha | \alpha, e; m \rangle$ . The approximation which is made in order to evaluate the expressions is that they are also eigenstates to the Hamiltonian of the full chain  $H = H_N$ , which amounts to saying that the effects from further environment sites, which due to the NRG setup couple with decreasing energies are only a small perturbation,

$$H | \alpha, e; m \rangle \approx E_m^\alpha | \alpha, e; m \rangle. \quad (\text{A.9})$$

This can be used in the expressions (A.8) above. We also assume that for zero temperature due to energy scale separation the density matrix can be given directly in the diagonal basis at the last iteration

$$\rho = \sum_l \frac{e^{-\beta_N E_N^l}}{Z} |l, N\rangle \langle l, N|. \quad (\text{A.10})$$

Here we can take  $\beta_N \sim \Lambda^{N/2}$  and  $Z = \sum_l e^{-\beta_N E_N^l}$ . As a consequence,  $\rho|l, \mathbf{e}; m\rangle = 0$  for  $m < N$ , since the states are orthogonal. Therefore, only the term in the second line in equation (A.8) contributes. Terms with kept states at step  $N_{\max}$  vanish, since by definition of the AS basis there are none. Taking into account the commutator term in the definition of the retarded Green's function [ $G_{AB}(t) = -i\theta(t)\text{tr}(\rho[A(t), B]_\varepsilon)$  ( $\varepsilon = -1$  bosonic,  $\varepsilon = 1$  fermionic)] and collecting the above the results the general Green's function  $G_{AB}(\omega) = \int dt e^{i\omega t} G_{AB}(t)$ ,

$$G_{AB}(\omega) = \sum_m \sum_{l_1, l_2, l_3} \frac{B_{l_2 l_3}(m) \rho_{l_3 l_1}^{\text{red}}(m) A_{l_1 l_2}(m) + \varepsilon A_{l_1 l_2}(m) \rho_{l_2 l_3}^{\text{red}}(m) B_{l_3 l_1}(m)}{\omega - (E_m^{l_2} - E_m^{l_1})} + \sum_m \sum_{l, k_1, k_2} \frac{B_{l k_1}(m) \rho_{k_1 k_2}^{\text{red}}(m) A_{k_2 l}(m)}{\omega - (E_m^l - E_m^{k_2})} + \frac{\varepsilon A_{l k_1}(m) \rho_{k_1 k_2}^{\text{red}}(m) B_{k_2 l}(m)}{\omega - (E_m^{k_1} - E_m^l)} \quad (\text{A.11})$$

The  $m$ -summation runs from  $m_0$ , where the truncation starts to  $N_{\max}$ . We have used

$$\langle l_1, \mathbf{e}_1; m | A | l_2, \mathbf{e}_2; m \rangle = \delta_{\mathbf{e}_1, \mathbf{e}_2} A_{l_1 l_2}(m), \quad (\text{A.12})$$

and the definition of the reduced density matrix

$$\rho_{k_1 k_2}^{\text{red}}(m) = \sum_{\mathbf{e}} \langle k_1, \mathbf{e}; m | \rho | k_2, \mathbf{e}; m \rangle. \quad (\text{A.13})$$

Since  $\rho|l, \mathbf{e}; m\rangle = 0$  for  $m < N$  the term in the first line only contributes for the last step  $N$  and then, since  $\rho$  is diagonal there, takes the form

$$G_{AB}^{(1)}(\omega) = \frac{1}{Z} \sum_{l_1, l_2} \frac{A_{l_1 l_2}(N) B_{l_2 l_1}(N) (e^{-\beta E_N^{l_1}} + \varepsilon e^{-\beta E_N^{l_2}})}{\omega - (E_N^{l_2} - E_N^{l_1})}. \quad (\text{A.14})$$

## A.2 Details for Quantum numbers $Q, S_z$

In the following sections we give the explicit expressions for the matrix elements appearing in the calculations, when  $Q$  and  $S_z$  are good quantum numbers. We describe how to calculate the reduced density matrix, the one-particle Green's function and other correlation functions. When different quantum numbers, e.g.  $Q$  and  $S$ , are used, the expressions are different due to the reduced matrix elements and Clebsch Gordon coefficients, which are usually used (Bauer 2007).

### A.2.1 Reduced density matrix

In this section we will give the expressions for the density matrix in terms of matrix elements and transformation matrices for the case where  $Q, S_z$  are good quantum numbers. Let the density matrix of the step  $N$ , which is not necessarily the last iteration, be given by

$$\rho_N = \sum_{Q, S_z, r_N, r'_N} |Q, S_z, r_N\rangle_N W_N(Q, S_z; r_N, r'_N) {}_N\langle Q, S_z, r'_N|. \quad (\text{A.15})$$

We start at  $N = N_{\max}$  with a diagonal  $\rho$  such that

$$W_N(Q, S_z; r_N, r'_N) = \delta_{r_N, r'_N} \frac{e^{-\lambda_N E_N(Q, S_z, r_N)}}{Z_N}, \quad (\text{A.16})$$

$Z_N = \text{tr}(e^{-\lambda_N H})$  and  $\lambda_N = \beta\lambda^{-\frac{N-1}{2}}$ .

The usual basis transformation in the NRG is given by (Bauer 2007)

$$|Q, S_z, r_N\rangle_N = \sum U_{QS_z}(r_N; r_{N-1}, i) |Q, S_z, r_{N-1}, i\rangle_N, \quad (\text{A.17})$$

where  $i = 1, \dots, 4$  and  $r_N = 1, \dots, 4r_{N-1}$ . Define the Fock basis for site  $N$  on the linear chain as  $|J_N\rangle$  ( $J_N = 1, \dots, 4$ ) with

$$|1_N\rangle := |0_N\rangle, \quad |2_N\rangle := f_{N,\uparrow}^\dagger |0_N\rangle, \quad |3_N\rangle := f_{N,\downarrow}^\dagger |0_N\rangle, \quad |4_N\rangle := f_{N,\uparrow}^\dagger f_{N,\downarrow}^\dagger |0_N\rangle. \quad (\text{A.18})$$

The basis for step  $N$  and  $N-1$  are related by

$$|Q, S_z, r_{N-1}, 1\rangle_N := |Q+1, S_z, r_{N-1}\rangle_{N-1} \otimes |1_N\rangle, \quad (\text{A.19})$$

$$|Q, S_z, r_{N-1}, 2\rangle_N := |Q, S_z - \frac{1}{2}, r_{N-1}\rangle_{N-1} \otimes |2_N\rangle, \quad (\text{A.20})$$

$$|Q, S_z, r_{N-1}, 3\rangle_N := |Q, S_z + \frac{1}{2}, r_{N-1}\rangle_{N-1} \otimes |3_N\rangle, \quad (\text{A.21})$$

$$|Q, S_z, r_{N-1}, 4\rangle_N := |Q-1, S_z, r_{N-1}\rangle_{N-1} \otimes |4_N\rangle. \quad (\text{A.22})$$

The first step is to substitute (A.17) into (A.15),

$$\rho_N = \sum W_N(Q, S_z; r_N, r'_N) U_{QS_z}(r_N; r_{N-1}, i) U_{QS_z}(r'_N; r'_{N-1}, j) \times \quad (\text{A.23}) \\ \times |Q, S_z, r_{N-1}, i\rangle_N \langle Q, S_z, r'_{N-1}, j|.$$

The reduced density matrix for step  $N-1$  is then found by the partial trace

$$\rho_{N-1} = \sum_{J_N=1}^4 \langle J_N | \rho_N | J_N \rangle. \quad (\text{A.24})$$

This is evaluated by substituting (A.23) into (A.24) and making use of (A.19)-(A.22).

This yields

$$\rho_{N-1} = \sum |Q, S_z, r_{N-1}\rangle_{N-1} W_{N-1}(Q, S_z; r_{N-1}, r'_{N-1}) {}_{N-1}\langle Q, S_z, r'_{N-1} | \quad (\text{A.25})$$

with

$$W_{N-1}(Q, S_z; r_{N-1}, r'_{N-1}) = \quad (\text{A.26}) \\ \sum_{r_N, r'_N} \left( U_{Q-1, S_z}(r_N; r_{N-1}, 1) W_N(Q-1, S_z; r_N, r'_N) U_{Q-1, S_z}(r'_N; r'_{N-1}, 1) \right. \\ + U_{Q, S_z + \frac{1}{2}}(r_N; r_{N-1}, 2) W_N(Q, S_z + \frac{1}{2}; r_N, r'_N) U_{Q, S_z + \frac{1}{2}}(r'_N; r'_{N-1}, 2) \\ + U_{Q, S_z - \frac{1}{2}}(r_N; r_{N-1}, 3) W_N(Q, S_z - \frac{1}{2}; r_N, r'_N) U_{Q, S_z - \frac{1}{2}}(r'_N; r'_{N-1}, 3) \\ \left. + U_{Q+1, S_z}(r_N; r_{N-1}, 4) W_N(Q+1, S_z; r_N, r'_N) U_{Q+1, S_z}(r'_N; r'_{N-1}, 4) \right).$$

### A.2.2 Expressions for the dynamic correlations functions

We give the relevant explicit expressions for the one-particle Green's function. The starting point is the Green's function in the general form (A.11) and we use  $A = c_{d,\sigma} = B^\dagger$ . Let us deal with the term in the first line in (A.11), where we directly take the representation (A.14). We use  $|l_1\rangle \rightarrow |Q-1, S_z - \sigma/2, l_1\rangle$  and  $|l_2\rangle \rightarrow |Q, S_z, l_2\rangle$  and find

$$G_{d,\sigma}^{(1)}(\omega) = \frac{1}{Z} \sum_{l_1, l_2} \frac{|\langle Q, S_z, l_2 | c_{d,\sigma}^\dagger | Q-1, S_z - \sigma/2, l_1 \rangle|^2 (e^{-\beta E(Q-1, S_z - \sigma/2, l_1)} + e^{-\beta E(Q, S_z, l_2)})}{\omega - [E(Q, S_z, l_2) - E(Q-1, S_z - \sigma/2, l_1)]}. \quad (\text{A.27})$$

Then we focus on the terms in the second line in (A.11) and look at the expression at a specific iteration  $m < N$  and

$$G_{d,\sigma}^{(2),m}(\omega) = \sum_{l, k_1, k_2} \frac{[c_{d,\sigma}^\dagger]_{lk_1}(m) \rho_{k_1 k_2}^{\text{red}}(m) [c_{d,\sigma}]_{k_2 l}(m)}{\omega - (E_m^l - E_m^{k_2})} + \frac{[c_{d,\sigma}]_{lk_1}(m) \rho_{k_1 k_2}^{\text{red}}(m) [c_{d,\sigma}^\dagger]_{k_2 l}(m)}{\omega - (E_m^{k_1} - E_m^l)}. \quad (\text{A.28})$$

Let us consider the first term, which describes positive excitations between discarded (higher) energies and kept (lower) energies. We omit the  $m$  index for the iteration and write for the discarded states  $|l\rangle \rightarrow |Q, S_z, l\rangle$ . The kept state  $|k_1\rangle$  is written as  $|Q-1, S_z - \sigma/2, k_1\rangle$ , whilst  $|k_2\rangle$  becomes  $|Q-1, S_z - \sigma/2, k_2\rangle$ . Therefore, the coefficient can be written as

$$\langle Q, S_z, l | c_{d,\sigma}^\dagger | Q-1, S_z - \sigma/2, k_1 \rangle W(Q-1, S_z - \sigma/2; k_1, k_2) \langle Q-1, S_z - \sigma/2, k_2 | c_{d,\sigma} | Q, S_z, l \rangle = \\ \langle Q, S_z, l | c_{d,\sigma}^\dagger | Q-1, S_z - \sigma/2, k_1 \rangle W(Q-1, S_z - \sigma/2; k_1, k_2) \langle Q, S_z, l | c_{d,\sigma}^\dagger | Q-1, S_z - \sigma/2, k_2 \rangle^*$$

where this term is summed over  $k_1$  from 1 to  $\text{rg}(Q-1, S_z - \sigma/2)$ , the corresponding range. We denote this expression including the summation by  $\alpha_\sigma(Q, S_z; l, k_2)$ . The whole term can then be written as

$$\sum_{Q, S_z, k_2} \sum_{l=\text{rg}(Q, S_z)+1}^{\text{rg\_bt}(Q, S_z)} \frac{\alpha_\sigma(Q, S_z; l, k_2)}{\omega - [E(Q, S_z, l) - E(Q-1, S_z - \sigma/2, k_2)]}, \quad (\text{A.29})$$

where the range before the truncation  $\text{rg\_bt}(Q, S_z)$  was used as summation limit. The second term in equation (A.28), which accounts for negative energy excitations, similarly has the form

$$\sum_{Q, S_z, k_1} \sum_{l=\text{rg}(Q, S_z)+1}^{\text{rg\_bt}(Q, S_z)} \frac{\alpha_\sigma(Q+1, S_z + \sigma/2; l, k_1)}{\omega - [E(Q+1, S_z + \sigma/2, k_1) - E(Q, S_z, l)]}, \quad (\text{A.30})$$

with  $\alpha_\sigma(Q+1, S_z + \sigma/2; l, k_1)$  given by

$$\langle Q, S_z, l | c_{d,\sigma} | Q+1, S_z + \sigma/2, k_1 \rangle W(Q+1, S_z + \sigma/2; k_1, k_2) \langle Q+1, S_z + \sigma/2, k_2 | c_{d,\sigma}^\dagger | Q, S_z, l \rangle = \\ \langle Q+1, S_z + \sigma/2, k_1 | c_{d,\sigma}^\dagger | Q, S_z, l \rangle^* W(Q+1, S_z + \sigma/2; k_1, k_2) \langle Q+1, S_z + \sigma/2, k_2 | c_{d,\sigma}^\dagger | Q, S_z, l \rangle$$

The higher  $F$ -Green's function, defined by

$$F_\sigma(t) = -i\theta(t)\langle\{[c_{d,\sigma}c_{d,-\sigma}^\dagger](t), c_{,\sigma}^\dagger\}\rangle, \quad (\text{A.31})$$

can be obtained starting from expression (A.11) in a similar way using  $A(t) = [c_{d,\sigma}n_{-\sigma}](t)$  and  $B = c_{,\sigma}^\dagger$  (Bauer 2007). In analogous way, the longitudinal spin correlation function, given by

$$\chi_l(t) = -i\theta(t)\langle[S_z(t), S_z]\rangle, \quad (\text{A.32})$$

is found. We can set  $A = B = S_z$  and use the Green's function in the form (A.11) with  $\varepsilon = -1$ . Similarly, with  $A = B^* = S^+$  the transverse spin correlation function can be calculated. For details we refer the reader to (Bauer 2007).

## Appendix B

# Renormalised parameters from NRG calculations

In this section we describe how renormalised parameters can be deduced from the excitations in the NRG calculations. We want to discuss the general case, which is valid for the impurity models in part 2 (chapters 3 and 4) as well as the lattice models in chapters 6 and 7. We start by considering a more general form of the linear chain Hamiltonian (2.1), including the impurity but without the interaction term. It is denoted by  $H_{-1,N}^0$ ,

$$H_{-1,N}^0 = \Lambda^{(N-1)/2} \sum_{\sigma,n=-1}^N \varepsilon_{n,\sigma} c_{n,\sigma}^\dagger c_{n,\sigma} + \Lambda^{(N-1)/2} \sum_{\sigma,n=-1}^N \beta_{n,\sigma} (c_{n,\sigma}^\dagger c_{n+1,\sigma} + \text{h.c.}). \quad (\text{B.1})$$

Here  $\beta_{n,\sigma}$  are the spin dependent hopping elements and on-site energies  $\varepsilon_{n,\sigma}$  of the linear chain. We defined  $\beta_{-1,\sigma} \equiv V_\sigma$  and  $\varepsilon_{-1,\sigma} = \varepsilon_{d,\sigma}$ . For the DMFT situation with magnetic symmetry breaking the medium can become polarised, which implies that the complex hybridisation function  $K_\sigma(\omega)$  is spin-dependent. Therefore we need to include a spin-dependent hopping amplitudes  $\beta_{n,\sigma}$  as well as on-site energies  $\varepsilon_{n,\sigma}$ . They can be obtained from  $\Delta_\sigma(\omega) = \text{Im}K_\sigma(\omega)$  in a procedure described in Bulla et al. (1997).

First we would like to derive the Green's function for this linear chain model. For a certain iteration  $N$  denote the linear chain model from site  $i$  to  $N$  by  $H_{i,N}^0$ ,  $i = 0, 1, \dots, N$ . The Green's function at the impurity site can be written in matrix notation  $\langle -1 | (\omega - H_{-1,N}^0)^{-1} | -1 \rangle$  and related to other matrix elements depending on  $H_{i,N}^0$  by a recursive procedure ( $|i\rangle = f_i^\dagger |\text{vac}\rangle$ ). In order to find this explicitly one needs to consider the inversion of the corresponding band matrices. Taking all factors into account one obtains the non-interacting Green's function for the linear chain model

$$G_{-1-1}^\sigma(\omega) = \frac{1}{\omega - \varepsilon_{d,\sigma} \Lambda^{(N-1)/2} - V_\sigma^2 \Lambda^{N-1} g_{00,\sigma}(\omega)} \quad (\text{B.2})$$

where  $g_{ii,\sigma}(\varepsilon)$  is the Green's function for site  $i$  and expressed as

$$g_{ii,\sigma}(\varepsilon) = \frac{1}{\varepsilon - \varepsilon_{i,\sigma} \Lambda^{(N-1)/2} - \beta_{i,\sigma}^2 \Lambda^{(N-1)} g_{i+1i+1,\sigma}(\varepsilon)}. \quad (\text{B.3})$$

Note that the Green's functions correspond to matrix elements  $g_{ii,\sigma}(\omega) = \langle i | (\omega - H_{i,N}^0)^{-1} | i \rangle$ .

As usual one-particle excitations  $E_\sigma$  are given by the poles of the Green's function and hence by the equations ( $\sigma = \pm 1$ )

$$E_\sigma - \varepsilon_{d,\sigma} \Lambda^{(N-1)/2} - V_\sigma^2 \Lambda^{N-1} g_{00,\sigma}(E_\sigma) = 0. \quad (\text{B.4})$$

For a certain iteration  $N$  denote the single particle excitation from the ground state for the non-interacting system by  $E_{p,\sigma}^0(N)$  and the hole excitations by  $E_{h,\sigma}^0(N)$ . For the hole excitation we have to include a negative sign for the energy and also the opposite spin corresponds to the value for the excitation, such that equation (B.4) gives in a slight rearrangement

$$\frac{E_{p,\sigma}^0(N) \Lambda^{-(N-1)/2}}{V_\sigma^2} - \frac{\varepsilon_{d,\sigma}}{V_\sigma^2} = \Lambda^{(N-1)/2} g_{00,\sigma}(E_{p,\sigma}^0(N)) \quad (\text{B.5})$$

and

$$\frac{-E_{h,\sigma}^0(N) \Lambda^{-(N-1)/2}}{V_{-\sigma}^2} - \frac{\varepsilon_{d,-\sigma}}{V_{-\sigma}^2} = \Lambda^{(N-1)/2} g_{00,-\sigma}(-E_{h,\sigma}^0(N)). \quad (\text{B.6})$$

We see therefore that the up/down spin hole excitations  $E_{h,\uparrow}^0(N)/E_{h,\downarrow}^0(N)$  are related to the parameters  $\varepsilon_{d,\downarrow}/\varepsilon_{d,\uparrow}$ , respectively.

This analysis of the non-interacting problem can be extended by switching on the interaction  $U$ . The aim is to determine the renormalised parameters  $\tilde{\varepsilon}_{d,\sigma}$  and  $\tilde{V}_\sigma^2$  for the quasiparticle excitations (Hewson et al. 2004). As above, for a certain iteration  $N$ , but now for the interacting system denote the single particle excitation from the ground state by  $E_{p,\sigma}(N)$  and  $E_{h,\sigma}(N)$  in analogy as hole excitation. The  $N$ -dependent free quasiparticle parameters  $\tilde{\varepsilon}_{d,\sigma}(N)$  and  $\tilde{V}_\sigma^2(N)$  are then in analogy to (B.5) and (B.6) given by

$$\frac{E_{p,\sigma}(N) \Lambda^{-(N-1)/2}}{\tilde{V}_\sigma^2(N)} - \frac{\tilde{\varepsilon}_{d,\sigma}(N)}{\tilde{V}_\sigma^2(N)} = \Lambda^{(N-1)/2} g_{00,\sigma}(E_{p,\sigma}(N)) \quad (\text{B.7})$$

and

$$\frac{-E_{h,\sigma}(N) \Lambda^{-(N-1)/2}}{\tilde{V}_{-\sigma}^2(N)} - \frac{\tilde{\varepsilon}_{d,-\sigma}(N)}{2\tilde{V}_{-\sigma}^2(N)} = \Lambda^{(N-1)/2} g_{00,-\sigma}(-E_{h,\sigma}(N)). \quad (\text{B.8})$$

Note that  $E_{p,\sigma}(N)$  and  $E_{h,\sigma}(N)$  are obtained numerically at each NRG step. The low energy renormalised parameters  $\tilde{\varepsilon}_{d,\sigma}, \tilde{\Delta}_\sigma$  are then defined by  $\tilde{\varepsilon}_{d,\sigma} = \lim_{N \rightarrow \infty} \tilde{\varepsilon}_{d,\sigma}(N)$  and  $\tilde{\Delta}_\sigma = \lim_{N \rightarrow \infty} \tilde{\Delta}_\sigma(N)$ . In practice for most cases, for  $\Lambda = 2$  a number of iterations  $N_{\max} \simeq 50$  is sufficient to determine the renormalised parameters accurately. We can give an explicit equation for  $\tilde{\Delta}(N)$  by subtracting the two equations above

$$\tilde{V}_\sigma^2(N) = \Lambda^{-(N-1)} \frac{E_{p,\sigma}(N) + E_{h,-\sigma}(N)}{g_{00,\sigma}(E_{p,\sigma}(N)) - g_{00,\sigma}(-E_{h,-\sigma}(N))} \quad (\text{B.9})$$

and from this  $\tilde{\varepsilon}_{d,\sigma}(N)$  is easily determined in (B.7).

We can also determine the local quasiparticle interaction  $\tilde{U}$  from the NRG results. The idea that helps to find it is to notice that it must be related to the difference between a two-particle excitation and two one-particle excitations. Having determined the quasiparticle parameters  $\tilde{\epsilon}_{d,\sigma}$  and  $\tilde{V}_{d,\sigma}$  via the procedure described above, we can give the free quasiparticle Hamiltonian [(1.12) without  $\tilde{U}$ ] in the linear chain form. It can be diagonalised numerically and written as

$$H_\sigma = \Lambda^{-\frac{N-1}{2}} \sum_{k=1}^{(N+2)/2} (E_{p,k,\sigma} p_{k,\sigma}^\dagger + E_{h,k,\sigma} h_{k,\sigma}^\dagger) \quad (\text{B.10})$$

where  $p_{k,\sigma}$  and  $h_{k,\sigma}$  are particle and hole operators, respectively. All terms involve a spin label  $\sigma$ , but no mixing of opposite spins occurs. Therefore, we can diagonalise the two spin components separately. We denote the energetically lowest one-particle excitation by  $E_{p,1,\sigma}$ , such that  $E_{p,1,\sigma} = E_{p,\sigma}$  (see above), and similarly for the holes. In order to relate the quasiparticle interaction term with  $\tilde{U}$  [cf. eq. (1.12)]

$$H_{\text{qp,int}} = \tilde{U} \Lambda^{(N-1)/2} : d_\uparrow^\dagger d_\uparrow d_\downarrow^\dagger d_\downarrow : \quad (\text{B.11})$$

to the one-particle and two-particle excitation  $E_{pp}^{\sigma,\sigma'}$ , which are calculated numerically in the NRG, we have to use inverse of the basis transformation to the eigenstates in (B.10)

$$d_\sigma = \sum_{k=1}^{(N+2)/2} [\psi_{p,k,\sigma}(-1) p_{k,\sigma} + \psi_{h,k,-\sigma}(-1) h_{k,-\sigma}^\dagger]. \quad (\text{B.12})$$

Then the corresponding to  $\tilde{U}_{pp}^{\sigma,\sigma'}$  particle particle term is

$$d_\uparrow^\dagger d_\uparrow d_\downarrow^\dagger d_\downarrow \sim \sum_{k_1, k_2, k_3, k_4} \psi_{p, k_1, \uparrow}^* (-1) \psi_{p, k_2, \uparrow} (-1) \psi_{p, k_3, \downarrow}^* (-1) \psi_{p, k_4, \downarrow} (-1) p_{k_1, \uparrow}^\dagger p_{k_2, \uparrow} p_{k_3, \downarrow}^\dagger p_{k_4, \downarrow}. \quad (\text{B.13})$$

If we only take into account the single lowest one-particle excitation  $E_{p,1,\uparrow}$  and  $E_{p,1,\downarrow}$  ( $k_1 = k_2 = k_3 = k_4 = 1$ ) and the two-particle excitation  $E_{pp}^{\uparrow,\downarrow}(N)$  the renormalised interaction  $\tilde{U}_{pp}^{\uparrow,\downarrow}(N)$  is seen to be inferred from (Hewson et al. 2004)

$$E_{pp}^{\uparrow,\downarrow}(N) - E_{p,\uparrow}(N) - E_{p,\downarrow}(N) = \tilde{U}_{pp}^{\uparrow,\downarrow}(N) \Lambda^{(N-1)/2} |\psi_{p,1,\uparrow}^*(-1)|^2 |\psi_{p,1,\downarrow}^*(-1)|^2. \quad (\text{B.14})$$

In a similar way we can look at particle-hole excitations  $E_{ph}^{\uparrow,\uparrow}$  (a hole  $\uparrow$  excitation corresponds to a particle  $\downarrow$ -excitation) to find an equation for the effective quasiparticle-quasihole interaction  $\tilde{U}_{ph}^{\uparrow,\uparrow}$

$$E_{ph}^{\uparrow,\uparrow}(N) - E_{p,\uparrow}(N) - E_{h,\uparrow}(N) = \tilde{U}_{ph}^{\uparrow,\uparrow}(N) \Lambda^{(N-1)/2} |\psi_{p,1,\uparrow}^*(-1)|^2 |\psi_{h,1,\uparrow}^*(-1)|^2, \quad (\text{B.15})$$

and also for hole-hole excitations

$$E_{hh}^{\downarrow,\uparrow}(N) - E_{h,\downarrow}(N) - E_{h,\uparrow}(N) = \tilde{U}_{hh}^{\downarrow,\uparrow}(N) \Lambda^{(N-1)/2} |\psi_{h,1,\downarrow}^*(-1)|^2 |\psi_{h,1,\uparrow}^*(-1)|^2. \quad (\text{B.16})$$

For large  $N$  these quantities are seen to converge to a certain value which is found to agree. We can therefore identify  $\tilde{U} = \tilde{U}_{pp}^{\uparrow,\downarrow} = -\tilde{U}_{ph}^{\uparrow,\uparrow} = \tilde{U}_{hh}^{\downarrow,\uparrow}$ .



# Appendix C

## Renormalised Perturbation Theory

In this part of the appendix we give a few more additional details for the RPT approach. First, we give a proof that the theory is well defined order by order. Then we outline an alternative formal description, which could form the basis for calculations in the equilibrium. We also describe the formal setup of a self-consistent theory based on the Luttinger Ward functional approach. In the last section we give details for the extension of the RPT to the non-equilibrium case.

The generating functional for the renormalised perturbation theory is given by equation (2.42),

$$\mathcal{Z}^r[J] = \int \mathcal{D}(d_\sigma^r, \bar{d}_\sigma^r) e^{-S^r[d_\sigma^r, \bar{d}_\sigma^r] - S^c[d_\sigma^r, \bar{d}_\sigma^r] - S_J[d_\sigma^r, \bar{d}_\sigma^r]}. \quad (\text{C.1})$$

The renormalised parameter action  $S^r$  is given in the earlier equation (2.43), the action for the counter-terms is given in (2.45) and the one-particle irreducible (1PI) source term is defined as in (2.47). This was used to generate the perturbation theory as in equation (2.52). First we give a proof that the RPT approach can be carried out order by order.

### C.1 Proof for the feasibility of the RPT approach

We want to prove generally that a renormalised perturbation theory as defined by (C.1) can be carried out order by order. We need to prove that the renormalisation conditions (2.40) and (2.41) can always be satisfied. This proof is carried out by induction. As a preliminary it is helpful to classify the contributions to the proper self-energy into three different types, as done before in the main text:

- (a) terms  $\Sigma_{\tilde{v}}(i\omega_n)$  coming purely from AIM interaction term  $e^{-S_{\tilde{v}}^r}$ . They correspond to the diagrams in the standard perturbation theory of the AIM.
- (b) terms coming purely from  $e^{-S_0^c}$ , which correspond to trivial counter-terms which can be collected to a self-energy contribution  $\Sigma^{ct}(i\omega_n) = -[\lambda_1 + \lambda_2 i\omega_n]$ .
- (c) mixed terms  $\Sigma_{\lambda_1, \lambda_2, \lambda_3}^{\text{mix}}(i\omega_n)$  generated by the combination  $e^{-S_{\tilde{v}}^r}$ ,  $e^{-S_0^c}$ , and  $e^{-S_{\lambda_3}^c}$ .

The perturbative renormalised self-energy to order  $n$  is given by

$$\tilde{\Sigma}^{(n)}(i\omega_n) = \sum_{k=1}^n \left[ \sum_m \Sigma_{\tilde{U}}^{(k,m)}(i\omega_n) + \sum_m \Sigma_{\lambda_1, \lambda_2, \lambda_3}^{\text{mix},(k,m)}(i\omega_n) \right] + \Sigma^{\text{ct}}(i\omega_n), \quad (\text{C.2})$$

where  $\Sigma^{(k,m)}$  denotes the  $m$ th diagrammatic contribution to the self-energy of order  $k$ . We have omitted the spin index for notational simplicity.

In order to classify different orders of the perturbation theory it is useful to think of the counter-term parameters as expanded in  $\tilde{U}$  (Hewson 2001),

$$\lambda_i = \sum_k \lambda_i^{(k)} \tilde{U}^k. \quad (\text{C.3})$$

Then for each order of the perturbation theory we have to determine the coefficients  $\lambda_i^{(n)}$  in this expansion, such that (2.40) and (2.41) are satisfied, whilst all mixed terms for the renormalised self-energy are included. Note that the mixed terms for a diagrammatic contribution to order  $n$  have generally a prefactor of the form

$$\tilde{U}^{m_0 + \sum_{i=1}^3 \sum_{m_i=1}^n m_i l_i^{(m_i)}} \prod_{i=1}^3 (\lambda_i^{(m_i)})^{l_i^{(m_i)}}, \quad (\text{C.4})$$

where  $l_i^{(m_i)} \in \mathbb{N}_0$  has to be chosen such that it gives the number of times a counter-term contribution of type  $i$  of the order  $m_i$  in  $\tilde{U}$  appears in the diagram;  $m_0$  gives the order from the standard AIM perturbative expansion in  $\tilde{U}$  corresponding to (a). For a diagram of order  $n$  we need to have the condition

$$m_0 + \sum_{i=1}^3 \sum_{m_i=1}^n m_i l_i^{(m_i)} = n \quad (\text{C.5})$$

Note that  $l_i^{(n)} = 0$  for  $i = 1, 2$ , and therefore to order  $n$  the terms  $\lambda_1^{(n)}$  and  $\lambda_2^{(n)}$  only appear in the last term  $\Sigma^{\text{ct}}$  in (C.2).

Similarly, we can classify the different contributions to the full renormalised vertex at zero frequency  $\tilde{\Gamma}(0)$ , where we use a simplified notation here. We have terms  $\tilde{\Gamma}_{\tilde{U}}(0)$ , such as in (a) above, which come from  $e^{-S_{\tilde{U}}^r}$  only. For later convenience let us take the first order term, which is just equal to  $\tilde{U}$ , separately. We also take the equivalent term for  $\lambda_3$  separately. As in (c) above we have mixed terms from original and counter-term contributions, which we denote by  $\tilde{\Gamma}_{\lambda_1, \lambda_2, \lambda_3}^{\text{mix}}(0)$ . They will generally have the same prefactor as in (C.4), but here we have  $m_i \in [0, n-1]$  for  $i = 0, 1, 2, 3$ , since we have taken out the  $\tilde{U}$  and  $\lambda_3$  term. The full renormalised vertex at zero frequency to order  $n > 1$  is then given by

$$\tilde{\Gamma}^{(n)}(0) = \tilde{U} + \lambda_3 + \sum_{k=2}^n \left[ \sum_m \tilde{\Gamma}_{\tilde{U}}^{(k,m)}(0) + \sum_m \tilde{\Gamma}_{\lambda_1, \lambda_2, \lambda_3}^{\text{mix},(k,m)}(0) \right], \quad (\text{C.6})$$

where similar to the case of the self-energy  $\tilde{\Gamma}^{(k,m)}$  denotes the  $m$ th diagram of order  $k$ . This is all the notation we need in the following.

To prove the induction step,  $n-1 \rightarrow n$ , we will assume that for an RPT to order  $n-1$  in  $\tilde{U}$  all constants  $\lambda_i^{(k)}$ ,  $k < n$  have been determined such that the renormalised self-energy and vertex satisfy the renormalisation conditions, i.e.,

$$\tilde{\Sigma}^{(n-1)}(0) = 0, \quad \frac{\partial}{\partial i\omega} \tilde{\Sigma}^{(n-1)}(i\omega = 0) = 0 \quad (\text{C.7})$$

and

$$\tilde{\Gamma}^{(n-1)}(0) = \tilde{U}. \quad (\text{C.8})$$

Now for order  $n$  one has to determine all diagrams of type (a) and (c) for the self-energy and vertex. These quantities to order  $n$  are then given by equation (C.2) and (C.6), respectively. The renormalisation condition for the vertex (2.41) reads

$$\tilde{U} + \sum_{k=1}^n \lambda_3^{(k)} \tilde{U}^k + \sum_{k=1}^n \left[ \sum_m \tilde{\Gamma}_{\tilde{U}}^{(k,m)}(0) + \sum_m \tilde{\Gamma}_{\lambda_1, \lambda_2, \lambda_3}^{\text{mix},(k,m)}(0) \right] = \tilde{U}. \quad (\text{C.9})$$

Note that only the second term contains  $\lambda_3^{(n)}$  and no term here can contain  $\lambda_1^{(n)}$  or  $\lambda_2^{(n)}$ . Now, according to the assumption of the induction, the counter-term parameters  $\lambda_i^{(k)}$  for  $k < n$  have been chosen such that (C.8) is satisfied, which implies that all terms with  $k < n$  vanish. This yields the equation

$$\lambda_3^{(n)} \tilde{U}^n + \left[ \sum_m \tilde{\Gamma}_{\tilde{U}}^{(n,m)}(0) + \sum_m \tilde{\Gamma}_{\lambda_1, \lambda_2, \lambda_3}^{\text{mix},(n,m)}(0) \right] = 0. \quad (\text{C.10})$$

All parameters entering the second and third term in this equation have been specified for  $k < n$  and thus (C.10) yields a unique solution for  $\lambda_3^{(n)}$ , provided that all diagrams have been evaluated. Similarly, we consider the first condition for the renormalised self-energy (2.40), which reads

$$0 = \tilde{\Sigma}^{(n)}(0) = \sum_{k=1}^n \left[ \sum_m \Sigma_{\tilde{U}}^{(k,m)}(0) + \sum_m \Sigma_{\lambda_1, \lambda_2, \lambda_3}^{\text{mix},(k,m)}(0) \right] + \sum_{k=1}^n \lambda_1^{(k)} \tilde{U}^k \quad (\text{C.11})$$

Note that the mixed terms do not contain  $\lambda_1^{(n)}$  or  $\lambda_2^{(n)}$ , but they can contain a term with  $\lambda_3^{(n)}$ , which has been determined from (C.10). According to the induction assumption terms for  $k < n$  are chosen such that (C.7) is satisfied, and therefore all terms for  $k < n$  cancel, which leaves us with

$$0 = \left[ \sum_m \Sigma_{\tilde{U}}^{(n,m)}(0) + \sum_m \Sigma_{\lambda_1, \lambda_2, \lambda_3}^{\text{mix},(n,m)}(0) \right] + \lambda_1^{(n)} \tilde{U}^n. \quad (\text{C.12})$$

This uniquely determines  $\lambda_1^{(n)}$ . A similar argument holds for the second part of the renormalisation condition (2.40) to determine  $\lambda_2^{(n)}$ , which concludes the induction step. For the proof it only remains to be shown that the case  $n = 1$  can be satisfied, which we have illustrated as one of the examples in section 2.2.2. We can therefore conclude at this stage that it is possible to carry out this RPT to any given order  $n$ .

## C.2 Alternative Setup for the RPT

We gave a formulation of how to generate a perturbation theory based on taking all counter-terms as interactions in chapter 2. A different formulation will be illustrated here, where terms of similar kind are collected. Starting again from (C.1) we can reformulate the theory slightly,

$$\mathcal{Z}^r[J] = \int \mathcal{D}(d_\sigma^r, \bar{d}_\sigma^r) e^{-S_0^r[d_\sigma^r, \bar{d}_\sigma^r] - S_{\tilde{U}}^r[d_\sigma^r, \bar{d}_\sigma^r] - S_0^c[d_\sigma^r, \bar{d}_\sigma^r] - S_{\lambda_3}^c[d_\sigma^r, \bar{d}_\sigma^r] - S_J[d_\sigma^r, \bar{d}_\sigma^r]} \quad (\text{C.13})$$

$$= e^{-S_{(\tilde{U}+\lambda_3)}^r[\delta J_\sigma, \delta \bar{J}_\sigma]} \int \mathcal{D}(d_\sigma^r, \bar{d}_\sigma^r) e^{-S_0^r[d_\sigma^r, \bar{d}_\sigma^r] - S_0^c[d_\sigma^r, \bar{d}_\sigma^r] - S_J[d_\sigma^r, \bar{d}_\sigma^r]} \quad (\text{C.14})$$

$$= e^{-S_{(\tilde{U}+\lambda_3)}^r[\delta J_\sigma, \delta \bar{J}_\sigma]} \mathcal{Z}_0^r[J]. \quad (\text{C.15})$$

We have collected the interaction terms corresponding to  $\tilde{U}$  and  $\lambda_3$  as they are of identical form, and did not treat the free counter-terms as interaction terms. The Gaussian integration gives similar as before

$$\mathcal{Z}_0^r[J] = e^{-\sum_\sigma \int_0^\beta d\tau \int_0^\beta d\tau' \bar{J}_\sigma(\tau) G_{\sigma, \lambda_1, \lambda_2}^r(\tau - \tau') J_\sigma(\tau')}, \quad (\text{C.16})$$

where

$$G_{\sigma, \lambda_1, \lambda_2}^r(\tau - \tau') = [G_0^{-1}(\tau - \tau') + [G_\sigma^{c,0}(\tau - \tau')]^{-1}]^{-1} \quad (\text{C.17})$$

The free counter-terms are included in the propagator, which now takes the general form

$$G_{\sigma, \lambda_1, \lambda_2}^r(\tau - \tau') = \frac{1}{\beta} \sum_n e^{-i\tau\omega_n} \frac{1}{i\omega_n - \tilde{\epsilon}_{d,\sigma} - K_\sigma^r(i\omega_n) + \lambda_1 + \lambda_2 i\omega_n}. \quad (\text{C.18})$$

As can be seen from the generating functional (C.15) the perturbation expansion is easier now consisting only of the terms, which were mentioned above under (a). These are the terms of the standard perturbation theory for the AIM. We denote these terms, which through the propagator depend on the counter-term constants by  $\Sigma_{(\tilde{U}+\lambda_3)}(i\omega_n, \lambda_1, \lambda_2)$ . The Dyson equation for this setup reads

$$G_{d,\sigma}(i\omega_n)^{-1} = G_{d,\sigma}^r(i\omega_n)^{-1} - \Sigma_{(\tilde{U}+\lambda_3)}(i\omega_n, \lambda_1, \lambda_2). \quad (\text{C.19})$$

Comparing with the earlier Dyson equation we can identify the renormalised self-energy in this scheme as

$$\tilde{\Sigma}(i\omega_n) = \Sigma_{(\tilde{U}+\lambda_3)}(i\omega_n, \lambda_1, \lambda_2) - \lambda_1 - \lambda_2 i\omega_n \quad (\text{C.20})$$

and the renormalisation conditions (2.40) become self-consistency equations

$$\lambda_1 = \Sigma_{(\tilde{U}+\lambda_3)}(0, \lambda_1, \lambda_2) \quad (\text{C.21})$$

and

$$\lambda_2 = \frac{\partial}{\partial i\omega} \Sigma_{(\tilde{U}+\lambda_3)}(i\omega = 0, \lambda_1, \lambda_2). \quad (\text{C.22})$$

The renormalisation condition for the vertex remains the same (2.40) taking into account that all propagators are given by (C.18) and the interaction is  $\tilde{U} + \lambda_3$ .

Although such a setup at first sight appears promising due the much simpler structure of the perturbation expansion it turns out that it is difficult to carry out the expansion in this form. We had seen that the counter-term parameters include contributions to different order [cf eq. (C.3)]. The setup defined by (C.15) and the free propagator (C.18) implies that counter-term contributions to all orders are included even in the low order diagrams discussed in the last section. They could be expanded again in orders of  $\tilde{U}$ , but that is like going back to the earlier section, or one has to devise a consistent way of including diagrams to all orders with these counter-term contributions. It turns out that these can in fact be done better in a frame work where also the renormalised self-energy is included in the propagators, or in other words the expansion is carried out in terms of the full propagators. This is then necessarily a self-consistent theory. The natural formalism for such an approach is the formulation in terms of a Luttinger Ward functional and the 2PI scheme, which will be described in the following section.

### C.3 Functional integral description in the 2PI formalism

The generating functional for the renormalised theory in the two-particle irreducible (2PI) scheme is given by

$$\mathcal{Z}^r[\eta] = \int \mathcal{D}(d_\sigma^r, \bar{d}_\sigma^r) e^{-S^r[d_\sigma^r, \bar{d}_\sigma^r] - S^c[d_\sigma^r, \bar{d}_\sigma^r] - S_\eta[d_\sigma^r, \bar{d}_\sigma^r]}, \quad (\text{C.23})$$

with the renormalised action  $S^r$  as in equation (2.43) and the action for the counter-terms as in (2.45). The difference to the earlier case is the source term, which is defined by

$$S_\eta = \sum_{\sigma, \sigma'_0} \int_0^\beta d\tau \int_0^\beta d\tau' \bar{d}_\sigma^r(\tau) \eta_{\sigma, \sigma'}(\tau, \tau') d_{\sigma'}^r(\tau'). \quad (\text{C.24})$$

We can define a generating functional for connected Green's functions,

$$W^r[\eta] = \log \mathcal{Z}^r[\eta]. \quad (\text{C.25})$$

The connected  $n$ -particle renormalised Green's function is obtained via

$$G_{\sigma_1, \dots, \sigma_n; \sigma'_1, \dots, \sigma'_n}^{r, (n)}(\omega_1, \dots, \omega_n; \omega'_1, \dots, \omega'_n) = \zeta^n \frac{\delta^{2n} W^r[\eta]}{\delta \eta_{\sigma'_1, \sigma_1}(\omega'_1, \omega_1) \dots \delta \eta_{\sigma'_n, \sigma_n}(\omega'_n, \omega_n)} \Big|_{\eta=0}. \quad (\text{C.26})$$

We can write

$$-\frac{\delta W^r[\eta]}{\delta \eta_{\sigma', \sigma}(\omega', \omega)} = -\langle \bar{d}_{\sigma'}^r(\omega') d_\sigma^r(\omega) \rangle_\eta = \langle d_\sigma^r(\omega) \bar{d}_{\sigma'}^r(\omega') \rangle_\eta = G_{\sigma, \sigma'}^r(\omega, \omega'), \quad (\text{C.27})$$

by which the generalised Green's function  $G_{\sigma,\sigma'}(\omega, \omega')$  is defined. It is suitable to perform a Legendre transform to a new generating functional  $\Gamma^r[G^r]$ ,

$$\Gamma^r[G^r] = \sum_{\sigma,\sigma',n,n'} G_{\sigma,\sigma'}^r(i\omega_n, i\omega'_n) \eta_{\sigma,\sigma'}(i\omega_n, i\omega'_n) - W^r[\eta], \quad (\text{C.28})$$

whose natural variable is  $G_{\sigma,\sigma'}^r(i\omega_n, i\omega'_n)$ . This functional generates proper vertex functions (Negele and Orland 1988). By functional differentiation we find

$$\frac{\delta \Gamma^r[G^r]}{\delta G_{\sigma,\sigma'}^r(\omega, \omega')} = -\eta_{\sigma,\sigma'}(\omega, \omega') \quad (\text{C.29})$$

For a non-interacting theory,  $\tilde{U} + \lambda_3 = 0$ , we can give an exact expression for the generating functional  $\Gamma^{0,r}[G^r]$ , since the integrals are Gaussian and can be carried out exactly. We find,

$$\Gamma^{r,0}[G^r] = \sum_{\sigma,\sigma',n,n'} [\log G_{\sigma,\sigma'}^r(i\omega_n, i\omega'_n) + 1 - ([G_{\sigma}^{r,0}(i\omega_n)]^{-1} + [G_{\sigma}^{c,0}(i\omega_n)]^{-1}) G_{\sigma,\sigma'}^r(i\omega_n, i\omega'_n)]. \quad (\text{C.30})$$

Note that

$$\frac{\delta \Gamma^{r,0}[G^r]}{\delta G_{\sigma,\sigma'}^r(i\omega_n, i\omega'_n)} = [G_{\sigma,\sigma'}^r(i\omega_n, i\omega'_n)]^{-1} - ([G_{\sigma}^{r,0}(i\omega_n)]^{-1} + [G_{\sigma}^{c,0}(i\omega_n)]^{-1}). \quad (\text{C.31})$$

In the interacting theory we can express the effective potential as

$$\Gamma^r[G^r] = \Gamma^{r,0}[G^r] + \Phi^r[G^r], \quad (\text{C.32})$$

with an additional functional  $\Phi^r[G^r]$ , which turns out to be the Luttinger Ward functional  $\Phi_{\text{LW}}^r[G^r]$  (Luttinger and Ward 1960, Abrikosov et al. 1963). It is well known and can be expressed diagrammatically in terms of closed skeleton diagrams. Its functional derivatives yield self-energy and irreducible vertex functions (Abrikosov et al. 1963). Note that the expansion is carried out with the effective interaction  $\tilde{U}_1 \equiv \tilde{U} + \lambda_3$  as expansion parameter as the interaction terms of the same structure have been collected again.

In this approach the renormalised Green's function is a variable. The physical Green's function, which corresponds to the stationary point of the functional  $\Gamma^r[G^r]$ , when the source is zero, satisfies the Dyson equation, which for the renormalised theory reads,

$$\tilde{\Sigma}_{\sigma}(i\omega_n) = [G_{\sigma}^{r,0}(i\omega_n)]^{-1} - [G_{\sigma,\sigma}^r(i\omega_n, i\omega_n)]^{-1}. \quad (\text{C.33})$$

In the stationary state invoking  $\eta = 0$  in equation (C.29) we find therefore using (C.31) that the renormalised self-energy  $\tilde{\Sigma}_{\sigma}(i\omega_n)$  is given by

$$\tilde{\Sigma}_{\sigma}(i\omega_n) = \frac{\delta \Phi^r[G^r]}{\delta G_{\sigma,\sigma}^r(i\omega_n, i\omega_n)} - [G_{\sigma}^{c,0}(i\omega_n)]^{-1} \quad (\text{C.34})$$

Note that explicitly we simply have  $[G_{\sigma}^{c,0}(i\omega_n)]^{-1} = \lambda_1 i\omega_n + \lambda_2$ .

We can now give the renormalisation conditions (2.40) and (2.41) in terms of the Luttinger Ward functional  $\Phi^r[G^r]$ . The equations (2.40) for the renormalised self-energy read

$$\frac{\delta\Phi^r[G^r]}{\delta G_{\sigma,\sigma}^r(0,0)} - [G_{\sigma}^{c,0}(0)]^{-1} = 0 \quad (\text{C.35})$$

and

$$\frac{\partial}{\partial i\omega} \left( \frac{\delta\Phi^r[G^r]}{\delta G_{\sigma,\sigma}^r(i\omega, i\omega)} - [G_{\sigma}^{c,0}(i\omega)]^{-1} \right) \Big|_{\eta=0, \omega=0} = 0. \quad (\text{C.36})$$

These equations determine  $\lambda_1$  and  $\lambda_2$ . It is convenient to define the self-energy  $\Sigma_{\sigma}^r(i\omega_n)$ , which is obtained from the perturbation expansion of  $\Phi^r[G^r]$ ,

$$\Sigma_{\sigma}^r(i\omega_n) = \frac{\delta\Phi^r[G^r]}{\delta G_{\sigma,\sigma}^r(i\omega_n, i\omega_n)}. \quad (\text{C.37})$$

The full retarded Green's function can therefore also be written as

$$G_{\sigma}^r(i\omega_n) = \frac{z_{\sigma}}{i\omega_n - \tilde{\varepsilon}_{d,\sigma} + i\tilde{\Delta} + \lambda_1 i\omega_n + \lambda_2 - \Sigma_{\sigma}^r(i\omega_n)}. \quad (\text{C.38})$$

In a self-consistent perturbative approach with (C.38) the self energy  $\Sigma_{\sigma}^r(i\omega_n)$  depends on the three renormalisation parameters  $\lambda_i$ , and the renormalisation conditions (C.35) and (C.36) are additional self-consistency equations

$$\Sigma_{\sigma}^r(i\omega_n = 0, \lambda_1, \lambda_2, \lambda_3) = \lambda_2 \quad (\text{C.39})$$

and

$$\frac{\partial}{\partial i\omega} \Sigma_{\sigma}^r(i\omega, \lambda_1, \lambda_2, \lambda_3) \Big|_{\omega=0} = \lambda_1. \quad (\text{C.40})$$

The condition (2.41) for the vertex has to be found by considering the particle hole irreducible vertex  $\tilde{I}_{ph}$ ,

$$\tilde{I}_{\sigma_1, \sigma_2}^{\sigma_3, \sigma_4}(\omega_1, \omega_2, \omega_3, \omega_4) = \frac{\delta^2\Phi[G^r]}{\delta G_{\sigma_3, \sigma_4}^r(\omega_3, \omega_4) \delta G_{\sigma_1, \sigma_2}^r(\omega_1, \omega_2)} \Big|_{\eta=0} \quad (\text{C.41})$$

In the particle hole channel this is related to the full renormalised vertex  $\tilde{\Gamma}$  through the Bethe Salpeter equation

$$\begin{aligned} \tilde{\Gamma}_{\sigma_1, \sigma_2}^{\sigma_3, \sigma_4}(\omega_1, \omega_2, \omega_3, \omega_4) &= \tilde{I}_{\sigma_1, \sigma_2}^{\sigma_3, \sigma_4}(\omega_1, \omega_2, \omega_3, \omega_4) \\ &+ \sum_{\omega'_2, \sigma'_2, \sigma'_4} \tilde{I}_{\sigma_1, \sigma'_2}^{\sigma_3, \sigma'_4}(\omega_1, \omega'_2, \omega_3, \omega'_2 + \omega_3 - \omega_1) G_{\sigma'_2}^r(\omega_2) G_{\sigma'_4}^r(\omega'_2 + \omega_3 - \omega_1) \times \\ &\times \tilde{\Gamma}_{\sigma'_2, \sigma_2}^{\sigma'_4, \sigma_4}(\omega'_2, \omega'_2 + \omega_3 - \omega_1, \omega_3, \omega_4). \end{aligned} \quad (\text{C.42})$$

This equation is represented graphically in figure C.1, where also the assignment of external frequencies is visible.

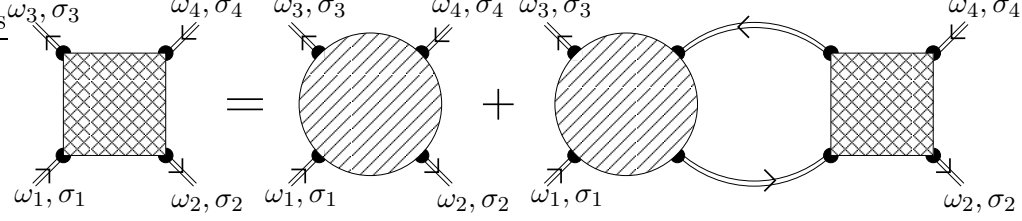


Figure C.1: Bethe Salpeter equation for full renormalised vertex  $\tilde{\Gamma}$  (box) expressed through the renormalised particle-hole irreducible vertex  $\tilde{I}_{ph}$  (circle) and full renormalised Green's function  $G^r$  (double line).

The renormalisation condition (2.41) is then given by

$$\tilde{\Gamma}_{\sigma, -\sigma}^{\sigma, -\sigma}(0, 0, 0, 0) \equiv \tilde{\Gamma}_{\sigma, -\sigma}(0, 0) = \tilde{U}. \quad (\text{C.43})$$

This equation determines  $\lambda_3$ .

An RPT in this scheme can be specified entirely by an approximation to the Luttinger Ward functional. From this the self-energy, the irreducible and full vertex can be calculated in terms of the full propagators and one has to iterate for self-consistency adjusting the counter-term parameters. Though in principle possible this approach is - even for simple approximations of the LW functional - difficult to carry out since the calculation of the full vertex with the Bethe-Salpeter equation is numerically cumbersome. Usually we are mainly interested in the renormalised self-energy and only really need the full vertex at zero frequency in order to satisfy the renormalisation condition. Therefore, we are calculating much more than we actually need in such an approach. A possibility to circumvent this additional effort is not to calculate the full vertex with all the dynamic dependence, but rather relate it to the self-energy via a Ward identity. This might be a promising route for future developments of the RPT, which at the time of writing has not been explored in detail.

## C.4 Non-equilibrium renormalised perturbation theory

Here we generalise the setup of the renormalised perturbation theory from chapter 2 to the non-equilibrium case, which is the subject of chapter 4. The renormalised parameters are defined for zero temperature and in the equilibrium limit,  $eV \rightarrow 0$ . The matrix Dyson equation (4.12) simplifies then to an equation for the  $(--)$  component,

$$G_{d,\sigma}^{--}(\omega)^{-1} = G_{d,\sigma}^{(0),--}(\omega)^{-1} - \Sigma_{\sigma}^{(--)}(\omega), \quad (\text{C.44})$$

where

$$G_{d,\sigma}^{(0),--}(\omega)^{-1} \Big|_{eV=0} = \omega - \varepsilon_{d,\sigma} + i\Delta \text{sgn}(\omega) \quad (\text{C.45})$$

and

$$\Sigma_{\sigma}^{(--)}(\omega) = \theta(\omega) \Sigma_{\sigma}^{\text{ret}}(\omega) + (1 - \theta(\omega)) \Sigma_{\sigma}^{\text{adv}}(\omega). \quad (\text{C.46})$$

We can therefore focus on the equilibrium retarded self-energy  $\Sigma_\sigma^{\text{ret}}(\omega)$  [ $\Sigma_\sigma^{\text{adv}}(\omega) = \Sigma_\sigma^{\text{ret}}(\omega)^*$ ] and carry out the usual Fermi liquid expansion. As seen in chapters 2 and 3 for the equilibrium RPT it is useful to include the magnetic field dependence in the self-energy, which we will do for the following definitions, which essentially coincide with (2.33) and (2.34) with  $\Sigma_\sigma(\omega) \rightarrow \Sigma_\sigma^{\text{ret}}(\omega)$ . Hence, with

$$z_\sigma(h)^{-1} = 1 - \frac{\partial \text{Re} \Sigma_\sigma^{\text{ret}}(0, h)}{\partial \omega}, \quad (\text{C.47})$$

the renormalised parameters are given by

$$\tilde{\Delta}_\sigma(h) = z_\sigma(h)\Delta, \quad \tilde{\varepsilon}_{d,\sigma}(h) = z_\sigma(h)(\varepsilon_{d,\sigma} + \text{Re} \Sigma_\sigma^{\text{ret}}(0, h)), \quad (\text{C.48})$$

The remainder of the self-energy  $\Sigma_\sigma^{\text{rem}}(\omega, h)$  defines the retarded renormalised self-energy  $\tilde{\Sigma}_\sigma^{\text{ret}}(\omega, h)$  [cf. (2.35)],

$$\tilde{\Sigma}_\sigma^{\text{ret}}(\omega, h) = z_\sigma(h)\Sigma_\sigma^{\text{rem}}(\omega, h). \quad (\text{C.49})$$

The renormalised interaction  $\tilde{U}(h)$  is defined as in equilibrium by the effective quasiparticle interaction of the problem, which is given by the full renormalised four point vertex function at zero frequency (2.37).

These renormalised parameters, which are the same ones as in the equilibrium RPT, are used for the low energy description of the non-equilibrium systems by replacing the original parameters. The effective action becomes  $\tilde{S} = \tilde{S}_0 + \tilde{S}_{\tilde{U}}$  with

$$S_0^r = \sum_\sigma \int_{-\infty}^{\infty} dt \int_{-\infty}^{\infty} dt' \bar{\mathbf{d}}_\sigma^r(t) \tilde{\mathbf{G}}_{d,\sigma}^{(0)}(t-t')^{-1} \mathbf{d}_\sigma^r(t') \quad (\text{C.50})$$

where  $\mathbf{d}_\sigma^r(t) := {}^t(d_{\sigma,-}^r(t), d_{\sigma,+}^r(t))$ ,  $d_{\sigma,\nu}^r(t) = d_{\sigma,\nu}(t)/\sqrt{z_\sigma}$ , and

$$\tilde{\mathbf{G}}_{d,\sigma}^{(0)}(t-t')^{-1} = \frac{1}{2\pi} \int d\omega \tilde{\mathbf{G}}_{d,\sigma}^{(0)}(\omega)^{-1} e^{-i\omega(t-t')}.$$

We have

$$\tilde{\mathbf{G}}_{d,\sigma}^{(0)}(\omega) = \begin{pmatrix} \tilde{G}_{d,\sigma}^{(0),--}(\omega) & \tilde{G}_{d,\sigma}^{(0),-+}(\omega) \\ \tilde{G}_{d,\sigma}^{(0),+-}(\omega) & \tilde{G}_{d,\sigma}^{(0),++}(\omega) \end{pmatrix}, \quad (\text{C.51})$$

where the matrix elements are given by [cf. (4.8)-(4.10)]

$$\tilde{G}_{d,\sigma}^{(0),--}(\omega) = \frac{\omega - \tilde{\varepsilon}_{d,\sigma} - i\tilde{\Delta}_\sigma(1 - 2f_{\text{eff}}(\omega))}{(\omega - \tilde{\varepsilon}_{d,\sigma})^2 + \tilde{\Delta}_\sigma^2}, \quad (\text{C.52})$$

$$\tilde{G}_{d,\sigma}^{(0),-+}(\omega) = \frac{2i\tilde{\Delta}_\sigma f_{\text{eff}}(\omega)}{(\omega - \tilde{\varepsilon}_{d,\sigma})^2 + \tilde{\Delta}_\sigma^2}, \quad (\text{C.53})$$

$$\tilde{G}_{d,\sigma}^{(0),+-}(\omega) = \frac{-2i\tilde{\Delta}_\sigma(1 - f_{\text{eff}}(\omega))}{(\omega - \tilde{\varepsilon}_{d,\sigma})^2 + \tilde{\Delta}_\sigma^2}, \quad (\text{C.54})$$

and  $\tilde{G}_{d,\sigma}^{(0),++}(\omega) = -\tilde{G}_{d,\sigma}^{(0),--}(\omega)^*$ . The interaction term reads

$$S_{\tilde{U}}^r = -\tilde{U} \int_{-\infty}^{\infty} dt (n_{d,\uparrow,-}^r(t)n_{d,\downarrow,-}^r(t) - n_{d,\uparrow,+}^r(t)n_{d,\downarrow,+}^r(t)). \quad (\text{C.55})$$

The renormalisation conditions for the renormalised retarded self-energy apply in the equilibrium limit, and are given as in (2.40) and (2.41). Generally in the Keldysh formalism, the retarded self-energy is given by

$$\Sigma_{\sigma}^{\text{ret}}(\omega) = \Sigma_{\sigma}^{--}(\omega) + \Sigma_{\sigma}^{-+}(\omega). \quad (\text{C.56})$$

In order to satisfy the renormalisation conditions (2.40) and (2.41) we have to include the counter-term action

$$\begin{aligned} S^c &= \sum_{\sigma} \int_{-\infty}^{\infty} dt \int_{-\infty}^{\infty} dt' \bar{\mathbf{d}}_{\sigma}^r(t) \underline{G}_{\sigma}^{c,0}(t-t')^{-1} \mathbf{d}_{\sigma}^r(t') \\ &\quad + \lambda_3 \int_{-\infty}^{\infty} dt n_{d,\uparrow,-}^r(t)n_{d,\downarrow,-}^r(t) - n_{d,\uparrow,+}^r(t)n_{d,\downarrow,+}^r(t) \\ &= S^{c,0} + S_{\lambda_3}^c \end{aligned} \quad (\text{C.57})$$

$$= S^{c,0} + S_{\lambda_3}^c \quad (\text{C.58})$$

where the matrix elements of  $\underline{G}_{\sigma}^{c,0}$  are generally given by  $G_{\sigma}^{c,\alpha\beta}(\omega)^{-1} = \lambda_2^{\alpha\beta}\omega + \lambda_1^{\alpha\beta}$ .  $G_{\sigma}^{c,\alpha\beta}(\omega)$  contains more degrees of freedom than needed for the renormalisation conditions. We will focus only on the relevant combinations for (2.40) and (2.41), and set all other  $\lambda_i^{\alpha,\beta}$  zero.

### Perturbation expansion in 1PI formalism

The renormalised perturbation theory can be set up in the one-particle irreducible scheme as described in section 2.2.2. The partition function of the model is then written as

$$\mathcal{Z}^r = \int \mathcal{D}(\mathbf{d}_{\sigma}^r, \bar{\mathbf{d}}_{\sigma}^r) e^{i(S^r[\mathbf{d}_{\sigma}^r, \bar{\mathbf{d}}_{\sigma}^r] + S^c[\mathbf{d}_{\sigma}^r, \bar{\mathbf{d}}_{\sigma}^r])}. \quad (\text{C.59})$$

A diagrammatic expansion can be generated by including a one-particle (1PI) source term of the form

$$S_J = \sum_{\sigma, \nu=\pm} \int_{-\infty}^{\infty} dt (\bar{\mathbf{d}}_{\sigma, \nu}^r(t) J_{\sigma, \nu}(t) + \text{h.c.}) \quad (\text{C.60})$$

$$= \sum_{\sigma} \int_{-\infty}^{\infty} dt (\bar{\mathbf{d}}_{\sigma}^r(t) \cdot \mathbf{J}_{\sigma}(t) + \text{h.c.}). \quad (\text{C.61})$$

The generating functional is generally written as

$$\mathcal{Z}^r[J] = \int \mathcal{D}(\mathbf{d}_{\sigma}^r, \bar{\mathbf{d}}_{\sigma}^r) e^{i(S^r[\mathbf{d}_{\sigma}^r, \bar{\mathbf{d}}_{\sigma}^r] + S^c[\mathbf{d}_{\sigma}^r, \bar{\mathbf{d}}_{\sigma}^r] + S_J[\mathbf{d}_{\sigma}^r, \bar{\mathbf{d}}_{\sigma}^r])}.$$

As before one obtains

$$\mathcal{Z}^r[J] = e^{iS_{(\bar{U}+\lambda_3)}^r[\delta J_{\sigma,\nu}, \delta \bar{J}_{\sigma,\nu}] + iS^{c,0}[\delta J_{\sigma,\nu}, \delta \bar{J}_{\sigma,\nu}]} \mathcal{Z}_0^r[J] \quad (\text{C.62})$$

where we have treated all counter-terms as interaction terms. By Gaussian integration we have

$$\mathcal{Z}_0^r[J] = e^{i \sum_{\sigma} \int_{-\infty}^{\infty} dt \int_{-\infty}^{\infty} dt' \bar{J}_{\sigma}(t) \underline{\tilde{G}}_{d,\sigma}^{(0)}(t-t') J_{\sigma}(t')} .$$

The connected Green's functions is formally obtained from

$$G_{\sigma_1 \sigma_2}^{\alpha_1, \alpha_2}(t_1, t_2) = \left. \frac{\delta^2 \log \mathcal{Z}^r[J]}{\delta \bar{J}_{\sigma_1, \alpha_1}(t_1) \delta J_{\sigma_2, \alpha_2}(t_2)} \right|_{J=0} . \quad (\text{C.63})$$

A diagrammatic perturbation expansion is obtained by expanding the exponential functions as explained in chapter 2 and follows from analogous arguments. One only needs to bear in mind the matrix structure of the theory, which accounts for the additional degrees of freedom. We are mainly interested in calculating the retarded renormalised self-energy (C.56). Therefore, we can focus on the combinations  $\lambda_i^{\text{ret}} \equiv \lambda_i^{--} + \lambda_i^{-+}$  for the counter-terms and in the simplest case determine the value directly by the renormalisation condition (2.40),

$$\lambda_1^{\text{ret}} = \Sigma_{\sigma}^{r,--}(0) + \Sigma_{\sigma}^{r,-+}(0) \quad (\text{C.64})$$

and

$$\lambda_2^{\text{ret}} = \frac{\partial}{\partial \omega} (\Sigma_{\sigma}^{r,--}(\omega) + \Sigma_{\sigma}^{r,-+}(\omega)) \Big|_{\omega=0} , \quad (\text{C.65})$$

where in all those equations we take the limit  $eV \rightarrow 0$ . The voltage dependent renormalised retarded self-energy is then given by

$$\tilde{\Sigma}_{\sigma}^{\text{ret}}(\omega, eV) = \Sigma_{\sigma}^{r,--}(\omega, eV) + \Sigma_{\sigma}^{r,-+}(\omega, eV) - \lambda_2^{\text{ret}} \omega - \lambda_1^{\text{ret}} . \quad (\text{C.66})$$



# Bibliography

- Abrikosov, A. A., Gorkov, L. P. and Dzyaloshinski, I. E.: 1963, *Methods of quantum field theory in statistical physics*, Dover, New York.
- Amasha, S., Gelfand, I. J., Kastner, M. A. and Kogan, A.: 2005, Kondo temperature dependence of the Kondo splitting in single-electron transistor, *Phys. Rev. B* **72**, 045308.
- Anders, F. B. and Schiller, A.: 2005, Real-time dynamics in a quantum impurity system: A time-dependent renormalization-group approach, *Phys. Rev. Lett.* **95**, 196801.
- Anderson, P. W.: 1961, Localized magnetic states in metals, *Phys. Rev.* **124**(1), 41.
- Anderson, P. W.: 1970, A poor man's derivation of scaling laws for the Kondo problem, *J. Phys. C* **3**, 2435.
- Aoki, H., Uji, S., Albessard, A. K. and Onuki, Y.: 1993, Transition of f electron nature from itinerant to localized: metamagnetic transition in CeRu<sub>2</sub>Si<sub>2</sub> studied via the de Haas – van Alphen effect, *Phys. Rev. Lett.* **71**(13), 2110.
- Balatsky, A. V., Vekhter, I. and Zhu, J.-X.: 2006, Impurity-induced states in conventional and unconventional superconductors, *Reviews of Modern Physics* **78**(2), 373.
- Bardeen, J., Cooper, L. and Schrieffer, J.: 1957, Theory of superconductivity, *Phys. Rev.* **108**, 1175.
- Bauer, J.: 2007, Details for the setup of numerical renormalisation group calculations for the Anderson impurity model, <http://www.ma.ic.ac.uk/~jb4/>.
- Bauer, J. and Hewson, A. C.: 2007a, Field-dependent quasiparticles in a strongly correlated local system. II., *Phys. Rev. B* **76**(3), 035119.
- Bauer, J. and Hewson, A. C.: 2007b, Field-dependent quasiparticles in the infinite-dimensional Hubbard model, *Phys. Rev. B* **76**(3), 035118.
- Bauer, J. and Hewson, A. C.: 2007c, Renormalized quasiparticles in antiferromagnetic states of the Hubbard model, *Eur. Phys. J. B* **57**, 235.

- Bauer, J., Hewson, A. C. and Oguri, A.: 2007a, Equilibrium and non-equilibrium dynamics of quasiparticles for locally correlated systems in a magnetic field, *J. Magn. Magn. Mat.* **310**, 1133.
- Bauer, J., Oguri, A. and Hewson, A. C.: 2007b, Spectral properties of locally correlated electrons in a BCS superconductor, *J. Phys.: Cond. Mat.* **19**, 486211.
- Buitelaar, M. R., Nussbaumer, T. and Schonberger, C.: 2002, Quantum dot in the Kondo regime coupled to superconductors, *Phys. Rev. Lett.* **89**, 256801.
- Bulla, R.: 1999, Zero-temperature metal-insulator transition in the infinite-dimensional Hubbard model, *Phys. Rev. Lett.* **83**, 136.
- Bulla, R., Costi, T. and Pruschke, T.: 2007, The numerical renormalization group method for quantum impurity systems, cond-mat/0701105.
- Bulla, R., Hewson, A. C. and Pruschke, T.: 1998, Numerical renormalization group calculations for the self-energy of the impurity Anderson model, *J. Phys.: Cond. Mat.* **10**, 8365.
- Bulla, R., Pruschke, T. and Hewson, A. C.: 1997, Anderson impurity in pseudo-gap Fermi systems, *J. Phys.: Cond. Mat.* **9**, 10463.
- Capone, M., Castellani, C. and Grilli, M.: 2002, First-order pairing transition and single-particle spectral function in the attractive Hubbard model, *Phys. Rev. Lett.* **88**, 126403.
- Caroli, C., Combescot, R., Nozières, P. and Saint-James, D.: 1971, Direct calculation of the tunneling current, *J. Phys. C* **4**, 916.
- Choi, M.-S., Lee, M., Kang, K. and Belzig, W.: 2004, Kondo effect and Josephson current through a quantum dot between two superconductors, *Phys. Rev. B* **70**, 020502.
- Coleman, P.: 2002, Local moment physics in heavy electron systems, cond-mat/0206003.
- Cooper, L.: 1956, Bound electron pairs in a degenerate Fermi gas, *Phys. Rev.* **104**, 1189.
- Costi, T. A.: 2000, Kondo effect in a magnetic field and the magnetoresistivity of Kondo alloys, *Phys. Rev. Lett.* **85**(7), 1504.
- Costi, T. A., Hewson, A. C. and Zlatić, V.: 1994, Transport coefficients of the Anderson model via the numerical renormalization group, *J. Phys.: Cond. Mat.* **6**, 2519.
- Cronenwett, S. M., Oosterkamp, T. H. and Kouwenhoven, L. P.: 1998, A tunable Kondo effect in quantum dots, *Science* **281**(8), 540.
- Dagotto, E.: 1994, Correlated electrons in high temperature superconductors, *Rev. Mod. Phys.* **66**, 763.

- De Franceschi, S., Hanson, R., van der Wiel, W. G., Elzerman, J. M., Wijkema, J. J., Fujisawa, T., Tarucha, S. and Kouwenhoven, L. P.: 2002, Out-of-equilibrium Kondo effect in a mesoscopic device, *Phys. Rev. Lett.* **89**(15), 156801.
- Dordevic, S. V., Beach, K. S. D., Takeda, N., Wang, Y. J., Maple, M. B. and Basov, D. N.: 2006, Heavy fermion fluid in high magnetic fields: An infrared study of CeRu<sub>4</sub>Sb<sub>12</sub>, *Phys. Rev. Lett.* **96**(1), 017403.
- Dupuis, N.: 2005, Effective action for superfluid Fermi systems in the strong-coupling limit, *Phys. Rev. A* **72**, 013606.
- Eagles, D. M.: 1969, Possible pairing without superconductivity at low carrier concentrations in bulk and thin-film superconducting semiconductors, *Phys. Rev.* **186**, 456.
- Edwards, D. and Green, A. C. M.: 1997, Heavy fermions in high magnetic fields, *Z. Phys. B* **103**, 243.
- Emery, V. J., Kivelson, S. A. and Lin, H. Q.: 1990, Phase separation in the  $t - j$  model, *Phys. Rev. Lett.* **64**(4), 475.
- Emery, V. J., Kivelson, S. A. and Tranquada, J. M.: 1999, Stripe phases in high temperature superconductors, *Proc. Natl. Acad. Sci. (USA)* **96**, 8814.
- Ferry, D. K. and Goodnick, S. M.: 1997, *Transport in Nanostructures*, Cambridge University Press.
- Freericks, J. K. and Jarrell, M.: 1995, Magnetic phase diagram of the Hubbard model, *Phys. Rev. Lett.* **74**(1), 186–189.
- Friedel, J.: 1956, On some electrical and magnetic properties of metallic solid solutions, *Can. J. Phys.* **54**, 1190.
- Fuji, T. and Ueda, K.: 2003, Perturbative approach to the nonequilibrium Kondo effect in a quantum dot, *Phys. Rev. B* **68**, 155310.
- Fuji, T. and Ueda, K.: 2005, Out-of-equilibrium transport phenomena through a quantum dot in a magnetic field, *J. Phys. Soc. Japan* **74**, 127.
- Garg, A., Krishnamurthy, H. R. and Randeria, M.: 2005, BCS-BEC crossover at  $t = 0$ : A dynamical mean field approach, *Phys. Rev. B* **72**, 024517.
- Georges, A., Kotliar, G., Krauth, W. and Rozenberg, M.: 1996, Dynamical mean-field theory of strongly correlated fermion systems and the limit of infinite dimensions, *Rev. Mod. Phys.* **68**, 13.

- Goldhaber-Gordon, D., Göres, J., Kastner, M. A., Shtrikman, H., Mahalu, D. and U.Meirav: 1998a, From the Kondo regime to the mixed-valence regime in a single-electron transistor, *Phys. Rev. Lett.* **81**, 5225.
- Goldhaber-Gordon, D., Shtrikman, H., Mahalu, D., Abusch-Magder, D., Meirav, U. and Kastner, M. A.: 1998b, Kondo effect in a single-electron transistor, *Nature* **391**, 156.
- Goodrich, R. G., Harrison, N., Teklu, A., Young, D. and Fisk, Z.: 1999, Development of the high-field heavy-fermion ground state in  $ce_xla_{1-x}b_6$  intermetallics, *Phys. Rev. Lett.* **82**(18), 3669–3672.
- Greiner, M., Regal, C. and Jin, D.: 2003, Emergence of a molecular Bose-Einstein condensate from a Fermi gas, *Nature* **426**, 537.
- Gutzwiller, M. C.: 1963, Effect of correlation on the ferromagnetism of transition metals, *Phys. Rev. Lett.* **10**(5), 159.
- Hausmann, R.: 1992, Crossover from BCS superconductivity to Bose-Einstein condensation: A self-consistent theory, *Z. Phys. B* **91**, 291.
- Hershfield, S., Davies, J. and Wilkins, J. W.: 1991, Probing the Kondo resonance by resonant tunneling through an Anderson impurity, *Phys. Rev. Lett.* **67**, 3720.
- Hertz, J. A. and Edwards, D. M.: 1972, Intermediate-coupling theory for itinerant ferromagnetism, *Phys. Rev. Lett.* **28**(20), 1334–1337.
- Hewson, A.: 1993a, *The Kondo Problem to Heavy Fermions*, Cambridge University Press, Cambridge.
- Hewson, A. C.: 1993b, Renormalized perturbation expansions and Fermi liquid theory, *Phys. Rev. Lett.* **70**(25), 4007.
- Hewson, A. C.: 2001, Renormalized perturbation calculations for the single-impurity Anderson model, *J. Phys.: Cond. Mat.* **13**, 10011–10029.
- Hewson, A. C.: 2005, The strong coupling fixed-point revisited, *J. Phys. Soc. Japan* **74**, 8.
- Hewson, A. C.: 2006, Spin and charge dynamics in a renormalised perturbation theory, *J. Phys.: Cond. Mat.* **18**, 1815–1832.
- Hewson, A. C., Bauer, J. and Koller, W.: 2006, Field dependent quasiparticles in strongly correlated local systems, *Phys. Rev. B* **73**(4), 045117.
- Hewson, A. C., Bauer, J. and Oguri, A.: 2005, Non-equilibrium differential conductance through a quantum dot in a magnetic field, *J. Phys.: Cond. Mat.* **17**, 5413.

- Hewson, A. C., Oguri, A. and Meyer, D.: 2004, Renormalized parameters for impurity models, *Eur. Phys. J. B* **40**, 177.
- Hofstetter, W.: 2000, Generalized numerical renormalization group for dynamical quantities, *Phys. Rev. Lett.* **85**(7), 1508.
- Horvatic, B. and Zlatic, V.: 1985, Equivalence of the perturbative and Bethe-ansatz solution of the symmetric Anderson Hamiltonian, *J. Physique* **46**(1), 1459.
- Hubbard, J.: 1963, Electron correlations in narrow energy bands, *Proc. R. Soc. London, Ser. A* **276**, 238.
- Hubbard, J.: 1964a, Electron correlations in narrow energy bands. II. the degenerate band case, *Proc. R. Soc. London, Ser. A* **277**, 237.
- Hubbard, J.: 1964b, Electron correlations in narrow energy bands. III. an improved solution, *Proc. R. Soc. London, Ser. A* **281**, 401.
- Kanamori, J.: 1963, Electron correlation and ferromagnetism of transition metals, *Prog. Theor. Phys* **30**, 275.
- Kato, M., Machida, K., Nakanishi, H. and Fujita, M.: 1990, Soliton lattice modulation of incommensurate spin density wave in two dimensional Hubbard model -a mean field study, *J. Phys. Soc. Japan* **59**, 1047.
- Keldysh, L. V.: 1965, Diagram technique for nonequilibrium processes, *Sov. Phys. JETP* **20**, 1018.
- Keller, M., Metzner, W. and Schollwöck, U.: 2001, Dynamics mean-field theory for pairing and spin gap in the attractive Hubbard model, *Phys. Rev. Lett.* **86**, 4612.
- Kogan, A., Amasha, S., Goldhaber-Gordon, D., G. Granger, Kastner, M. A. and Shtrikman, H.: 2004, Measurement of Kondo and spin splitting in single-electron transistors, *Phys. Rev. Lett.* **93**, 166602.
- Koller, W., Hewson, A. C. and Edwards, D. M.: 2005, Polaronic quasiparticles in a strongly correlated electron band, *Phys. Rev. Lett.* **95**, 256401.
- Kondo, J.: 1964, Resistance minimum in dilute magnetic alloys, *Prog. Theor. Phys* **32**, 37.
- Korbel, P., Spalek, J., Wójcik, W. and Acquarone, M.: 1995, Spin-split masses and metamagnetic behavior of almost-localized fermions, *Phys. Rev. B* **52**(4), R2213–R2216.
- Kotliar, G. and Ruckenstein, A.: 1986, New functional integral approach to strongly correlated Fermi systems: The Gutzwiller approximation as a saddle point, *Phys. Rev. Lett.* **57**(11), 1362.

- Kouwenhoven, L. and Glazman, L.: 2001, Revival of the Kondo effect, *Physics World* p. 33.
- Krishna-murthy, H. R., Wilkins, J. W. and Wilson, K. G.: 1980a, Renormalization-group approach to the Anderson model of dilute magnetic alloys. I. Static properties for the symmetric case, *Phys. Rev. B* **21**(3), 1003.
- Krishna-murthy, H. R., Wilkins, J. W. and Wilson, K. G.: 1980b, Renormalization-group approach to the Anderson model of dilute magnetic alloys. II. static properties for the asymmetric case, *Phys. Rev. B* **21**(3), 1044.
- Laloux, L., Georges, A. and Krauth, W.: 1994, Effect of a magnetic field on Mott-Hubbard systems, *Phys. Rev. B* **50**(5), 3092.
- Landau, L.: 1957, The theory of a Fermi liquid, *Sov. Phys. JETP* **3**, 920.
- Langreth, D.: 1966, Friedel sum rule for Anderson's model of localized impurity states, *Phys. Rev.* **150**(2), 516.
- Leggett, A. J.: 2006, *Quantum Liquids*, Oxford University Press, Oxford.
- Lieb, E.: 1989, Two theorems on the Hubbard model, *Phys. Rev. Lett.* **62**, 1201.
- Logan, D. and Dickens, N.: 2001, Field-dependent dynamics of the Anderson impurity model, *J. Phys.: Cond. Mat.* **13**, 9713–9738.
- Luttinger, J. M.: 1960, Fermi surface and some simple equilibrium properties of a system of interacting fermions, *Phys. Rev.* **119**(4), 1153.
- Luttinger, J. M.: 1961, Analytic properties of single-particle propagators for many-fermion systems, *Phys. Rev.* **121**, 942.
- Luttinger, J. M. and Ward, J. C.: 1960, Ground-state energy of a many-fermion system II, *Phys. Rev.* **118**(5), 1417.
- Manekar, M., Chaudhary, S., Chattopadhyay, M. K., Singh, K. J., Roy, S. B. and Chaddah, P.: 2000, First order metamagnetic transition in CeFe<sub>2</sub> based pseudobinary alloys, *J. Phys.: Cond. Mat.* **12**, 9645.
- Matsumoto, D.: 2001, A simple perturbation theory of a quantum dot coupled to superconducting leads, *J. Phys. Soc. Japan* **70**(2), 492.
- Matsuura, T.: 1979, The effects of impurities on superconductors with Kondo effect, *Prog. Theor. Phys.* **57**(6), 1823.
- Mehta, P. and Andrei, N.: 2006, Nonequilibrium transport in quantum impurity models: The bethe ansatz for open systems, *Physical Review Letters* **96**(21), 216802.

- Meir, Y. and Wingreen, N.: 1992, Landauer formula for the current through an interacting electron region, *Phys. Rev. Lett.* **68**, 2512.
- Metzner, W. and Vollhardt, D.: 1989, Correlated lattice Fermions in  $d = \infty$  dimensions, *Phys. Rev. Lett.* **62**, 324.
- Meyer, D. and Nolting, W.: 2001, Strong-coupling scenario of a metamagnetic transition, *Phys. Rev. B* **64**(5), 052402.
- Micnas, R., Ranninger, J. and S.Robaszkiewicz: 1990, Superconductivity in narrow-band systems with local nonretarded attractive interactions, *Rev. Mod. Phys.* **62**, 113.
- Mielke, A.: 1993, Ferromagnetism in the Hubbard model and Hund's rule, *Phys. Let. A* **174**, 443.
- Moore, J. E. and Wen, X.-G.: 2000, Anomalous magnetic splitting of the Kondo resonance, *Phys. Rev. Lett.* **85**, 1722.
- Mott, N. F.: 1949, The basis of the electron theory of metals, with special reference to the transition metals, *Proc. R. Soc. London, Ser. A* **62**, 416.
- Mott, N. F.: 1968, Metal-insulator transitions, *Rev. Mod. Phys.* **40**, 677.
- Müller-Hartmann, E.: 1989, Correlated fermions in a lattice in high dimensions, *Z. Phys. B* **74**, 507.
- Nagaoka, Y.: 1966, Ferromagnetism in a narrow, almost half-filled  $s$  band, *Phys. Rev.* **147**(1), 392–405.
- Negele, J. W. and Orland, H.: 1988, *Quantum Many-Particle Systems*, Adelson-Wesley.
- Nozières, P. and Schmitt-Rink, S.: 1985, Bose condensation in an attractive fermion gas: From weak to strong coupling superconductivity, *J. Low Temp. Phys.* **59**, 195.
- Oguri, A.: 2001, Fermi-liquid theory for the Anderson model out of equilibrium, *Phys. Rev. B* **64**(1), 153305.
- Oguri, A.: 2002, Out-of-equilibrium Anderson model at high and low bias voltages, *J. Phys. Soc. Japan* **71**, 2969.
- Oguri, A.: 2005, Fermi liquid theory for the nonequilibrium Kondo effect at low bias voltages, *J. Phys. Soc. Japan* **74**(1), 110.
- Oguri, A.: 2006, Transport theory for interacting electrons connected to reservoirs, cond-mat/0606316.
- Oguri, A.: 2007, Mixed-state aspects of an out-of-equilibrium Kondo problem in a quantum dot, *Phys. Rev. B* **75**(3), 035302.

- Oguri, A., Tanaka, Y. and Hewson, A. C.: 2004, Quantum phase transition in a minimal model for the Kondo effect in a Josephson junction, *J. Phys. Soc. Japan* **73**, 2496.
- Ono, Y.: 1998, Theory of metamagnetism in the heavy fermion compound CeRu<sub>2</sub>Si<sub>2</sub>, *J. Phys. Soc. Japan* **67**(7), 2197.
- Peters, R., Pruschke, T. and Anders, F. B.: 2006, Numerical renormalization group approach to Green's functions for quantum impurity models, *Phys. Rev. B* **74**(24), 245114.
- Ralph, D. C. and Buhrman, R. A.: 1994, Kondo-assisted and resonant tunneling via a single charge trap: A realization of the Anderson model out of equilibrium, *Phys. Rev. Lett.* **72**(21), 3401–3404.
- Rammer, J. and Smith, H.: 1986, Quantum field-theoretical methods in transport theory of metals, *Rev. Mod. Phys.* p. 323.
- Randeria, M.: 1995, Crossover from BCS to Bose-Einstein Condensation, *in* A. Griffin, D. Snoke and S. Strinagari (eds), *Bose-Einstein Condensation*, Cambridge University Press, Cambridge.
- Riseborough, P. S.: 2006, The magnetic field and spin dependence of quasi-particle mass enhancements in CeB<sub>6</sub>, *Phil. Mag.* **86**, 2581.
- Rosch, A., Costi, T. A., Paaske, J. and Wölfle, P.: 2003, Spectral function of the Kondo model in high magnetic fields, *Phys. Rev. B* **68**, 014430–1.
- Rozhkov, A. V. and Arovas, D. P.: 1999, Josephson coupling through a magnetic impurity, *Phys. Rev. Lett.* **82**(13), 2788.
- Ryder, L. H.: 1996, *Quantum Field Theory*, Cambridge University Press, Cambridge.
- Sachdev, S.: 1999, *Quantum Phase Transitions*, Cambridge University Press, Cambridge.
- Sakai, O., Shimizu, Y. and Kasuya, T.: 1989, Single-particle and magnetic excitation spectra of degenerate Anderson model with finite f-f coulomb interaction, *J. Phys. Soc. Japan* **58**(10), 3666.
- Sakai, O., Shimizu, Y., Shiba, H. and Satori, K.: 1993, Numerical renormalization group study of magnetic impurities in superconductors II: Dynamical excitation spectra and spatial variation of the order parameter, *J. Phys. Soc. Japan* **62**(9), 3181–3197.
- Sangiovanni, G., Gunnarsson, O., Koch, E., Castellani, C. and Capone, M.: 2006a, Electron-phonon interaction and antiferromagnetic correlations, *Phys. Rev. Lett.* **97**, 046404.

- Sangiovanni, G., Toschi, A., Koch, E., Held, K., Capone, M., Castellani, C., Gunnarsson, O., Mo, S.-K., Allen, J. W., Kim, H.-D., Sekiyama, A., Yamasaki, A., Suga, S. and Metcalf, P.: 2006b, Static versus dynamical mean-field theory of Mott antiferromagnets, *Phys. Rev. B* **73**(20), 205121.
- Saso, T. and Itoh, M.: 1996, Insulator-to-metal transition in Kondo insulators under a strong magnetic field, *Phys. Rev. B* **53**(11), 6877.
- Satori, K., Shiba, H., Sakai, O. and Shimizu, Y.: 1992, Numerical renormalization group study of magnetic impurities in superconductors, *J. Phys. Soc. Japan* **61**(9), 3239.
- Schrieffer, J. R. and Wolff, P. A.: 1966, Relation between the Anderson and Kondo Hamiltonians, *Phys. Rev.* **149**(2), 491.
- Schulz, H. J.: 1990, Incommensurate antiferromagnetism in the two-dimensional Hubbard model, *Phys. Rev. Lett.* **64**(12), 1445.
- Shraiman, B. I. and Siggia, E. D.: 1989, Spiral phase of a doped quantum antiferromagnet, *Phys. Rev. Lett.* **62**(13), 1564–1567.
- Siano, F. and Egger, R.: 2004, Josephson current through a nanoscale magnetic quantum dot, *Phys. Rev. Lett.* **93**, 047002.
- Spalek, J. and Gopalan, P.: 1990, Almost-localized electrons in a magnetic field, *Phys. Rev. Lett.* **64**(23), 2823–2826.
- Tasaki, H.: 1995, Ferromagnetism in Hubbard models, *Phys. Rev. Lett.* **75**(25), 4678.
- Toschi, A., Capone, M. and Castellani, C.: 2005, Energetic balance of the superconducting transition across the BCS-Bose Einstein crossover in the attractive Hubbard model, *Phys. Rev. B* **72**, 235118.
- Tsvetlik, A. M. and Wiegmann, P. B.: 1983, Exact results in the theory of magnetic alloys, *Adv. Phys.* **32**(25), 453.
- van Dam, J. A., Nazarov, Y. V., Bakkers, E. P. A. M., Franceschi, S. D. and Kouwenhoven, L. P.: 2006, Supercurrent reversal in quantum dots, *Nature* **442**, 667.
- van Dongen, P. G. J.: 1995, Phase separation in the extended Hubbard model at weak coupling, *Phys. Rev. Lett.* **74**(1), 182.
- van Dongen, P. G. J.: 1996, Phase diagram of the extended Hubbard model at weak coupling, *Phys. Rev. B* **54**, 1584.
- Vecino, E., Martin-Rodero, A. and Yeyati, A. L.: 2003, Josephson current through a correlated quantum level: Andreev states and pi junction behavior, *Phys. Rev. B* **68**, 035105.

- von der Linden, W. and Edwards, D. M.: 1991, Ferromagnetism in the Hubbard model, *J. Phys.: Cond. Mat.* **3**, 4917.
- Weichselbaum, A. and von Delft, J.: 2006, Sum-rule conserving spectral functions from the numerical renormalization group, cond-mat/0607497.
- Wilson, K.: 1975, The Renormalization Group: Critical phenomena and the Kondo problem, *Rev. Mod. Phys.* **47**, 773.
- Yamada, K.: 1975a, Perturbation expansion for the Anderson Hamiltonian, *Prog. Theo. Phys.* **54**, 316.
- Yamada, K.: 1975b, Perturbation expansion for the Anderson Hamiltonian, *Prog. Theo. Phys.* **53**, 1970.
- Yoshioka, T. and Ohashi, Y.: 2000, Numerical renormalization group studies on single impurity Anderson model in superconductivity: A unified treatment of magnetic, non-magnetic impurities, and resonance scattering, *J. Phys. Soc. Japan* **69**(6), 1812.
- Zagoskin, A. M.: 1998, *Quantum theory of Many-Body Systems*, Springer, New York.
- Zitzler, R., Pruschke, T. and Bulla, R.: 2002, Magnetism and phase separation in the ground state of the Hubbard model, *Eur. Phys. J. B* **27**, 473.
- Zwierlein, M., Abo-Shaeer, J., Shirotzek, A., Schunck, C. H. and Ketterle, W.: 2005, Vortices and superfluidity in a strongly interacting Fermi gas, *Nature* **435**, 1047.
- Zwierlein, M., Stan, C. A., Schunck, C. H., Raupach, S. M. F., Kerman, A. J. and Ketterle, W.: 2004, Condensation of pairs of fermionic atoms near a Feshbach resonance, *Phys. Rev. Lett.* **92**, 120403–1.

# Acknowledgement

First and foremost I would like to express my gratitude to Dr AC Hewson for accepting me as a PhD student at Imperial College. In no other constellation could I have had such a thorough introduction to the application of renormalisation group methods to strongly correlated electron systems, from “The Kondo Problem to Heavy Fermions”. I have benefited enormously from the many ideas and suggestions for the work throughout these years. A thesis with such a variety of topics would have been impossible without his continuous support and invaluable advice.

I would also like to thank Dr W Koller and Dr D Meyer. It was my pleasure to continue their excellent work on the “IC\_NRG” program. Many of the results presented in this thesis could not have been achieved without their earlier contributions. In addition I would like to acknowledge numerous helpful discussions ranging from technical issues with the program over physics questions to personal matters. Moreover, I would like to express my gratefulness to Dr N Dupuis. He was always open to discuss questions on condensed matter theory with me. I owe a lot to him, as well, for many useful suggestions to improve parts of this thesis. I would also like to acknowledge a number of very helpful discussions with Prof DM Edwards throughout the course of this work.

A special “arigato” goes to Prof A Oguri and the group at Osaka City University for their hospitality. Many important contributions for this work developed during my stay there. I would like to thank Prof Oguri for taking so much time for discussions and for much helpful advice. I am also very grateful to Dr R Bulla and Prof D Vollhard for giving me the opportunity to spend some weeks in Augsburg towards the end of my PhD. I had many fruitful and interesting discussions in the inspiring environment there. Finally, I would also like to thank my examiners Dr DKK Lee and Prof DE Logan for taking the time and providing many useful comments about the work.

As much as the scientific support it is important to acknowledge the thorough personal support I benefitted from throughout the last three years. I am very grateful to my parents and family for their open ears and encouragement. Finally, and maybe more important than anyone else, I would like to express deep gratitude to Mayra. Listening to my complaints on a regular basis, and standing my ill humour, when things did not work out, must have been a considerable challenge. Without her love and support I would not be where I am now.

